NASA/DOD
Control/Structures
Interaction Technology
1986

NASA

NASA/DOD Control/Structures Interaction Technology 1986

Compiled by
Robert L. Wright
NASA Langley Research Center
Hampton, Virginia

N/\S/

National Aeronautics
and Space Administration

**Scientific and Technical
Information Office**

1987

PREFACE

The National Aeronautics and Space Administration (NASA) and the Department of Defense (DOD) are actively involved in the development of a validated technology data base in the areas of control/structures interaction, deployment dynamics, and system performance for large flexible spacecraft. The generation of these technologies is essential to the efficient and confident development of this new class of spacecraft to meet stringent goals in safety, performance, and cost. As a major element of this technology effort, the NASA Office of Aeronautics and Space Technology (OAST) has initiated the Control of Flexible Structures (COFS) Program that provides a major focus for the Research and Technology base activities in structural dynamics and controls and complements long-range development programs at the Air Force Wright Aeronautical Laboratories (AFWAL). These activities provide a systematic approach to address technology voids through development and validation of analytical tools, extensive ground testing of representative structures, and in-space experiments for verification of analysis and ground test methods.

In order to promote timely dissemination of technical information acquired in these programs, the NASA Langley Research Center and the AFWAL will alternately sponsor an annual conference to report to industry, academia, and government agencies on the current status of control/structures interaction technology. The First NASA/DOD CSI Technology Conference is the beginning of this series.

This publication is a compilation of the papers presented at the conference and is divided into two parts. Part I was distributed at the conference, and Part II is being distributed after the conference.

The use of trade names or names of manufacturers in this publication does not constitute an official endorsement of such products or manufacturers, either expressed or implied, by the National Aeronautics and Space Administration.

H. L. Bohon
General Chairman

CONTENTS

PRECEDING PAGE BLANK NOT FILMED

CONTROL OF FLEXIBLE STRUCTURES (COFS)

SELECTED NASA RESEARCH IN CONTROL/STRUCTURES INTERACTIONS

J. F. Garibotti
Ametek, Inc.
Anaheim, California

BACKGROUND

NASA, recognizing the need for a proven Control/Structures Interaction (CSI) technology, formed an Ad Hoc Subcommittee composed of members of the NASA Space Systems and Technology Advisory Committee in August 1982. The purpose of the Subcommittee was to assess the readiness of this technology and evaluate potential NASA alternative activities to remedy any deficiencies. The results of the Subcommittee's activities were an initial step in providing for the flight readiness of the CSI technology. The Subcommittee completed its work with a report in June 1983, which included a number of major findings and recommendations.

The intent of the Subcommittee was that a CSI technology program be implemented and include activities such as COFS (Control of Flexible Structures).

o   FORMATION OF AD HOC SUBCOMMITTEE ON CONTROL/STRUCTURES INTERACTION (CSI) IN AUGUST 1982

o   TASK COMPLETED IN JUNE 1983

o   MAJOR RECOMMENDATIONS INCLUDED:

- OBTAIN AND ASSESS QUANTIFIED REQUIREMENTS OF SYSTEMS NEEDING CSI TECHNOLOGY

- ESTABLISH ANALYSIS/GROUND TEST/ ON-ORBIT TEST RELATIONSHIP

- IDENTIFY DOD NEEDS/COORDINATE WITH DOD

o   CSI TECHNOLOGY INCLUDES COFS

INDUSTRY OVERVIEW/ISSUES

    To prepare for this overview contacts with members of Industry, DoD, NASA, and the University community were made to obtain a broad cross section of views on the CSI technology program and COFS. This presentation, while incorporating many of these views, primarily represents the thoughts of the author.

    It must be emphasized that the principal objective of this briefing is to enhance the chance that the CSI technology program will be successful, i.e. that a flight-ready CSI technology will be made available in a timely manner. A secondary objective is to promote a better understanding of how industry can contribute to and benefit from the CSI technology program.

    o   INDUSTRY CONTACTS MADE

    o   OBJECTIVE OF BRIEFING

        - HELP CSI TECHNOLOGY PROGRAM

        - UNDERSTAND HOW INDUSTRY CAN CONTRIBUTE TO AND
          BENEFIT FROM CSI TECHNOLOGY PROGRAM

    o   PRESENTATION IS IN FORM OF COMMENTS/QUESTIONS

CSI TECHNOLOGY JUSTIFICATION

In order to properly direct the CSI technology program to achieve the most usable results, it is necessary to understand what the system (spacecraft, components) requirements are that dictate the need for a flight-ready CSI technology. For some systems CSI technology will be enabling, for others it will be enhancing and for still others, not needed at all. It is important that this understanding be quantified as much as possible. As a minimum, a quantified comparison of open loop response and required response should be made.

System needs dictate the importance of CSI technology for a given system and it should be kept in mind that there are other key technologies that will be, or are now, demanding resources to solve their problems, e.g. achievement of appropriate on-orbit power, increased launch capability. To justify the importance of CSI technology, quantified requirements for CSI technology must be established.

o   WHAT PLANNED NASA, DoD SYSTEMS

- REQUIRE CSI TECHNOLOGY?
- BENEFIT FROM CSI TECHNOLOGY OPTION?

o   CAN CSI TECHNOLOGY REQUIREMENTS BE QUANTIFIED?

o   WHAT IS SIGNIFICANCE OF CSI/COFS VS. OTHER SYSTEM, PERFORMANCE, AND SURVIVABILITY REQUIREMENTS, E.G.

- POWER
- OPTICS
- LAUNCH VEHICLE CAPABILITY

INDUSTRY MOTIVATION

To motivate industry to participate in the CSI technology program it is necessary to realize there are two types of industrial organizations. Large businesses or organizations will participate, in large part, because they think of CSI technology as a building block technology leading toward the acquisition of a large system contract and the resulting benefit. Small businesses, which can offer a lot to the CSI technology program, will participate only if they can achieve a near-term benefit. As far as this Conference is concerned there are only 18 papers out of 52 co-authored by industry representatives and some of these discuss activity completed over two years ago.

To further motivate industry, it would be helpful to let them know what technical capability is intended to be developed, e.g. what engineering software, test techniques, or test facilities. In regard to this, industry should be kept appraised of the status of the Large Spacecraft Laboratory and its relationship to analysis development and validation and on-orbit testing of the CSI technology program.

o   MECHANISMS TO MOTIVATE PARTICIPATION

- LARGE BUSINESS
- SMALL BUSINESS
- 18 OF 52 PAPERS FROM INDUSTRY

o   WHAT CAPABILITY WILL BE DEVELOPED?

o   WHAT TEST FACILITIES WILL BE DEVELOPED?

o   WHAT IS STATUS OF LARGE SPACECRAFT LABORATORY?

WHAT IS NASA INVESTMENT STRATEGY FOR
CSI TECHNOLOGY?

So that Industry can better participate in the CSI technology program it would be most helpful to know what the program plan and investment strategies are. The more industry knows about this the more meaningful can be its interaction with NASA, for example at meetings such as this. The figure lists key elements of an investment strategy which should be put forth by NASA for information and for discussion by all concerned.

o   CSI TECHNOLOGY OBJECTIVES

o   ON-GOING RELATED PROGRAMS

o   NASA/INDUSTRY JOINT ENDEAVOR AGREEMENTS

o   PRESENT CSI TECHNOLOGY SOA FOR KEY ISSUES

o   SPECIFIC CSI TECHNOLOGY PROGRAMS/TASKS

o   SCHEDULE
    - WHAT IS EXPECTED PROGRESS VS. TIME?
    - WHEN WILL WE BE DONE?

o   FUNDING

o   PLANS FOR TRANSITION TO APPLICATION

SATISFYING NEEDS VERSUS ADVANCING TECHNOLOGIES

The COFS part of the CSI technology program is primarily directed at testing and appears to include all of the flight or on-orbit testing presently planned for CSI.

At the present COFS appears to be oriented toward advancing the state of the art of individual technologies as opposed to satisfying a system need; e.g. achieving a specified geometrical precision of a spacecraft structure during the operation of the spacecraft. The expense of a program like COFS will require an approach focused on satisfying a need in order to command the resources necessary for success. The need to be satisfied, no doubt, will have to be important to DoD as well as NASA.

At present perceived shortcomings of COFS include the fact that development of key technologies such as materials and structural design, both important to achieving geometrical precision, are not part of COFS.

o   COFS APPEARS TO BE TECHNOLOGY DEVELOPMENT

o   PERCEIVED DIFFICULTIES/SHORTCOMINGS

   - BALANCE OF PASSIVE/ACTIVE APPROACHES MISSING
   - KEY DISCIPLINES NOT INCLUDED
   - PLAN FOR TRANSITION TO APPLICATION UNDEFINED

o   COST VS. POTENTIAL PAYOFF

COFS II

The figure represents the COFS II test article, which appears to represent the structure for a communications or surveillance antenna, the wave length of operation of which may be such as not to require CSI technology. The resources needed for COFS II will require that the COFS II test article represent a real problem.
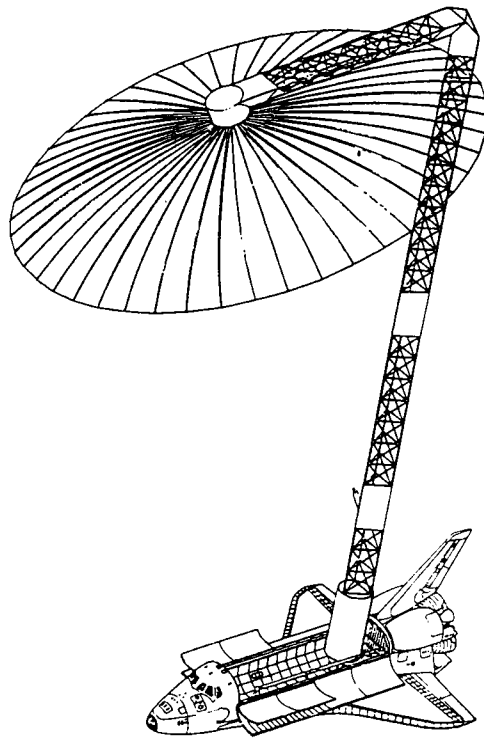
HALO*

The structure shown in this figure may not be exactly what COFS II should be but it is closer to being the type of test article we should be looking at. CSI technology needs should be determined first and then the test article should be designed.

*High Altitude Large Optics (HALO)
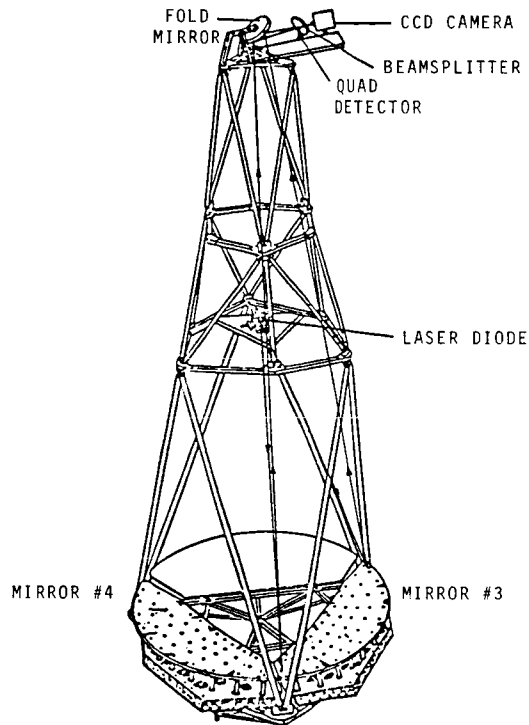
GUEST INVESTIGATOR OPPORTUNITIES

This is a list of guest investigator opportunities for COFS. Note the lack of any "opportunity" to investigate materials and structural design, e.g. optimization, issues whose resolution would support the achievement of geometrically precise structures.

Selection criteria for guest investigators should be based on how well their proposed experiments support development of a flight ready CSI technology.

- **STRUCTURAL DYNAMICS**

- **FLEX-BODY CONTROL ALGORITHMS**

- **SYSTEM IDENTIFICATION ALGORITHMS**

- **FLIGHT & GROUND TEST METHODS**

- **MATH MODELLING**

- **VIBRATION SUPPRESSION**

- **ANALYSIS OF GROUND & IN-SPACE TEST DATA**

- **FLIGHT TESTING OF UNIQUE HARDWARE**

COFS

Although COFS is a subset of CSI there is no clear exposition of this relationship. This relationship is extremely important because it will dictate in large part the relationship between analysis and ground test development and validation, and on-orbit testing. This relationship is key to flight test justification and thus, development of a flight-ready CSI technology.

A key element of CSI technology and thus COFS, is the inter-disciplinary nature of the problem. Every effort should be made to permit materials and structures on-orbit experiments, if required, to be part of COFS. If these experiments cannot be accommodated in COFS and they are required, resources should be made available for them.

o   HOW DO CSI TECHNOLOGY AND COFS RELATE?

o   ANALYSIS/GROUND TEST/ON-ORBIT TEST RELATIONSHIP
     IS KEY TO CSI TECHNOLOGY (AND TO FLIGHT TEST JUSTIFICATION)

     - TO VALIDATE ANALYSIS AND GROUND TEST METHODS
     - TO DETERMINE WHAT CAN ONLY BE DONE ON-ORBIT
     - HOW WILL COFS I RESULTS BE USED IN THIS REGARD?

o   WHAT ARE SELECTION CRITERIA FOR GUEST INVESTIGATORS?

o   WHAT IS CURRENT COFS SCHEDULE?

o   ARE USERS AND TECHNOLOGY DEVELOPERS "IN SYNC"?

o   CAN MATERIALS AND STRUCTURAL CONCEPT EXPERIMENTS BE
     ACCOMMODATED, E.G. MEASUREMENT OF THERMAL CYCLING EFFECTS?

o   CAN PROPRIETARY DESIGNS BE AVOIDED?

CSI TECHNOLOGY PROGRAM

This figure illustrates the relative proportion of resources devoted to Base R&T and to COFS for the CSI technology program. On a yearly basis COFS is estimated to receive six times the resources available for Base R&T.

BASE R&T

° STRUCTURES
° MATERIALS
° STRUCTURAL DESIGN
° CONTROLS

COFS*

° DYNAMICS
° ACTIVE STRUCTURAL
  CONTROL
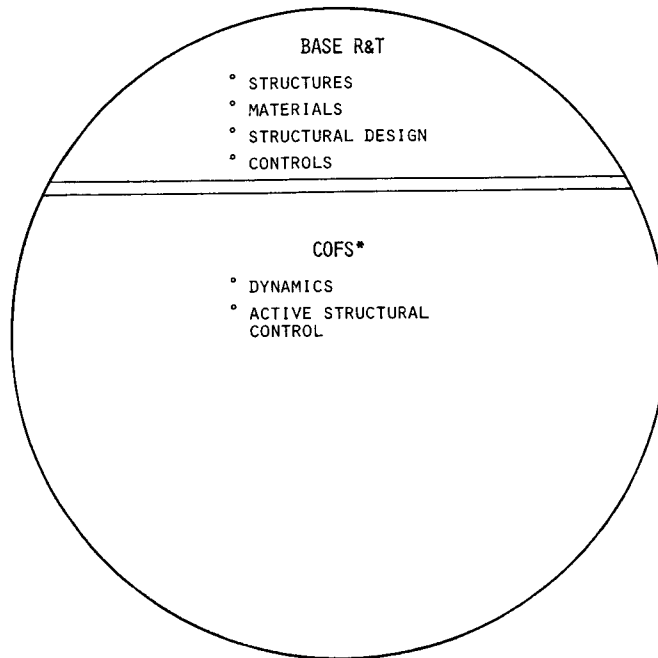
* COFS WILL PROVIDE FUNDAMENTAL DATA FOR ANALYTICAL DEVELOPMENT AND FOR VALIDATION
  OF ANALYSIS/GROUND TEST

574

STRUCTURAL CONCEPTS

This figure illustrates a concept for a structurally efficient truss element, the development of which would enhance our ability to design geometrically precise structures. This is an example of structural design activity relevant to COFS and CSI.

MONOCOQUE TUBE   GEODETIC TAPERED TUBE

THERMAL CYCLING EFFECTS

To achieve geometrically precise structure the effect of thermal cycling on composite materials must be investigated and understood. To do this requires a thermal cycling test facility that is large enough and properly equipped. This must be accounted for in the CSI technology program.

o   BEHAVIOR OF "THERMALLY STABLE" REINFORCED COMPOSITES UNDERGOING THERMAL CYCLING IS NOT WELL UNDERSTOOD

o   THIS IS CRITICAL TO ACHIEVEMENT OF GEOMETRICALLY PRECISE STRUCTURE

o   THERMAL CYCLING TEST FACILITY IS NEEDED

o   NEED TO ESTABLISH THERMAL CYCLING EFFECTS, BOUND THEM, DEAL WITH THEM

o   HOW IS THIS ACCOUNTED FOR IN CSI TECHNOLOGY?

o   ARE THERE OTHER ISSUES LIKE THIS?

SUMMARY

To achieve an "optimum" solution to the achievement of geo-
metrical precision requires that all key technologies, e.g. materials,
structures, dynamics, and controls, be brought to bear on the problem.
This in turn will require individuals to be aware of the role of each
of these technical disciplines in achieving this "optimum", and to
make an effort to thoroughly understand these disciplines.

o   SYSTEM NEEDS MUST BE ASSESSED PERIODICALLY

o   EMPHASIZE TECHNOLOGY DEVELOPMENT TO MEET
     SYSTEM NEEDS

o   ON-ORBIT TESTING FOR MATERIALS AND STRUCTURAL DESIGN
     TECHNOLOGY MUST BE CONSIDERED IN CSI TECHNOLOGIES, IF
     NOT IN COFS

o   PROPER PHASING OF ANALYSIS/GROUND TEST/ON-ORBIT TEST
     MUST BE MAINTAINED

o   COFS IS PART OF CSI TECHNOLOGY

o   MAINTAIN/ENHANCE COORDINATION WITH DOD

SPACE STATION: A PROGRAM OVERVIEW

Judith H. Ambrus
Office of Space Station
National Aeronautics and Space Administration
Washington, D.C.

Mankind is at the threshold of a new age. Before the end of this century we will have taken the next logical step in space exploration: we will have established man's permanent presence in space. We will have a facility in low Earth orbit consisting of a manned base with working and living facilities for a crew of eight and several unmanned platforms carrying experiments, tended and serviced by the Station or the Shuttle crew (Figure 1). The Shuttle will be a regular visitor delivering new crews, supplies, new experiments or spacecraft for launch into different orbit and returning with completed experiments, crews that have finished their tour of duty, waste material, and perhaps items to be repaired on the ground. An orbital maneuvering vehicle, a robotic space tug, will assist in hauling in spacecraft for servicing or possibly logistics modules delivered by expendable launch vehicles. This is the vision, but the hard facts must be considered.

The idea of a Space Station is not new to anyone engaged in the business of space. Even while the Apollo project was still on the drawing boards, future plans which included various concepts of space stations were being drawn up. Over the years, as we gained more experience, the concepts changed. For instance, we now know that artificial gravity is not necessary for men to survive and not suffer irreversible damage to their health, after living in space for a period of a few weeks or months. We also know what our transportation system to space is, its strength and its limitations. These and other data are enabling us now to realistically plan, design and develop the next logical step.
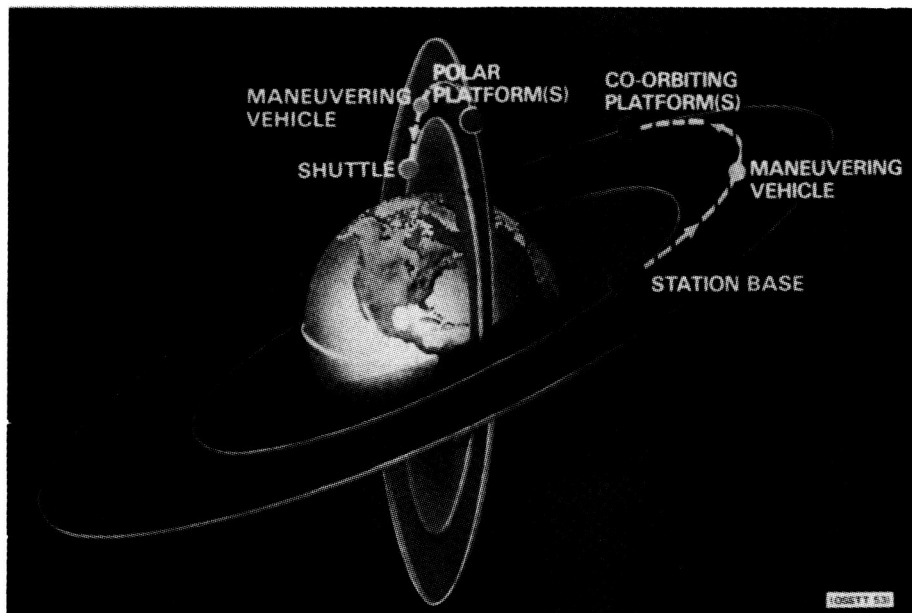

Figure 1

---

*Original figures not available at time of publication.

SPACE STATION GOALS

When the President directed NASA in January, 1984 (in his State
of the Union Address) to develop a Space Station, he set very
important goals for this program (Figure 2).

The preliminary design of the facility (Figure 2) might
contribute to the accomplishement of all of these goals. It is a
multi-purpose facility, serving as a microgravity laboratory in
space where basic research and technology development experiments
will be performed in a "shirt sleeve" environment. Some of these
will lead to enhanced knowledge about human physiology in the
weightless environment; others might lead to materials processes
which, once automated, will develop into commercial ventures.
Scientific instruments will be mounted on the upper and lower
booms for the observational sciences. These instruments will be
serviced or changed by either crew members via EVA*, or by a
mobile telerobotic servicer. Spacecraft, such as the Gamma Ray
Observatory and the Hubble Space Telescope, will be serviced in
the servicing bay. It will also be possible to assemble
spacecraft to be launched into other orbits or toward
outer space. Finally, several elements will be contributed by
the European Space Agency, Japan, and Canada -- our international
partners in this endeavor.

- ASSURE FREE WORLD LEADERSHIP IN SPACE DURING THE 1990's
- STIMULATE ADVANCED TECHNOLOGY
- PROMOTE INTERNATIONAL COOPERATION
- ENHANCE CAPABILITIES FOR SPACE SCIENCE AND APPLICATIONS
- DEVELOP FURTHER THE COMMERCIAL POTENTIAL OF SPACE
- CONTRIBUTE TO PRIDE AND PRESTIGE
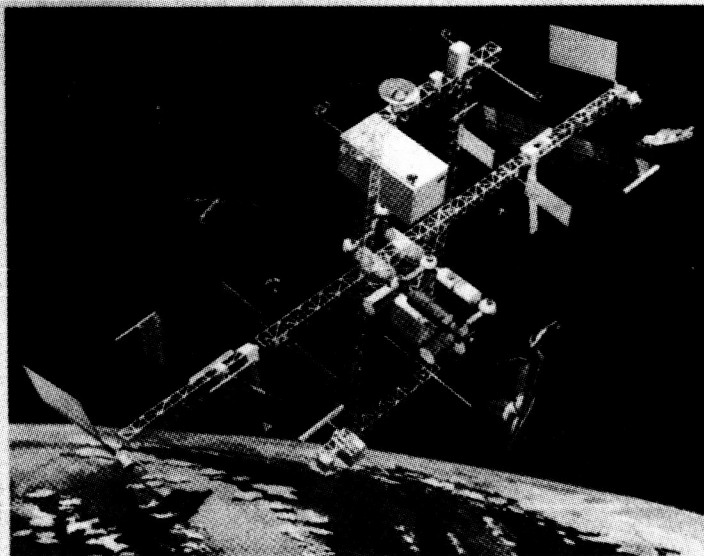- STIMULATE INTEREST IN SCIENCE AND ENGINEERING EDUCATION

Figure 2

---

*EVA (extravehicular activity).

SPACE STATION PROGRAM OBJECTIVES

The key program objectives that have been set to meet these goals (Figure 3) take into consideration the environment in which we have to attain our goals. We are committed by Presidential directive to have a permanently manned facility in 1994; we also have limited resources. The facility has to provide more than useful capabilities. These capabilities will have to be affordable. We are not yet sure what the most useful aspects of the Station might be; therefore, we will have to build a Station which is capable of evolution. Man in space is very expensive; therefore, we have to design a facility with a judicious mix of manned and unmanned elements. We also have to make sure that those expensive man-hours are not used up trying to keep the Station afloat; thus, development of automation and robotics technologies is imperative for long-term affordability of the capabilities. Finally, we have to secure international cooperation in both building and using the Station.

It is obvious that this is the most challenging program ever undertaken by NASA. The challenges are both technical and managerial.

o We have to design for "permanence," which means both easy maintainability and design for evolution

o We have to build to cost and schedule, meeting both the presidentially mandated milestone for permanent manned presence in 1994 and the budget constraints placed upon us by Congress

o We have to design within a realistic transportation environment, which is currently undergoing redefinition

o We have to manage systems engineering and integration for a program far bigger and more complex then any in our experience

o We have to learn to efficiently communicate without drowning in paper

o We have to incorporate new technologies, balancing cost, schedule, and risk; trading off the potential of long-term, operational cost savings versus the risk of having a new technology develop unexpected flaws

o We have to try to design operations during the hardware design stage, so as to design to the operational environment. This will mean hard choices involving possibly an as yet unknown user versus a problem here and now, which might delay a launch schedule

o We have to learn new techniques, such as assembly and checkout on orbit, potentially while parts of the Station are already operational

o Finally, we have to orchestrate the international dimensions of
the program, which involves meshing not only schedules and costs
not under our control but also dealing with unfamiliar technical
and management practices

SPACE STATION PROGRAM OBJECTIVES

- Develop a permanently manned Space Station by 1994

- Provide useful and affordable capabilities

- Enhance space science and applications

- Stay within $8 billion cost envelope*

- Secure international cooperation

- Design for evolution

- Push automation and robotics technologies

- Incorporate potential for man-tended concept in baseline program

- Blend manned and unmanned systems and capabilities

*FY 1984 Dollars

Figure 3

SPACE STATION PROGRAM SCHEDULE

Because of its complexity, the program has been planned in different phases (Figure 4). The official program start of 1984 drew heavily on planning and concept development work accomplished over the years by NASA and its contractors. Thus it was possible to convene an in-house Concept Development Group, which in the span of a year (Phase A) developed the so-called reference concept, which became the basis of the RFP for Phase B of the program, the Concept Development and Preliminary Design Phase. To manage this phase the work was divided into four "work packages," each managed by a different NASA Center and involving two contractors per work package doing parallel work. System integration was accomplished in-house in the Program Office established at the Johnson Space Center.

During this phase the reference configuration was critically examined from aspects of user capability, development cost, technical risk, maintainability, and other factors to evolve into the baseline configuration. The most obvious changes were the manned base configuration change from the "power tower" to the "dual keel." This provides a stiffer structure, allows for placement of the modules in the most favorable microgravity environment and has considerably more space for attaching payloads. The module pattern was changed from the "racetrack" configuration which included internal airlocks to a simpler design consisting of modules with nodes and tunnels to interconnect. This allowed for easier traffic patterns as well as providing more volume.

It was also during this process that technologies for the various subsytems were selected. For example the decision was made to have a "hybrid" power system consisting of both solar array/battery modules and solar dynamic modules. The much smaller area of the solar collectors reduces drag and saves operating costs and thus has more growth capability. The technical risk of not having fight experience with a solar dynamic system was outweighed by the operational considerations and high near-term power demands. It was also decided to close the Environmental Control and Life Support System to the point where only nitrogen would be resupplied to the pressurized atmosphere (the oxygen being regenerated). Recycling water would allow only food to be supplied and solid waste to be returned. Again, the long-term savings in logistic resupply costs were considered worth the higher development costs of such a system.

SPACE STATION PROGRAM SCHEDULE

CY 1984   1986   1988   1990   1992   1994   1996

▼ PRESIDENTIAL DIRECTIVE TO NASA

   ▼ NASA PROGRAM CONCEPT (RFP)

   ◤◢ ADVANCED DEVELOPMENT PROGRAM

   ◤☐ DEFINITION & PRELIMINARY DESIGN

   ◹ SYSTEM DEVELOPMENT ◸

ASSEMBLY LAUNCHES ▽▽.............▽

POSSIBLE MAN-TENDED CAPABILITY (MTC) ▽

PERMANENTLY MANNED ◿

PLATFORM LAUNCHES ▽ ▽   ▽▽
                  POLAR   COORBITING

BASELINE CONFIGURATION COMPLETED ▽◿
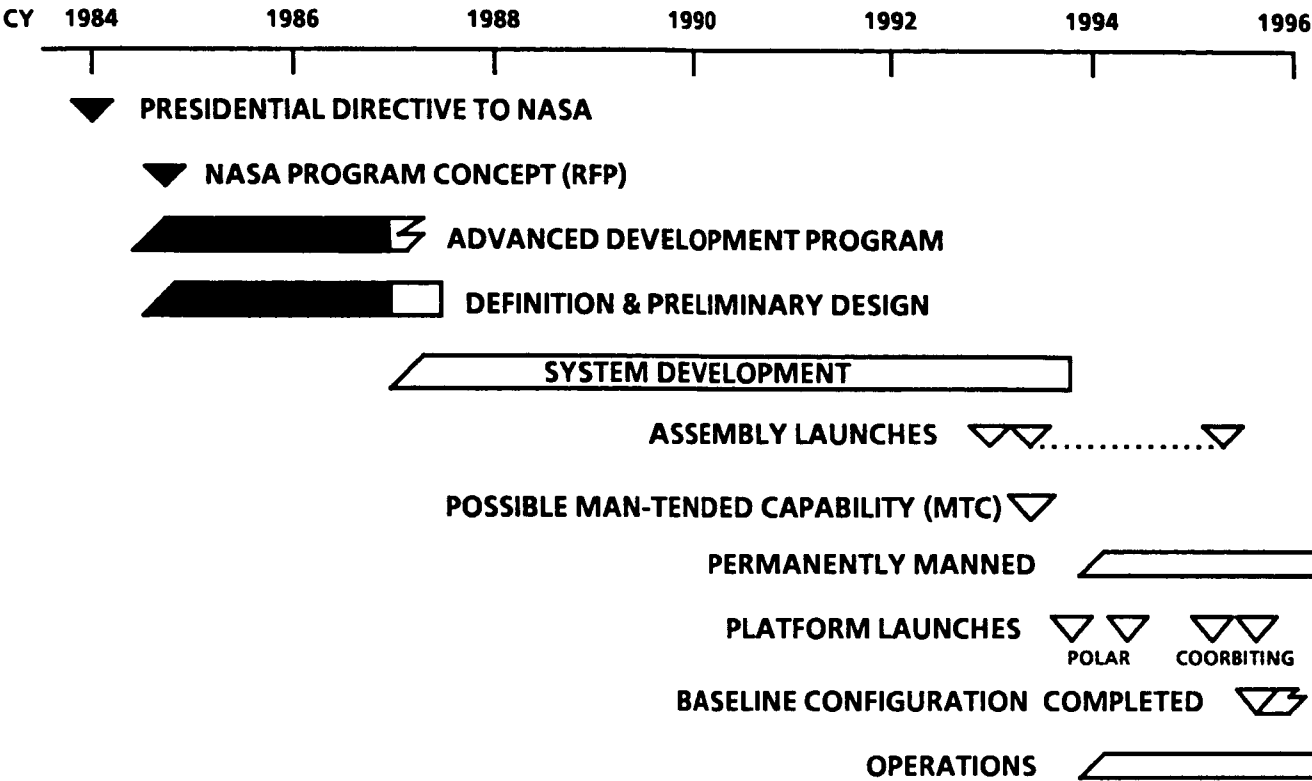
OPERATIONS ◿

Figure 4

ADVANCED DEVELOPMENT PROGRAM

These choices were greatly aided by the results from the Advanced Development Program that was conducted parallel to the Phase B effort (Figure 5). During the early planning process it had become apparent that there were several promising technologies in NASA's generic technology base program which, if focused towards the Space Station application, would have high pay-off in operational cost savings.

The program was designed for a three year effort in thirteen different areas. After the first year some technologies were selected for prototype development and testing. This program was also used to establish test beds, which are being used for prototype testing now, but will be retained for use in test bed verification of flight hardware as well as serve the evolutionary technologies. Several decisive flight experiments were also conducted.

It was the advanced development program that lowered the risks to an acceptable level and enabled the choices mentioned above in power and ECLSS*. Other examples include the choice of the high efficiency, two-phase thermal management system (outside the pressurized volumes), the hydrogen/oxygen propulsion system, the erectable instead of deployable structure, the sea level pressure in the pressurized volumes, and others.

As the second phase of the Space Station Program neared completion, the Baseline Configuration underwent another hard scrutiny. This had been necessitated by the changed environment following the loss of the Challenger, which includes the change in the availability (and possibly mode) of transportation, the heightened awareness of crew safety, the concern over early uses of the Space Station and the cost of the baseline configuration raised by Congress and the management concerns highlighted by the Roger's Commission. The Administrator, therefore, ordered a comprehensive technical, cost, and management review of the program.

---

*Environmental Control and Life Support Systems.

ADVANCED DEVELOPMENT PROGRAM

- Current technology is, in some areas, inadequate for desired Space Station capabilities

- Purpose of Advanced Development Program is to provide advanced technology options that are reliable and cost effective

- Five key program elements:

    Focused Technology - provides proper application focus to the generic R&T base program and continues technology development through demonstration at the breadboard level

    Prototype Hardware - provides for development of protypical hardware that embodies the advanced technologies

    Test Beds - provides for proper testing of the new technologies at the brassboard or prototype level

    Flight Experiments - provides in-space demonstrations of advanced technologies using the Shuttle

    Subsystem Studies - provides for additional studies of technical options resulting from advanced development efforts

Figure 5

CRITICAL EVALUATION TASK FORCE REFERENCE CONFIGURATION

The configuration resulting from this review (Figure 6) has the following features:

o It combines the nodes and interconnecting tunnels into "resource nodes." This results in more useable pressurized volume, thus enabling the inside accommodation and servicing of instruments, which previously required EVA

o It increased the initial deployed power to allow for early user operations

o It adjusted the assembly sequence to achieve permanent habitability in 1994, and user operations during assembly to allow for the limited transportation capabilities
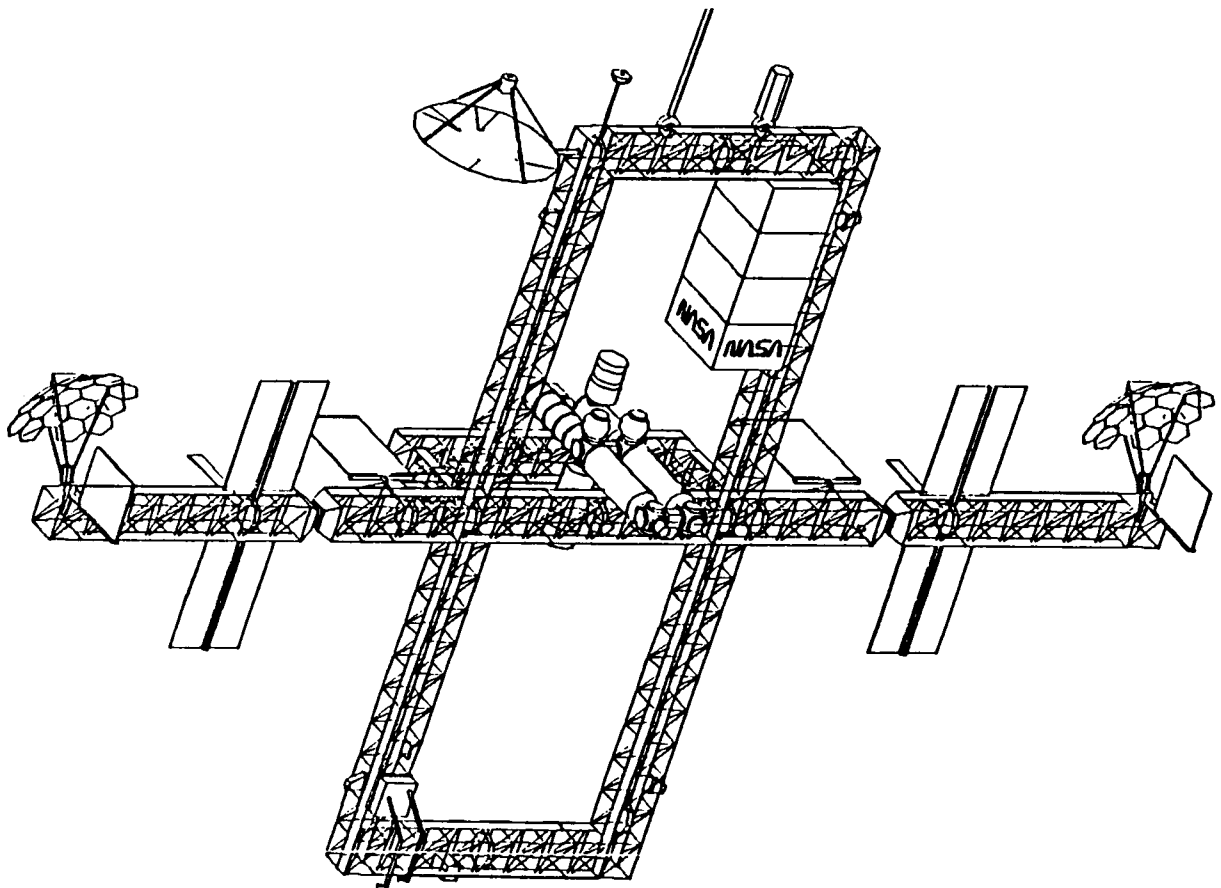
Figure 6

PROGRAM MANAGEMENT APPROACH

The concurrent management review of the Space Station Program resulted in a somewhat changed management structure (Figure 7), with a Program Office being established in the Washington area as part of Headquarters. This Program Office will accomplish the system engineering and integration which involve the interfaces between the hardware elements developed by four NASA centers with their contractor teams and the three international partners.

LEVEL A

NASA Headquarters, Washington, D.C.

• Policy and overall program direction

LEVEL A'

Washington Metropolitan Area

• Program management and technical content

LEVEL C

Various NASA Centers

• Project management: element definition and development

CONTRACTORS

Multiple Locations

• Detail design, manufacturing, integration and test, plus engineering and technical services
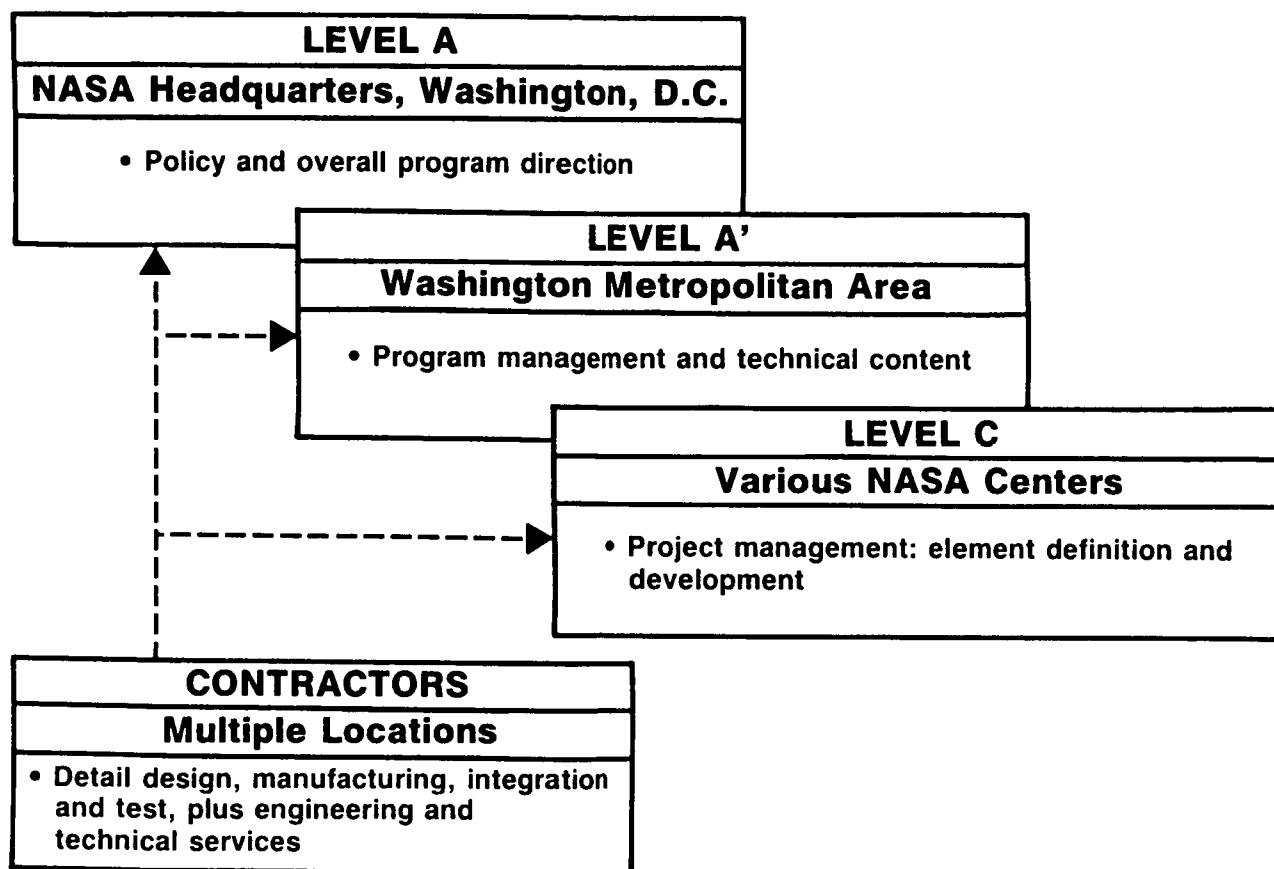
Figure 7

SPACE STATION PLAN

The Space Station elements with the responsible organization
(NASA and international) are shown in Figure 8. Present
activities are focused on the start of Phase C/D, the Design and
Development Phase. The major challenges at present include the
synchronization of four RFPs*, the international negotiations, the
still ongoing cost review, and the effort to define and plan
operations. And while we are working to build the initial Space
Station, we also look toward the twenty-first century, when the
Space Station will be the base from which we plan manned missions
to other planets, to mine the asteroids, and to further explore
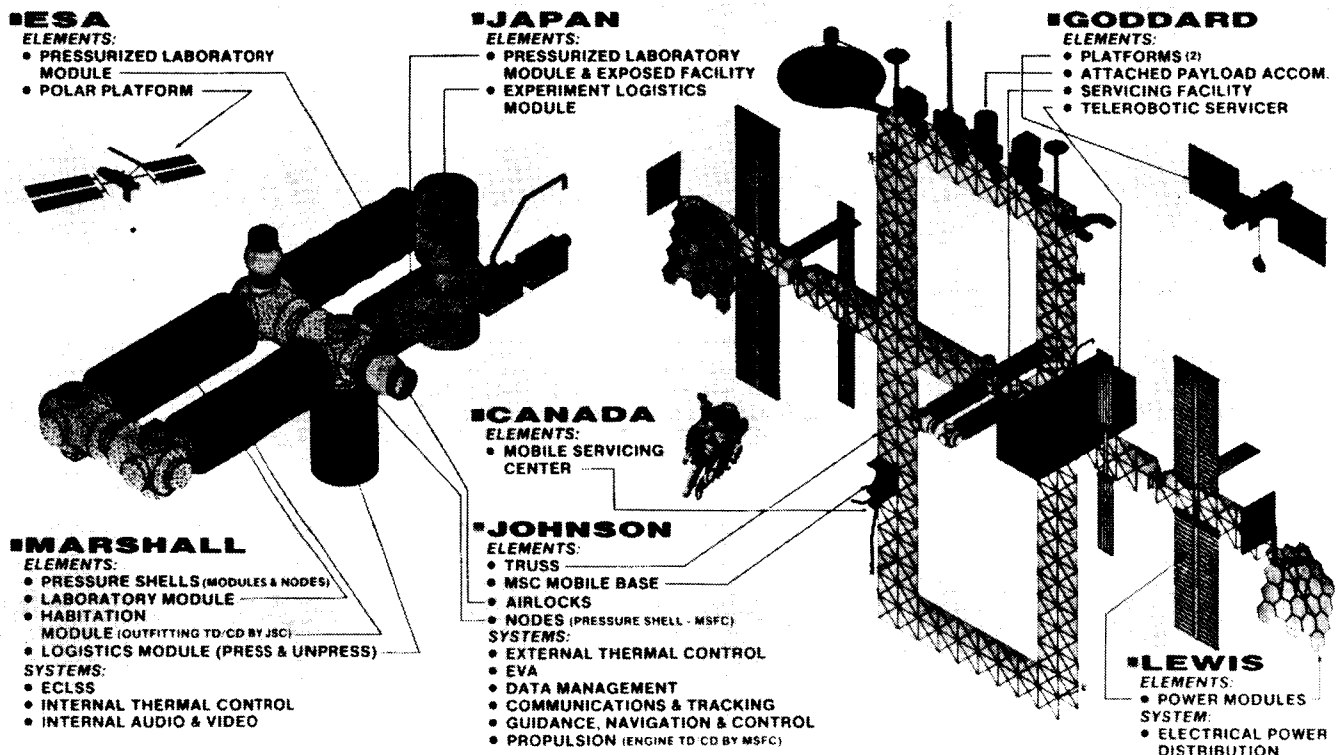our solar system and beyond.

ESA
ELEMENTS:
- PRESSURIZED LABORATORY MODULE
- POLAR PLATFORM

JAPAN
ELEMENTS:
- PRESSURIZED LABORATORY MODULE & EXPOSED FACILITY
- EXPERIMENT LOGISTICS MODULE

GODDARD
ELEMENTS:
- PLATFORMS (2)
- ATTACHED PAYLOAD ACCOM.
- SERVICING FACILITY
- TELEROBOTIC SERVICER

CANADA
ELEMENTS:
- MOBILE SERVICING CENTER

MARSHALL
ELEMENTS:
- PRESSURE SHELLS (MODULES & NODES)
- LABORATORY MODULE
- HABITATION MODULE (OUTFITTING TO/CD BY JSC)
- LOGISTICS MODULE (PRESS & UNPRESS)
SYSTEMS:
- ECLSS
- INTERNAL THERMAL CONTROL
- INTERNAL AUDIO & VIDEO

JOHNSON
ELEMENTS:
- TRUSS
- MSC MOBILE BASE
- AIRLOCKS
- NODES (PRESSURE SHELL - MSFC)
SYSTEMS:
- EXTERNAL THERMAL CONTROL
- EVA
- DATA MANAGEMENT
- COMMUNICATIONS & TRACKING
- GUIDANCE, NAVIGATION & CONTROL
- PROPULSION (ENGINE TO CD BY MSFC)

LEWIS
ELEMENTS:
- POWER MODULES
SYSTEM:
- ELECTRICAL POWER DISTRIBUTION

Figure 8

*Request for Proposals.

JOINT OPTICS STRUCTURES EXPERIMENT (JOSE)*

David Founds
Air Force Weapons Laboratory
Kirtland Air Force Base, N.M.

*Original figures not available at time of publication.

The objective of the JOSE program is to develop, demonstrate, and evaluate active vibration suppression techniques for Directed Energy Weapons (DEW). DEW system performance is highly influenced by the line-of-sight (LOS) stability and in some cases by the wave front quality. The missions envisioned for DEW systems by the Strategic Defense Initiative require LOS stability and wave front quality to be significantly improved over any currently demonstrated capability.

Earlier work sponsored by the Defense Advanced Research Project Agency (DARPA) in the Active Control of Space Structures (ACOSS) program led to the development of a number of promising structural control techniques. However, the ACOSS theory was developed for well characterized structures with narrow bandwidth disturbances. Further these techniques were applied to relatively simple beam, plate, and truss type structures. These techniques were able to, at best, demonstrate vibration suppression of a factor of 100. DEW structures are vastly more complex than any structures controlled to date. They will be subject to disturbances with significantly higher magnitudes and wider bandwidths, while holding higher tolerances on allowable motions and deformations.

Meeting the performance requirements of the JOSE program will require: upgrading the ACOSS technologies to meet new more stringent requirements, the development of requisite sensors and actuators, improved control processors, highly accurate system identification methods, and the integration of the above hardware and methodologies into a successful demonstration.

1. Demonstrate the effect of Disturbances on line of sight error

2. Demonstrate use of Active Structural control to correct LOS error caused by Disturbances

3. Compare simulation predictions to experimental results

JOSE OBJECTIVES

A realistic test article for the JOSE demonstration was provided by the High Altitude Large Optics (HALO) program. The HALO program run by the Rome Air Development Center (RADC) was to develop techniques for the manufacture of lightweight optics. In the final phase of the program, two HALO active mirror panels and a third mirror mass simulator were integrated into a large graphite-epoxy structure. This assembly was designed to have many of the characteristics of a large, lightweight, optical system. It utilizes lightweight, tubular graphite-epoxy structural members which may be typical of DEW type structures. The ends of the structural members are fit with Invar joints. The optics include large ultra-lightweight mirrors that are actively controlled by surface and alignment actuators to maintain optical performance. Each mirror is supported by three pairs of position actuators. Each pair forms a "V" shape with the vertex resting on the truss. The actuators are flexured at both ends to reduce the bending moments transmitted to the mirror surface. The dummy mirror is supported on three pairs of struts in place of the actuators. The struts are also fitted with flexures at the ends. In addition to its unique construction, the HALO truss was sized to fit inside a vacuum chamber at Itek. The JOSE program has taken advantage of the existing HALO structure to provide optical performance and structural vibration data.
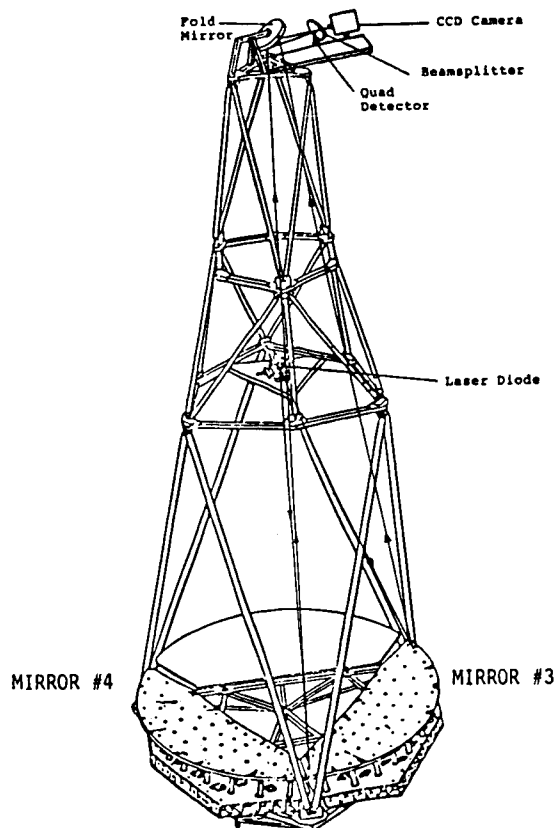

High Altitude Large Optics

During the delay prior to the start of the JOSE program an opportunity to test the HALO truss occurred. The objectives of the test were:

1. Measure the important modes of vibration, i.e., those likely to contribute to line-of-sight error under in-service excitations. Modal data including natural frequencies, damping ratios, mode shapes, and associated modal masses were measured. These data were used to "tune" a finite-element model of the truss.

2. Measure the damping of selected modes in air and in the Itek vacuum chamber.

3. Measure selected frequency response functions between input force and LOS error. These were used to calculate the power spectral density (PSD) of the LOS motion for specified disturbance PSD's.

4. Characterize the local bending modes of one of the primary mirror panels. These modes are of particular interest for the tuning of the finite element of the mirror supports.

During the planning for the test it was decided to support the truss on soft, pneumatic springs at the corners of its triangular base. This simulates the isolation system that may be used in a DEW system. Approximately 650 frequency response functions were measured in determining the structural characteristics of the HALO truss. Determining which of the modes contributed significantly to the LOS error required the use of a three milliWatt laser diode and a quad cell detector. Frequency response functions were measured between the input force and the output of the quad cell detector. The importance of these measurements can be seen from the following plots. The frequency of the first structural mode is below 10 Hz, while there are no optically significant modes until 21 Hz.
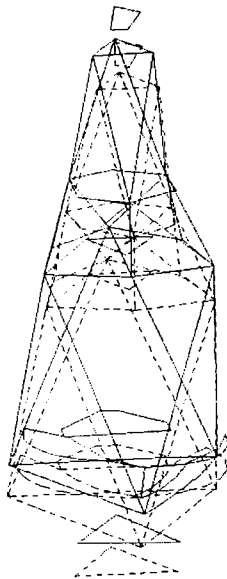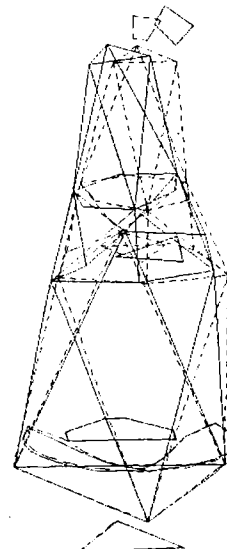
Shape of vibration mode
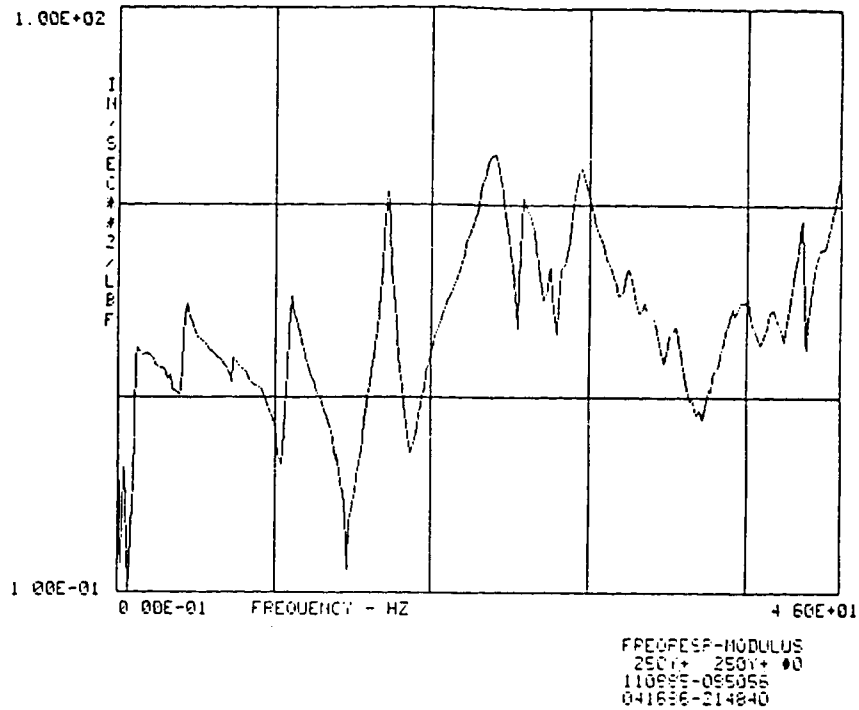at 3.51 Hz.
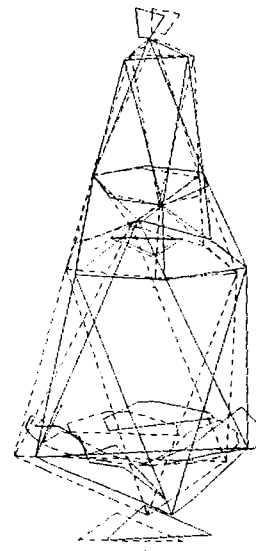
Shape of vibration mode
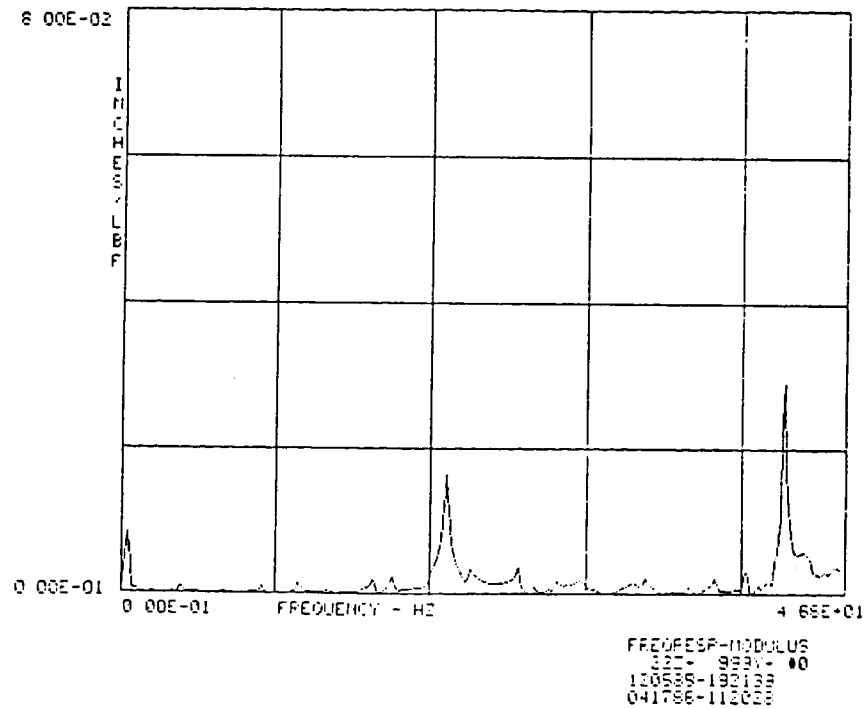at 4.63 Hz.
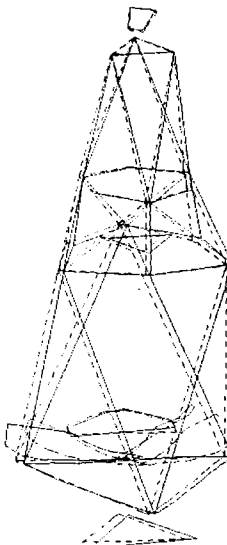
Shape of vibration mode
at 20.80 Hz.

Shape of vibration mode
at 23.98 Hz.

FREQUENCY RESPONSE FUNCTIONS

FREQRESP-MODULUS
25CY+   25CY+ #0
110995-095056
041696-214840

HALO truss with mirrors main sweep 1 burst random.

FREQRESP-MODULUS
32+   993Y+ #0
120595-192133
041796-112028

Line-of-sight motion FRF
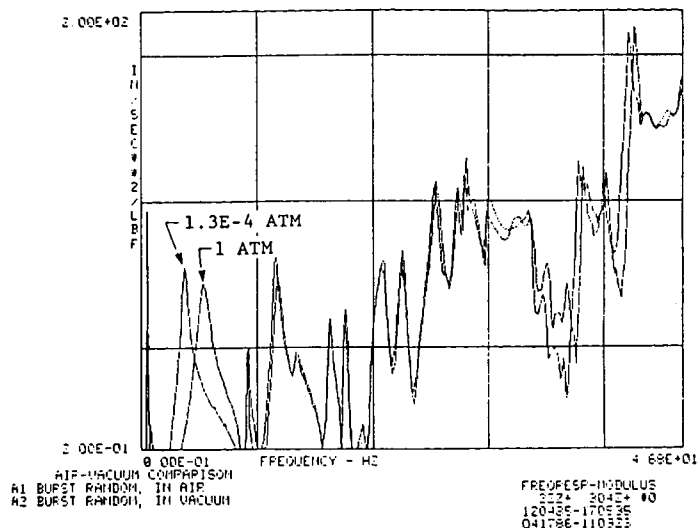burst random, in vacuum.

596
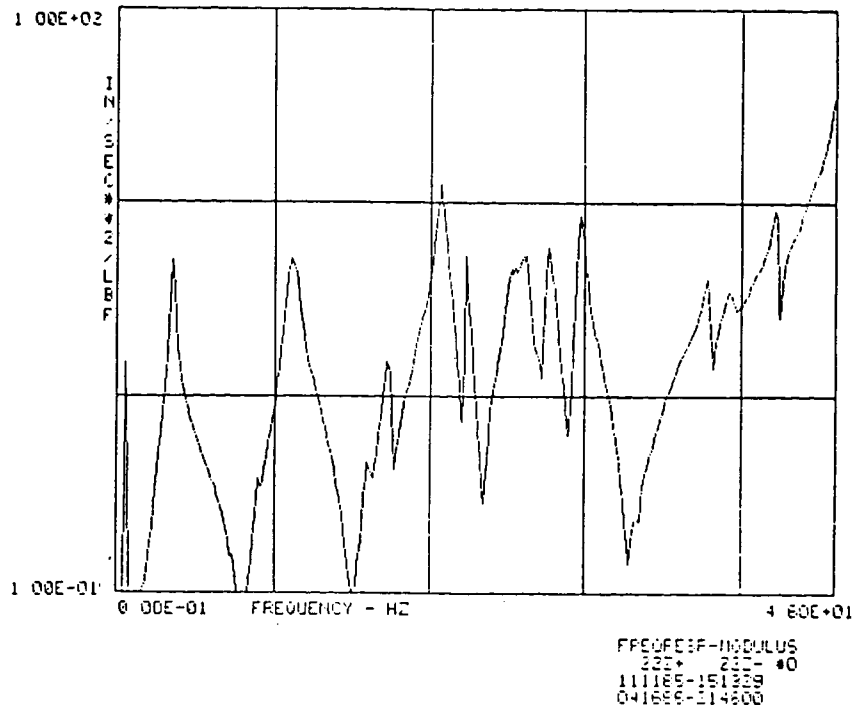
HALO truss with mirrors main sweep 2.
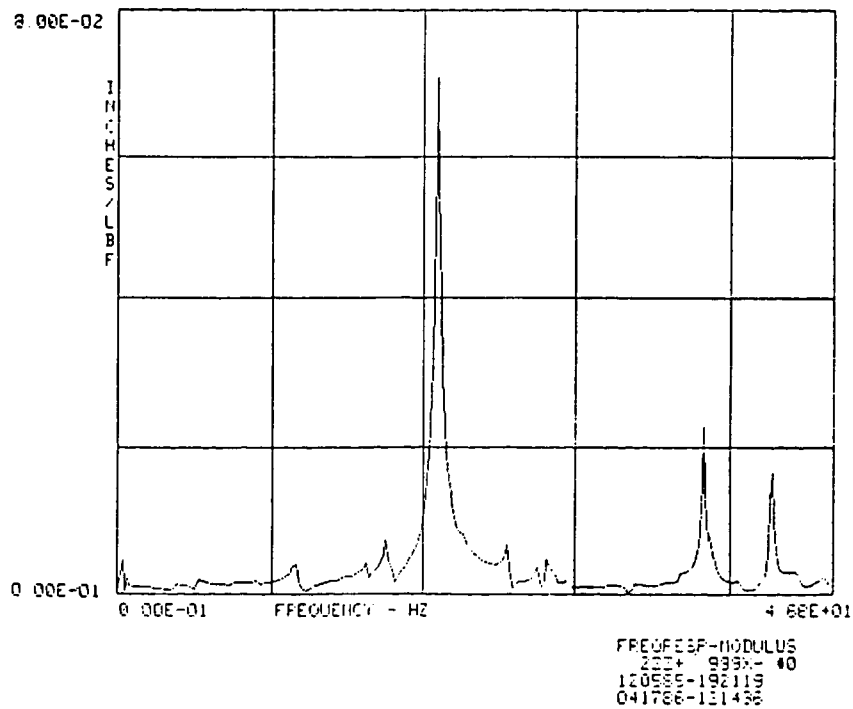
Line-of-sight motion FRF
burst random, in vacuum.

In order to determine the effect of vacuum on the structural damping the HALO truss was placed in a vacuum chamber and selected frequency response functions were remeasured. The following plot and table indicate that the effect of the vacuum was negligible and the changes that did occur are most likely related to the slight difference in the mounting of the pneumatic supports.


AIR-vacuum comparison,
A1 burst random, in air,
A2 burst random, in vacuum.

Response Coordinate	Natural frequency f_r, Hz		Viscous damping ratio ζ_r	
	Air	Vacuum	Air	Vacuum
351Y-	9.20	9.14	0.010	0.0085
22Z+	11.79	11.50	0.020	0.022
120Y-	13.42	13.28	0.033	0.023
351Y-	16.17	16.19	0.0096	0.0084
410Z-	17.46	17.48	0.0067	0.0078
22Z+	20.82	20.84	0.013	0.012
410Z-	22.46	22.57	0.0087	0.0069
351Y-	25.39	25.58	0.0077	0.0076
410Z-	27.28	27.48	0.0064	0.0064
351Y-	27.89	28.03	0.0056	0.0049
351Y-	29.39	29.53	0.0073	0.0066
410Z-	31.71	32.07	0.0043	0.0061
410Z-	33.53	33.92	0.0076	0.0058
410Z-	36.43	36.74	0.0048	0.0048
351Y-	37.89	38.26	0.0031	0.0036
304Z+	39.96	40.25	0.0029	0.0034
304Z+	42.10	42.65	0.0034	0.0018

Damping of the HALO Experimental Structure
In Air and In Vacuum.

A specialized modal test was performed to examine the local modes of one of the mirrors on its fine figure actuators. The local mode test was performed using a roving impulse excitation and multiple fixed accelerometers. A total of 159 frequency response functions were measured on the mirror and used to determine the bending modes. The mirror exhibited modes corresponding to rigid body motion of the mirror on its supports and classical plate bending. Both may be important to LOS and wavefront error. The data were used to tune the finite-element model of the truss with respect to the stiffness of the coarse and fine figure actuators, and the mirrors themselves.
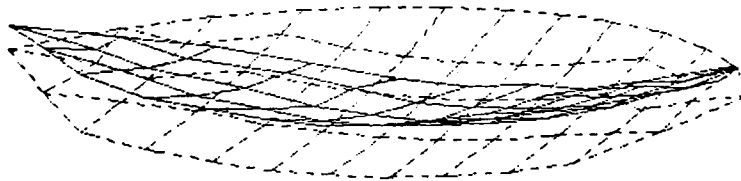
Shape of vibration mode at 36.44 Hz.
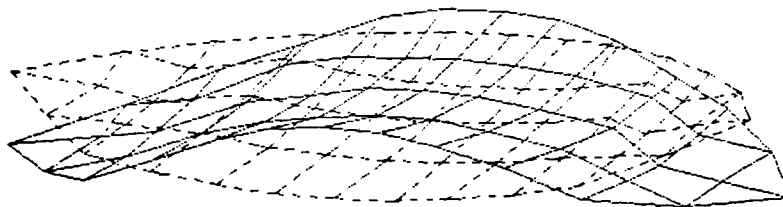
Shape of vibration mode at 37.96 Hz.
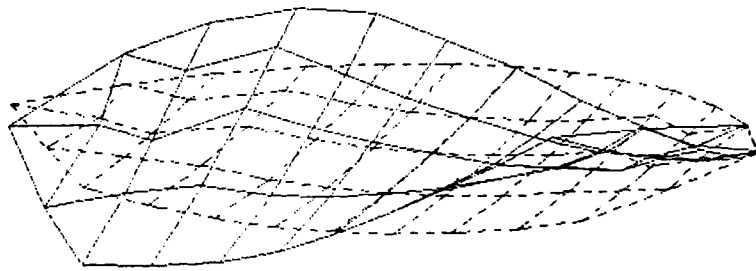
Shape of vibration mode at 39.22 Hz.
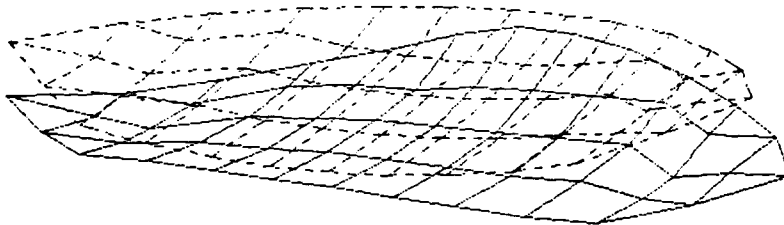
Shape of vibration mode at 44.87 Hz.

A 100 x 100 pixel array, 3mm x 4mm in size, was used to record the effect of the structural vibrations on the wavefront quality. The rms wavefront error was calculated from the peak spread function.
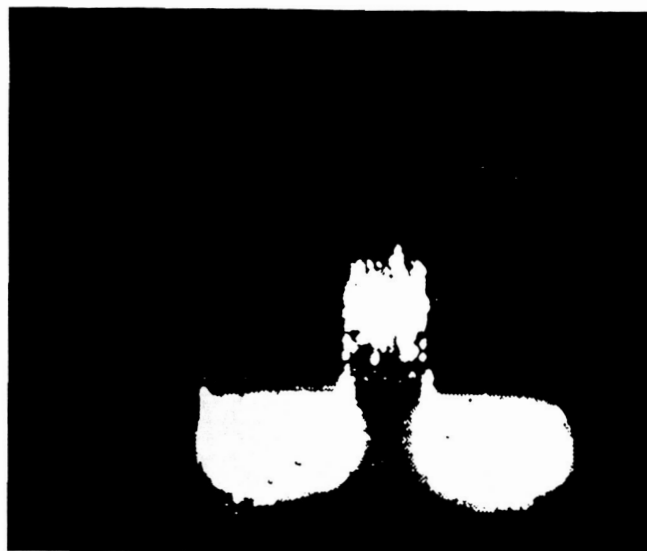
PIXEL ARRAY

The results of both the LOS and wavefront error were used to estimate the equivalent errors that could be expected from the vibrations that are likely in a DEW system.

Vibration Source	Frequency Range	Approx. WFE, m RMS
Coolant Lines (Bends)	0.1 - 10Hz	0.05 u m RMS
	10 - 100Hz	0.01 u m RMS
Resonator Forward End Cap	0.1 - 100Hz	7.7 u m RMS

Wavefront Error Predictions

LARGE SPACECRAFT POINTING AND SHAPE CONTROL

Arthur L. Hale
General Dynamics
San Diego, California

This presentation summarizes work performed under contract to the Flight Dynamics Laboratory (FIGC), Air Force Wright Aeronautical Laboratories. The contract, entitled Large Spacecraft Pointing and Shape Control (LSPSC), was initiated in September 1983. Technical work was completed in August 1986.

The major objectives and the scope of the study are listed below. The overall objective was the development of control algorithms that allow the concurrent operation of slewing, pointing, vibration, and shape control subsystems. This objective is important for near-term space surveillance missions that require the rapid-retargeting and precise pointing of large flexible satellites. The success of these missions requires the design and concurrent operation of the various interacting control subsystems.

LSPSC PROGRAM

MAJOR OBJECTIVES

- **DEVELOP TECHNIQUES NECESSARY TO DESIGN A CONTROL SYSTEM TO SLEW AND PRECISELY SETTLE A LARGE FLEXIBLE ANTENNA SPACECRAFT**

- **EXPLORE THE INTEGRATION OF AND INTERACTIONS BETWEEN THE DIFFERENT CONCURRENTLY OPERATING CONTROL SUBSYSTEMS ONBOARD**

  CONTROL SUBSYSTEMS:

  - SLEW
  - POINT/TRACK
  - VIBRATION SUPPRESSION
  - SHAPE

- **IDENTIFY GAPS IN THE TECHNOLOGY REQUIRED FOR CONTROLLING A LARGE ANTENNA SPACECRAFT**

SCOPE

- AN UNCLASSIFIED THEORETICAL STUDY, NOT A SYSTEMS STUDY

- LEVEL OF DETAIL CONSISTENT WITH A PREDESIGN EFFORT

- SUFFICIENT REALISM TO GUARANTEE THE RELEVANCE AND ACCURACY OF MAJOR CONCLUSIONS

The program was conducted in two phases. Phase I was primarily mathematical model development, while Phase II was primarily control development.

LSPSC PROGRAM TASKS

PHASE I

- REVIEW THREATS AND MISSIONS

- DEFINE MATHEMATICAL MODEL OF ANTENNA SPACECRAFT

- DEFINE CONTROL REQUIREMENTS AND GOALS

- EVALUATE EXTERNAL AND INTERNAL DISTURBANCES

- EVALUATE ACTUATORS/SENSORS FOR LSS CONTROL APPLICATIONS

PHASE II

- REVIEW LSS CONTROLS LITERATURE AND ON-GOING PROGRAMS

- DEVELOP CONTROLLERS USING HEURISTIC LOCATIONS OF ACTUATORS/SENSORS FOR:

  - SLEWING
  - VIBRATION SUPPRESSION
  - POINTING/TRACKING
  - SHAPE CONTROL

- DETERMINE OPTIMAL LOCATIONS OF ACTUATORS/SENSORS AND REPEAT CONTROLLER DEVELOPMENT

- EVALUATE ROBUSTNESS OF BOTH CONTROLLERS

- EXAMINE THE INFLUENCE OF PASSIVE DAMPING

The baseline generic mission for the study was a tactical surveillance mission for a space based radar. The satellite was to be in a 5600 n.mi. polar orbit and have a chase mode slew rate of 2 deg/sec. Both a coning mode of operation and a star-scan mode were examined initially. Due to the very high momentum requirements of a coning mode, the staring mode was chosen for the control development phase. For the staring mode, target acquisition and target tracking were required. A slow reorientation was required at least once per orbit. An occasional fast slew was required for surveying multiple targets.

MISSION GEOMETRY AND REQUIREMENTS
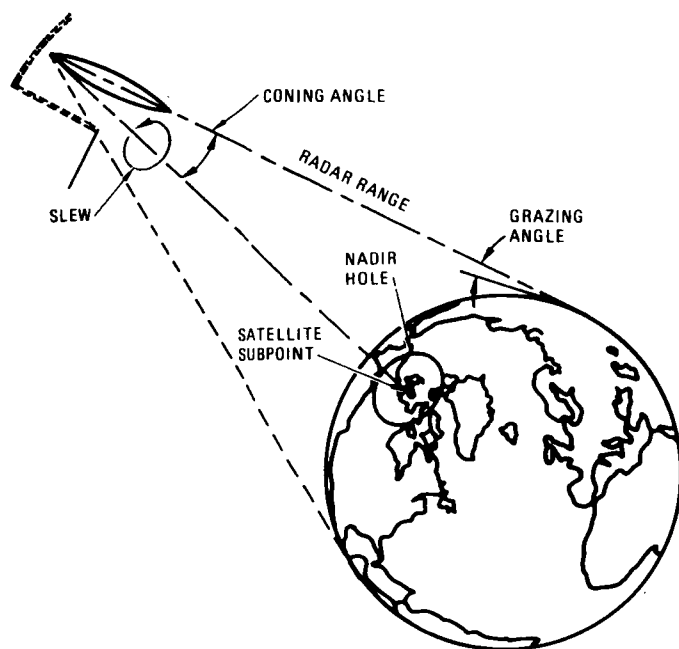
SYSTEM PARAMETERS	
ORBIT ALTITUDE	5,600 N.MI.
ORBIT PLANE	POLAR
STRUCTURE	
• TYPE	DISH ANTENNA
• DIAMETER	100M
• SLEW RATES	2 DEG/SEC
	(0.8 DEG/SEC)
OPERATING FREQUENCY	10 GHz (3 CM)
CONING ANGLE	22.4 DEG

| DERIVED PARAMETERS	
ANTENNA DIRECTIVITY GAIN	80 dB
ANTENNA BEAMWIDTH	0.02 DEG
ACCESS RADIUS	4,060 N.MI.
INSTANTANEOUS COVERAGE-	
• MAXIMUM LENGTH	460 N.MI.
• OPERATIONAL LENGTH	170 N.MI.*
• WIDTH	2.7 N.MI.
SATELLITE SUBPOINT VELOCITY	3,600 KTS
MAXIMUM RADAR RANGE	8,360 N.MI.
OPERATIONAL RADAR RANGE	8,065 N.MI.*
NOMINAL SEARCH RATES	19,300 N.MI.^{2}/SEC*
	8,700 N.MI.^{2}/SEC
PRIME POWER	20-50 KILOWATTS

*5 DEGREE GRAZING ANGLE MINIMUM

606

The table below summarizes pointing and surface accuracy requirements for the generic mission. The requirements for X-band operation were chosen in order to create the most challenging control problem.

SPACECRAFT POINTING REQUIREMENTS

	L-Band	S-Band	X-Band
Band			
• Wavelength (frequency)	24 CM (1.25 GHz)	10 CM (3 GHz)	3 CM (10 GHz)
• Gain	64 dB	72 dB	80 dB
• Beamwidth	0.1° (1,750μr)	0.04° (700μr)	0.02° (350μr)
Antenna pointing accuracy			
• Threshold	0.01° (175μr)	0.004° (70μr)	**0.002° (35μr)**
• Goal	0.001° (17.5μr)	0.0004° (7μr)	**0.0002° (3.5μr)**
Feed angular orientation			
• Threshold	0.01° (175μr)	0.004° (70μr)	**0.002° (35μr)**
— Lateral movement/120M	2 CM (0.08λ)	0.8 CM (0.08λ)	0.4 CM (0.13λ)
• Goal	0.001° (17.5μr)	0.0004° (7μr)	**0.0002° (3.5μr)**
— Lateral movement/120M	0.2 CM (0.008λ)	0.08 CM (0.008λ)	0.04 CM (0.013λ)
Search mode slew rate	5.0°/sec	1.2°/sec	0.8°/sec
Tracking mode slew rate	0.004°/sec	0.004°/sec	0.004°/sec
Tracking mode pointing accuracy	0.0025° (44μr)	0.001° (18μr)	0.0005° (8.8μr)
Surface accuracy			
• Surface tolerance (RMS)	1.2 CM (0.05λ)	0.5 CM (0.05λ)	0.15 CM (0.05 λ)
• Surface accuracy (absolute)			
— Threshold	1.7 CM (0.07λ)	0.7 CM (0.07λ)	**0.35 CM (0.10λ)**
— Goal	0.17 CM (0.007λ)	0.07 CM (0.007λ)	**0.035 CM (0.01λ)**

The spacecraft model itself was chosen to be a geodetic-truss, 100-meter diameter, offset-feed antenna.

## SPACECRAFT MODEL — OFFSET CONFIGURATION
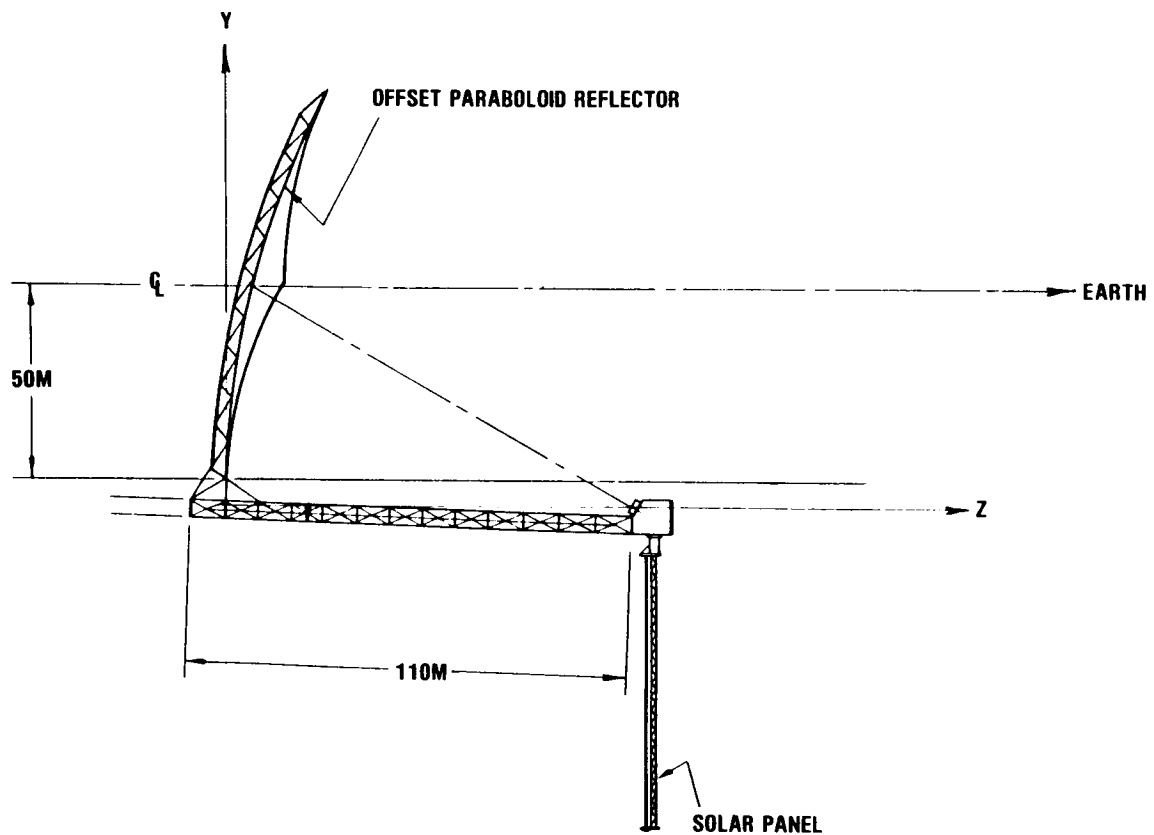
An extensive parametric study of unattached (free-free) truss reflectors was conducted. The goal was to investigate and provide data concerning low-frequency truss-reflector behavior. A strawman objective was to achieve a reflector with a first-mode frequency on the order of 0.1 Hz. This objective could not be achieved using standard geo-truss design practices to obtain a reasonable design. Consequently, a reasonably designed 100-meter reflector was chosen. The reflector's lowest free-free modal frequency is 1.7 Hz.

PARAMETRIC STUDY:
UNATTACHED REFLECTOR DISH

Trial No.	1	2	3	4	5	6	7	8	9	10	11	12	13	14	15	16	17	18	19	20	21	22
E (mpsi)	20	15	10	10	2	10	10	10	10	10	10	10	10	10	10	10	10	10	10	10	34	34
No. of bays	12	12	12	16	20	20	24	28	20	16	20	16	20	20	20	20	20	16	20	16	12	12
Strut angle (degree)	30	30	30	24	24	24	24	24	15	15	12	12	10	8	24	24	24	24	24	24	40	40
F/D_p	0.5	0.5	0.5	0.5	0.5	0.5	0.5	0.5	0.8	0.8	1.0	1.0	1.2	1.5	0.5	0.5	0.8	0.8	0.8	0.8	0.5	0.5
Diameter (m)	50	50	50	50	50	50	50	50	50	50	50	50	50	50	80	100	100	100	150	150	50	100
Truss depth (m)	1.1	1.1	1.1	0.4	0.3	0.3	0.3	0.3	0.1	0.1	0.1	0.1	0.1	0.03	0.5	0.7	1.2	1.4	1.7	2.1	2.0	3.9
Diagonal length (m)	3.2	3.2	3.2	2.3	1.8	1.8	1.5	1.3	1.7	2.2	1.7	2.1	1.7	1.7	2.9	3.6	3.6	4.6	5.5	6.8	3.6	7.3
Tube diameter (cm)	2.2	2.2	2.2	2.7	2.3	2.3	2.0	1.8	2.2	2.6	2.2	2.5	2.2	2.2	3.1	3.6	3.6	4.2	4.8	5.5	2.4	3.8
Weight (kg)	1,193	1,193	1,193	2,040	2,234	2,234	2,412	2,570	2,139	1,956	2,117	1,932	2,100	2,095	4,733	6,768	6,587	6,047	12,721	11,746	1,236	3,945
Package diameter (cm)	282	282	282	448	481	481	510	535	472	441	470	438	468	468	653	754	743	693	967	905	283	442
Package height (cm)	494	494	494	357	285	285	238	203	272	340	269	336	267	265	456	571	563	705	845	1,057	536	1,071
1st vib mode (Hz) (free-free)	1.66	1.44	1.17	0.604	0.233	0.498	0.422	0.365	0.256	0.306	0.196	0.231	0.157	0.118	0.316	0.254	0.332	0.406	0.223	0.271	3.43	1.70

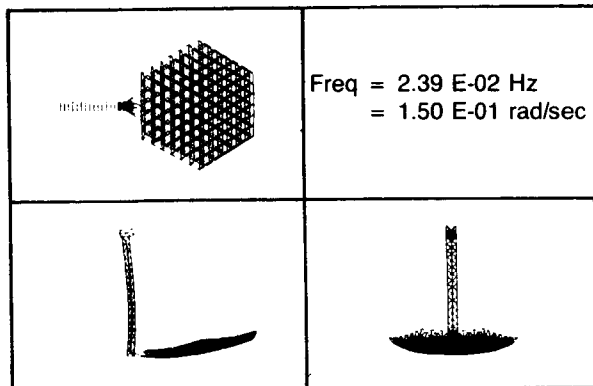Independent variables: E (mpsi), No. of bays, Strut angle (degree), F/D_p, Diameter (m)

A quite flexible feed-boom was coupled to the reflector. A simulated solar array and a feed-bus structure were attached to the end of the feed-boom opposite the reflector. The lowest frequency of vibration of the vehicle is 0.024 Hz. There are 33 elastic modes below 1 Hz. The flexible feed-boom was chosen to facilitate technological development by creating a challenging control problem.
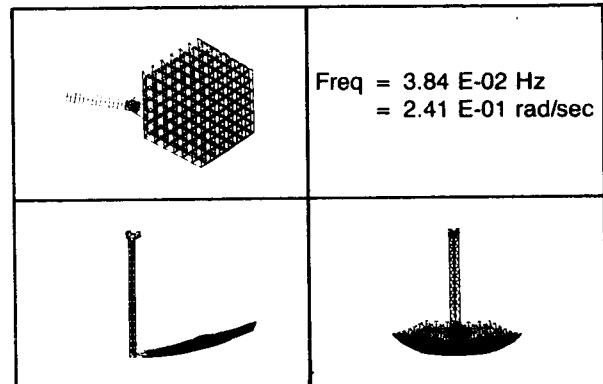
VIBRATION MODES
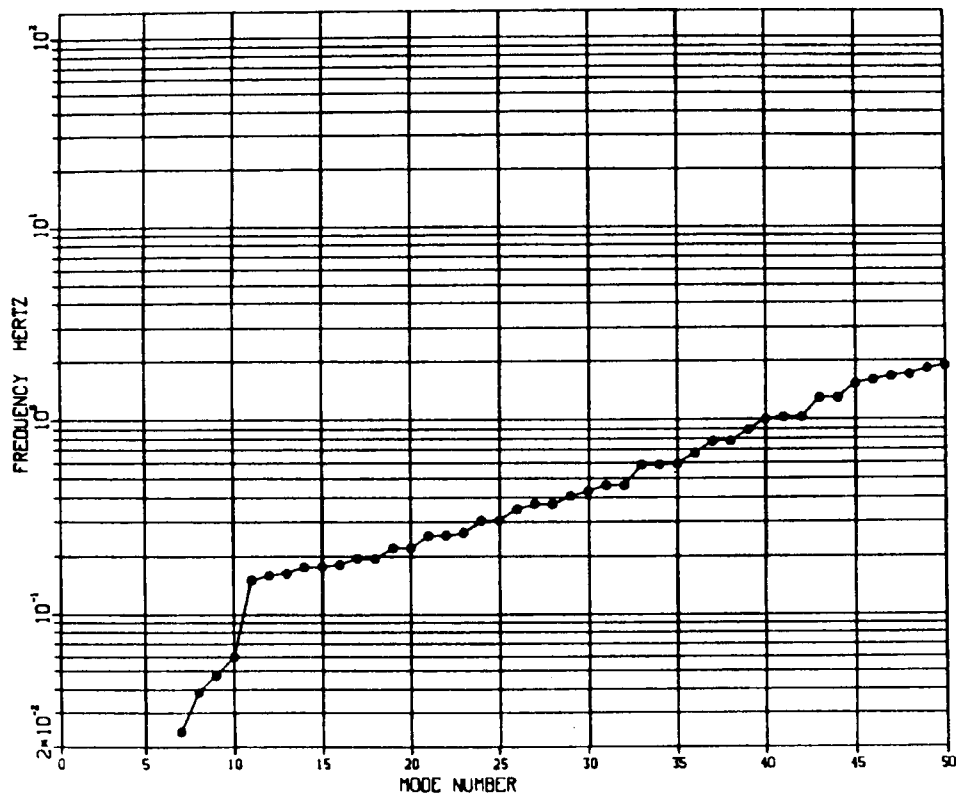
The lowest 4 elastic modes are significantly excited by maneuvering disturbances. The first elastic mode, mode 7, is primarily boom bending in the Y-Z plane. Mode 8 is primarily a torsion mode of the feed-boom. Mode 9 is primarily a boom bending mode in the Y-Z plane coupled with solar array bending. Finally, mode 10 is primarily a reflector rocking mode with boom bending in the X-Z plane.
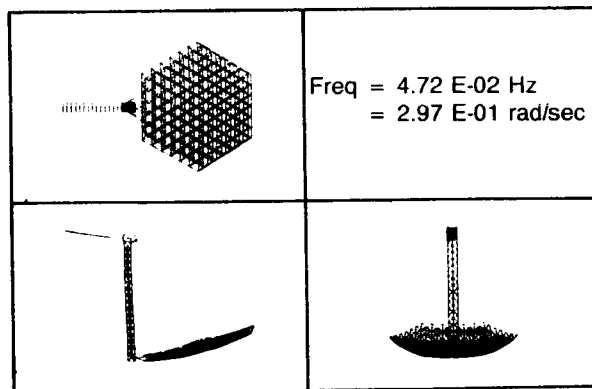
DEFORMED SHAPE — MODE 7

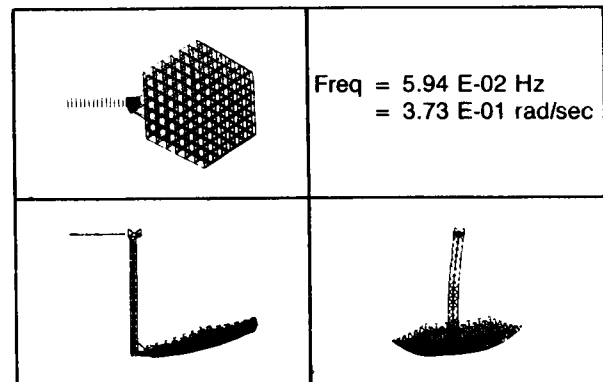Freq = 2.39 E-02 Hz
= 1.50 E-01 rad/sec

DEFORMED SHAPE — MODE 8

Freq = 3.84 E-02 Hz
= 2.41 E-01 rad/sec

DEFORMED SHAPE — MODE 9

Freq = 4.72 E-02 Hz
= 2.97 E-01 rad/sec

DEFORMED SHAPE — MODE 10

Freq = 5.94 E-02 Hz
= 3.73 E-01 rad/sec

Conclusions of the structural model development task are summarized below.

STRUCTURAL MODEL DEVELOPMENT SUMMARY

- Geodetic-truss reflector was chosen for:
  - Ability to accommodate fast slewing maneuvers
  - High achievable surface accuracy
  - High failure & attack survivability (structural redundancy)

- Parametric studies of the reflector show that very low natural frequencies are not inherent (even for 100-meter diameter reflectors)

- A "reasonably designed" 100-meter diameter (1.7Hz) reflector was chosen as representative of this class of reflectors

- An offset antenna configuration was chosen over center-fed because it offers a more challenging control problem

- The truss-boom's bending stiffness was chosen to be small (mode 7 frequency = 0.024 Hz) to provide a challenging slewing/vibration/pointing/shape control problem

Many disturbances, both internal and external, affect the spacecraft. The table shows that by far the dominant disturbances are due to the slewing maneuvers. The effect of gravity gradient torques is comparable to that of pointing/tracking torques for this spacecraft with a flexible boom.

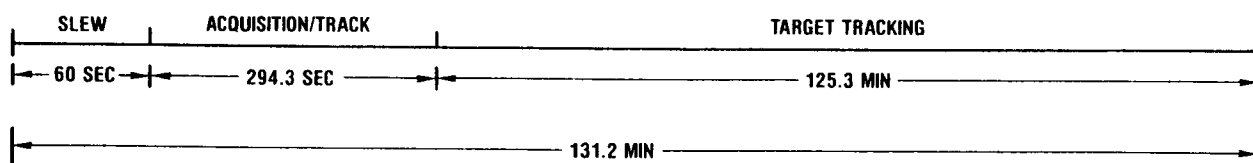## LSPSC FAST-SLEWING DISTURBANCE DOMINATES ALL OTHER DISTURBANCES

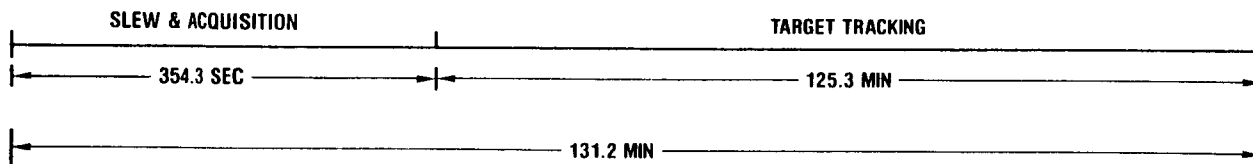| Disturbances	LOS Error/LOS[*] goal
Thermal gradient	$\ll 1.0$
Solar pressure	< 1.0
Gravity gradient	1.1 - 4.0
Pointing/tracking torques (CMGs)	0.1 - 7.2
Reboost (RCS)	490
Slow slewing (CMGs)	500
Fast slewing (RCS)	56 - 39,000

*Line of sight (LOS).

All the generic orbit scenarios considered include a slew and target acquisition phase followed by an operational phase in which a target is tracked. RCS-thrusters were used to perform the fast slewing maneuvers, while CMGs were used to perform the slow slewing and target tracking maneuvers. In the case of a fast slewing maneuver, settling of vibrations must be completed during the acquisition phase. To reduce the elastic excitation following the fast slewing maneuver, the RCS pulses were tuned to periods of the lower modes.
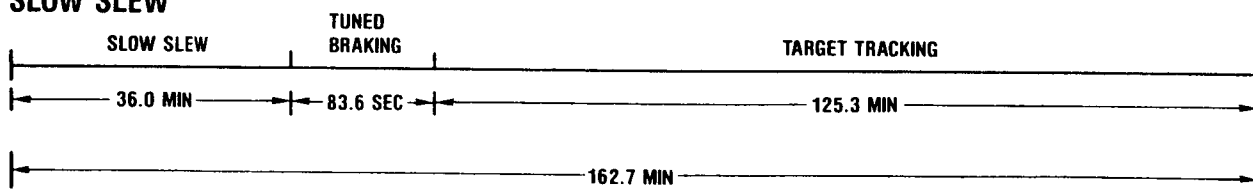
ORBIT SCENARIO SEQUENCES
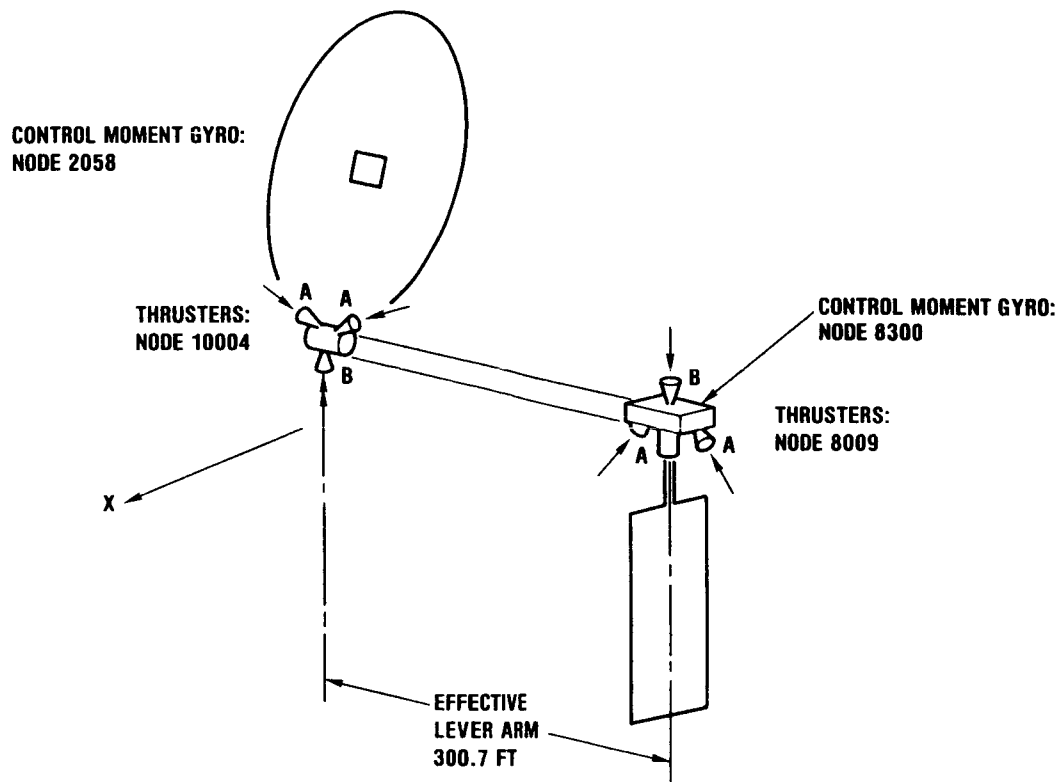### (Not to Scale)

ORIGINAL FAST SLEW

SLEW	ACQUISITION/TRACK	TARGET TRACKING

├── 60 SEC ──┤├──── 294.3 SEC ────┤├──────── 125.3 MIN ────────┤

├──────────────── 131.2 MIN ────────────────┤

TUNED FAST SLEW

SLEW & ACQUISITION	TARGET TRACKING

├──────── 354.3 SEC ────────┤├──────── 125.3 MIN ────────┤

├──────────────── 131.2 MIN ────────────────┤

SLOW SLEW

SLOW SLEW	TUNED BRAKING	TARGET TRACKING

├──── 36.0 MIN ────┤├── 83.6 SEC ──┤├──────── 125.3 MIN ────────┤

├──────────────── 162.7 MIN ────────────────┤

614

Locations of the RCS-thrusters and the CMGs are shown below.

LOCATION OF SLEWING DEVICES

CONTROL MOMENT GYRO: NODE 2058

THRUSTERS: NODE 10004

A A
B

CONTROL MOMENT GYRO: NODE 8300

B

A A

THRUSTERS: NODE 8009

X

EFFECTIVE LEVER ARM 300.7 FT

As mentioned, the fast slewing torque profile was tuned to the periods of modes 7 and 9. Two "tuned" torque profiles were compared to an original profile.

FAST-SLEW DISTURBANCES

44.6 DEGREE REST-TO-REST SLEW

ORIGINAL FAST SLEW - NO. 0

ACTUATOR FORCE (POUNDS)

TIME (SECONDS)

TUNED-SLEW DISTURBANCE NO. 1

ACTUATOR FORCE (POUNDS)

TIME (SECONDS)

TUNED-SLEW DISTURBANCE NO. 2

ACTUATOR FORCE (POUNDS)

TIME (SECONDS)
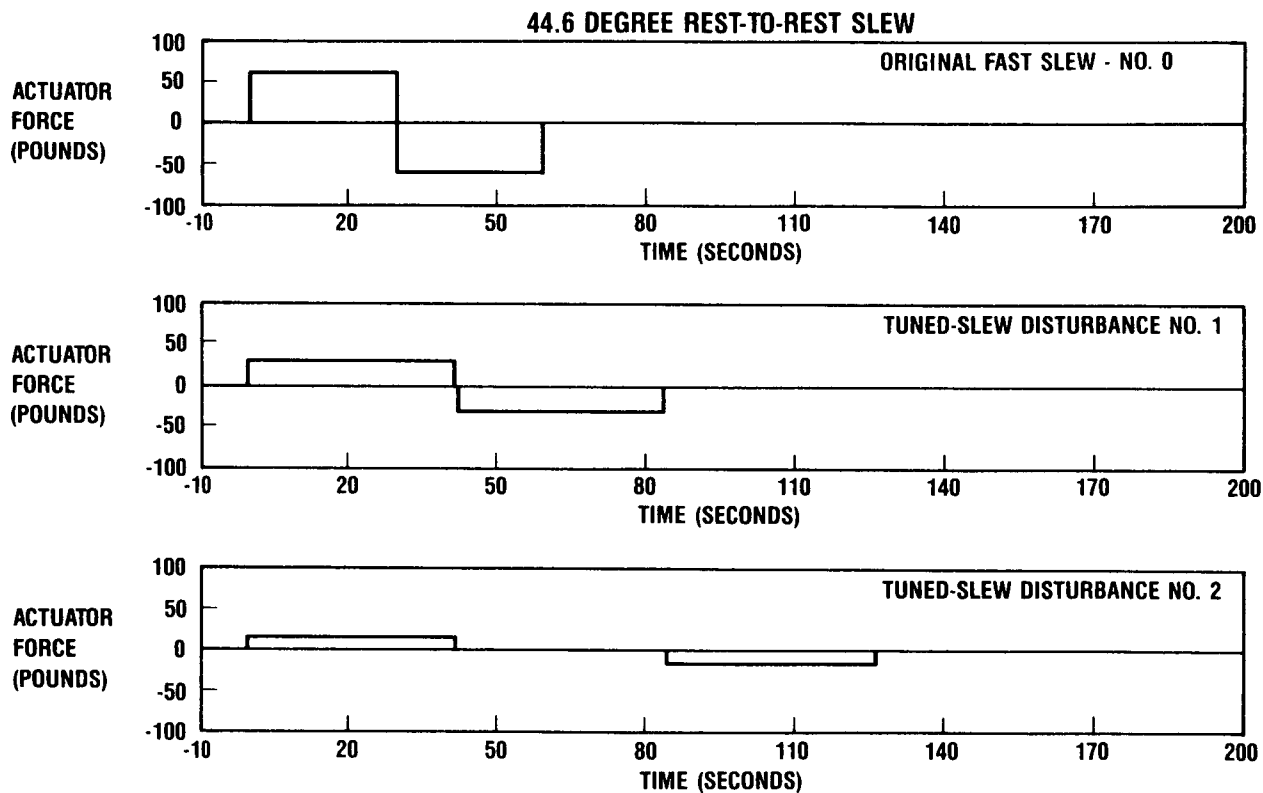
Tuning the slewing pulses is seen to significantly reduce the post-slew dynamic response. This is important as it reduces the vibration control torques required to settle the vehicle. Tuned slew number 1 was chosen as a baseline.

COMPARISON OF POST FAST-SLEW EXCITATION LEVELS CLEARLY SHOWS THE BENEFITS OF TUNING

DESCRIPTION	PERFORMANCE (PEAK NEAREST T = 130 SEC)		
	TOTAL LOS ERRORS (ARC-SEC)	RMS SURFACE ERRORS (10^{-3} IN.)	PATH LENGTH Δ (10^{-3} IN.)
ORIGINAL FAST SLEW BANG/BANG (29.6/29.6)	38,785	56	55,000
TUNED SLEW NO. 1 BANG/COAST/BANG (41.7/0.64/4.17)	402	2	50
TUNED SLEW NO. 2 BANG/COAST/BANG (41.7/42.98/41.7)	56	2	85
PERFORMANCE SPECIFICATIONS	7	59	59

Conclusions of the disturbance evaluation task are summarized below.

EVALUATION OF DISTURBANCES

- **FAST SLEWING DISTURBANCE DOMINATES**

    – ORDERS OF MAGNITUDE LARGER THAN ALL OTHERS EXCEPT SLOW SLEW

    – SLOW-SLEW IMPULSE IS HIGH BUT TIME TO DAMP IS LONG

- **VIBRATION CONTROL REQUIREMENTS DRIVEN BY**

    – ELASTIC MODE RESPONSE TO FAST SLEW

    – TIME AVAILABLE IN ACQUISITION PHASE FOR DAMPING

- **ORIGINAL FAST SLEW LEADS TO VERY LARGE (UNREALISTIC) VIBRATION-CONTROL TORQUES**

- **TUNING THE FAST-SLEW PULSES TO PERIODS OF FUNDAMENTAL ELASTIC MODES**

    – LEADS TO A REALISTIC VIBRATION CONTROL PROBLEM

    – IS PRACTICALLY IMPLEMENTED

The control system development task designed decentralized control subsystems for vibration suppression, three-axis pointing, and required shape control. Fast slewing was taken to be open loop.

CONTROL SYSTEM DEVELOPMENT

Tasks
- Review LSS controls literature & on-going programs
- Develop decentralized pointing/vibration/shape controllers using:
  - Heuristically located actuators & sensors
  - Optimally located actuators & sensors

Approach
- Fast-slewing is open loop
- Vibration suppression system designed using filter-accommodated MESS
  - Control lower elastic modes, suppress rigid-body modes & a few higher elastic modes
  - Collocated actuators (reaction wheels) & sensors (rate gyros)
  - Filter rigid-body rates from rate gyro measurements
- Three-axis attitude controller for pointing & tracking
  - Each axis designed independently
  - Low-gain "coarse pointing" controller for target acquisition
  - High-gain "fine pointing" controller for target tracking
- Shape control consists of aligning the antenna feed over the reflector
  - Alignment for the tracking maneuver was demonstrated by simulations
  - The same controller will accommodate solar pressure & gravity gradient torques (these disturbance torques are comparable to the tracking torques)

The Large Space Structures (LSS) controls literature was reviewed and the Model Error Sensitivity Suppression (MESS) design method was chosen as a method for designing the vibration control subsystem.

COMPARISON OF SOME LSS CONTROL DESIGN APPROACHES

TECHNIQUE	DESCRIPTION	ADVANTAGES	DISADVANTAGES
MESS	LQG — BASED APPROACH EXTENDED TO ACCOUNT FOR TRUNCATION OF KNOWN DYNAMICS; HEAVILY PENALIZES UNCONTROLLED DYNAMICS IN COST FUNCTION; CAN INCORPORATE ROLL-OFF FILTERS TO DECREASE EXCITATION OF UNKNOWN DYNAMICS.	• HIGH PERFORMANCE • ALLOWS DECENTRALIZED CONTROL • DIRECT METHODOLOGY TO SUPPRESS SUBSYSTEM INTERACTION	• DECOUPLING MECHANISM REQUIRES KNOWN DYNAMICS • MAY REQUIRE ADDITIONAL ACTUATORS TO ACHIEVE DECOUPLING • LQG ROBUSTNESS CONCERNS
IMSC	TRANSFORMATION APPLIED TO THE CONTROL INFLUENCE MATRIX SUCH THAT PRODUCT OF IT AND GAIN MATRIX IS DIAGONAL; EACH MODE CONTROLLED INDEPENDENTLY.	• CONTROLLED MODES ARE COMPLETELY DECOUPLED • EASY TO DESIGN	• FOR COMPLETE DECOUPLING, REQUIRES ONE ACTUATOR PER CONTROLLED MODE • "MODAL FILTERS" REQUIRE MANY SPATIALLY DISTRIBUTED SENSORS
HAC/LAC	HAC CONTROLLER DESIGNED VIA FREQUENCY — SHAPED LQG; LAC CONTROLLER DESIGNED USING OUTPUT FEEDBACK; FREQUENCY SHAPING PROVIDES A MEANS TO DECREASE EXCITATION OF UNKNOWN DYNAMICS.	• HIGH PERFORMANCE • FREQUENCY SHAPING ALLOWS INCORPORATION OF COMMON FREQUENCY DOMAIN CONSTRAINTS INTO STATE-SPACE FORMULATION	• HAC MAY DESTABILIZE LAC • FREQUENCY SHAPING MAY RESULT IN HIGH-ORDER SYSTEM • LQG ROBUSTNESS CONCERNS
POSITIVE REAL	A POSITIVE REAL COMPENSATOR APPLIED TO A LSS WITH FORCE ACTUATORS AND COLOCATED LINEAR VELOCITY SENSORS REMAINS POSITIVE REAL AND THUS STABLE REGARDLESS OF MODEL UNCERTAINTY	•TOTALLY STABILITY-ROBUST CONTROL DESIGN DUE TO PARAMETER INDEPENDENT STABILITY	• ACTUATOR DYNAMICS DESTROY POSITIVITY • DIGITAL IMPLEMENTATION ALSO DEGRADES STABILITY THROUGH THE ELIMINATION OF POSITIVITY USUALLY LOW PERFORMANCE CONTROL
MATHEMATICAL PROGRAMMING	LINEAR AND NONLINEAR MATHEMATICAL OPTIMIZATION TECHNIQUES USED TO DESIGN CONTROLLER; DESIGN CONSTRAINTS AND POSSIBLY AN OBJECTIVE FUNCTION ARE INCORPORATED INTO A CONSTRAINED MINIMIZATION PROBLEM SUBJECT TO THE LSS DYNAMICS.	• OPTIMIZES THE ACTUAL DESIGN VARIABLES • MECHANIZES THE ACTUAL ENGINEERING PROCESS • HANDLES NONLINEAR PROBLEMS • VERY GENERAL APPROACH	• SINCE THE TECHNIQUE EMULATES THE ENGINEER, THE ALGORITHM AND INTERFACE SOFTWARE CAN BE DIFFICULT TO DEVELOP • SENSITIVITY COMPUTATION CAN BE COSTLY
ALGEBRAIC METHODS (ESPECIALLY H_{∞})	DESIGN THE COMPENSATOR DIRECTLY RATHER THAN A CONTROL LAW PLUS AN ESTIMATOR; FUNCTIONAL ANALYSIS METHOD OFTEN USED.	• ROBUSTNESS OF DESIGN EMPHASIZED • DESIGN CONSTRAINTS BASED ON FREQUENCY DOMAIN MEASURES	• COMPUTATIONALLY INTENSIVE • OFTEN RESULTS IN HIGH-ORDER COMPENSATORS • IMMATURE STATE OF DEVELOPMENT

Each of the concurrently operating subsystems is shown in the block diagram below.

LSPSC DECENTRALIZED CONTROL CONFIGURATION
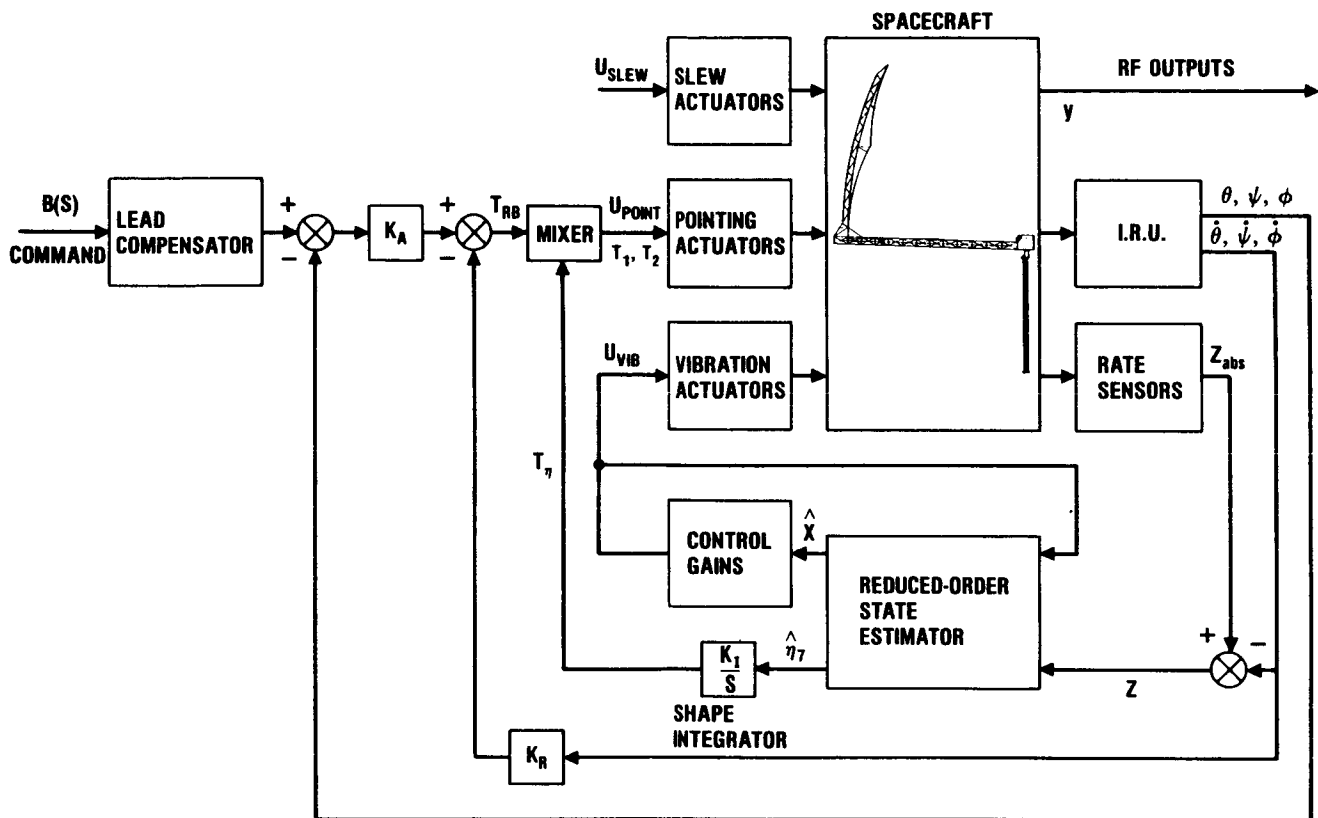
Only the lowest 4 elastic modes (modes 7-10) contribute significantly to the LOS error. They are the modes that are actively controlled in the vibration control subsystem.

INDIVIDUAL MODAL CONTRIBUTIONS TO TOTAL LOS ERROR (PEAK NEAREST T = 130 SECONDS)

SLEW DESCRIPTION	MODE NUMBER			
	MODE 7 (.024 Hz)	MODE 8 (.038 Hz)	MODE 9 (.047 Hz)	MODE 10 (.059 Hz)
ORIGINAL FAST SLEW BANG/BANG (29.6/29.6 SEC)	37500 (96.7)	2 (.005)	1000 (2.6)	283 (.695)
TUNED SLEW NO. 1 BANG/COAST/BANG (41.7/0.64/41.75 SEC)	21 (5.2)	4 (1.0)	2 (.5)	375 (93.3)
TUNED SLEW NO. 2 BANG/COAST/BANG (41.7/42.98/41.7 SEC)	28 (50.0)	2 (3.6)	1 (1.8)	25 (44.6)

NOTE: ENTRIES ARE IN ARC-SECONDS. NUMBER IN PARENTHESIS INDICATES APPROXIMATE PERCENT OF TOTAL LOS ERROR

Both heuristically and optimally located actuators and sensors were investigated. Ten collocated actuators and sensors were used in each case. Ten actuators were needed since the torque per actuator was constrained.
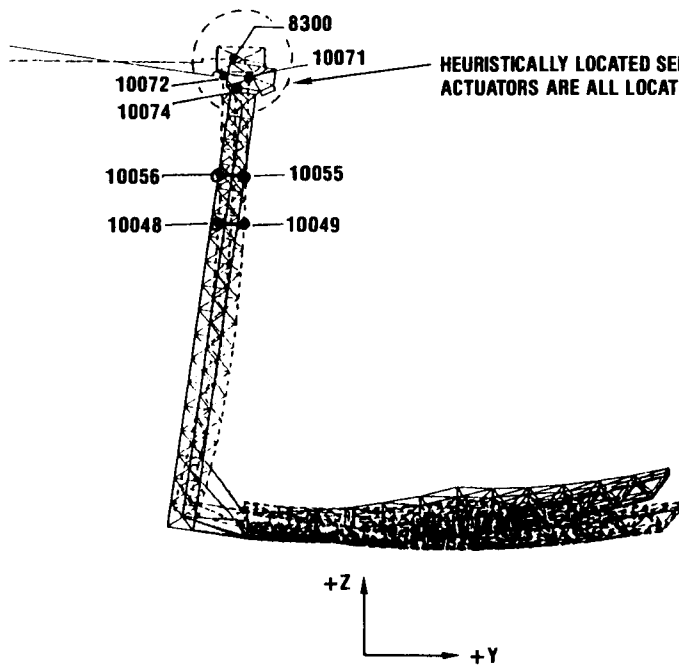
HEURISTICALLY LOCATED ACTUATORS FOR
ACTIVE VIBRATION SUPPRESSION

UNDEFORMED SHAPE

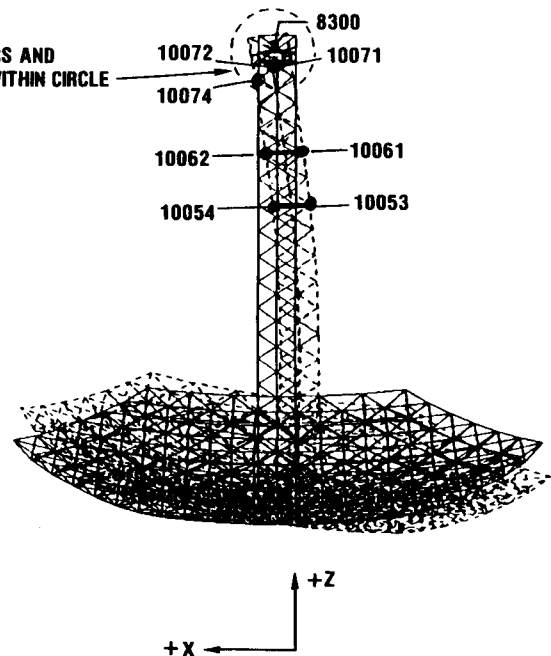| NODE	TORQUE DIRECTIONS
8,006	X,Y,Z
10,071	X,Y,Z
10,072	X,Y,Z
10,074	Y
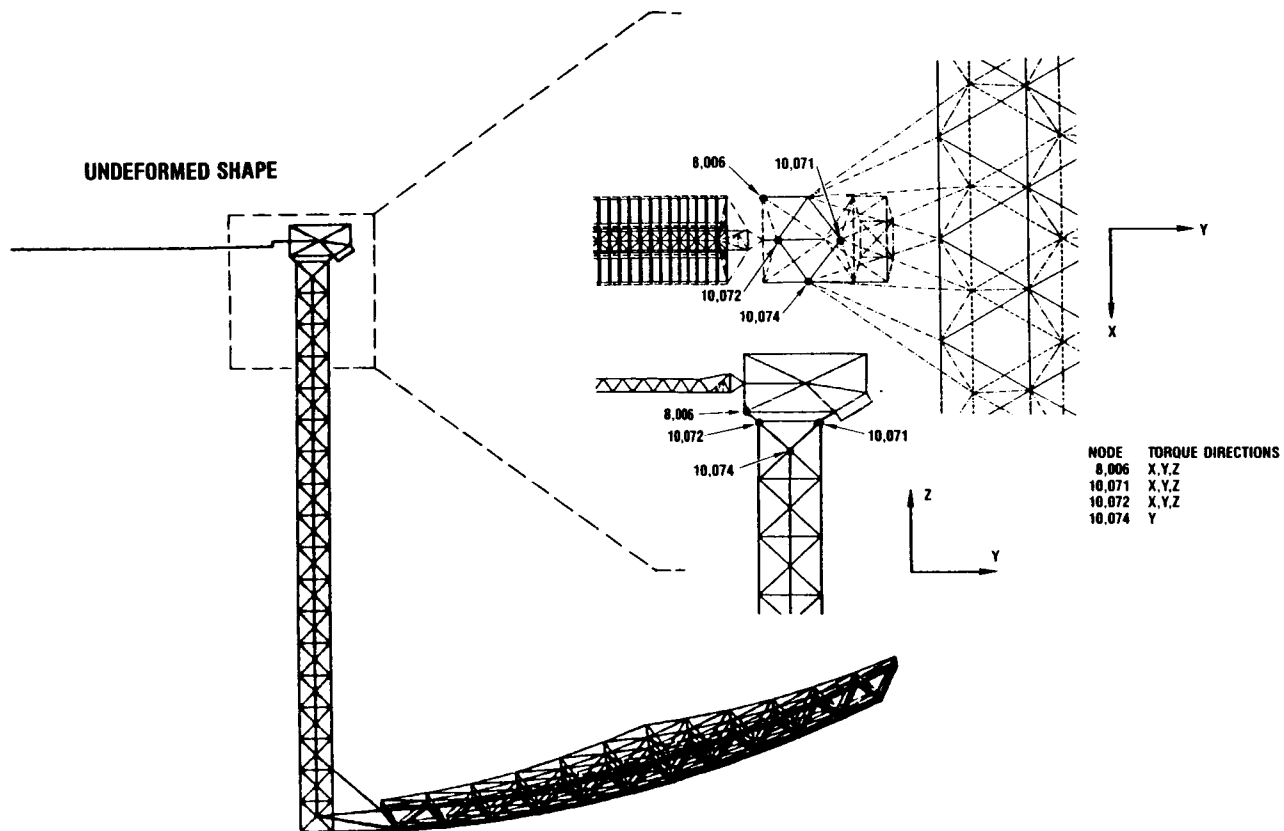
Optimizing the locations of actuators and sensors led to distributing them to locations of high modal kinetic energy.

OPTIMALLY LOCATED VIBRATION CONTROL SENSORS AND ACTUATORS SUPERIMPOSED ON MODES 7 AND 10 DEFLECTIONS

MODAL DEFORMATION: MODE 7 — 0.024 Hz

MODAL DEFORMATION: MODE 10 — 0.059 Hz

8300
10071
10072
10074
HEURISTICALLY LOCATED SENSORS AND ACTUATORS ARE ALL LOCATED WITHIN CIRCLE
10056 — 10055
10048 — 10049

8300
10072 — 10071
10074
10062 — 10061
10054 — 10053

+Z
+Y

+Z
+X

NOTE: BOOM MOUNTED SENSORS/ACTUATORS LOCATED AT POSITIONS OF MAXIMUM MODE 7 AND 10 SLOPES
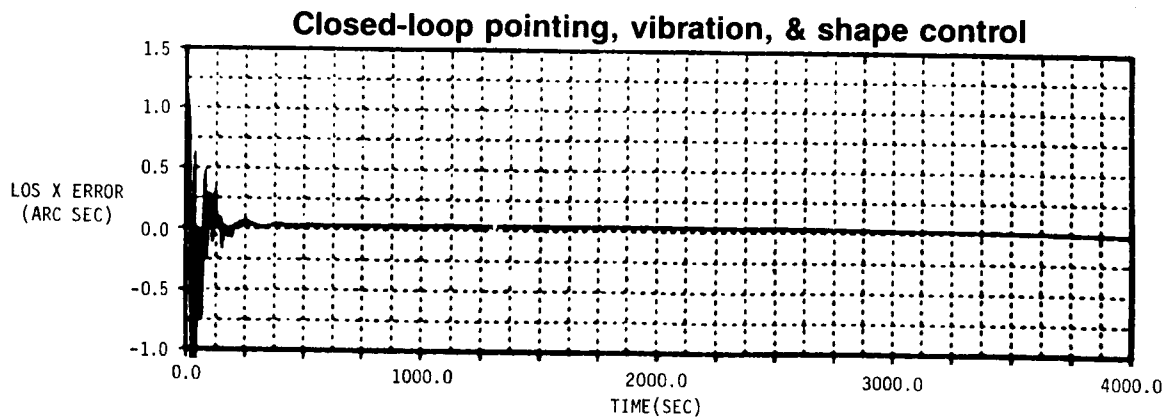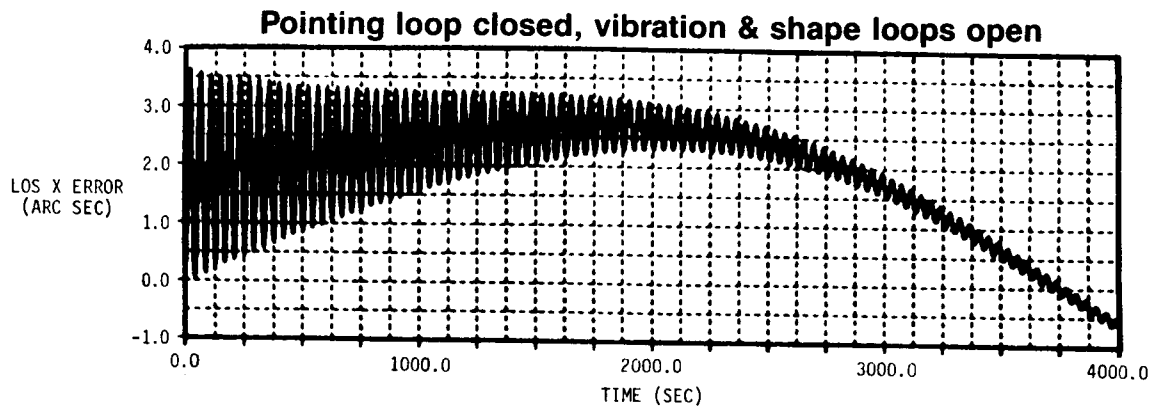
The torque per actuator was substantially smaller for the optimally located actuators.

COMPARISON OF MAXIMUM ABSOLUTE VIBRATION-CONTROL TORQUE LEVELS (MESS-COMPENSATORS)
Heuristic Vs Optimal Locations
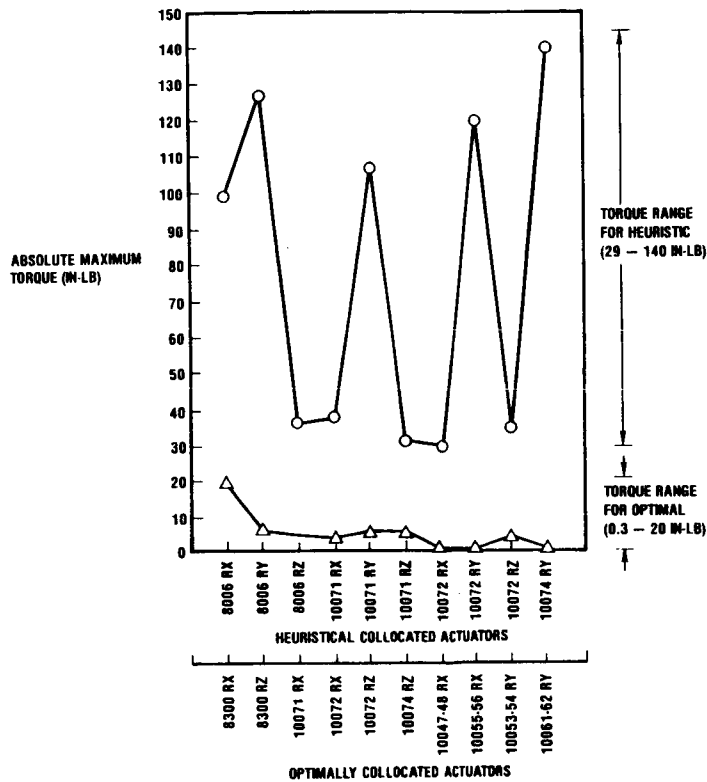
Open- and closed-loop LOS response is compared in the plots below. The open-loop response shows a significant slowly varying LOS error which is corrected by the shape control loop. The closed-loop response is well within our threshold for LOS error and also within our goal.

TRACKING MANEUVER RESPONSE

Pointing loop closed, vibration & shape loops open

LOS X ERROR (ARC SEC)

TIME (SEC)

Closed-loop pointing, vibration, & shape control

LOS X ERROR (ARC SEC)

TIME(SEC)

Conclusions from the control system design and nominal evaluation task are summarized below.

CONTROL SYSTEM DEVELOPMENT SUMMARY

- For this LSS with 0.5% assumed modal damping, only the lowest four elastic modes (modes 7, 8, 9 & 10) require active vibration suppression
- Distributed (optimally) actuators & sensors are able to suppress vibrations using much less control torque
- For this class of LSS, a larger number of actuators & sensors may be required than previously expected for the heuristically located actuator
  - Driven by performance, maximum torque level, & hardware failure constraints
  - We needed more actuators than controlled modes
- The nominal performance of the final closed-loop pointing/vibration/shape controller is within the goal
- Redesigns of each subsystem were required to achieve the performance goal; this suggests that a centralized approach may be more efficient

To evaluate the performance and stability robustness of each control system, both direct perturbations and frequency-domain singular value analysis were used.

ROBUSTNESS MEASURES

- Perturbation case studies — parameter variations made directly on the evaluation model; closed-loop stability & performance directly assessed

- Frequency domain singular value analysis (G_0, G stable)
    - Stability robustness

        - Additive perturbations
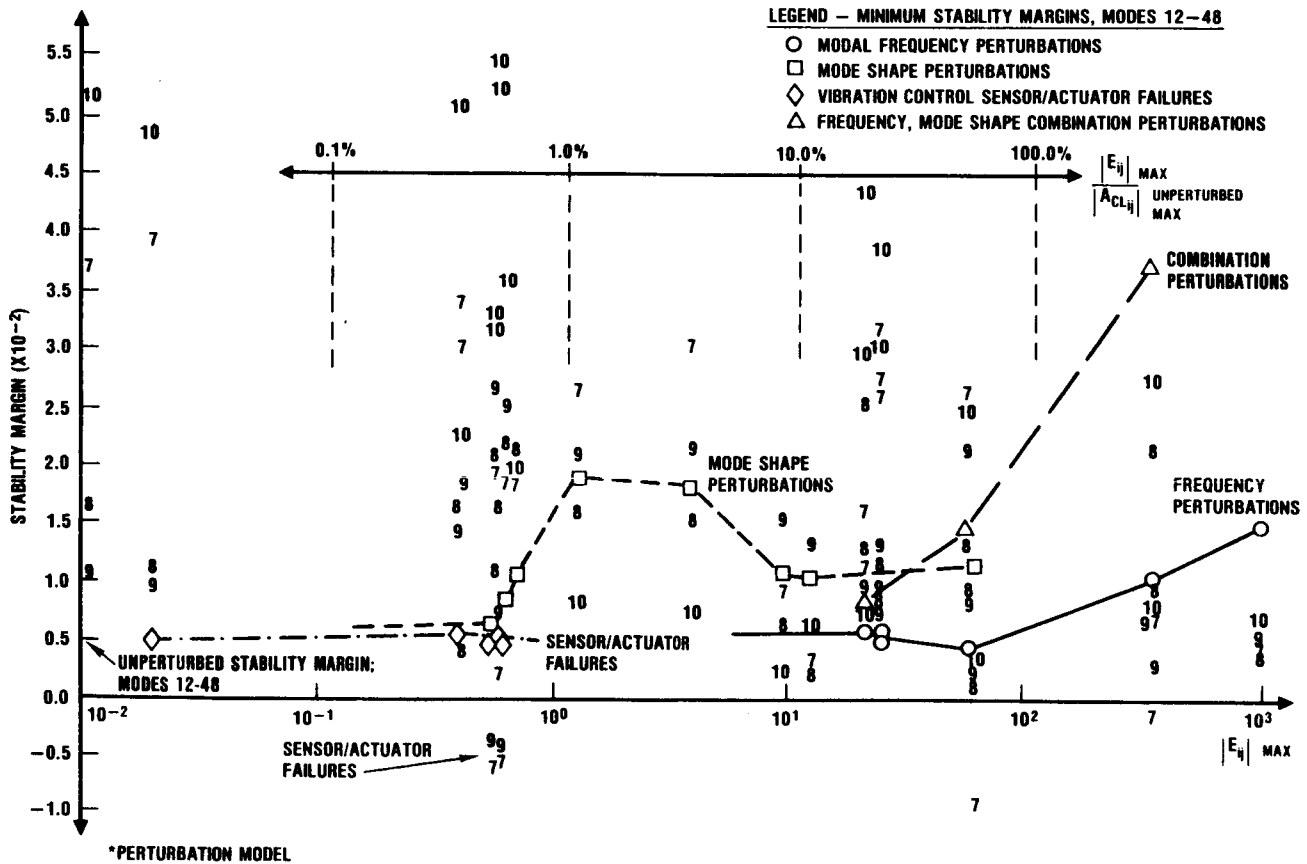 $$\bar{\sigma}(G(j\omega)) < \underline{\sigma}(I + G_0(j\omega)) \qquad , \omega \geq 0$$

        - Multiplicative perturbations
        $$\bar{\sigma}(G(j\omega)) < 1 / \bar{\sigma}[G_0 (I + G_0)^{-1}] \qquad , \omega \geq 0$$
    - Sensitivity
    $$\Delta Y = (I + G_0)^{-1}G \qquad \Rightarrow \text{Make } (I + G_0) \text{ Large}$$

The vibration control system is most sensitive to actuator and sensor failures.

VARIOUS PERTURBATIONS:* STABILITY MARGIN VS. MAXIMUM PERTURBATION MAGNITUDE

LEGEND — MINIMUM STABILITY MARGINS, MODES 12—48
- O MODAL FREQUENCY PERTURBATIONS
- □ MODE SHAPE PERTURBATIONS
- ◇ VIBRATION CONTROL SENSOR/ACTUATOR FAILURES
- △ FREQUENCY, MODE SHAPE COMBINATION PERTURBATIONS


*PERTURBATION MODEL

629

The minimum singular value of the return difference matrix gives the distance from the critical point. The closer the minimum singular value gets to zero, i.e. minus infinity decibels, the closer the closed-loop system is to being unstable.

Comparing the minimum singular value of this plot with that on the following plot, one sees that the high-gain pointing loop increases the system's sensitivity to parameter variations by an order of magnitude.

SINGULAR VALUES OF RETURN DIFFERENCE
MATRIX VS. FREQUENCY
Closed-Loop Vibration Control Only
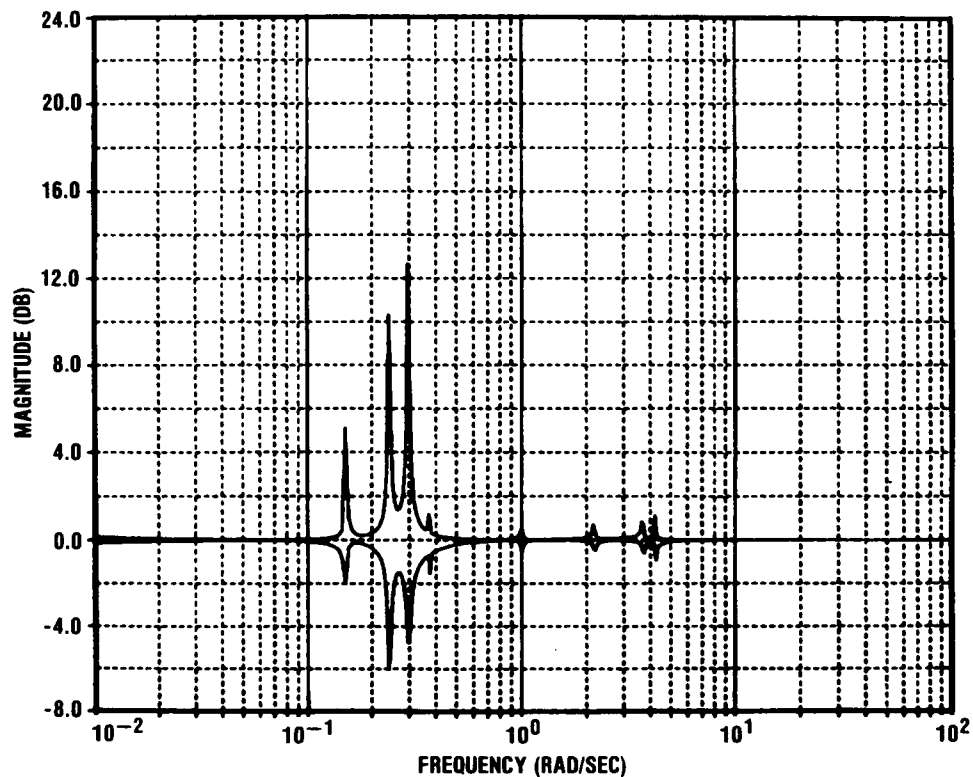
SINGULAR VALUES OF RETURN DIFFERENCE
MATRIX VS. FREQUENCY
Closed-Loop Pointing, Vibration, and Shape Control
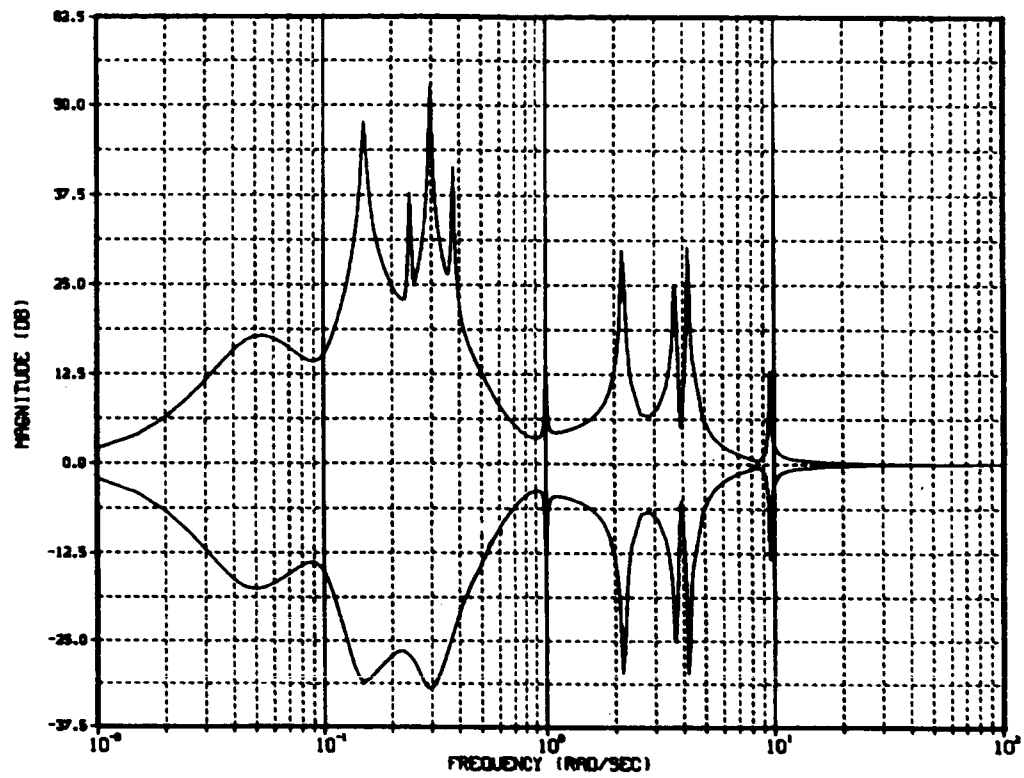
Conclusions concerning controller robustness are summarized below.

CONTROL ROBUSTNESS CONCLUSIONS

- The vibration suppression subsystem, when considered alone, possesses reasonable stability robustness qualities to modal frequency & mode shape perturbations
- The MESS compensator design is sensitive to certain actuator & sensor failures
  - The MESS algorithm depends on these sensors & actuators for subsystem decoupling
  - Collocated actuator & sensor failures do provide a degree of stability robustness, but not necessarily performance robustness
- Unstructed singular value analysis is useful in identifying frequencies at which sensitivity to perturbations is significant
- Interaction between the high-gain pointing & the flexible modes (primarily mode 9) in the perturbed system are extremely destabilizing to the integrated control system·

The feasibility of adding passive damping to the vehicle was assessed and the effects of passive damping on the closed-loop system's performance were examined.

PASSIVE VS ACTIVE DAMPING TRADEOFFS

- An assessment of the LSPSC-spacecraft structure concludes that from 1% to 15% passive modal damping in the lower modes is achievable
- To achieve the highest levels of passive damping, it is important to consider it in the initial structural design
- For the LSPSC spacecraft, the optimum mix of passive & active damping is to use the highest achievable level and supplement it with active controls as necessary
- The slewing torque tuning we did is sensitive to passive damping levels
    - We actually found higher active-control torques with the addition of passive damping
    - This is considered a disadvantage of tuning the torques rather than a disadvantage of added passive damping

A number of important major conclusions resulted from the LSPSC study. The conclusions are summarized below.

LSPSC MAJOR CONCLUSIONS

Truss antenna structures are inherently stiff

- It takes "heroic" efforts to achieve reflector vibration frequencies less than 0.1 Hz, even with a reflector the size of 100 meters
- While the feed boom bending can have low frequencies, damping of these modes requires a different type control than does correction of reflector distortions

Slewing maneuvers are dominant design drivers

- Settling after fast-slew drives vibration control design
- Acquisition/tracking after fast-slew drives pointing control design

Rapid slewing/pointing of this size vehicle will require very large, fast responding actuators

- Large actuators add large nonstructural mass to the vehicle
- Locating the actuators leads to conflicting demands on minimizing vehicle moments of inertia & minimizing flexible-body modal excitation

Maturity of shape control technology is well behind other control technologies

- Actuators require development
- Sensors require a great deal of development

For a large truss antenna, only a few lower elastic modes require vibration control

- Slewing disturbances significantly excite only the fundamental boom bending & torsion modes
- RF parameters are most sensitive to these lowest modes

Spatially distributed actuators/sensors are advantageous

- The torque per actuator is reduced with more actuators
- Optimizing the locations of actuators/sensors leads to distributing to locations of high modal kinetic energy
- For same number actuators, torque per optimally located actuators is substantially smaller than the torque per heuristically located actuators

Decentralized control design leads to complex series of analyses

- Interaction among controllers with overlapping bandwidths is difficult to avoid
- Constant interaction analysis & subsystem redesign of decentralized controllers suggests that centralized approach may be more efficient
- Robustness of the integrated controllers should be considered from the outset

A significant level of passive damping is possible for truss structures (PACOSS conclusion)

- 5-15% passive modal damping reduces requirements for active vibration control
- Achieving 5% passive modal damping is very feasible
- With significant effort, can probably achieve 10%
- It is important to design for passive damping from the outset

ROBUST CONTROL FOR LARGE SPACE ANTENNAS

M. F. Barrett
Honeywell Systems and Research Center
Minneapolis, Minnesota

OUTLINE OF PAPER

An outline for the presentation is shown in this figure. We begin with a brief description of program objectives and the space-based radar application. Next, we describe general characteristics of the 100-m diameter reflector spacecraft, the intended mission and associated requirements, and dynamic characteristics relevant to that mission. Preliminary control analyses are then carried out for the critical rapid slew and settle maneuver to establish feedback control requirements and fundamental limitations in meeting those requirements with state-of-the-art control hardware for a baseline reaction control system (RCS) jet placement assumed for the open-loop bang-bang slew maneuver. An improved RCS jet placement is proposed which greatly alleviates these limitations. Control moment gyros (CMGs), angular position sensors (integrating rate gyros), and linear translation sensors (double integrating accelerometers) are placed for feedback control. Next, control laws are designed for the improved sensor and actuator placement and evaluated for performance and robustness to unstructured model uncertainty. The robustness of this final control design is also assessed with respect to modal parameter uncertainty. Finally, results of these control designs analyses are summarized, conclusions are drawn, and recommendations for future studies are presented.

PROGRAM OBJECTIVES AND APPLICATION

SPACECRAFT/MISSION DEFINITION

PRELIMINARY CONTROL ANALYSES FOR FAST SLEW MANEUVER

FINAL CONTROL DESIGN AND EVALUATION

SUMMARY, CONCLUSIONS, AND RECOMMENDATIONS

AFFDL SPONSORED PROGRAM

Current Air Force plans to develop large spacecraft antennas for surveillance and reconnaissance missions pose significant challenges for structural and control designers. The objectives of this AFFDL-funded study were to develop robust control laws for pointing and shape control of a large space antenna and to assess the robustness of such controllers to structural mode parameter uncertainty.

The application for this study was a 100-m diameter offset feed reflector satellite of the class required for radar surveillance missions. The model was developed by General Dynamics (GD) Convair under their AFFDL-funded Large Spacecraft Pointing and Shape Control (LSPSC) study. The most stressing mission requirement was to execute a 45 deg slew maneuver in 60 sec, and settle to meet accuracy specifications of 35 µrad for pointing and 59 milli-in for surface shape within 5 minutes. Angular rate requirements for the primary tracking maneuver were more modest. Accuracy goals were taken to be a factor of 10 smaller than these specifications.

A self-imposed goal of the study was to satisfy all maneuver requirements with current actuator capability. Current CMG capability was assumed to be that of the Bendix MA2000 Double-Gimbaled Advanced Development CMG for Skylab, which has a torque capability of 175 ft-lb and a momentum storage capability of 3000 ft-lb-sec. Corresponding specifications were taken to be a factor of 10 larger than goal. Current force and impulse capability for RCS jets imposed no limitations for the study.

OBJECTIVES:

- To Develop Robust Control Laws For Pointing And Shape Control Of A Large Space Antenna.
- To Assess Robustness Of Such Controllers To Structural Mode Parameter Uncertainty.

APPLICATION: SPACE-BASED RADAR MISSION

- 100-m Offset Feed Reflector (GD's LSPSC Study)
- Maneuver Requirements

    - Target Tracking: 0.004 deg/sec
    - Max. Rate Slew: 45 deg In 60 sec, 1.5 deg/sec ⟍ Total Time
    - Settling Time To Reach Specifications: 5 min. ⟋ To Spec: 6 min.

- Pointing/Shape Specifications

    - Pointing Accuracy : 35 µrad (3.5 µrad Goal)
    - Surface Accuracy: 59 milli-in (5.9 milli-in. Goal)

- CMG Control Limitations (Goal $\triangleq$ Advanced Devel. CMG For SKYLAB)

    - Max. Torque: 1750 ft-lb (175 ft-lb Goal)
   - Max. Momentum: 30,000 ft-lb-sec (3000 ft-lb-sec Goal)

SPACECRAFT DEFINITION

The spacecraft model employed was for an offset feed reflector satellite. It consists of a 100-m diameter hexagonal reflector dish, which is attached to a 110 m boom through the mount. The spacecraft bus, which is attached to the opposite end of the boom, supports the antenna feed and a 50 m by 9 m solar panel to supply the necessary power for both radar surveillance and control requirements. Total weight of the spacecraft was more than 17,000 lb and largest moment of inertia (about the x axis) was 2.5×10^7 slug-ft-sq.
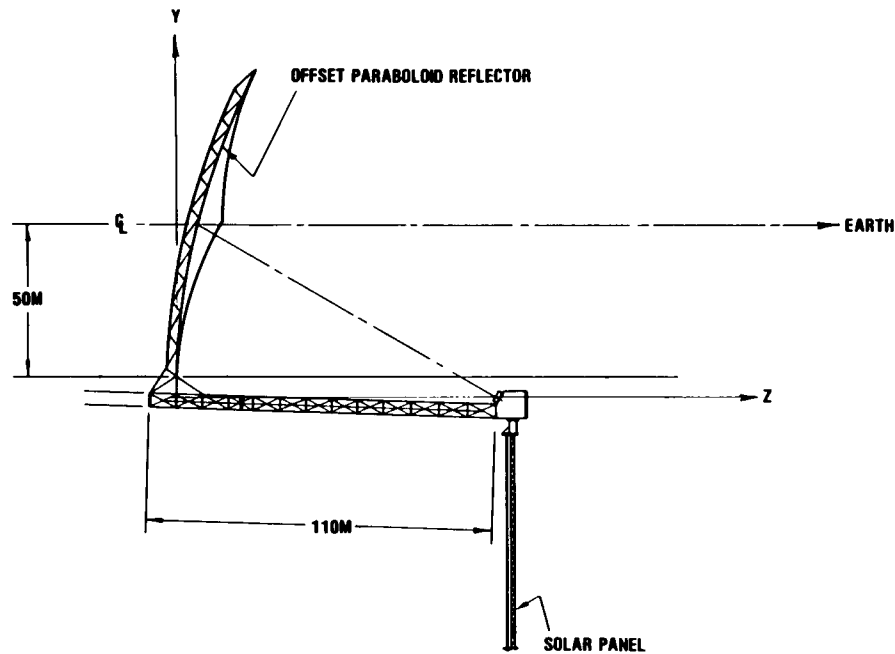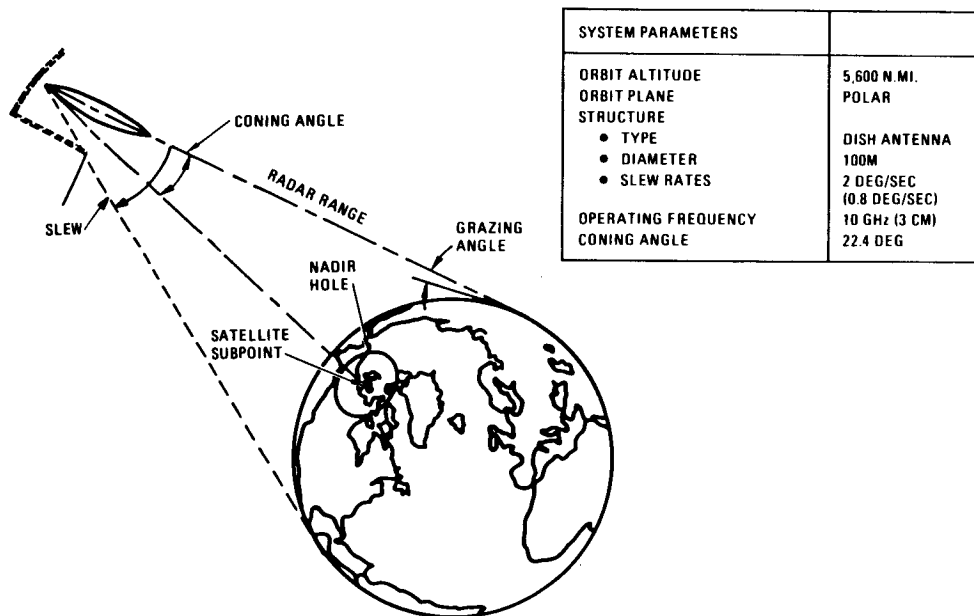
SPACECRAFT GEOMETRY

The GD geodetic truss forms the primary building block for the satellite reflector and boom. It is deployable, employs graphite/epoxy construction, and is designed to be accommodated by the Space Shuttle orbiter cargo bay. Due to the inherent stiffness of this truss structure, the primary free-free mode of the unattached reflector dish was determined by GD to be 1.70 Hz, which is well above the 0.1 Hz estimate typically assumed by the large space structure controls community.
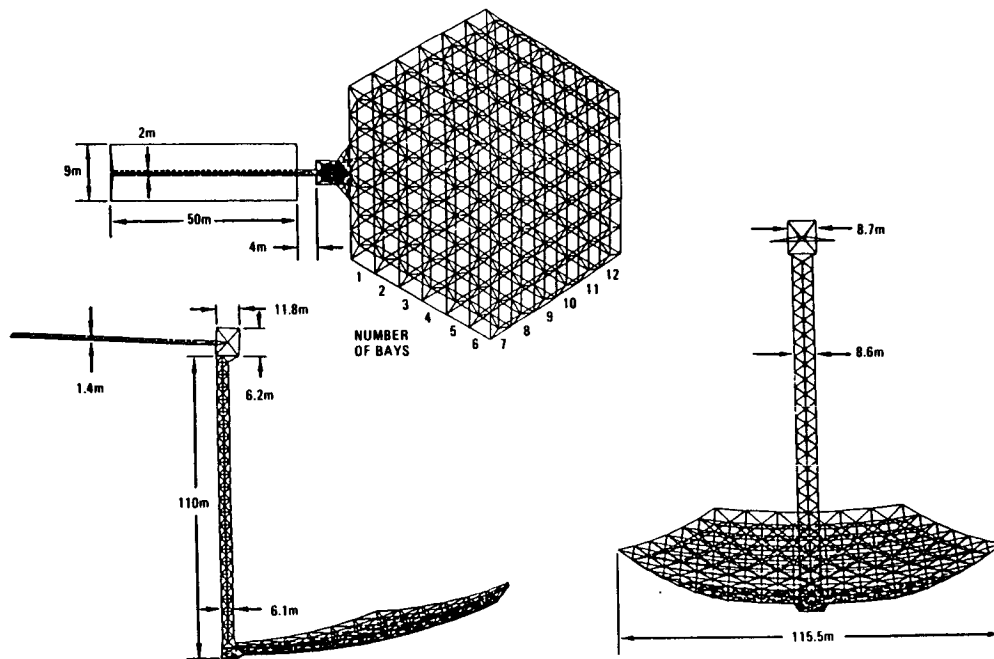
SPACECRAFT MISSION

The spacecraft mission characteristics are illustrated in this figure. The spacecraft operates in a 6 hr polar orbit at an altitude of 5600 nmi. Its primary purpose is to track fixed targets on the surface of the Earth or moving targets (such as aircraft) near the Earth. The most stressing mission requirement, which is considered an uncommon occurrence, is to execute a large angle (45.6 deg) fast slew maneuver in 60 sec and settle to within pointing specifications of 35 μrad in minimum time. This maneuver is motivated by a requirement to occasionally acquire and track a critical target (without warning) anywhere near the Earth's surface, which defines a cone of radius 22.4 deg. Thus, the maximum slew angle is roughly twice this angle.

| SYSTEM PARAMETERS	
ORBIT ALTITUDE	5,600 N.MI.
ORBIT PLANE	POLAR
STRUCTURE	
• TYPE	DISH ANTENNA
• DIAMETER	100M
• SLEW RATES	2 DEG/SEC
	(0.8 DEG/SEC)
OPERATING FREQUENCY	10 GHz (3 CM)
CONING ANGLE	22.4 DEG

MISSION SCENARIO

To provide continuous coverage of the Earth's surface, a constellation of three satellites would be required as shown in this figure. In order to hand off targets from one satellite to the next, there is also a regular requirement to execute a slow slew from the trailing edge of the Earth to the leading edge, and then track a target until the next satellite hand off some two hours later.
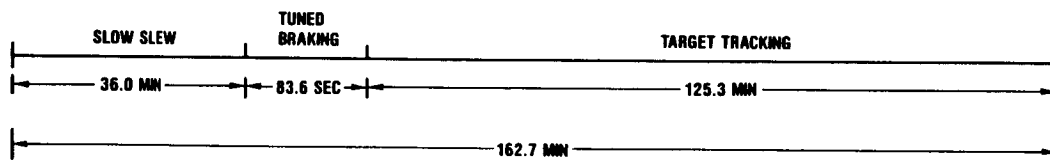

643
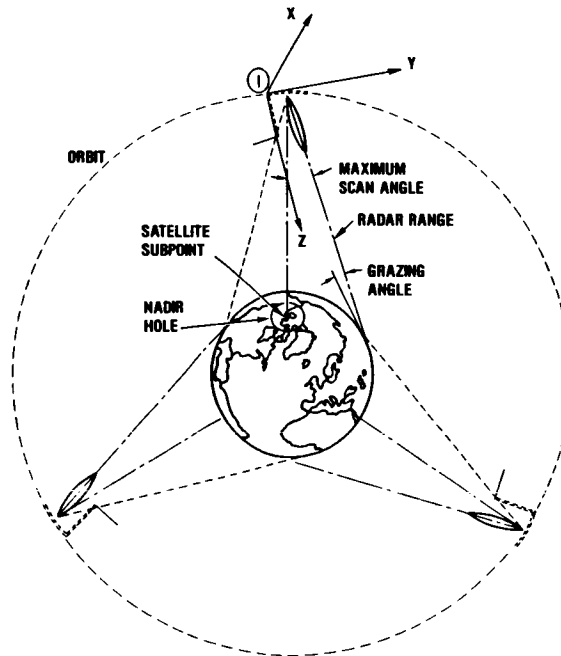
NOMINAL SLEW MANEUVER TIMELINES (NOT TO SCALE)

Nominal timelines for these slew and tracking maneuvers are shown in this figure. In both cases the primary tracking maneuver spans just over 2 hr to allow for a smooth handoff of targets between satellites. For the fast slew maneuver, total time to slew and settle within specifications for target acquisition is roughly 6 min. For the slow slew maneuver, total time to slew and settle is roughly 37 min.

FAST SLEW (UNCOMMON OCCURRENCE)

SLEW	ACQUISITION/TRACK	TARGET TRACKING
60 SEC	294.3 SEC	125.3 MIN

131.2 MIN
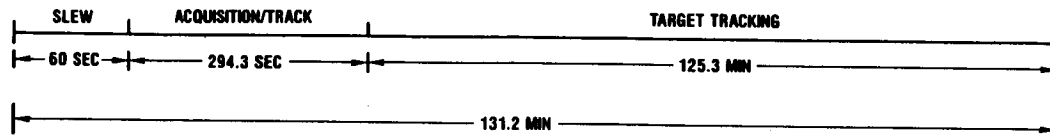
SLOW SLEW (NORMAL OCCURRENCE)

SLOW SLEW	TUNED BRAKING	TARGET TRACKING
36.0 MIN	83.6 SEC	125.3 MIN

162.7 MIN

MODEL FOR STRUCTURE/ANTENNA

A finite element model was developed by GD using NASTRAN. This model employs 370 nodes and contains mode frequencies and six degree of freedom mode shapes at all nodes for some 207 modes (6 rigid, 201 flexible). This defines 2220 (= 370 × 6) total degrees of freedom for each mode. The model used here, however, contained only the first 103 of these modes, which covers flexible mode frequencies from 0.15 r/s to 78.1 r/s. Modal damping for all flexible modes was assumed to 0.5 percent (ζ = 0.005). Due to the inherent stiffness of truss structures, only the first four flexible modes proved to be critical to antenna performance. These include the first bending and torsion modes for the boom and the first bending mode for the solar panel. To facilitate mixing of translational and rotational degrees of freedom, modal shapes data were scaled to give units of milli-in. for translation and μrad for rotations.

Four of some 15 antenna parameters defined by GD were selected to measure the effects of modal displacements on RF performance. These effects are illustrated in the next two figures.
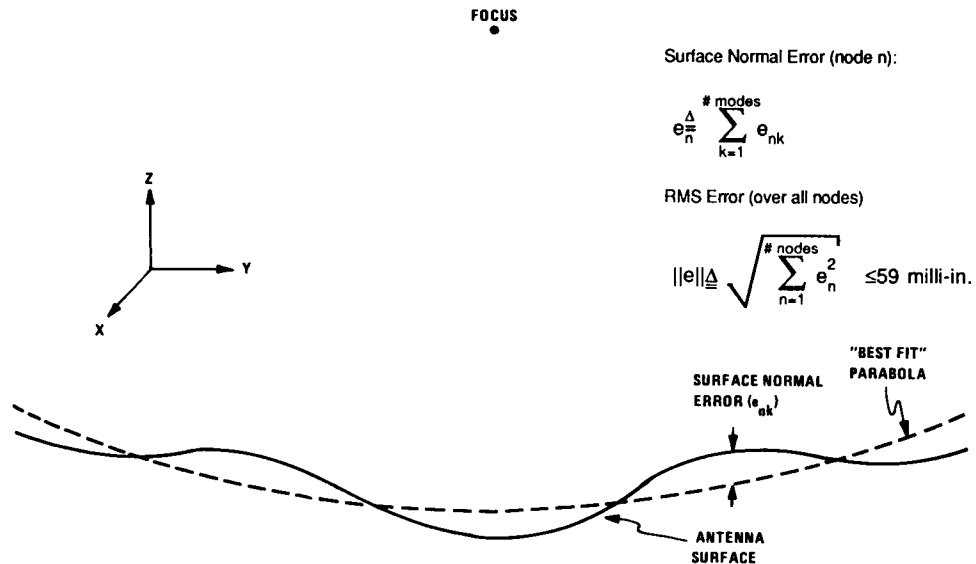
STRUCTURE

- 2220 DOFs (= 370 Nodes x 6 DOFs/Node)

- 103 Modes (0.15 r/s $\leq \omega_k \leq$ 80 r/s)

- 0.5% Modal Damping (ζ_k = 0.005)

- Four Critical Flexible Modes
  - Y - Axis Boom Bending: Mode 7 -- 0.15 r/s
  - X - Axis Boom Bending: Mode 10 -- 0.37 r/s
  - Z - Axis Boom Torsion: Mode 8 -- 0.24 r/s
  - Z - Axis Solar Panel Bending: Mode 9 -- 0.30 r/s

ANTENNA

- Four Critical Responses
  - Beam Rotation X (LOS $_X$) : 35 μ rad
  - Beam Rotation Y (LOS $_Y$) : 35 μrad
  - Beam Path Length Change (Defocus): 59 milli-in.
 - RMS Surface Normal: 59 milli-in

EFFECTS OF FLEXIBILITY ON
ANTENNA PERFORMANCE: SURFACE ERRORS

This figure shows the effect of flexibility on antenna surface accuracy, which provides a measure of antenna gain. To do so, requires definition of a *best fit* parabola, in a least squares sense, to the distorted dish for each flexible mode. Total surface error in the normal (z axis) direction for any node n then consists of the sum of the contributions due to each mode. Rms normal surface error is, in turn, given by the RSS contribution over all nodes on the antenna.


FOCUS

Surface Normal Error (node n):

$$e_n \overset{\Delta}{=} \sum_{k=1}^{\# \text{modes}} e_{nk}$$

RMS Error (over all nodes)

$$\|e\| \overset{\Delta}{=} \sqrt{\sum_{n=1}^{\# \text{nodes}} e_n^2} \quad \leq 59 \text{ milli-in.}$$

"BEST FIT" PARABOLA

SURFACE NORMAL ERROR (e_{nk})

ANTENNA SURFACE

EFFECTS OF FLEXIBILITY ON
ANTENNA PERFORMANCE: BEAM POINTING ERRORS

This figure shows the effect of flexibility on beam pointing errors. The solid line denotes the ideal beam generated by a ray traced from the feed to the center of the undistorted reflector to a normal reference plane. The dashed line denotes the corresponding beam for a similar ray traced from the feed on the distorted boom to the center of the distorted best-fit reflector to a second reference plane parallel to the first. Both rays travel an equal distance (8 units) in equal time. The angle between the two beams defines beam rotation error about the x axis. A similar picture defines beam rotation error about the y axis. These errors correspond to traditional line-of-sight errors in optical systems. The distance between the two reference planes defines beam path length change in the normal (z axis) direction. This error corresponds to the traditional defocus error in optical systems.
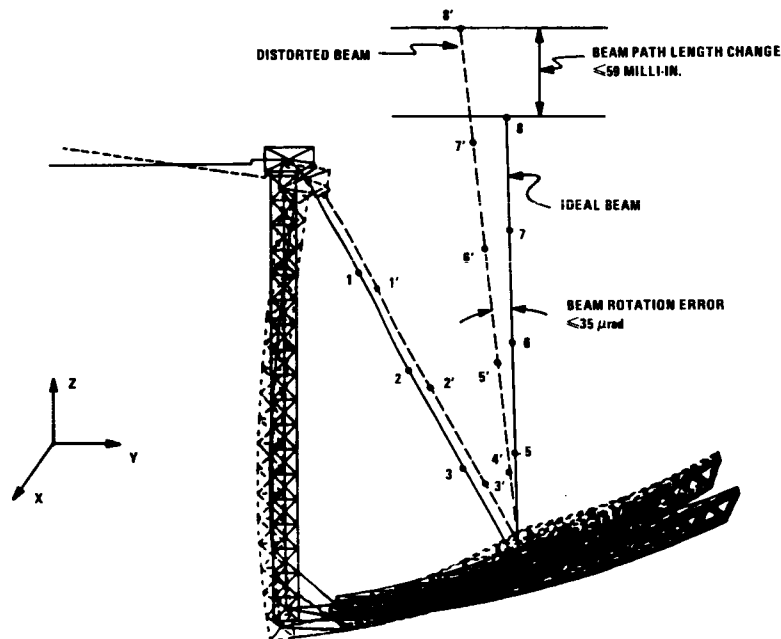
NOMINAL FAST SLEW MANEUVER (FULL EARTH DIAMETER)

Recall that a critical maneuver for the large space antenna is a requirement to execute a large angle (45.6 deg) slew maneuver about the spacecraft +x axis in 60 sec and settle to within specifications in minimum time. This slew can be accomplished with the open-loop time-optimal bang-bang control scheme shown in this figure.
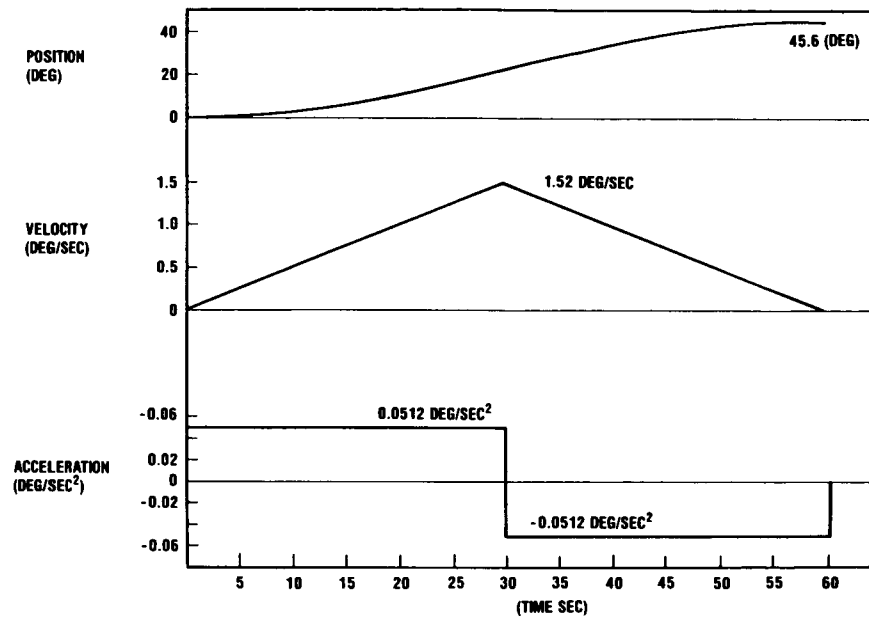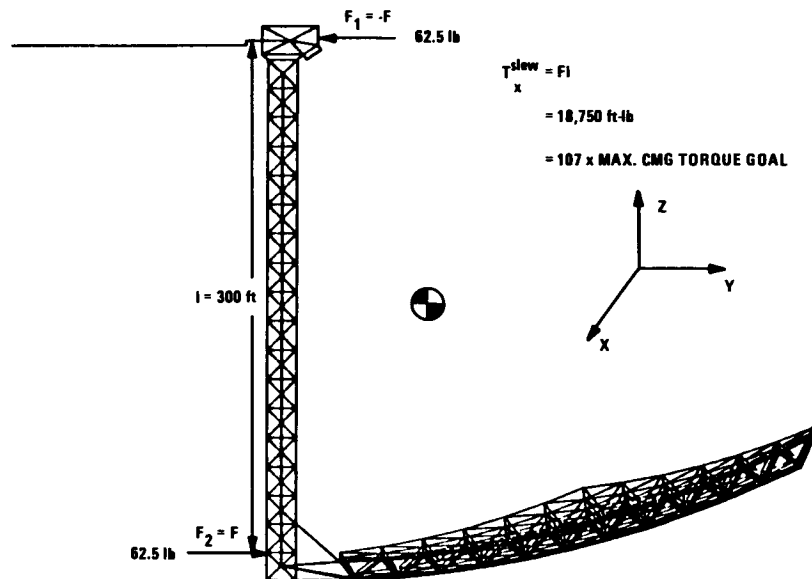
NOMINAL RCS JET PLACEMENT

The nominal placement of reaction control system (RCS) jets chosen by GD to accomplish the nominal fast slew maneuver is shown in this figure. It requires simultaneous firing of the "B" RCS jets for the first 30 sec of the maneuver: a +y axis jet at node 10004 (near the mount) and a -y axis jet at node 8009 (center of bus). To arrest the resulting angular accelerations, opposing forces generated in the latter 30 sec of the maneuver by the "A" jets require the use of two pairs of jets in a skewed configuration to avoid thrust impingement on either the solar panels or the antenna surface. Taking into account spacecraft inertia about the x axis, the effective moment arm, the allowable maneuver time, and the desire for no net translation implies jet sizing of 61.5 lb for each of the "B" jets. Assuming a 45 deg skew angle for the "A" jets gives a nominal sizing of 43.5 lb for these jets. Also indicated is GD's nominal placement of three-axis control moment gyros (CMGs) for slow slew and tracking maneuvers.
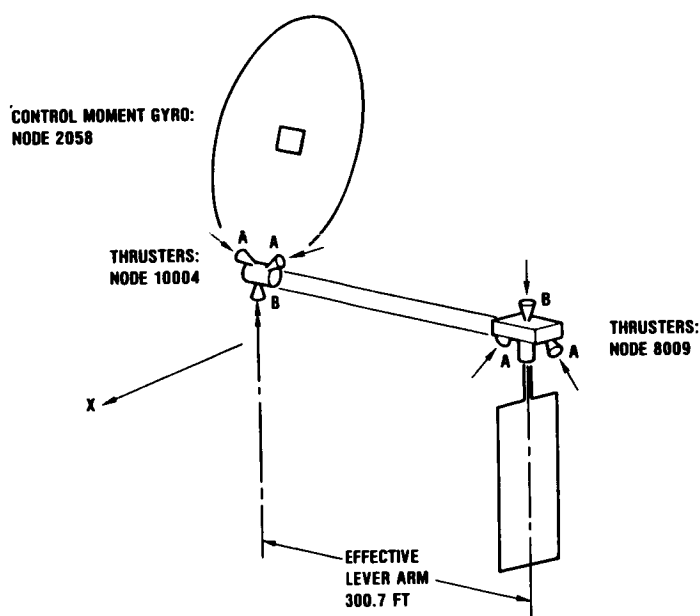
CRITICAL DISTURBANCE: SLEW MANEUVER

Although RCS jets are essential to provide the necessary control power for the fast slew maneuver, the resulting disturbance torque of 18,750 ft-lb (= 61.5 lb × 300 ft) easily dominates all natural disturbances. This torque is more than two orders of magnitude larger than current CMG capability (goal). Since nominal slew torques for each half of the slew maneuver are designed to oppose one another, the net effect on the rigid body is ideally only an attitude change. In practice, force imbalances between jets and misalignments of the jet plumes produce disturbances in all axes. Even in the absence of such imperfections, however, flexible mode excitations due to RCS jet forces during the first half of the slew maneuver are not in general canceled by those generated during the second half. Therefore, residual antenna parameter errors due to these excitations that remain after the open-loop slew maneuver must be reduced by feedback control to meet specifications.

$F_1 = -F$

62.5 lb

$T_x^{slew} = Fl$

= 18,750 ft-lb

= 107 x MAX. CMG TORQUE GOAL

$l = 300$ ft

$F_2 = F$

62.5 lb

CONTROL PROBLEM FOR FAST SLEW MANEUVER
(WITH BASELINE RCS JET PLACEMENT)

To assess the enormous difficulty of the feedback control problem, transient responses of both rigid-body and flexible-body models were compared for the nominal open-loop RCS jet force profile. Responses for the flexible-body model show large excitation of mode 7 for all four antenna parameters and some excitation of modes 9 and 10 for beam y. Beam rotation x overshoots the commanded value by roughly 15 deg, which is nearly 7000 times the 35 μrad specification that applies after settling. Note that for the nominal 0.5 percent natural damping assumed for all modes, beam x would require a settling time of roughly 200 min (40 $\times$ spec) to reach specification without closed-loop feedback control for settling. Specification violations for beam rotation y and path length are far less severe. Nevertheless, settling time requirements for these parameters would still exceed reasonable limits. The response for rms normal, however, never exceeds its specification of 59 milli-in. and therefore requires no closed-loop feedback control for settling. Thus a factor-of-40 increase in closed-loop over open-loop damping is required to meet specifications for all antenna parameters.

PEAK ANTENNA RESPONSES

- Beam Rotation x : 15 deg (7000 x spec)

- Beam Rotation y : 0.75 deg (350 X spec)

- Beam Path Length : 60 in. (1000 x spec)

- RMS Surface Normal: 50 milli-in. (0.8 x spec)

SETTLING TIME: $\zeta_{ol} = 0.005$ (0.5%)

- $T_s = 200$ min. (40 x spec)

REQUIRED CLOSED-LOOP DAMPING (CRITICAL MODES)

- $\zeta_{cl} > 40 \ \zeta_{ol} = 0.2$ (20%)

FEEDBACK CONTROL STRUCTURE
FOR SLEW MANEUVER: SINGLE-AXIS (IDEALIZED)

A candidate feedback control structure for the RCS slew maneuver is shown in this figure for an ideal case in which measurements y are equal to the regulated variables z and control inputs u enter at the disturbance inputs d. Here we have assumed that the primary disturbance, due to the open-loop RCS jet command, drives the antenna structure directly through a feed forward gain K_{ff} and the command generation logic through a command shaping prefilter $G_{rb}(s)$. A natural candidate for this prefilter is a rigid-body model of the antenna response to RCS jet command inputs. When the feed forward gain K_{ff} is set equal to one, this ensures that the feedback compensator $K(s)$ controls only the error e between the flexible-body and rigid-body response to RCS jet inputs. This particular structure was chosen because it ensures that the bulk of the control power required for the slew maneuver is supplied by the RCS jets to move the rigid body. A much smaller control effort is supplied by the actuators used for feedback control which, for the preliminary analyses that follow, will be assumed to be *continuous* RCS jets. Although this assumption is unrealistic, results produced for this ideal case serve to define an upper bound on achievable performance for feedback control using more realistic actuators.
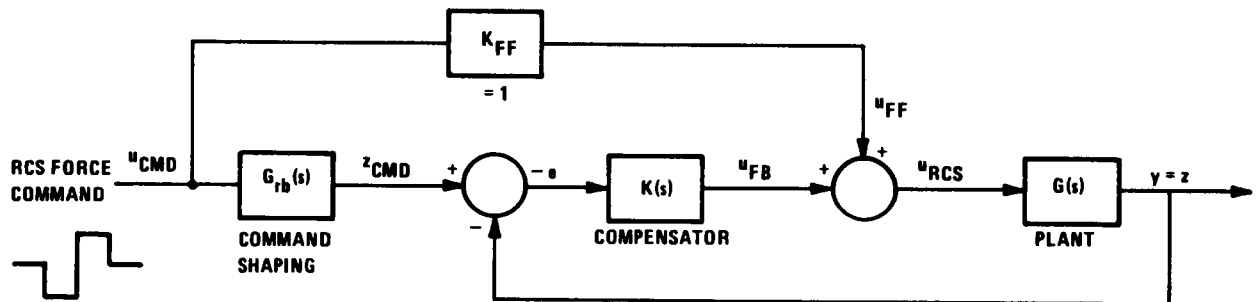
SUMMARY OF PRELIMINARY CONTROL DESIGN RESULTS

A nominal feedback control law was designed for this case using the LQG/LTR methodology with loop transfer recovery at the input to achieve a desired crossover frequency (or bandwidth) of roughly 1 r/s. This design achieved good stability margins for the feedback loop broken at the input. An examination of closed-loop eigenvalues indicates that this design provides substantial damping ($\zeta = 0.87$) for the critical mode 7 at 0.15 r/s, but much smaller damping for modes 9 and 10.

Transient responses for this control design show that beam rotation errors require 15 min to fall within their specifications of 35 μrad (3 × spec). Note also that peak values in control force are about 100 lb. These imply control torques of 30,000 ft-lb peak assuming a 300 ft moment arm. To achieve continuous control inputs, these torques must in practice be supplied by continuous actuators such as CMGs. These peak torque requirements exceed spec by a factor of 17, and the current CMG torque capability goal by a factor of 170. To meet the 5 min settling time spec implies peak torque requirements of 50 times spec, or 500 times goal. These results emphasize a fundamental tradeoff between control power and time to settle following the slew maneuver.

SUMMARY

- Design Has Good Stability Margins (± 10 db, 55 deg)
- Mode 7 Is Well Damped ($\zeta_{cl} = 0.87$)
- But, Modes 9 & 10 Are Less Well Damped ($\zeta_{cl} = 0.03, 0.05$)
- Thus Settling Time of $T_s = 15$ min Is Long (3 x spec)
- Implied Peak Control Torque Is Excessive (300 ft Moment Arm)
    - 30,000 ft-lb In First 60 sec (17 x spec)
    - 90,000 ft-lb Required To Meet T_s spec (50 x spec)

OBSERVATIONS

- Jet Input For Slew Puts Enormous Momentum Into Structure
    H = 62.5 lb x 300 ft x 30 sec = 562 500 ft-lb-sec
- Momentum Put into Flexible Modes Must Be Removed

∴ | Fundamental Tradeoff: Control Power vs. Time To Settle |

C - 2

IMPROVED RCS JET PLACEMENT FOR FAST SLEW MANEUVER

To appreciably improve the potential for improved slew maneuver performance requires drastic measures to minimize excitation of y-axis boom bending. One approach, which has been pursued by GD in their LSPSC study, is to adjust the period of the open-loop slew so that some even harmonic of the RCS jet input (which is zero for a symmetric waveform) coincides with the period of the critical mode 7 boom bending mode. This also minimizes excitation of mode 9, which has a frequency that is approximately twice that of mode 7. The effectiveness of this approach, however, is quite sensitive to mode frequency, and could in practice require on-orbit identification to isolate this mode frequency.

An alternative approach, that was pursued in this study, is to spatially distribute RCS jets in such a manner as to essentially eliminate excitation of the critical mode 7 boom bending mode. This fundamental change in objectives, however, can be accomplished with only minor modification to the baseline GD-defined placement. The new placement uses the two existing jet locations plus one additional location at the outer edge of the antenna to achieve the desired x-axis rotation, no translation in the y or z axes, and (ideally) no excitation of the critical mode 7 boom bending. To account for RCS jet imperfections, thrust imbalances of 5 percent of nominal (3 σ) and plume misalignments of 3 deg (3 σ) were also assumed. The latter misalignments give rise to cross-axis thrust errors that are also 5 percent of nominal. The resulting jets produce net translations and rotations in all axes and excite all flexible-body modes. Thus, three-axis control of rotations is unavoidable in practice.

OBJECTIVE: PLACE RCS JETS TO MINIMIZE EXCITATION OF FLEXIBILITY

NEW PLACEMENT

- Uses Existing Y-Axis Jets At Base And Tip Of Boom

- But Allows Combined Y And Z Axis Forces At Base

- Adds New Z-Axis Jet To Outer Edge Of Antenna

RCS BLENDING SCHEME: DISTRIBUTE NOMINAL JET FORCES TO ACHIEVE

- Desired Rotation About X Axis (1)

- No Translation In Y or Z Axes (2)

- No Excitation Of Mode 7 Y-Axis Beam Bending (1)

RCS JET IMPERFECTIONS: EACH JET ASSUMES RANDOM

- Thrust Imbalances   : 5% Of Nominal (3 σ)

- Plume Misalignments   : 5% Of Nominal (3 σ)

- • | Actual Jets Produce Net Translations and Rotations In All Axes And Excite All Flex Modes! $\Rightarrow$ Need 3-Axis Control Of Rotations

IMPROVED RCS JET PLACEMENT FOR FAST SLEW MANEUVER (CONT.)

The resulting improved RCS jet placement for the fast slew maneuver is shown in this figure. Note that the jet at the top of the boom (node 8009) allows only y-axis force (-44 lb), while that at the outer edge of the antenna (node 1025) allows only z axis force (+16.3 lb). The jet at bottom of the boom (node 10004) allows a combination of y and z axis forces to ideally balance net forces and thereby eliminate translation. This scheme can be expected to yield greater performance robustness to model uncertainty than tuned slew maneuvers since it depends only on mode shapes rather than on mode frequencies.
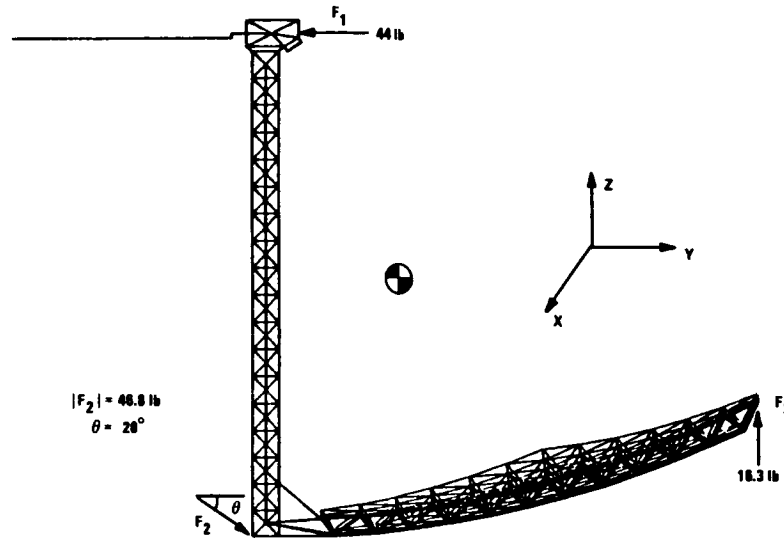
CONTROL PROBLEM FOR FAST SLEW MANEUVER
(WITH IMPROVED RCS JET PLACEMENT)

To illustrate the dramatic reduction in modal excitation for this RCS placement, a transient response was generated for a 60 sec open-loop slew maneuver. Peak errors for beam x and y rotations and path length change are now all roughly 100 times specification, while rms surface normal is well within specification. Comparing these plots with those for the original placement shows error reductions of 70 for beam x, 3 for beam y, 10 for path length, and 1.6 for rms surface. The magnitude of these reductions indicates a strong potential for improved performance with this new RCS jet placement. For the nominal 0.5 percent natural damping assumed for all modes, a settling time of roughly 52 min (10 × spec) is required to reach specification without closed-loop feedback control for settling. Thus a factor of 10 increase in closed-loop over open-loop damping is required to meet specifications for all antenna parameters.

PEAK ANTENNA RESPONSES (IDEAL JETS)

- Beam Rotation x   : 3500 μrad   (100 x spec)

- Beam Rotation y   : 3500 μrad   (100 x spec)

- Beam Path Length   : 4500 milli-in.   (75 x spec)

- RMS Surface Normal :   30 milli-in.   (0.5 x spec)

SETTLING TIME: ζ_{ol} = 0.005 (0.5%)

- T_S = 52 min. (10 x spec)

REQUIRED CLOSED-LOOP DAMPING (CRITICAL MODES)

- ζ_{cl} > 10 ζ_{ol} = 0.05 (5%)

ASSUMED SENSOR AND ACTUATOR PLACEMENT: 3-AXIS

Prior to final feedback control design, a set of actuators was placed with a simple least-squares algorithm to best approximate the effect of disturbances on desired antenna responses. Similarly, a set of sensors was placed with a simple least-squares algorithm to best approximate the effect of disturbances on desired antenna responses. The resulting actuator set had x, y and z axis CMGs at node 2083 (bottom of the dish) and at node 10072 (top of the boom). The sensor set was made up of x, y and z rotation sensors at node 2033 (bottom of the dish), a z rotation sensor at node 10072, and x and y translation sensors at node 10008 (near the bottom of the boom).
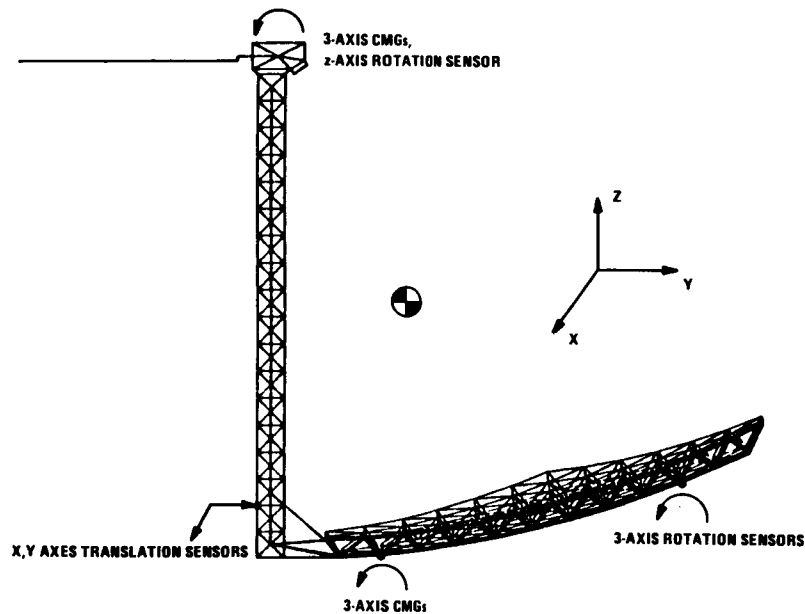
FEEDBACK CONTROL SOLUTION

For the final feedback control design, these latter translation sensors were compensated with second-order hi-passes to washout low-frequency measurements due to rigid-body translations, which are uncontrollable with CMGs. This also washes out rigid-body rotations. The LQG/LTR methodology was again applied with loop transfer recovery at the output to achieve an LQG loop crossover frequency (or bandwidth) of about 0.5 r/s. The resulting compensator included 40 states, but could likely be reduced to 10-20 states using model reduction.

ASSUMPTIONS

- 6 CMG Actuators (3 Dish, 3 Bus)

- 4 Rotation Sensors (3 Dish, 1 Bus)

- 2 Translation Sensors (Boom) With Second-Order Hi-Passes
  (To Eliminate Uncontrollable Translations)

LQG/LTR METHODOLOGY: OUTPUT RECOVERY

- KF Loop Crossover : ω_f = 0.5 r/s

- LQ Loop Crossover : ω_c = 5 r/s

COMPENSATOR COMPLEXITY

- 6 Inputs

- 6 Outputs

- 40 States (Could Be Reduced To 10-20 States With Model Reduction)

FEEDBACK CONTROL STRUCTURE FOR SLEW MANEUVER: 3-AXIS

For closed-loop simulation, the feedback control design was implemented as shown here. This loop is equivalent, in a feedback sense, to a loop that feeds back the four rotation measurements plus the two high-passed translation measurements. In addition, it also high-passes the commanded translations, as desired. The matrix D distributes thrust imbalances and misalignments for both positive and negative RCS jets to produce net forces in three directions for each of the three jet locations.
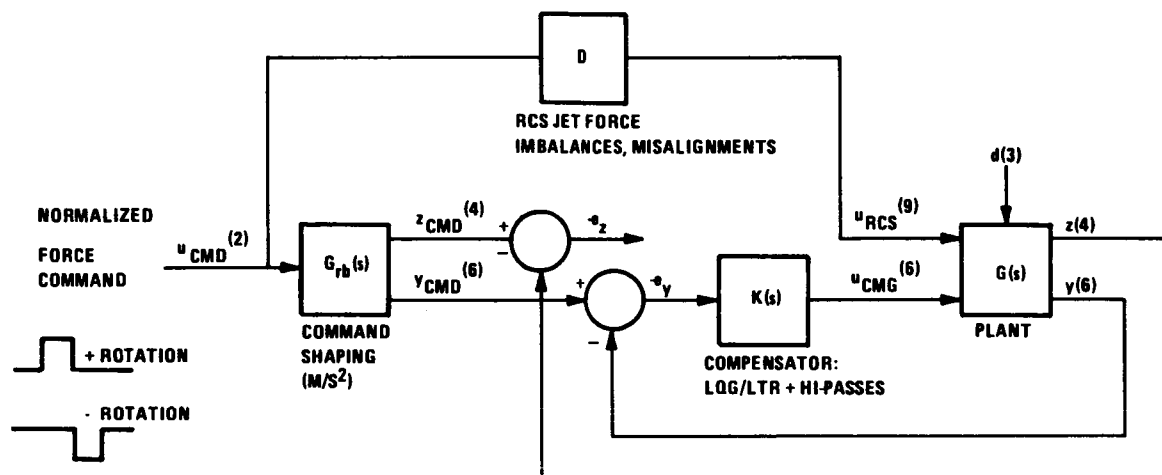
FINAL CONTROL DESIGN PERFORMANCE FOR FAST SLEW MANEUVER

Closed loop transient responses using the perturbed RCS jet disturbances were run for several different slew periods. In all cases the time for all antenna responses to fall within performance specifications is well within the 5 min settling time specification, while peak CMG torques lie well within spec (but outside of goal). In addition, time to goal in all cases is roughly 7 min. Results also show that a slew period cf 1.5 min with 2.7 min settling gives a minimum time to spec of 4.2 min, with peak control torques that are 2.6 times goal. However, a slew period of 2.5 min with 2.2 min settling gives only a slightly longer time to spec of 4.7 min, with peak control torques that approach goal. The latter choice represents a much better compromise between time to spec and required control torque.

SLEW PERIOD (MIN.)	TIME TO SPEC (MIN.)	TIME TO GOAL (MIN.)	PEAK CMG TORQUE (FT-LB.)	
1.0	4.3	6.7	920 (5.2 X Goal)	
1.5	4.2	6.7	430 (2.6 x Goal)	TIME OPTIMAL!
2.0	4.4	7.0	280 (1.6 x Goal)	
2.5	4.7	7.2	200 (1.1 X Goal)	BETTER COMPROMISE!

STABILITY/ROBUSTNESS PROPERTIES FOR FINAL CONTROL DESIGN

Robustness to unstructured uncertainty, as measured by multivariable singular value analyses of sensitivity and complementary sensitivity, was mixed for this control design. That at the output (design point) was good since it allows sensor uncertainty as large as 67 percent. That at the input was poor since it only allows actuator uncertainty as large as 10 percent. This poor robustness is due to the standard problem of achieving good robustness an evaluation point different than the design point. It is further aggravated by the ambiguity in controlling only three rigid-body rotation modes at low frequency with six inputs and six outputs.

Robustness to modal parameter uncertainty, as measured by structured singular value analysis for real perturbations, is quite encouraging. Allowable relative error variations in all parameters of 24 percent or more are reasonable for the first few modes in a dynamic model. Even greater robustness to modal frequencies would be highly desirable, however.

ROBUSTNESS TO UNSTRUCTURED UNCERTAINTY (SVs): SENS./COMP. SENS.

- Good At Output : $\sigma \leq 1.5 \Rightarrow$ 67% Sensor Uncertainty (Design Point)

- Poor At Input : $\sigma \leq 10 \Rightarrow$ 10% Actuator Uncertainty

- Poor Input Robustness At Low Frequency Due To
  - Evaluation Point Different From Design Point
  - Six Inputs/Outputs With Only Three RB Modes (Rotations)

ROBUSTNESS TO MODAL PARAMETER UNCERTAINTY (REAL μ):
ALLOWABLE VARIATIONS IN

- Mode Frequency $\leq$ 24% Of Nominal   ⎫
- Mode Damping $\leq$ 1200% Of Nominal   ⎬   For first 4 Flex Modes
- Mode Shapes (Input or Output) $\leq$ 63% Of Nominal ⎭

> THESE ALLOWABLE VARIATIONS ARE REASONABLE FOR FIRST FEW FLEXIBLE MODES!

SUMMARY

Performance results for this study can be summarized as follows. Control torque requirements for the nominal fast slew maneuver with nominal RCS jet placement are 500 times goal. Using a longer slew period with correspondingly shorter settling time buys a factor of 25 reduction in control torque, but this is still not enough. A new RCS jet placement using one additional jet allows a factor of 70 reduction in boom bending excitation. An LQG/LTR control design for the fast slew maneuver using the new RCS jet placement meets performance specifications within a 5 min settling period and performance goals within a 7 min period. This design also meets performance requirements for more modest slow slew and target tracking maneuvers, and could meet goal in the face of solar and gravity gradient torques with minor redesign.

PERFORMANCE

- Control Torque Requirements For Fast Slew Maneuver
  (1 min. Slew + 5 min. Settling) Using Nominal RCS Jet Placement
  Are Unacceptable (500 X SKLYLAB)

- Using Longer Slew Period (~3 min.) With Shorter Settling Time (~ 3 min.)
  Allows Substantial Reduction In Control Torque (20 X SKYLAB)
  ...But, Not Enough!

- New RCS Placement, Using One Additional Jet, Allows Factor Of 70
  Reduction In Beam Bending Excitation!

- LQG/LTR Control Design Performance For New RCS Placement
  And SKYLAB-Sized CMGs Meets

  - 35 μ rad Spec Within 5 min. For Fast Slew Maneuver

  - 3.5 μ rad Goal Within 7 min. For Fast Slew Maneuver

  - 35 μ rad "Spec" Throughout Slow Slew Maneuver } Not Presented
  - 3.5 μ rad Goal For Target Tracking   } Here!

- Control Performance In The Face Of Solar Torques Nearly Meets Spec,
  And Could Meet Goal With Minor Refinements To Control Design!
  (Also Not Presented Here!)

SUMMARY (CONT.)

Robustness to unstructured uncertainty was mixed for this control design. That at the input (design point) was good since it allows sensor uncertainty as large as 67 percent. That at the output was poor since it only allows actuator uncertainty as large as 10 percent. A dual LQG/LTR control design procedure with loop transfer recovery at the input would reverse these results. More sophisticated design techniques would allow a better compromise between input and output robustness.

Robustness to modal parameter uncertainty is quite encouraging. Allowable relative error variations in all parameters of 24 percent or more are reasonable for the first few modes in a dynamic model.

ROBUSTNESS TO UNSTRUCTURED UNCERTAINTY

- Good At Output: $\sigma \leq 1.5 \Rightarrow$ 67% Sensor Uncertainty
  (Design Point)

- Poor At Input: $\sigma \leq 10 \Rightarrow$ 10% Actuator Uncertainty

- LQG/LTR With Input Recovery Reverses These Results

- More Sophisticated Design Techniques (μ Synthesis)
  Could Achieve A Better Compromise Between Input and Output

ALLOWABLE VARIATIONS IN MODAL PARAMETERS

- 24% for Mode Frequencies

- 1200% for Mode Dampings

- 63% for Mode Shapes (Input or Output)

RECOMMENDATIONS

The final LQG/LTR control design would require at least two modifications before practical implementation: further refinements to meet performance in the face of solar and other environmental disturbances and compensator simplification via model reduction. A number of more fundamental research issues might also be addressed to achieve improved robustness to unstructured and parametric uncertainty. Ultimately more efficient methods for analysis of robustness to parametric uncertainty would be desirable.

FINAL LQG/LTR CONTROL DESIGN REQUIRES

- Further Refinements To Meet Performance Specs (Goals) In The Face Of Solar And Other Environmental Disturbances

- Simplication Via Model Reduction Before Practical Implementation

MORE FUNDAMENTAL RESEARCH ISSUES

- Improved Robustness At Both Input And Output (μ Synthesis)

- Improved Robustness At Input And/Or Output When Number Of Rigid-Body Modes Is Less Than Number Of Controls Or Measurements

- Improved Robustness To Parametric Uncertainty (e. g., Mode Frequencies)

- More Efficient Methods For Analysis Of Robustness To Parametric Uncertainty

LARGE SPACE SYSTEMS TECHNOLOGY AND REQUIREMENTS*

James M. Romero
National Aeronautics and Space Administration
Washington, D.C.

*Viewgraphs only; original figures not available at time of publication.

NASA SPACE EMPHASIS

☒ RECONSTITUTE SHUTTLE CAPABILITY

☒ MAINTAIN SPACE STATION MOMENTUM

☒ RESOLVE SCIENCE MISSION BACKLOG

AND

☒ REBUILD TECHNOLOGY BASE

STATE OF TECHNOLOGY

☒ TECHNOLOGY BASE IS DEFICIENT
   - LIVING OFF PAST
   - TECHNOLOGY NO LONGER LEADS WITH
     SOLUTIONS... IT CHASES PROBLEMS

☒ EXPECTATIONS EXCEED WHAT TECHNOLOGY
   CAN DELIVER

☒ U.S. LEADERSHIP CHALLENGED

☒ DECLINE OF NASA EXPERTISE

SPACE R & T FUNDING TREND

(CONSTANT FY 87 DOLLARS)

($,M)

(EXCLUDES NUCLEAR ELECTRIC & NUCLEAR ROCKET PROGRAMS 1965-1973)

FISCAL YEAR
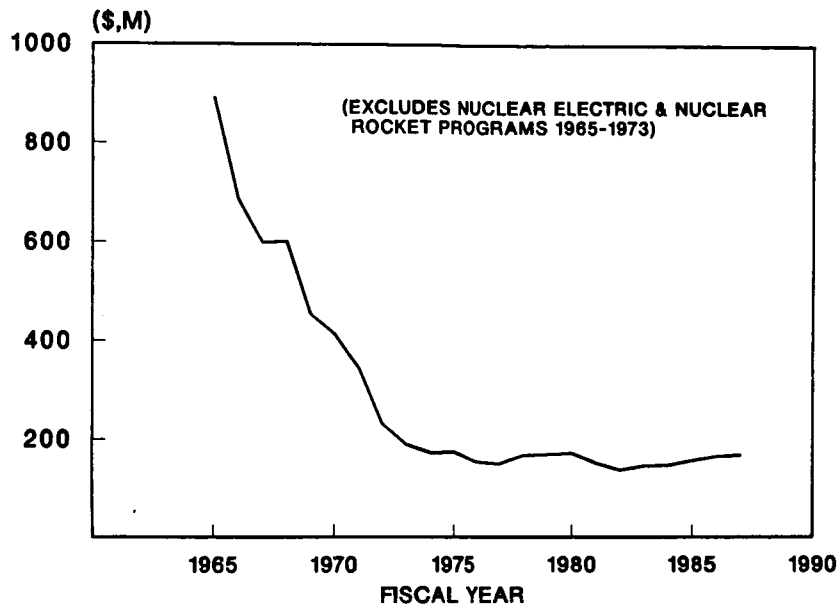
CIVIL SPACE TECHNOLOGY INITIATIVE

FOCUSED THRUSTS
TO REMEDY GAPS
IN TECHNOLOGY BASE
TO ENABLE HIGH PRIORITY PROGRAMS

CSTI FOCUS

- ☒ **PROPULSION**
  - EARTH-TO-ORBIT
  - ORBIT TRANSFER
  - BOOSTER TECHNOLOGY

- ☒ **VEHICLE**
  - AEROASSIST FLIGHT EXPERIMENT

- ☒ **INFORMATION SYSTEMS**
  - SCIENCE SENSOR TECHNOLOGY
  - DATA: HIGH RATE/CAPACITY

- ☒ **LARGE STRUCTURES AND CONTROL**
  - CONTROL OF FLEXIBLE STRUCTURES
  - PRECISION SEGMENTED REFLECTORS

- ☒ **POWER**
  - HIGH CAPACITY
  - SPACECRAFT

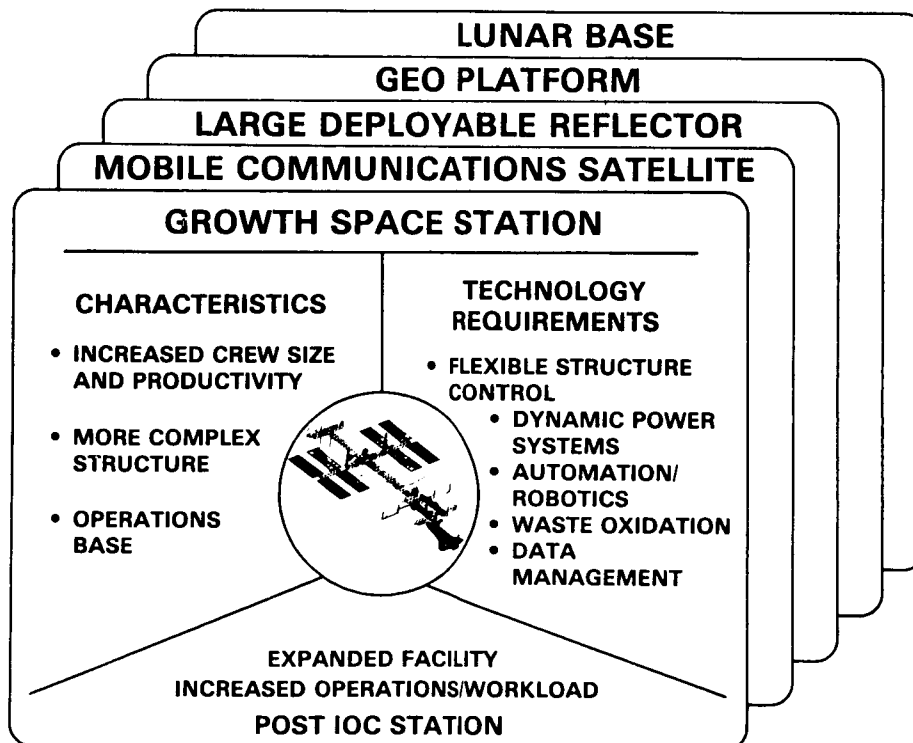- ☒ **AUTOMATION AND ROBOTICS**
  - ROBOTICS
  - AUTONOMOUS SYSTEMS

OAST RESPONSIBILITY IS TO DEVELOP TECHNOLOGIES

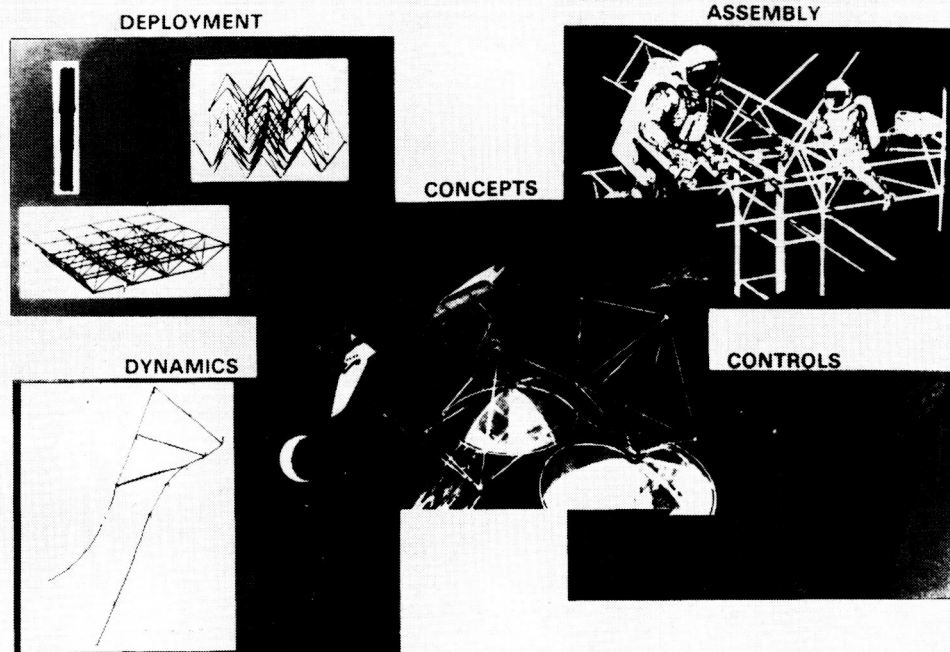## THAT WILL ENABLE OR ENHANCE FUTURE NATIONAL MISSIONS
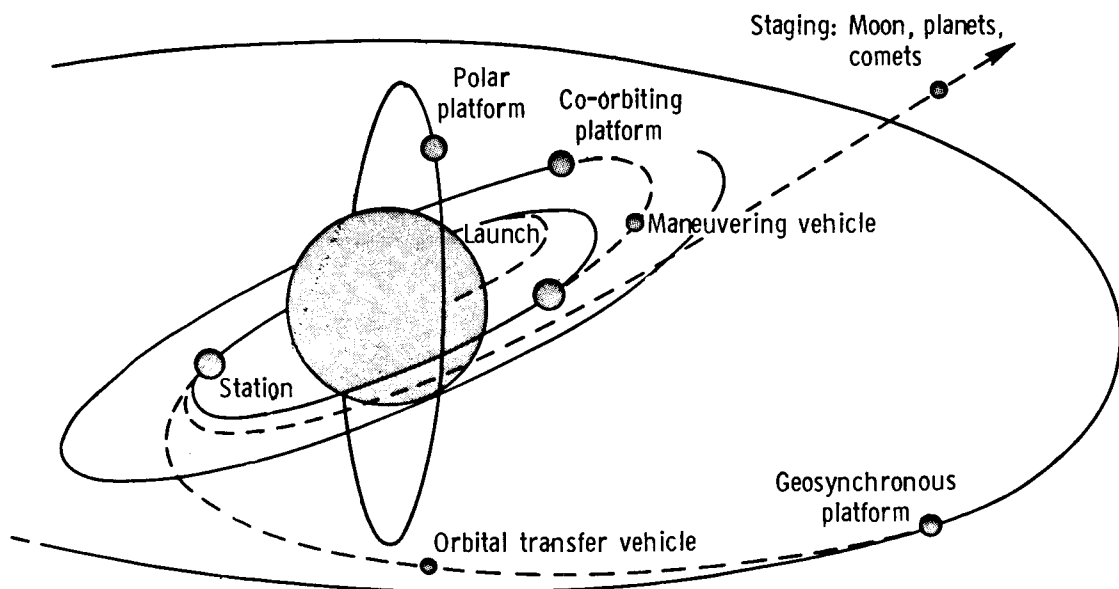
PROGRAM FOCUS ON DRIVER MISSIONS

	1980's	1990's	2000's	2010's
TRANSPORTATION	SSME IMPROVEMENTS	ADVANCED CRYO ENGINE, SPACE BASED OTV, SHUTTLE REPLACEMENT, HEAVY LIFT VEHICLES		TRANSLUNAR OTV
SPACECRAFT	COMET RENDEZVOUS	SATURN ORBITER TITAN PROBE, MARINER MARK II, EARTH OBSERVING SYSTEMS, LEO	MARS/COMET SAMPLE RETURN, GEO CONTINUOUS COVERAGE, PLANETARY PROBES	OUTER PLANET ORBITERS
LARGE SPACE SYSTEMS		IOC SPACE STATION, GROWTH SPACE STATION, MOBILE COMMUNICATIONS SATELLITE, 5M 20M 50M	GEO PLATFORM, LARGE DEPLOYABLE REFLECTOR	LUNAR BASE

LARGE SPACE SYSTEMS

LUNAR BASE
GEO PLATFORM
LARGE DEPLOYABLE REFLECTOR
MOBILE COMMUNICATIONS SATELLITE
GROWTH SPACE STATION

CHARACTERISTICS

- INCREASED CREW SIZE AND PRODUCTIVITY

- MORE COMPLEX STRUCTURE

- OPERATIONS BASE

TECHNOLOGY REQUIREMENTS

- FLEXIBLE STRUCTURE CONTROL
  - DYNAMIC POWER SYSTEMS
  - AUTOMATION/ROBOTICS
  - WASTE OXIDATION
  - DATA MANAGEMENT

EXPANDED FACILITY
INCREASED OPERATIONS/WORKLOAD

POST IOC STATION

LARGE FLEXIBLE STRUCTURES
AND THEIR CONTROL

DEPLOYMENT
ASSEMBLY
CONCEPTS
DYNAMICS
CONTROLS

LARGE HABITATS

LARGE DEPLOYABLE REFLECTOR
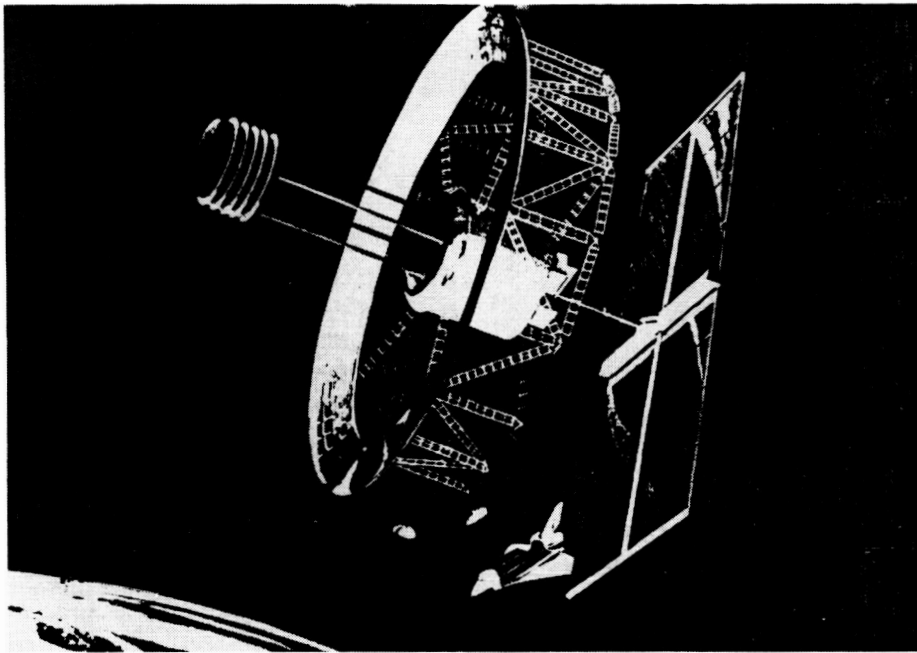
LUNAR BASE TECHNOLOGIES

- LOW "G" STRUCTURES
- LONG LIFE POWER
- CLOSED LIFE SUPPORT
- RADIATION PROTECTION
- TELEROBOTICS
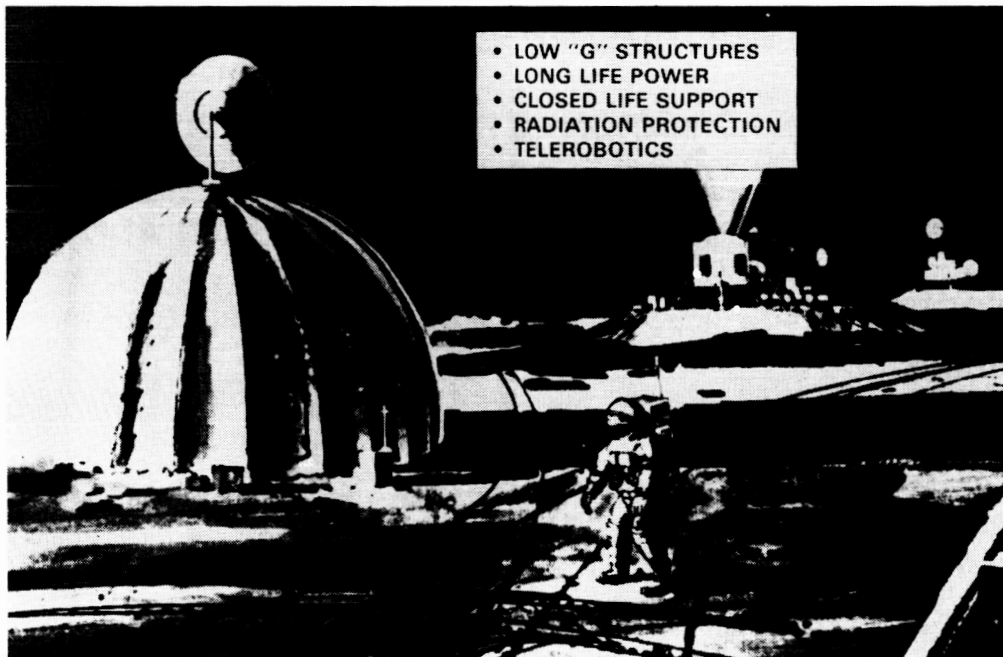
IN-SPACE TECHNOLOGY EXPERIMENTS

AN EXPONENTIALLY EXPANDING PROGRAM
DRIVEN BY THE CONVERGENCE OF:

USER NEEDS	&	SPACE FACILITIES

• RESEARCH
  - MATERIALS
  - FLUIDS
  - DEVICES
  - STRUCTURES, CONTROLS
 	
• DEMONSTRATION
  - PROOF OF CONCEPT
  - ENGINEERING DEMO
  - FLIGHT QUALIFICATION
		• SHUTTLE
		  - PAYLOAD BAY
		  - MID-DECK
		  - CANNISTERS
		  - HITCHHIKERS
		
		• SPACE STATION
		  - INTERNAL PAYLOADS
		  - EXTERNALLY MOUNTED
		  - TECHNOLOGY LAB. MODULE
		  - PLATFORM BASED
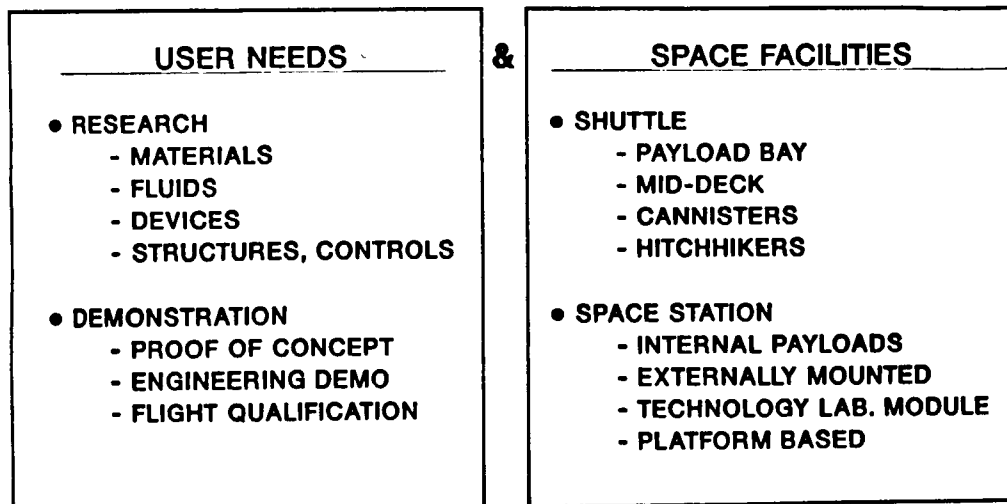
IN-SPACE R & T APPROACH

☒ ESTABLISH OAST AS NATIONAL FOCAL POINT FOR IN-SPACE R&T

☒ COORDINATE USER COMMUNITY REQUIREMENTS AND PLANS

- WORKSHOPS
- SYMPOSIA

☒ STIMULATE COOPERATIVE VENTURES

- OUTREACH
- GUEST INVESTIGATOR

IN-SPACE EXPERIMENT PROGRAM POTENTIALS

LAUNCH MASS (KG × 10³)

COST ($M)

NSSD (CIVIL TECHNOLOGY) LAUNCH MASS PROFILE

INDUSTRY & OTHER GOV'T FUNDING

PROJECTED OAST FUNDING

30 — — 300

20 — — 200

10 — — 100

84 86 88 90 92 94 96 98

YEAR
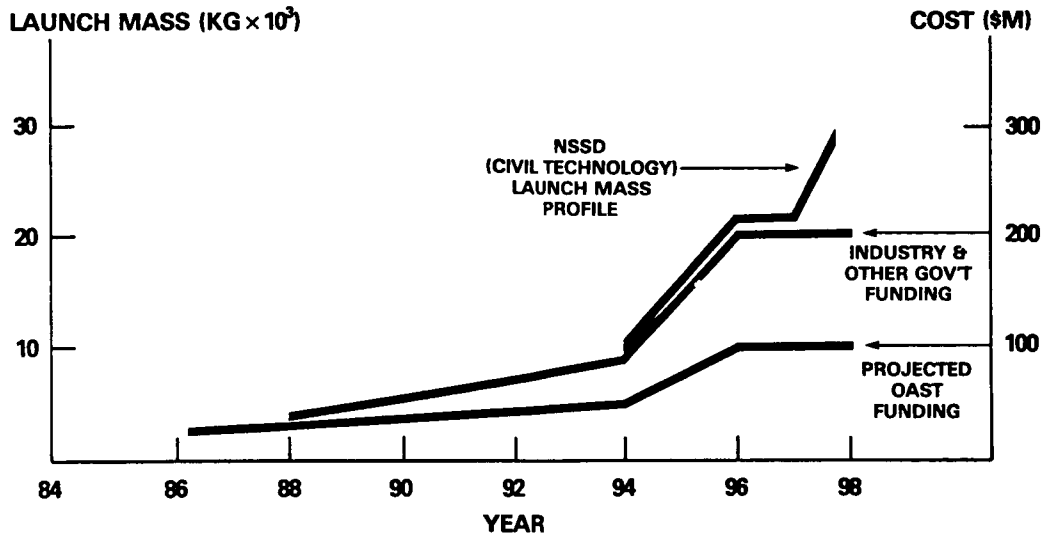
WHAT A STRONG TECHNOLOGY PROGRAM BUYS

- ADDED TECHNOLOGY OPTIONS

- INCREASED MISSION CAPABILITIES

- ADDED MISSION OPPORTUNITIES

- REDUCED DEVELOPMENT AND OPERATING COSTS

DESIGN, CONSTRUCTION, AND UTILIZATION OF A SPACE STATION
ASSEMBLED FROM 5-METER ERECTABLE STRUTS

Martin M. Mikulas, Jr. and Harold G. Bush
NASA Langley Research Center
Hampton, Virginia

ABSTRACT

This paper presents the primary characteristics of the 5-meter erectable truss which has been baselined for the Space Station. The relatively large 5-meter truss dimension was chosen to provide a deep beam for high bending stiffness yet provide convenient mounting locations for space shuttle cargo bay size payloads which are ~14.5 ft. (4.4 m) in diameter. Truss nodes and quick-attachment erectable joints are described which provide for evolutionary three-dimensional growth and for simple maintenance and repair. A mobile remote manipulator system is described which is provided to assist in station construction and maintenance. A discussion is also presented of the construction of the Space Station and the associated extra-vehicular activity (EVA) time.

INTRODUCTION

The truss structure is a key element in enabling the Space Station to be a highly versatile facility capable of essentially unlimited evolutionary growth and use. Construction of the Space Station is planned in the 1990's and it is expected to provide a space operation base for the next 20 years or more. Due to this long life it is important that the truss structure be capable of evolutionary growth in all three dimensions, and be capable of easily accommodating unanticipated alterations. It should be capable of accommodating a wide variety of shuttle-compatible payloads in a customer friendly fashion with a minimum of interference to growth and station operations. The truss must also provide a stiff and stable framework to: (1) minimize structure-control interaction, (2) simplify the pointing systems of stellar, solar, and earth observation instruments, and (3) accommodate micro-g experiments. Several truss structures which have been considered for the Space Station are described in ref. 1. A trade study which dealt in depth with the merits of the various trusses is presented in ref. 2. In ref. 2, it was concluded that the most desirable truss for the Space Station should be as deep as possible for maximum bending stiffness and for minimum weight and part count. However, the truss should also be sized to be compatible with space shuttle cargo bay size payloads. With these considerations in mind, a 5-meter-deep, square cross-section truss has been baselined for the Space Station support structure. Another feature of the 5-meter erectable truss is that it is constructed in a cubic arrangement using three-dimensional nodal clusters that permit architectural evolution for construction and growth in three orthogonal directions.

A major consideration in the design of the Space Station is on-orbit construction. In ref. 2 a trade study was conducted of deployable and erectable trusses for the Space Station. The study showed that deployable trusses, though

*NASA TM-89043.

676

attractive for space trusses because of the reduced EVA required for initial construction, are limited in size due to launch volume constraints. Erectable trusses offer the freedom to configure and size the truss size to operational needs. Thus the decision is to choose between reduced EVA construction hours for initial assembly of the deployable truss, or the additional bending stiffness and architectural freedom offered by the larger erectable truss. In January 1986, the 5-meter erectable truss was selected as a baseline for the Space Station. This paper summarizes the primary operational characteristics and structural details of the current baseline truss.

DUAL-KEEL STATION

The current baseline 5-meter truss, Dual-Keel Space Station is shown in fig. 1 and schematic details are shown in fig. 2. As shown in the side view, the two vertical keels fly in a gravity gradient earth pointing mode. The outboard solar power systems rotate relative to the central portion of the station to continuously point to the sun. The two long vertical keels (110 m.) are to provide space for mounting the numerous payloads to be attached to the station. The pressurized living modules are placed at the center of gravity of the Space Station to minimize artificial gravity effects. Stellar pointing payloads are placed on the upper transverse boom, while earth pointing payloads are placed on the lower transverse boom. The solar power systems are widely spaced to reduce plume impingement problems and contamination from the space shuttle during docking. The 5-meter truss provides a stiff support for the pressurized modules, the solar power systems, and numerous stellar and earth-pointing payloads. The Space Station will have several independent pointing control systems; thus, the truss should be stiff to avoid excessive interaction among these control systems. Since the station is too large to be assembled and tested on the ground, it is necessary that the structural response be linear and predictable for control purposes.

TRUSS REQUIREMENTS

There is no precedent for an on-orbit structure as large and complex as that being considered for the Space Station. The truss structure must provide a stiff, redundant framework to support massive pressurized modules, a large solar power system, and numerous scientific payloads, many of which require accurate pointing systems. It must be designed to permit the integral attachment of large protective hangars and to provide a location for the construction of other large spacecraft. The primary requirements which drive the truss design are:

o   Stiffness, Mass, and Cost
o   Customer Accommodations
     Payloads, Growth, Spacecraft Construction
o   Space Station Operations
     Payload Movement, Maintenance, Servicing
o   Space Station Construction
     EVA Time, Reliability and Safety, Construction Experience

In the present paper these four requirements will be discussed and it will be shown how they entered into the selection of the 5-meter erectable truss for the Space Station.

In this section the stiffness, mass, and cost of truss structures are compared as a function of the depth of the truss. In all cases the truss bays are assumed to be cubic and only the size is varied. Since the Space Station truss is stiffness designed, the struts are assumed to be constructed of high modulus graphite/epoxy.

The struts are assumed to be clad inside and out with aluminum to protect against erosion due to atomic oxygen, eliminate out-gassing, and provide a mechanism to tailor the coefficient of thermal expansion of the strut. The nominal strut is assumed to have a wall laminate as follows:

Aluminum layer	.006"	(.152 mm)
P-70 Gr/Ep layer	.060"	(1.52 mm)
Aluminum layer	.006"	(.152 mm)
Total Wall Thickness	.072"	(1.83 mm)

Average Density = .068 lb/in^3 (1880 Kg/m^3)
Average Modulus ~ 40 x 10^6 psi   (276 GPa)

The relative thickness of aluminum and graphite/epoxy was chosen to achieve a nominal zero coefficient of thermal expansion in the strut.

The operational loads experienced by the Space Station are very low due to the zero-g environment. The largest loads are a result of docking with the Space Shuttle. Attenuators are being designed for the docking maneuver so that even those loads will be small. Thus, the primary structural requirement for the truss is that of high stiffness to minimize structure-control interaction and to minimize the magnitude and duration of transient responses.

Part Count. The effect of truss size on part count is shown in fig. 3. As shown in the top two sketches, the total length of strut material required to construct a beam is independent of the depth of the beam. Further, the number of parts in such beams is inversely proportional to the beam depth. The lower sketches show that the number of parts for a two-dimensional area type truss is inversely proportional to the square of the depth. For area trusses, the length of struts per unit of area covered increases linearly as the strut length decreases. Because of these size characteristics, longer length truss struts result in lower total weight and cost. There are practical limits, however, to the maximum length of the individual struts for different applications. In the case of the Space Station, the upper limit to the strut length was selected to make the truss compatible with payloads having the diameter of the Space Shuttle cargo bay. The maximum payload diameter for the cargo bay is 14.5 ft. The truss strut length was chosen to be 5-meters (16.4 ft.) to permit a clearance between the truss and payload for operations.

Truss Mass and Stiffness. The mass and part count for the current Dual-Keel Space Station 5-meter erectable truss is shown in fig. 4-a as a function of beam depth. These results show that for struts of constant wall thickness, a 3-meter deep beam would be 20 percent heavier than a 5-meter deep beam. If the bending stiffness of the beam were constrained to be equal to the 5-meter truss, the weight of the smaller depth beams increases dramatically. It is shown in the figure that a 3-meter deep beam of equal bending stiffness would weigh twice as

much as a 5-meter deep beam. Due to the added launch cost for the extra weight and the higher costs for the material, the smaller depth beam is considerably more expensive to put in orbit. Another factor that affects this trade is assembly time which is almost directly proportional to the number of parts to be handled. Again, the deeper truss shows an advantage (e.g., reduced assembly time).

The importance of stiffness of the Space Station truss was studied in ref. 3. In ref. 3, a detailed finite element analysis of the station indicated that the framework frequencies of the 5-meter configuration were almost double those of the 9-ft. bay configuration. This increase results in reduced dynamic response as shown by an example of results from ref. 3, in fig. 4-b. This figure shows a continuous trace of the flexible sunline at the outer solar dynamic collector during a reboost maneuver. The maximum allowable angular excursion for the solar dynamic system is 0.1 degree. The angular excursions for the 9-foot truss are three times as great as the 5-meter truss and as can be seen in the figure, there is very little margin for the 9-foot truss system. These results are typical of other examples studied in ref. 3 and demonstrate the importance of the increased stiffness offered by the 5-meter strut construction.

OTV Hangar Construction. The OTV hangar is representative of a number of protective hangars that are anticipated on the Space Station. Construction of the support truss for the hangar is also typical of the construction that will be required for other large space systems to be built on the Space Station. In fig. 5 a comparison is given for constructing a hangar from 9-ft. struts and 5-meter (16.4 ft.) struts. As can be seen in the figure, a 9-ft. strut hangar requires three times as many struts and nodes as a 5-meter strut hangar. The weight of the 9-ft. strut hangar is twice the weight of a 5-meter strut hangar and the construction time is about three times as long. These differences are significant and are an indication of the long term benefits that will result from the 5-meter strut construction approach.

CUSTOMER ACCOMMODATIONS

The Space Station is planned to be placed in orbit in the early 1990s and is expected to provide a space operations base for the next 20 years or more. It is highly likely that the functional use of this space base will continually evolve as operational experience accumulates. For this reason it is important that the truss structure, which forms the backbone of the station, be capable of evolutionary change and growth in all three dimensions and must readily accommodate unanticipated changes. The truss structure must accommodate a wide range of shuttle-compatible payloads with minimum interference to growth and station operations.

Growth Potential. To provide a truss with growth capability in all three dimensions, it is necessary that the nodal cluster at the intersection of the struts be designed so that struts in all dimensions can be added as needed. Such a node is shown schematically in fig. 6 for an orthogonal truss. To permit complete three-dimensional growth of such a truss, it is necessary that each node possess 18 strut attachment positions. There are 6 strut attachment positions in the x, y, and z directions, and 12 strut attachment positions at 45 degrees to the coordinate axes for the diagonals. For the current baseline node, 8 additional strut attachment positions are provided for attachment of payloads. These 8 positions are shown as triangles on the node in fig. 6. The direction of these positions coincides with a diagonal line which passes through

the center of the cube. A photograph of such a node is shown in fig. 7 with two quick attachment erectable joints. Such spherical nodes have been used for many years in the construction of ground structures and there is a large body of knowledge relative to their use. The main difference in the current node is the use of quick attachment joints to minimize the EVA effort required to assemble the structure. For applications in space, the node would be shipped to orbit with the necessary number of quick attachment joints bolted in place to construct the initial structure. Extra joints could be attached initially or could be bolted on in orbit if needed for growth.

Payload Accommodations. The most common types of payloads to be accommodated by the station are either small instruments or experiments, or large cargo-bay-sized payloads. It is likely that even the smaller payloads will be integrated onto a standardized pallet in the shuttle/station mission system. For launch efficiencies, this pallet would likely be sized to make maximum use of the cargo bay volume (pallet size is approximately 14.5 ft. in diameter). Most larger payloads (storage tanks, large instruments, spacecraft, etc.) will also be sized to maximize use of the cargo bay. The 5-meter truss has been sized specifically to be compatible with cargo-bay-sized payloads. The payloads can be attached to the interior or exterior of the truss with no interference to adjacent bays. This feature is important to minimize congestion on the station and to ensure that attached payloads do not interfere with operations such as payload movement and additional construction.

A schematic showing the growth capability of the 5-meter truss is shown in fig. 8. As can be seen in the schematic, the payloads are attached to the cubic diagonal attachment positions. Such an attachment scheme does not interfere with structural attachment positions so that the truss can be constructed over previously attached payloads for growth if desired. It is also shown that cargo-bay-sized payloads fit nicely within each truss bay and do not interfere with operation of the mobile remote manipulator system (MRMS).

The growth shown in fig. 8 could occur in a gradual, evolutionary fashion using the erectable method of construction. Because of the high redundancy of the truss, many selected struts may be omitted to enhance accessibility or to accommodate payloads longer than one bay.

A sketch of an octagonal cargo bay sized pallet is shown attached to the 5-meter structure in fig. 9. Attachment arms which would fold to fit in the cargo bay are shown in the inset. A payload attachment fixture is shown attached to the truss node in a cubic diagonal position, and the pallet arm with a simple protrusion connector is shown in position prior to insertion and lock up. Since the four longeron truss is redundant, the face diagonal can be removed for payload insertion without destroying the integrity of the truss. In a multiple bay keel or in an area where there are many bays, the high redundancy of the truss would permit the diagonal to be permanently omitted if desired. Such a subsurface attachment of the pallet permits complete unobstructed movement and operation of the MRMS over the truss surface yet still provides access for servicing.

For some payloads it may be necessary to provide protection from propulsion plumes, radiation, micrometeoroids, or to provide thermal control. A concept for providing such shielding is shown in fig. 10. In this concept, deployable "curtains" would be added as needed to provide the protection necessary. A hatch would be provided for access and, as can be seen in the figure, the

5-meter truss provides a large interior volume for servicing. An alternate, more highly preintegrated system is shown in fig. 11. In this concept, an octagonal pallet similar to that shown in fig. 9 would have a collapsible protective covering attached which would be deployed on-orbit. A hatch is shown on top of the shield for access. Such a system could provide protection from plume contamination by the shuttle during docking maneuvers and the hatch could be left open during other times. The high versatility for attaching payloads is shown in fig. 12. The upper left hand sketch demonstrates how a cargo bay size storage tank longer than one truss bay may be accommodated. The other sketches demonstrate the capability of the 5-meter truss for accommodating a variety of space shuttle type payloads.

SPACE STATION OPERATIONS

The construction, operation, and maintenance of the Space Station will require numerous on-orbit operations of unprecedented complexity and duration. The truss, being the basic support structure for the station, must be designed to facilitate these operations in a reliable, safe fashion. The truss must support the pressurized modules, the subsystems, and all utility lines. Since these are widely dispersed on the station, there must be some means to transport materials and to support EVA or robotic operations.

Transport Systems. A mobile transport system designed to support Space Station operations is presented in refs. 4 and 5. A sketch of this system called the mobile remote manipulator system (MRMS) is shown in fig. 13. The transporter is attached to guide pins which are provided at each node of the truss. Mobility is provided by a push-pull draw bar which can move the mobile transporter one bay at a time. The transporter can turn 90 degrees and move in orthogonal directions. The transporter can also change planes to accomplish movement in all three dimensions. Thus, the combination of the cubic truss and MRMS represents a versatile system in which construction and operations can be accomplished in all three dimensions. Two mobile foot restraints are provided on the MRMS to provide astronauts, and possibly robots, with a positioning device to assist in construction and maintenance operations. A remote manipulator system (RMS) similar to the shuttle RMS is also provided to assist in material movement and positioning.

An alternate technique for maintenance and servicing is to provide a smaller mobile transporter inside the truss. This transporter could either be on rails or operate on internal guide pins in a fashion similar to the MRMS. A schematic of such a transporter is shown in fig. 14. In this figure the transporter is shown operating on rails and a robot is attached for servicing. The same concept could be used to provide mobility and support for an astronaut.

A simple system for transporting an astronaut about the station which is under consideration is a monorail, two truss bays long, which operates on the MRMS guide pins. A battery driven endless belt or chain would provide the mobility for the system. The astronaut would be attached to a controllable foot restraint which would provide a stable work platform to facilitate maintenance or servicing. A similar system could also be used for robotic operations.

Spacecraft Construction. One anticipated use of the Space Station is to serve as a base for constructing other spacecraft. The 5-meter erectable truss and the MRMS represent a versatile system for conducting a wide variety of construction scenarios. The truss can be expanded to provide the necessary area

for construction and the MRMS can provide the capability to move materials and support construction operations.

Crew Safety and ACCESS. The 5-meter erectable truss has been designed specifically to accommodate manual assembly by astronauts. The diameter of the quick attachment end joints as shown in fig. 15 was limited to 2 inches to be compatible with a pressured glove. The joints and struts were kept smooth and snag free for safety reasons. As can be seen in fig. 16, the whole truss system (struts and joints) has been kept as hazard free as possible to facilitate safe astronaut operations.

A major consideration in the design of the truss is to provide adequate access for a space suited astronaut. For comparison purposes, an astronaut is shown inside of two different size truss in fig. 17. The astronaut is shown outfitted with a Manned Maneuvering Unit (MMU). It is anticipated that the MMU will be used for some Space Station operations. As can be seen in the figure, mobility and access in a 9-foot truss would be quite limited while there is ample access in a 5-meter truss.

SPACE STATION CONSTRUCTION

Detailed studies have been conducted on various approaches for constructing the Space Station on-orbit. Both erectable and deployable trusses for the Space Station are discussed in ref. 1, and a detailed trade study of the different approaches is presented in ref. 2. As mentioned previously, the 5-meter truss is desirable for the Space Station for high bending stiffness and size compatibility with space shuttle payloads. However, since it must be erected strut by strut on-orbit, the alternative of a smaller truss which could be folded like an accordion and deployed on orbit must be considered.

EVA Construction Hours. In ref. 2 the trade-offs between deployable and erectable approaches are discussed in detail. A significant issue involved in that trade study is the amount of EVA required to construct the station. Results presented in fig. 18 show that the initial station can be constructed in seven shuttle flights. As expected, the station with deployable structure takes less time to construct than the erectable version. However, due to the large number of subsystems that must be installed on-orbit in both cases, the difference between total construction time is small. In fact, the advantages gained from the 5-meter truss over the 20 year lifetime of the station outweigh the extra EVA hours required for initial assembly.

For the erectable structures, the construction times used in these studies were taken from neutral-buoyancy assembly tests conducted on a large truss beam with 18 ft. struts (ref. 6). The results were also validated by a shuttle flight experiment where 10 bays of an erectable structure were assembled on-orbit (ref. 7). These tests will be discussed later in this section. Since there is no experience with deployable structures in this size range, engineering estimates were made of the construction times.

Construction Experience. Prior to 1980, studies were conducted of techniques for erecting large structures on orbit. Timeline investigations were performed both analytically and by testing in a neutral buoyancy facility. The earliest neutral buoyancy tests involved pressure suited test subjects erecting a truss with 18 ft. long struts with no assembly aids. The test subjects reported that unassisted assembly was very difficult and tiring. An assembly aid was then

682

designed to provide mobile foot restraints for the test subjects, and to provide an assembly line like assembly fixture for the truss. This device, called a mobile work station is shown in fig. 19. In fig. 19, two astronauts are shown in the mobile foot restraints constructing the truss. The foot restraints can position the astronauts at any point required to construct a single bay. After one bay is completed, an endless chain moves the truss on a rail in an assembly line fashion so that the next bay can be constructed. These underwater construction studies indicated that such structures could be space erected at the rate of one strut every 38 seconds.

Flight Experiments. In November 1985, a 10-bay truss was erected on-orbit by two astronauts out of the space shuttle cargo bay (refs. 7 and 8). In this experiment called ACCESS, the two astronauts were in fixed foot restraints while the truss was on an assembly fixture that could be rotated and registered one bay at a time as the truss was erected (fig. 20). A photograph of the actual on-orbit assembly is shown in fig. 21. The results of these tests are given in fig. 22. In this test the 10-bay truss comprised of 96 struts was constructed in 25 minutes on-orbit. Although this truss is smaller than that being considered for Space Station, the test results clearly demonstrated the practicality and economy of erected trusses on-orbit. During the ACCESS flight test the astronauts detached the 10-bay-long truss from the shuttle to demonstrate truss manipulation on-orbit. The astronauts indicated that the open truss was relatively easy to maneuver on-orbit. After the manipulation demonstration, they readily reattached the truss to the assembly fixture, and disassembled and restowed the truss.

The ACCESS flight experiment provided valuable data in validating neutral buoyancy zero-g construction simulations. The flight test demonstrated that neutral buoyancy simulations are quite good for an ACCESS size truss. The need for a flight experiment to assist in the development of construction techniques for a 5-meter truss Space Station is currently being evaulated. A study of a large scale flight experiment was conducted and reported on in ref. 9. This study considered the construction and dynamic testing of a "T"-shaped truss 16-bays long with a 5-bay wide cross member, as shown in fig. 23. The length and geometry of the truss was chosen to achieve low bending and torsional frequencies for on-orbit dynamic testing. The results of this study indicated that one-half of the space shuttle cargo bay would be required to place such an experiment in orbit. The results also indicated that two 6-hour EVAs would be required to construct and test the structure. A sequence of the construction process for the first 6-hour EVA is shown in figs. 24, 25, and 26. The remaining 8 truss bays are constructed and utility lines are installed during the second EVA which is not shown. These studies of the construction process for the flight experiment verified that construction of the Space Station from 5-meter erectable struts was indeed practical.

Such a flight experiment would provide an interim step toward the construction of large structural systems such as the Space Station. In-orbit dynamic tests could be conducted to provide insight into the 0-gravity dynamic response predictability of such truss structures. Due to the large economic resources required to conduct such a test, however, it may be prudent to combine the test with early construction of a portion of the station.

An alternate flight experiment would be to construct a truss of about 5 bays on-orbit. Due to the highly reduced number of struts to be constructed, a less elaborate assembly aid could be used. For example, the shuttle RMS could

provide the movable foot restraint for the construction process. Such a test
would provide information about the handling characteristics of such long struts
and details on joining techniques. The results again would be valuable in
calibrating neutral buoyancy simulations.

Once constructed, such a truss could be left on-orbit to provide a test facility
for future flight experiments. A schematic of such a test bed is shown in fig.
23. The experiments to be tested on the orbiting truss would be built on
standard space shuttle pallets. The 5-meter truss is sized to handle such
payloads so installation would be the same as that for attaching experiments to
Space Station. All attachments would be of Space Station type so that the
experiment would provide early information on station operations as well as
providing an early test bed for scientific experiments.

CONCLUDING REMARKS

This paper presents primary characteristics of the 5-meter erectable truss
structure which has been baselined for the Space Station. A primary design
consideration for the Space Station is to provide adequate stiffness to minimize
structure-control interaction during operation. This consideration tends to
require the station truss to be as deep as possible to provide maximum beam
bending stiffness with the least structural mass. However, the truss must also
provide convenient attachment locations for space shuttle cargo bay size
payloads (~14.5 ft. in diameter).

These two considerations led to the 5-meter truss design for the Space Station.
The deep truss provides both high bending stiffness, and a lower number of
struts and nodes. This reduced part count is directly reflected in lower costs
and reduced construction time. The truss is compatible with shuttle
cargo-bay-sized payloads and reduces congestion on the station since every
payload can be contained within the dimensions of each truss bay. This is an
important consideration in simplifying long term operations on the station. A
truss node fitting was designed to permit the truss to grow in all three
orthogonal directions. This feature permits versatile evolutionary architecture
and, together with the quick-attachment erectable joint, provides a truss system
which can be readily repaired or updated with unanticipated alternations.

A mobile remote manipulator system (MRMS) is provided on the station to assist
in construction, maintenance, and spacecraft servicing and construction. The
cubic truss is designed to permit orthogonal movement of the MRMS in all three
dimensions. Guide pins are provided at each of the truss nodes for attachment
and movement of the MRMS. Detailed construction studies of each phase of the
Space Station construction have been conducted to ensure compatibility with
shuttle EVA resources. Although EVA timelines were slightly longer than
desirable for comfortable margins, studies are continuing to reduce the amount
of EVA required.

REFERENCES

1.   Mikulas, Martin M., Jr.; Croomes, Scott D.; Schneider, William; Bush,
     Harold G.; Nagy, Kornell; Pelischek, Timothy; Lake, Mark S.; and Wesselski,
     Clarence. Space Station Truss Structures and Construction Considerations.
     NASA TM-86338. (1985).

2. Mikulas, Martin M., Jr.; Wright, Andrew S., Jr.; Bush, Harold G.; Watson, Judith J.; Dean, Edwin B.; Twiggn, Leonard T.; Rhodes, Marvin D.; Cooper, Paul A.; Dorsey, John T.; Lake, Mark S.; Young, John W.; Stein, Peter A.; Housner, Jerrold M.; and Ferebee, Melvin J., Jr. Deployable/Erectable Trade Study for Space Station Truss Structures. NASA TM-87573. (1985).

3. Young, John W.; Lallman, Frederick J.; Cooper, Paul A.; and Giesy, Daniel P. Control/Structures Interaction Study of Two 300 KW Dual-Keel Space Station Concepts. NASA TM-87679. (1986).

4. Mikulas, Martin M., Jr.; Bush, Harold G.; Wallsom, Richard E.; Dorsey, John T.; and Rhodes, Marvin D. A Manned-Machine Space Station Construction Concept. NASA TM-85762. (1984).

5. Bush, Harold G.; Mikulas, Martin M., Jr.; Wallsom, Richard E.; and Jensen, J. Kermit. Conceptual Design of a Mobile Remote Manipulator System. NASA TM-86262. (1984).

6. Heard, Walter L., Jr.; Bush, Harold G.; Wallsom, Richard E.; and Jensen, J. Kermit. A Mobile Work Station Concept for Mechanically Aided Astronaut Assembly of Large Space Trusses. NASA TP-2108. (1983).

7. Heard, Walter L., Jr. and Watson, Judith J. Results of the ACCESS Space Construction Shuttle Flight Experiment. AIAA Paper No. 86-1186-CP, Presented at the AIAA Space Systems Technology Conference, San Diego, California, June 9-12, 1986. (1986).

8. Card, Michael F.; Heard, Walter L., Jr.; and Akin, David L. Construction and Control of Large Space Structures. NASA TM-87689. (1986).

9. Russell, R. A.; Raney, J. P.; and DeRyder, L. J. A Space Station Structures and Assembly Verification Experiment - SAVE. NASA TM-89004. (1986).
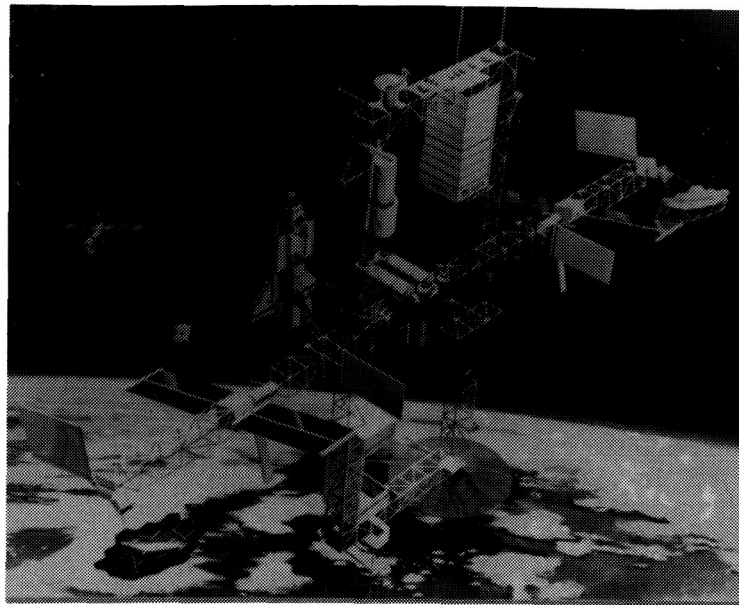
Fig. 1. Dual-Keel Space Station constructed with 5-meter struts.

Truss data

No. of struts   1100
No. of nodes   330
Truss mass   11,900 lbs
                 5,400 Kg

Top View

TDRS Antenna
Photovoltaic Array
Power Radiator
Solar Dynamic Collector
Remote Manipulator
RCS Thruster
Thermal Radiator
Front View

Flight Path
NADIR
Side View
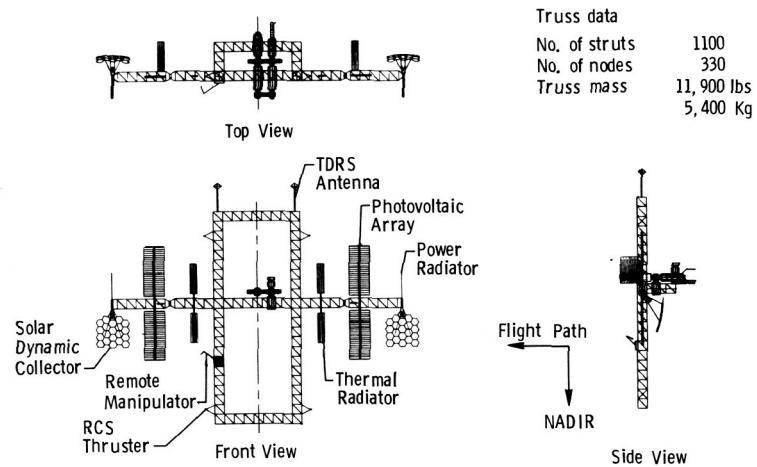
Fig. 2. Schematic of 5-meter truss, Dual-Keel Space Station.

26 struts
8 joints

13 struts
4 joints

Number of parts ~1/ℓ

Total length
of struts
Independent
of size

Larger beams are stiffer,
lighter and have fewer parts

Part count effect magnified in area trusses

Number of parts ~1/ℓ^2

Total length of struts ~1/ℓ
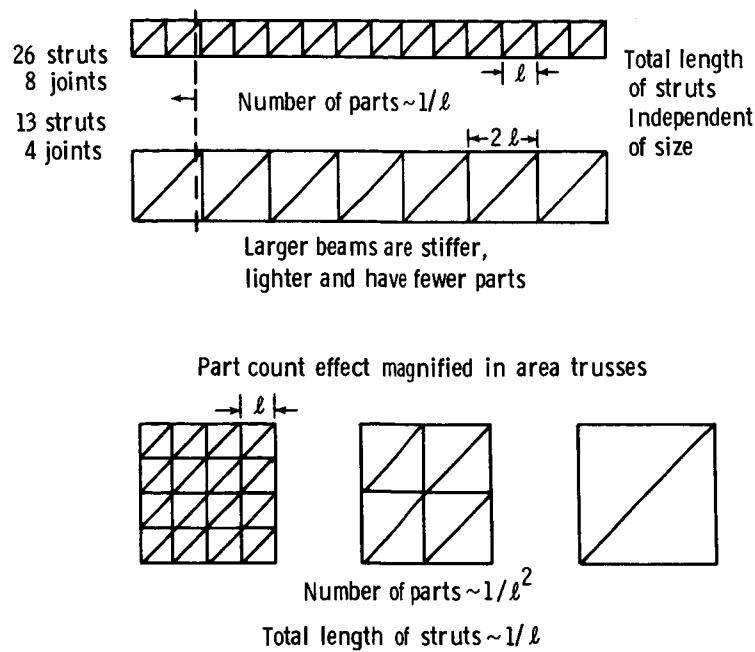
Fig. 3.   Size effects in stiffness designed trusses.

$\dfrac{Mass}{length}$, $\dfrac{lbm}{ft}$

Equal bending
stiffness trusses

Equal thickness
struts

$\dfrac{kg}{m}$

Meters

Feet
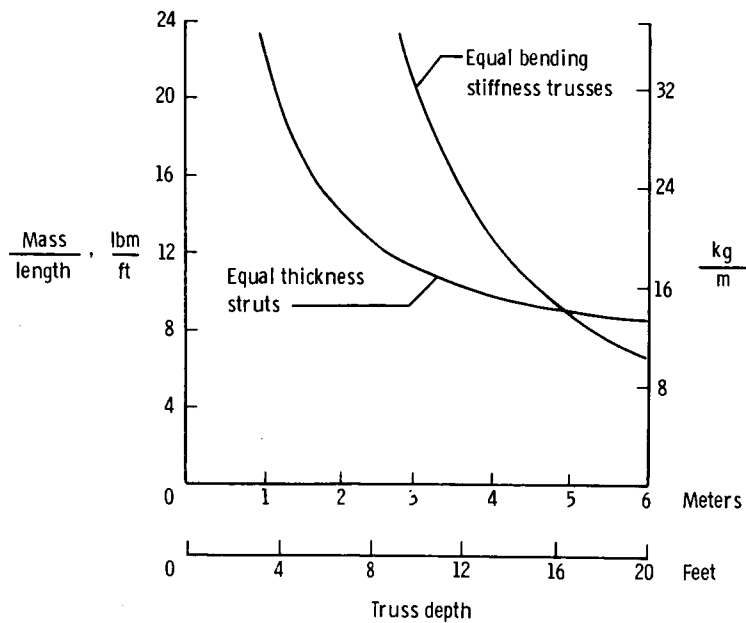
Truss depth

Fig. 4a.   Effect of truss depth of structural mass.
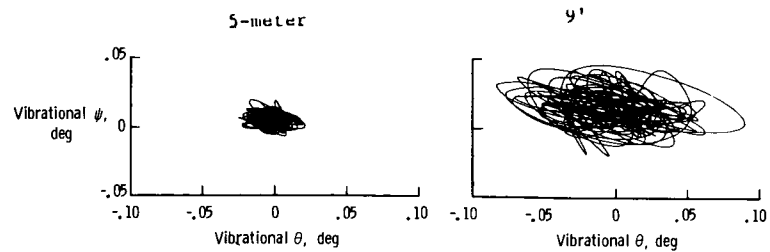
Fig. 4b. Flexible sun line variations at outer solar collector during reboost maneuver.
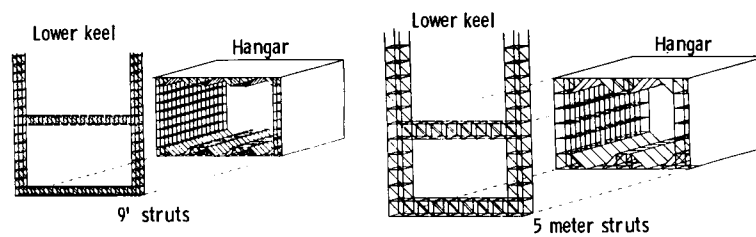
	9'	5 meter
Number of struts	4,660	1,590
Number of nodes	1,380	460
Mass	32,600 lbs 14,790 kg	16,000 lbm 7,260 kg
Construction time	78 hours	27 hours

Fig. 5. OTV Hangar construction comparison.

26 strut locations
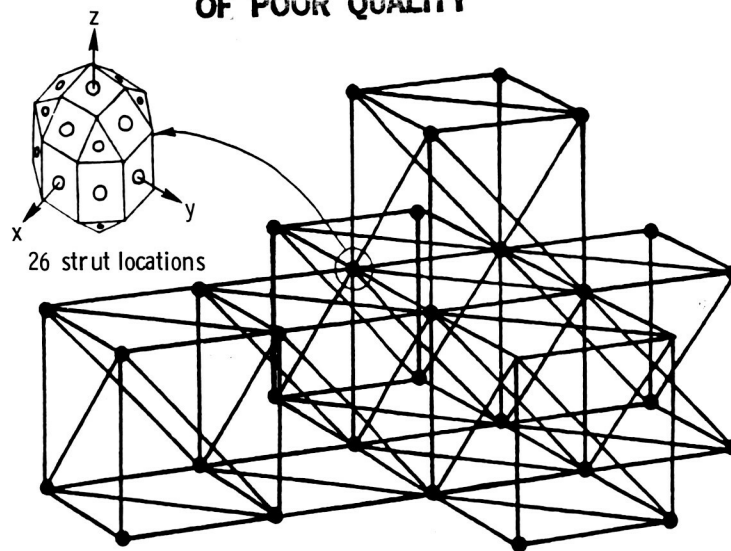
Fig. 6. Three-dimensional node permits highly
versatile growth.
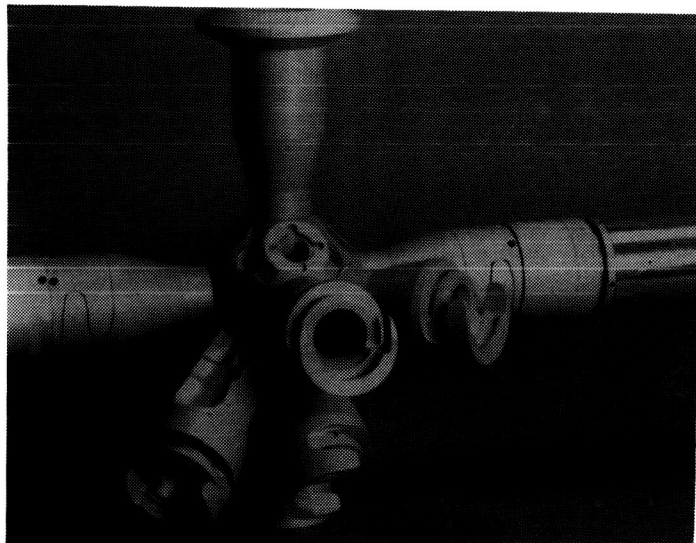
Fig. 7. Three-dimensional quick attachment
erectable node.

- Symmetric payload attachment potential
- Increase stiffness
- Increase payload space
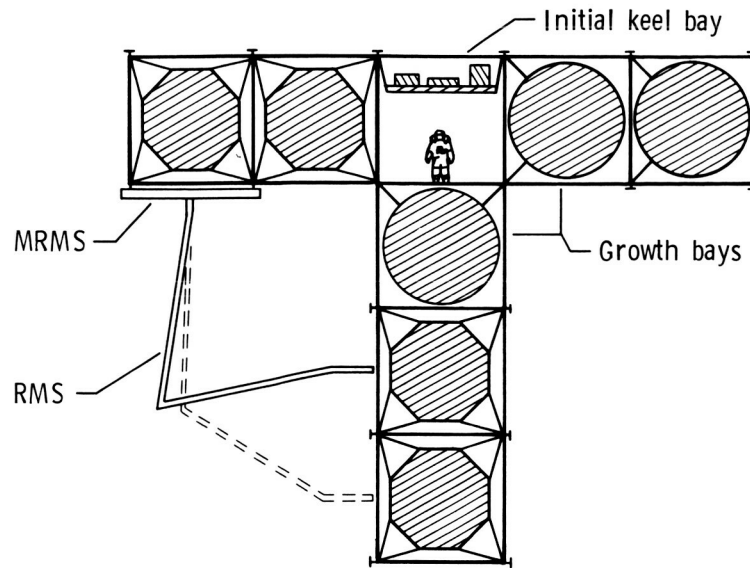
Fig. 8. Three-dimensional growth capability of 5-meter truss.
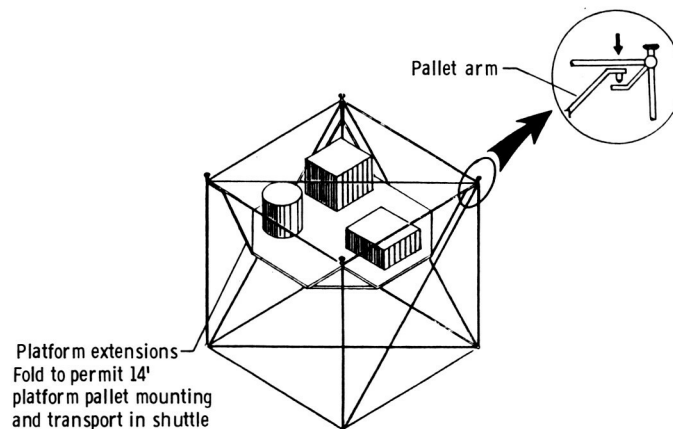
These shuttle-compatible pallets provide an "LDEF-LIKE" scenario for accommodating a large number of flight experiments with minimal interference to space station operations

Fig. 9. Cargo bay size equipment pallets can be recessed in 5-meter truss to minimize station congestion.
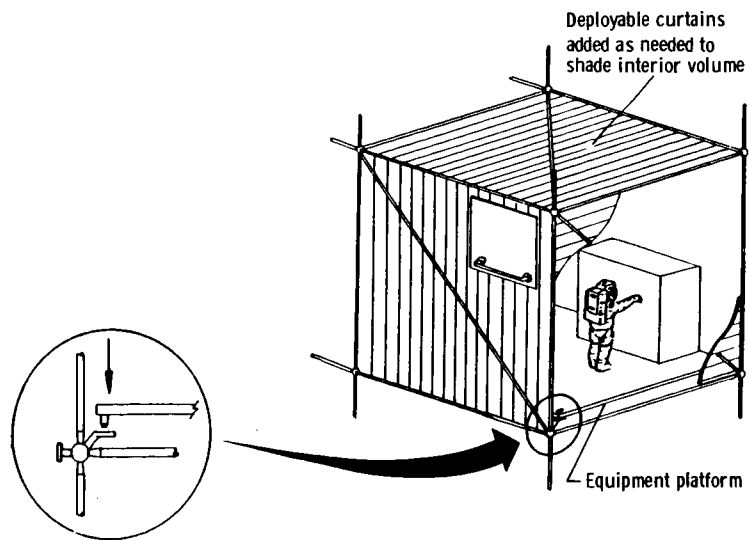
Fig. 10.   Five-meter structure provides useable
           interior volume.
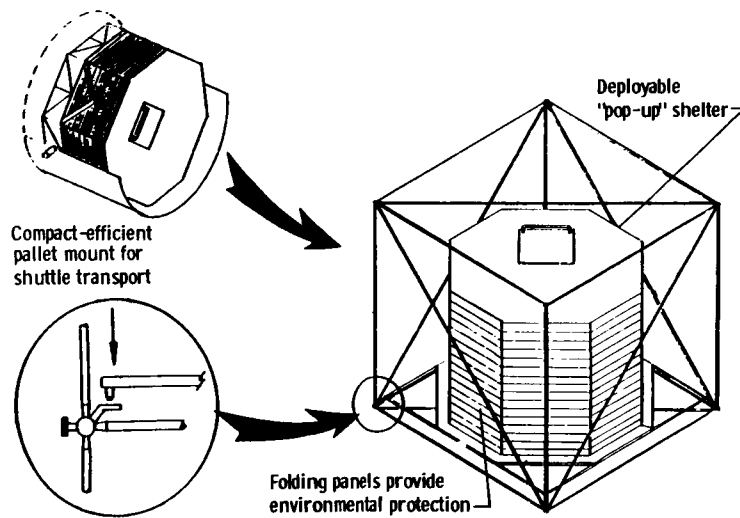
Fig. 11.   Five-meter truss can accommodate cargo
           bay size environmental protection
           shelter.

Propellant tank

Launch pallets

Net or
insulation cover

Maintenance/storage area

Ground integrated subsystem modules
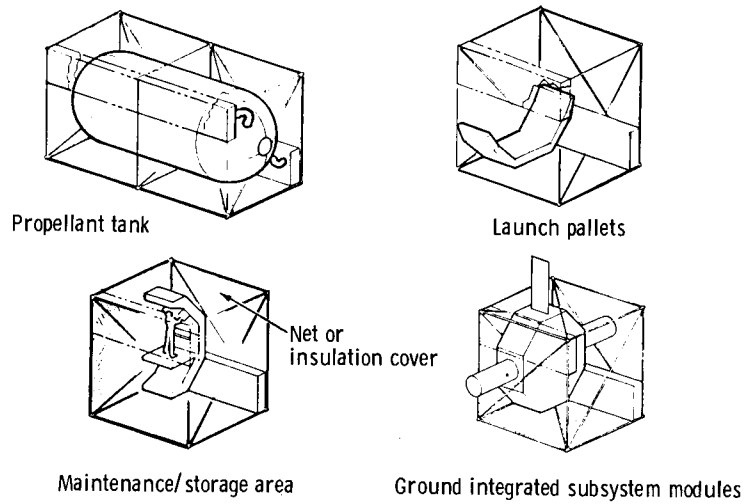
Fig. 12. Cargo bay size payloads can be stored
on interior of 5-meter truss.

Guide pins

Drawbar

Mobile foot
restraints
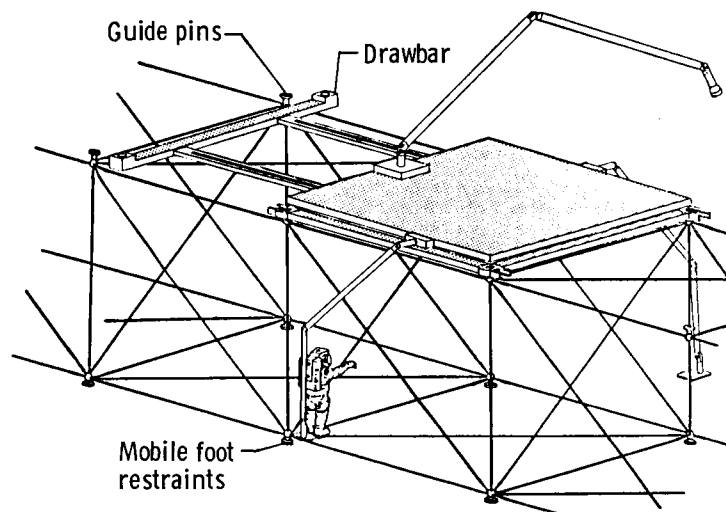
Fig. 13. Mobile remote manipulator system
attached to 5-meter truss.

692
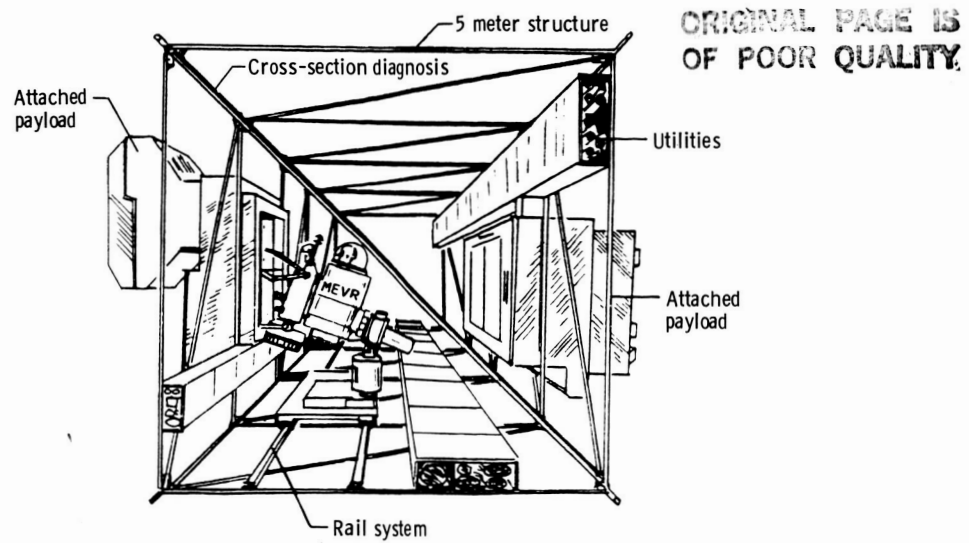
Fig. 14.   5-meter truss provides sufficient room
for an interior mobile transporter.
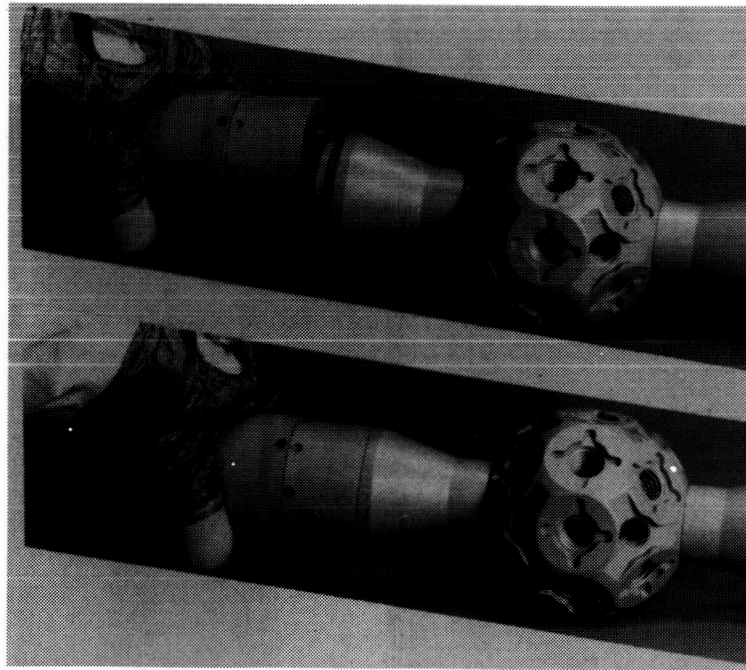
Fig. 15.   Quick-attachment joints designed for
astronaut glove handling.
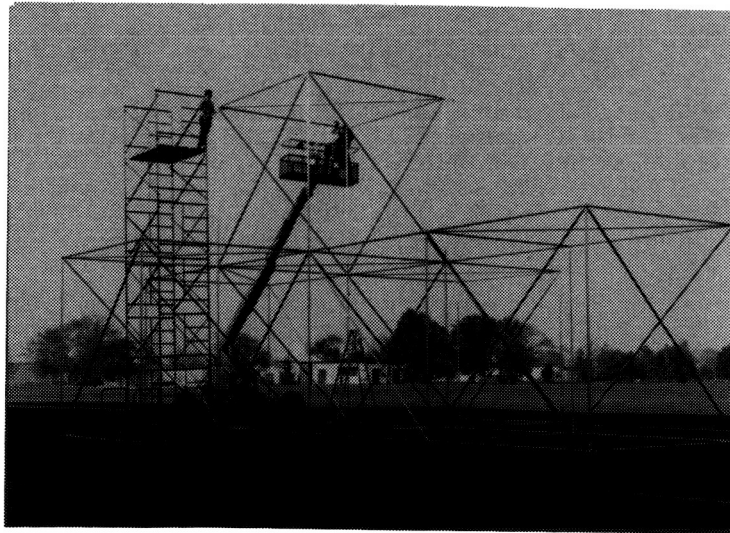
Fig. 16.   Space Station structural model.
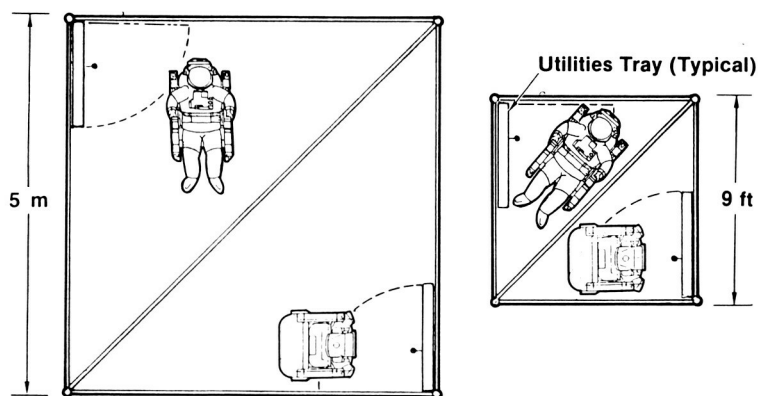
Fig. 17.   5-meter truss provides ample room for
           EVA operations.
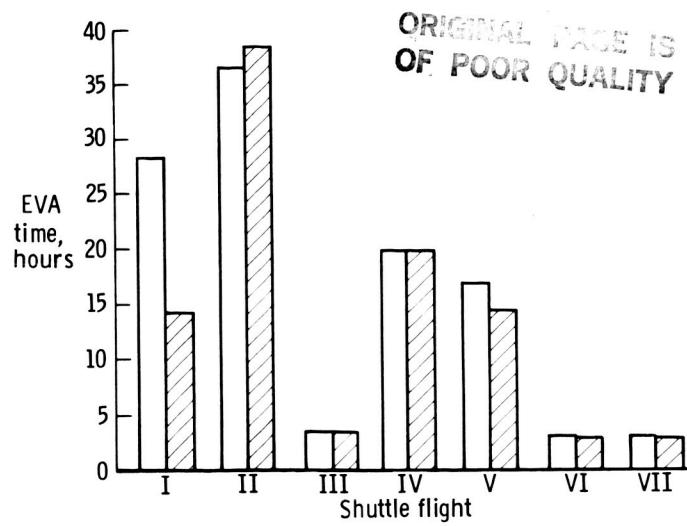
Fig. 18. Comparison of EVA hours to construct IOC Space Station configurations.
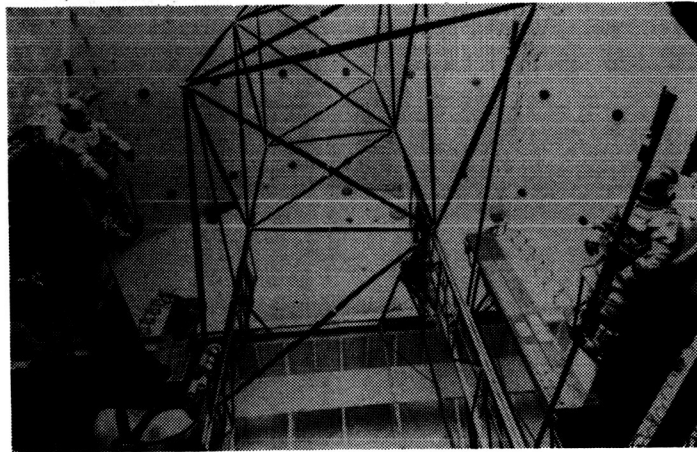
Fig. 19. 38-strut truss assembly in mobile work station.
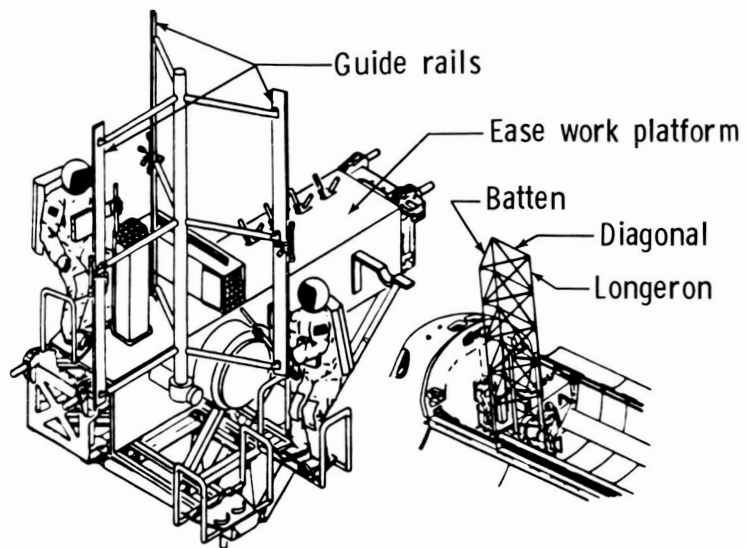
Fig. 20.   ACCESS baseline experiment setup.
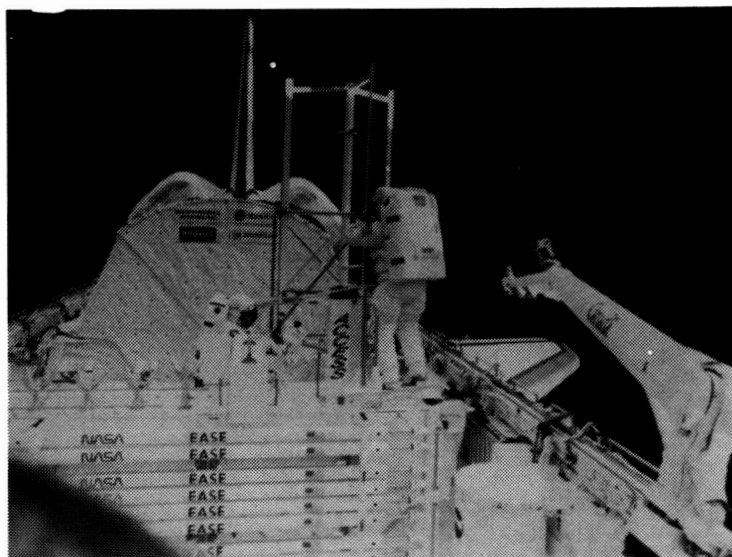
Fig. 21a.   Initiation of ACCESS truss
construction experiment.

Fig. 21b.   Photograph of on-orbit ACCESS
assembly.

Preliminary results

Task	Time min: sec		
	NBS	NBS	Flight
	Avg all tests	Trained	Trained
Setup	4:00	3:04	3:31
Assemble 10 bays	30:13	21:44	25:27
Disassemble 10 bays	18:45	15:00	18:52
Stow and close up	5:23	4:30	4:41
	58:21	44:18	52:31

Fig. 22.   Correlation of space truss
construction time for ACCESS.
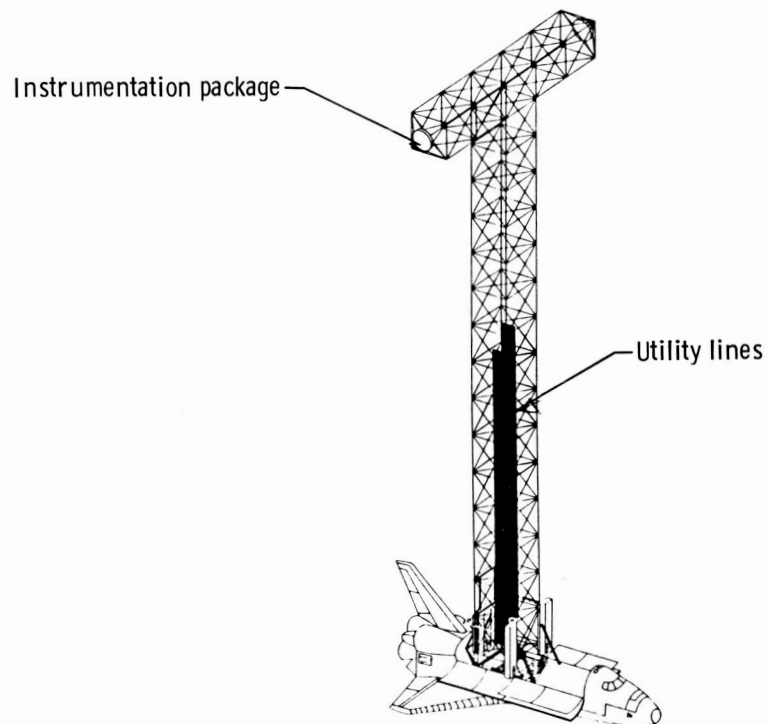
Fig. 23.   16 bay-long truss flight experiment.
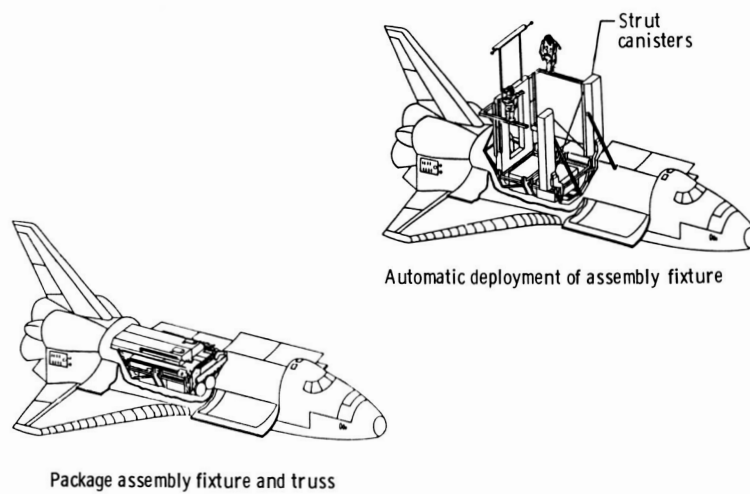
Fig. 24.   Packaged flight experiment and assembly fixture.

Instrument package

Erection of first bay

Five bays of erected truss
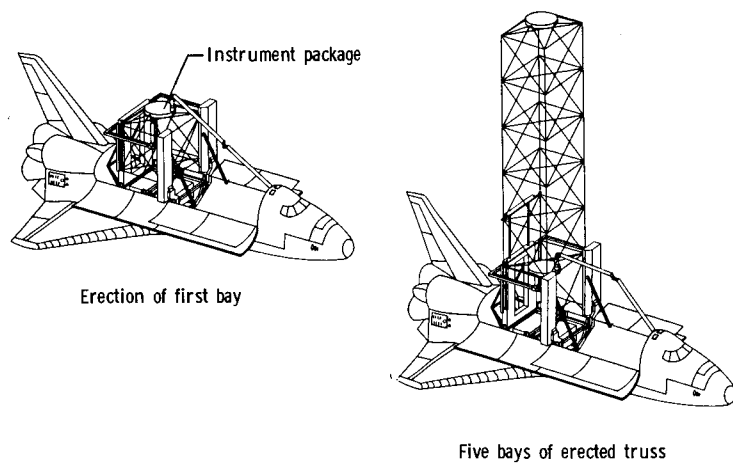
Fig. 25.   Initial assembly of 5-meter erectable truss.

Five bays rotated and reattached
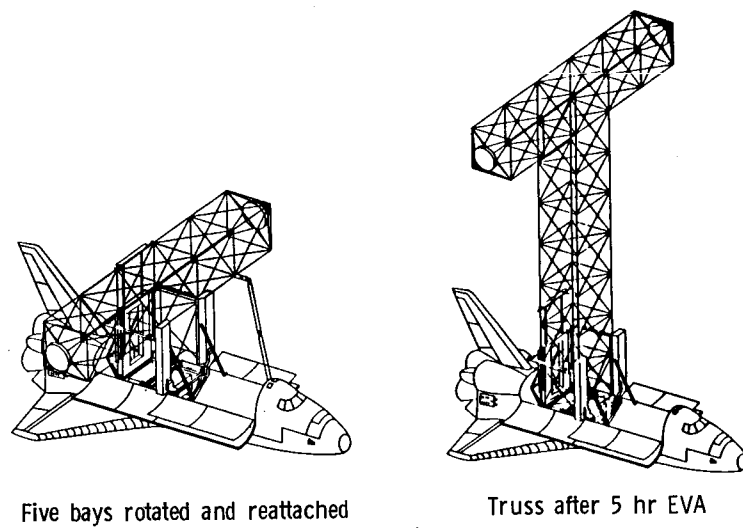
Truss after 5 hr EVA

Fig. 26.   12 bays of erected truss after a 5-hour EVA.

CONTROLS-STRUCTURES-ELECTROMAGNETICS INTERACTION PROGRAM

William L. Grantham, Marion C. Bailey,
Wendell K. Belvin, and Jeffrey P. Williams
NASA Langley Research Center
Hampton, Virginia

SUBJECTS TO BE DISCUSSED

This paper describes a 4 year technology development program involving Controls/Structures/Electromagnetics/Interaction (CSEI) for large space structures. The CSEI program has been developed as part of Langley Research Center's continuing effort following the successful kinematic deployment and RF tests of the 15 meter Hoop/Column antenna which has just been completed. One of the "lessons learned" in the program so far is the necessity and importance of being able to make reflector surface adjustment after fabrication and deployment. Cumulative manufacturing errors have proven to be much larger than expected even when great care is taken to maintain highly accurate templates, etc. during the fabrication and assembly stages.

- **Program Objectives**
- **Ground-Based Test Configuration**
- **Intelsat Adaptive Feed**
- **Reflector Shape Prediction Model**
- **Control Experiment Concepts**
- **Master Schedule**
- **COFS-II Baseline Configuration**

PROGRAM OBJECTIVES

The CSEI Program objectives are to extend the 15 meter antenna tests and examine interdisciplinary issues important in optimizing Large Space Antenna (LSA) performance for a variety of potential users. This will be accomplished by analytical code development as well as testing of the modified 15 meter antenna. New antenna features are being added which include automated remote control of the reflector surface and feed location, utilization of electronic adaptive feed compensation techniques, and incorporation of real-time antenna figure measurements for open and closed loop control tests of the flexible structure.

(CSEI)
GROUND-BASED TECHNOLOGY DEVELOPMENT FOR LARGE SPACE ANTENNAS

Objective:

Develop Methodology For Optimizing RF Performance Of Large Space Antennas By Application Of Controls-Structures-Electromagnetic Interactive Technologies.

Approach:

Extend 15-Meter Antenna Tests To Include

- Surface Control For Reflector Figure Improvement.
- Integrated Structural-Dynamics-Electromagnetics Code Development
- Adaptive Feed Techniques For Surface Distortion Compensation
- Real Time Figure Meas.

ANTENNA GEOMETRY

This chart shows the 15 meter Hoop/Column antenna geometry with interconnecting block diagrams for the remote surface control unit, adaptive feed controller, and surface state estimator-recorder. The antenna has been named Hoop/Column after its dominate structural members: a central telescoping column supporting a circumferential hoop. The hoop is supported by quartz cords attached to the top of the column and graphite cords attached to the opposite end of the column. The reflecting mesh surface is shaped by cord trusses and by graphite control cords as illustrated in the figure. Whereas these control cords were adjusted manually in the 1985 RF tests to improve the smoothness of the reflector surface, motorized control is now being added for more rapid remote actuation. Details concerning the surface control cords are shown on the next figure and in reference 1.
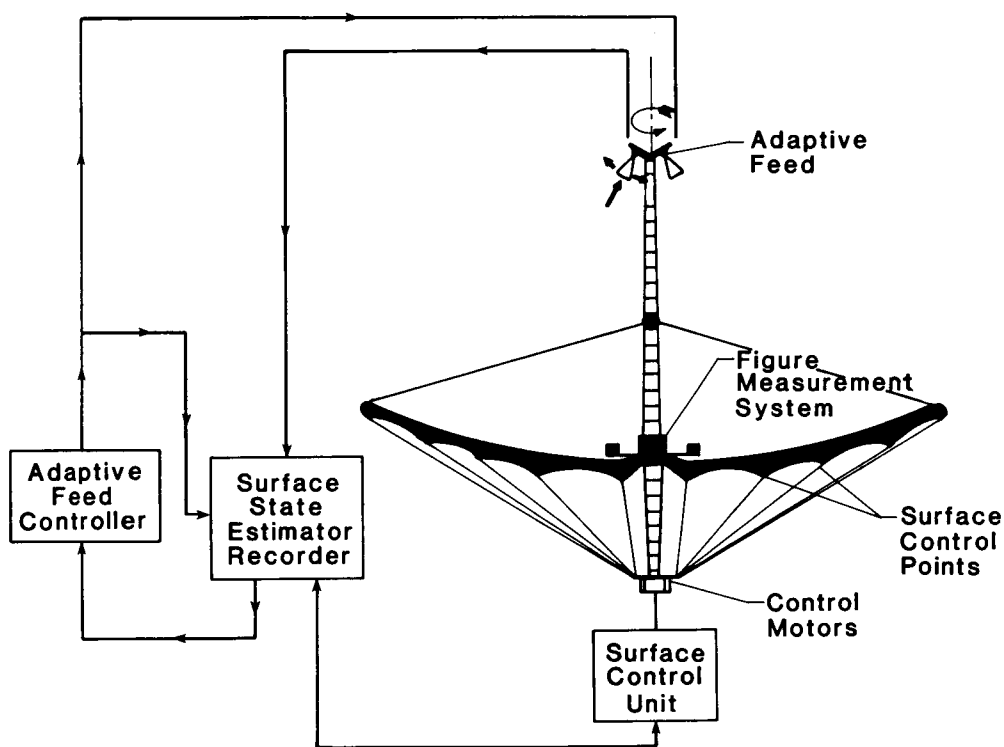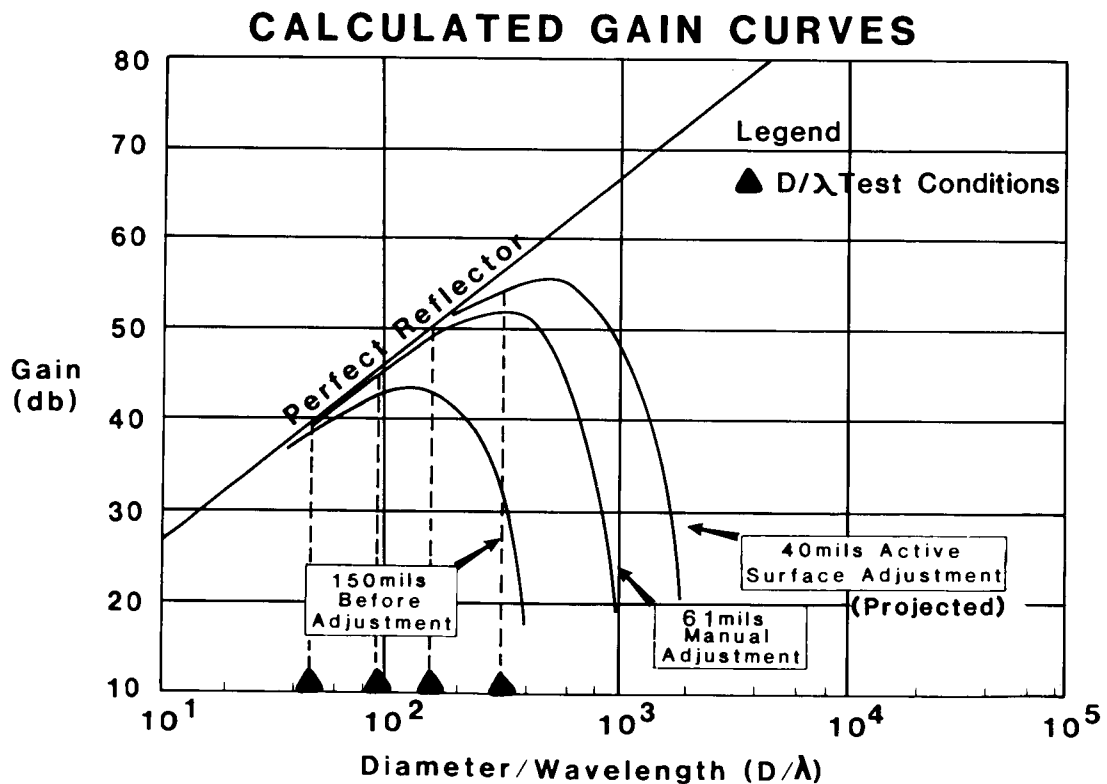
SURFACE SHAPE CONTROL CABLES

The geometry of one radial cord and its catenary rear truss cords is detailed in this chart. As can be seen, the reflector surface is shaped by the 4 cords which originate from the base of the column where the control motors are located. To minimize cost, only one quadrant of the reflector is planned for surface control so that there are a total of 28 control cords motorized on the antenna. Complete surface control is possible at a later time if funds become available. The control motor design is compatible with launch/stow requirements for potential future flight experiments on Shuttle as are planned in the COFS II Program (ref. 2).
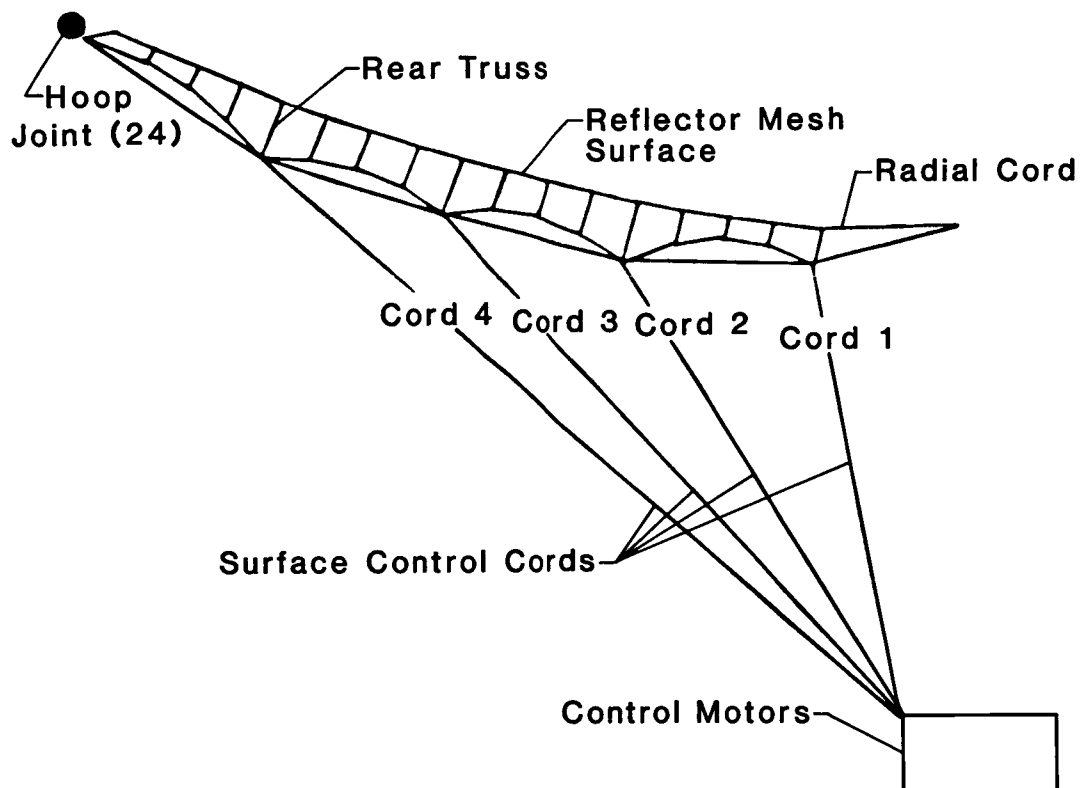
This graph shows the importance of reflector surface smoothness for achieving RF gain values near the diffraction limit (straight line function). The lower curve labeled "Before Adjustment" shows the Ruze calculated gain as a function of D/ for the 4 wavelengths tested at the Martin Marietta Near-Field Facility in 1985, before the reflector surface smoothness was manually adjusted using the control cords. As expected, boresite gain for the highest test frequency (11.6 GHz) showed serious performance loss for this 150 mils RMS surface accuracy. This condition was greatly improved by the control cord adjustment of the reflector surface to an RMS error of 61 mils as seen by the curve labeled "Manual Adjustment". Still further improvement is anticipated after the motorized control cord system has been put in place, since finer surface control will be possible and the structure will not be subject to hystersis errors which may have been introduced by cord tension release when the manual method was used. Although the Ruze model is useful in showing gain trends for random roughness reflector surfaces, more exact calculations are possible (ref. 3).

CALCULATED GAIN CURVES

Gain (db) vs Diameter/Wavelength (D/λ)

Legend: ▲ D/λ Test Conditions

Perfect Reflector

150 mils Before Adjustment

61 mils Manual Adjustment

40 mils Active Surface Adjustment (Projected)

PHASE COMPENSATION

Several researchers have suggested that compensation for distortions in large parabolic reflectors is possible by means of an electronically controlled feed array. The principle of this concept is shown here. On the left side of this figure is shown an ideal reflector-feed combination working together to form an undistorted plane wave in the aperture plane of the antenna with a corresponding well formed far field pattern.

If a physical distortion in the reflector occurs, as shown in the center depiction, a proportional phase distortion will occur in the aperture plane with a resultant field pattern degradation in shape and boresite gain. For a feed that has phase front adjustment capability as is planned in the CSEI Program, a compensating distortion can be introduced to offset the phase perturbation caused by the physical reflector warp as shown on the right side of the chart. This type of performance correction would be possible for both rapid and slowly changing conditions.

Far Field Pattern

Feed

Adaptive Feed

Ideal Reflector

Distorted Reflector
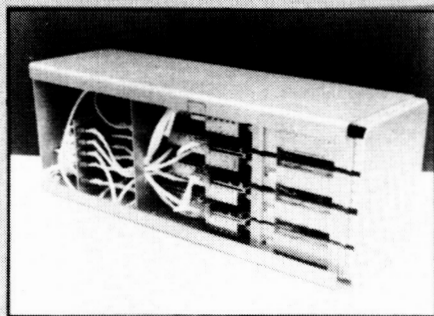
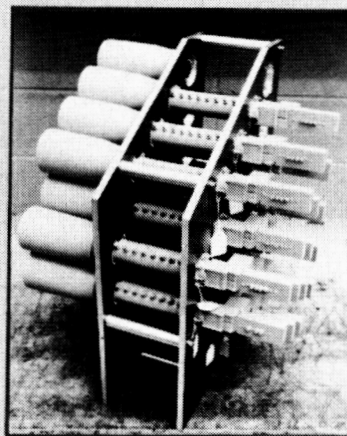**Distorted Reflector With Adaptive Feed**
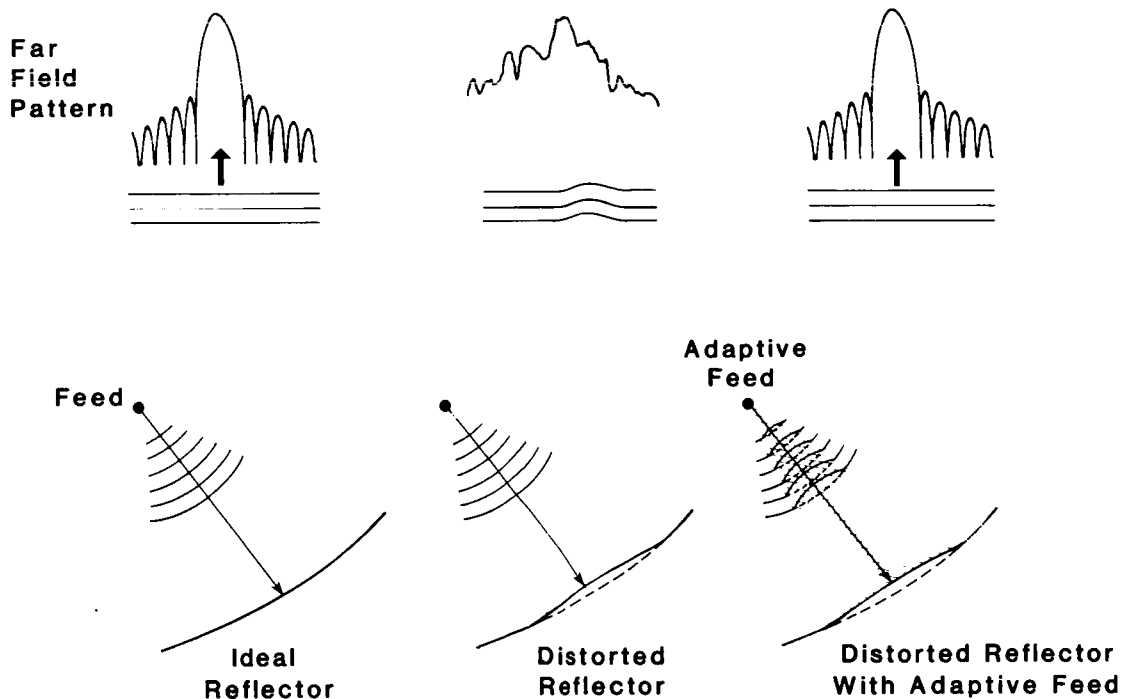
INTELSAT MULTI-HORN FEED

One of the feed designs being considered for compensation tests in the early phases of the program is the Intelsat multimode horn array. This photo shows the 24 element horn array mounted in the strong-back structure and the beam forming electronics network which controls the signal phase and amplitude to each active horn. This design, as well as an advanced feed design, is being evaluated for possible tests with the 15 meter antenna as part of the 4 year CSEI ground-based program.
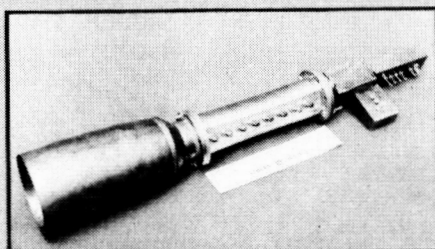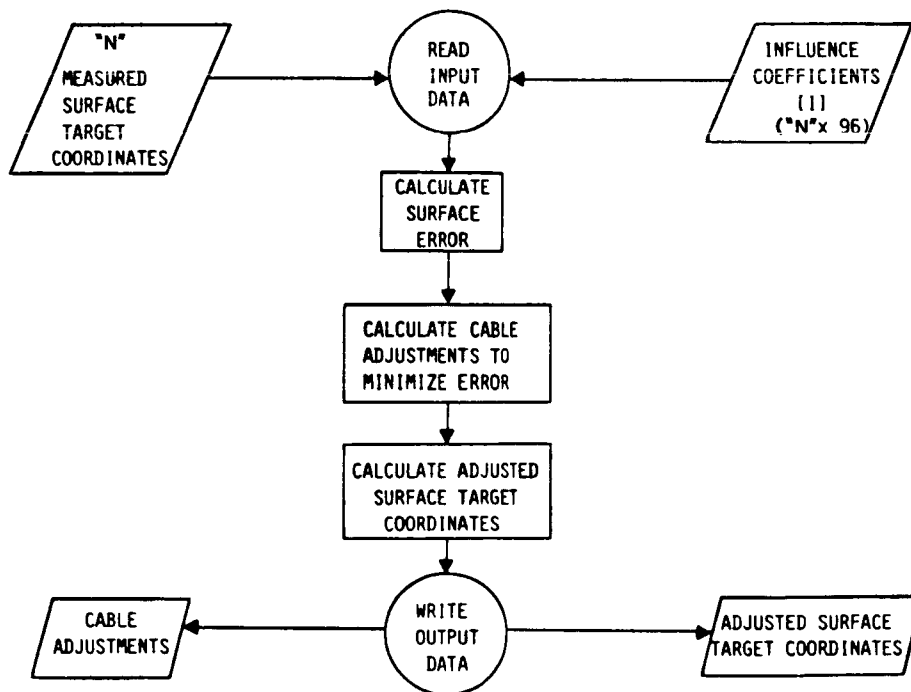

SINGLE MULTIMODE HORN CONFIGURATION WITH POLARIZER

RADIATING SOURCE ARRAY

Beam Forming Network Assy.

REFLECTOR SHAPE CONTROL ALGORITHM

The procedure for surface adjustment is shown in this chart. Surface figure data will be provided by the optical sensor to the algorithm which will then determine the extent of deviation from an ideal parabolic reflector surface. Subsequently, these residuals will be used to set the control cable adjustments necessary to optimize the surface shape using influence coefficients derived from a finite elements model (EAL). This cable adjustment information is fed to the control circuit of the motorized control cords and implemented as a surface change. The intent of the design is to have the ability to control the surface up to approximately 15 Hz for small surface displacements. Initial tests will be restricted to quasi-static type surface adjustments with man-in-the-loop review at each step of adjustment. Later tests in the program may include closed loop surface control experiments.

"N"
MEASURED
SURFACE
TARGET
COORDINATES

READ
INPUT
DATA

INFLUENCE
COEFFICIENTS
[I]
("N"x 96)

CALCULATE
SURFACE
ERROR

CALCULATE CABLE
ADJUSTMENTS TO
MINIMIZE ERROR

CALCULATE ADJUSTED
SURFACE TARGET
COORDINATES

CABLE
ADJUSTMENTS

WRITE
OUTPUT
DATA

ADJUSTED SURFACE
TARGET COORDINATES

ANTENNA STRUCTURAL MODEL

The Engineering Analysis Language (EAL) finite-element program was used to structurally model and analyze the antenna. A separate paper on this model is given by W. K. Belvin et. al. (ref. 4). The reflector shape for each quadrant is that of a parabolic segment with the vertex located about 50 cm from the column center. The design of the Hoop/Column antenna can accommodate other reflector shapes as needed by the user such as spherical, parabolic torus, and planar.

Although the minimum number of optical targets needed for surface definition has not yet been determined, it is expected that there will need to be at least one for every surface control cord. Measurements will also be required for the feed location relative to the surface in order to complete the definition of antenna figure. The optical system required to accomplish this has not yet been selected but several sensor candidates are available including a recently demonstrated laser radar sensor as well as a number of conventional angle sensing systems. The measurement accuracy goal is 7 mils RMS with each target sampled 100 times each second.

TOP VIEW
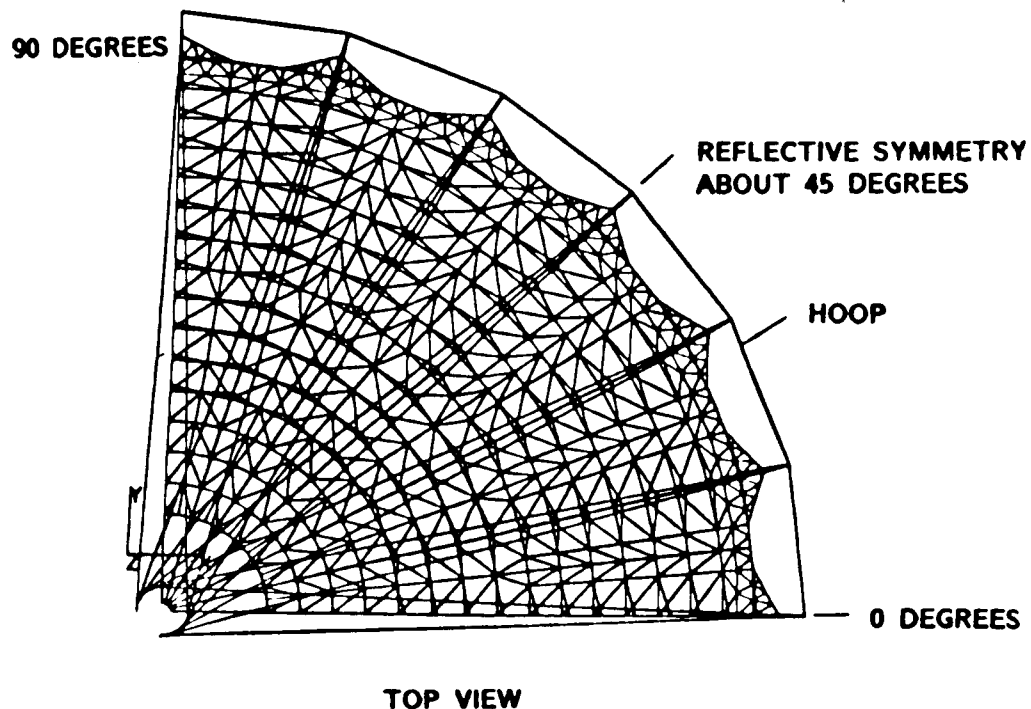
CONTROL EXPERIMENT CONCEPTS

The Hoop/Column antenna is a flexible structure which will experience excitation of flexible motion of the support structure, and static and dynamic distortion of the reflector surface. It is expected that such structural vibrations will degrade the R-F performance of the antenna. The purpose of the controls investigations is to demonstrate and define the performance improvement realized through active control of the structural dynamics.

It is intended to perform ground-based experiments which admit a high degree of fidelity to the on-orbit mission environment of the antenna. This should include both maneuvering of the structure and the rejection of on-board disturbances. The reflector shape sensors and cord actuators described in this paper will permit some damping augmentation of the reflector surface, but additional sensors and actuators will be needed for the slew maneuver.

OBJECTIVE:

- Demonstrate That Active Control Of The Structural Dynamics Can Improve The R-F Performance Of The Hoop-Column Antenna.

APPROACH:

- Emulate The Dynamic Environment Which Might Be Expected On-Orbit-i.e. Slew Maneuvers And On-Board Disturbance Sources.

- Use Base-Line Sensors And Actuators For Dynamic Shape Control.

- Add Cord Actuators For Hoop Control And Torque Actuators On Column For Slew Control (Phase III).

Two primary controls experiments are presently envisioned. The first is to use the planned reflector shape sensors and cord actuators to control the nominal shape and augment the damping of the reflector surface. The reflector shape adjustment would be accomplished in a quasi-static manner for Phases I and II. Damping augmentation would be accomplished using the actuator/load-cell micro-controller assemblies as decentralized control systems which implement local damping loops.

The second control task will be to implement a rapid slew maneuver of the antenna and maintain surface accuracy during that maneuver (Phase III). It may be possible to suspend the Hoop/Column antenna from a universal joint located in the center of the column. To accomplish the slew, it would be necessary to instrument the hoop with accelerometers and the column with angular rate sensors and accelerometers. These will provide feed-back for rigid body attitude control and structural vibration suppression. Actuators will consist of hoop cord actuators similar to those used for the surface cords. Scissors gyros (SG's) are proposed for each end of the mast to provide the slew control torques. The bandwidth of the SG's may be sufficient for column vibration suppression.

SHAPE CONTROL:

- Use Optical Sensor And Cord Actuators To Perform Quasi-Static (Automated) Shape Adjustments Of One Quadrant.

- Use Load Cells And Cord Actuators/Micro-Controllers To Augment Mesh Damping.

SLEW MANEUVER-RAPIDLY SLEW 10 DEGREES

- Suspend H/C From A Fixed Universal Joint.

- Instrument Hoop With Accelerometers And Column Ends With Angular Rate Sensors.

- Add Hoop Cord Actuators Around The Hoop To Control The Out-Plane Motion.

- Add Scissor Gyro Torquers To Ends Of Mast To Effect Slew.

Static and dynamic testing of the antenna has just been completed in the Langley 16 meter vacuum chamber (ref. 4). Completion of this structural dynamics testing marks the beginning of the CSEI program. The design and fabrication of the CSEI surface adjustment system has now started and is expected to be completed by spring of 1987. The first testing phase of the CSEI program will begin with an evaluation of the surface adjustment system in the fall of 1987 to determine its ability to upgrade the reflector surface smoothness prior to going to the MMA Near-Field Facility for quasi-static RF testing (Phase II). Phase III of the program will include a return to the MMA facility with an advanced adaptive feed design and possibly closed loop surface control experiments. After completion of these three phases of testing, the antenna will be transferred to the COFS II Project Office for refurbishment as a potential flight article in that program. Flight tests are currently planned for FY 1994-95.
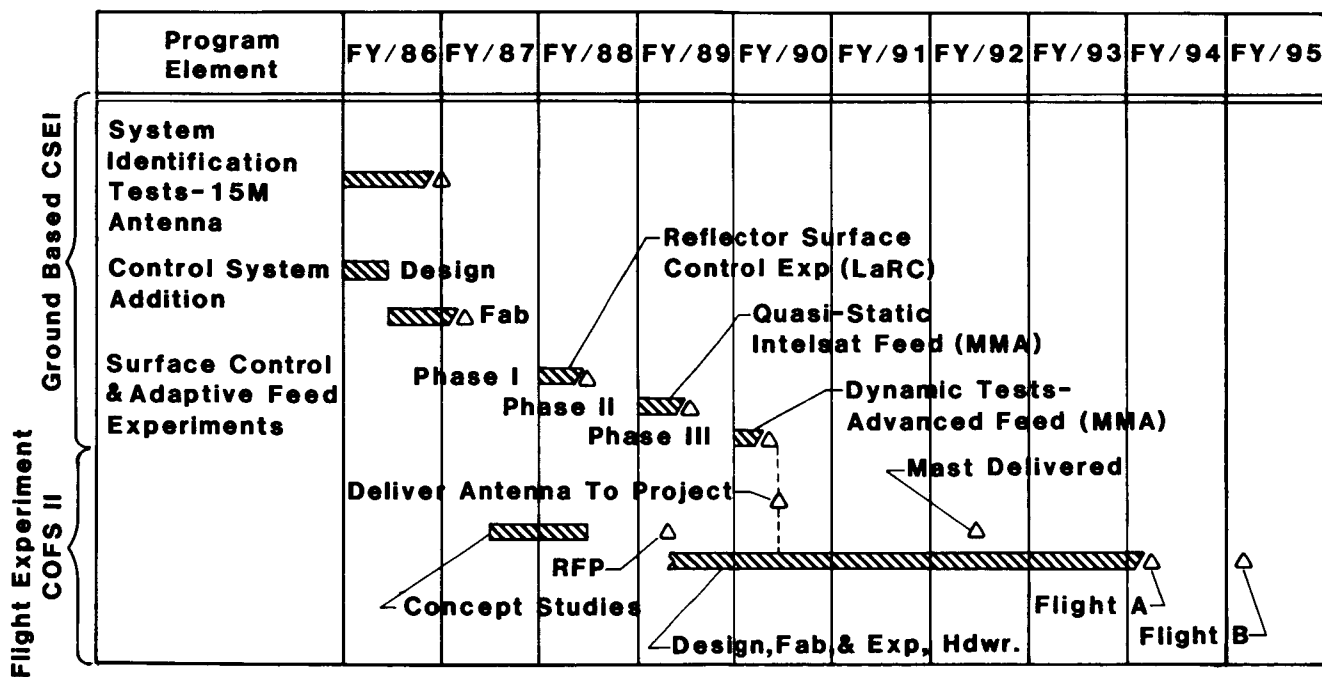
This artist's sketch shows the baseline Hoop/Column configuration for COFS II flight experiment described in more detail by J. S. Pyle (ref. 2). The baseline configuration will utilize a portion (30 to 40 meters) of the COFS I MAST mounted on the STEP pallet in the Space Shuttle bay as the basic structure for the flight system. The tip of the Mast will be modified with an adapter structure for the purpose of mounting a two degree-of-freedom gimbal and the Hoop/Column antenna (baseline configuration). Shape control of one quadrant of its surface and control of the hoop also will be part of the baseline capability.
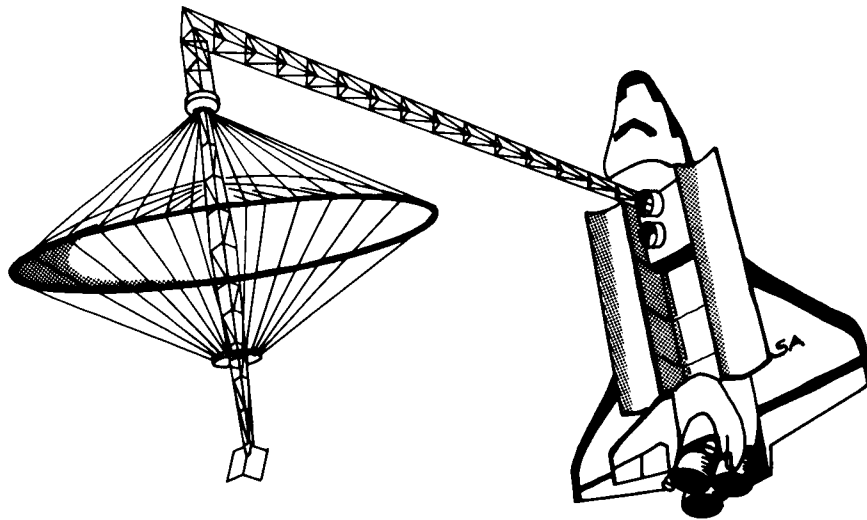
REFERENCES

1. James B. Miller, Elvin L. Ahl, Jr., David H. Butler, and Frank Peri, Jr.: Surface Control System for the 15 Meter Hoop/Column Antenna, NASA CP-2447, Part 1, 1986. pp. 533-546.

2. Jon S. Pyle and Raymond Montgomery: COFS II 3-D Dynamics and Controls Technology, NASA CP-2447, Part 1, 1986, pp. 327-346.

3. M. C. Bailey: Hoop/Column and Tetrahedral Truss Electromagnetic Tests, NASA CP-2447, Part 2, pp. 737-746, 1987.

4. W. K. Belvin and Harold H. Edighoffer: 15 Meter Hoop/Column Antenna Dynamics: Test and Analysis, NASA CP-2447, Part 1, 1986, pp. 167-186.

BOX TRUSS ANTENNA TECHNOLOGY STATUS*

J. V. Coyner and
E. E. Bachtell
Martin Marietta Denver Aerospace
Denver, Colorado

BOX TRUSS ANTENNA DEVELOPMENT

This paper summarizes recent technology development activities for box truss structures and box truss antennas. Three primary activities will be reported: the development of an integrated analysis system for box truss mesh antennas; dynamic testing to characterize the effect of joint freeplay on the dynamic behavior of box truss structures; and the fabrication of a 4.5-meter diameter offset fed mesh reflector integrated to an all graphite-epoxy box truss cube (fig. 1).

O   ANALYSIS OF BOX TRUSS MESH ANTENNAS

O   DYNAMIC TESTING OF BOX TRUSS SPACE STRUCTURE

O   FABRICATION OF 4.5M BOX TRUSS ANTENNA

Figure 1

HISTORY OF BOX TRUSS

Each year significant steps were taken in the maturity of the box truss design and the understanding of the supporting analysis. Figure 2 summarizes the evolution of the deployable box truss and related technology activities. During 1977 and 1978, the emphasis was placed on design and analytical verification of the box truss structure performance. During 1979, 1980, and 1981, design refinements and hardware fabrication were directed towards GFRP integration with primary emphasis on low cost. This activity culminated in the fabrication and demonstration of the 4.5-meter cube. During 1982, a full-scale prototype of a gate frame truss was fabricated and tested. Also, a mesh test model was fabricated to validate the mesh reflector analytical tools and to demonstrate fabrication techniques. During 1983 and 1984, mesh analytical work continued, metal matrix composite development made significant progress, precision joint designs were fabricated and demonstrated, and passive damping augmentation concepts were developed. During 1985 and 1986 a 4.5-meter mesh reflector was fabricated and dynamic testing of a 20 meter truss was performed.

1977	-	BOX TRUSS DESIGN CONCEIVED ON IR&D
	-	DESIGN DEVELOPED AND ANALYZED ON "ON ORBIT ASSEMBLY" PROGRAM
	-	SINGLE FRAME DEMONSTRATION MODEL FABRICATED
1978	-	DESIGN AND FABRICATION OF SINGLE FRAME PROTOTYPE STRUCTURE (GFRP TUBES AND METALLIC FITTINGS)
1979	-	DESIGN REFINEMENT INTEGRATING LOW COST GFRP FITTINGS AND MEMBERS
1980	-	DESIGN OF GFRP 4.6-METER CUBE
	-	FABRICATION OF ALL COMPONENTS
1981	-	ASSEMBLY AND TEST OF 4.6-METER CUBE
1982	-	MESH MODEL FABRICATION AND TEST
	-	ASSEMBLY AND TEST OF GATE FRAME TRUSS
1983	-	METAL MATRIX COMPONENT DESIGN, FABRICATION, TEST
	-	PRECISION JOINT DESIGN, FABRICATION, TEST

Figure 2

HISTORY OF THE BOX TRUSS (CONCLUDED)

1984   –   METAL MATRIX COMPONENT DESIGN. FABRICATION. TEST
           –   MESH TIE SYSTEM ANALYTICAL DEVELOPMENT
           –   PASSIVE DAMPING COMPONENT DEVELOPMENT

1985   –   FABRICATION OF 4.5 METER BOX TRUSS ANTENNA
           –   DYNAMIC TEST OF STATICALLY DETERMINATE AND INDETERMINATE TRUSSES

1986   –   TESTING OF 4.5 METER BOX TRUSS ANTENNA

BOX TRUSS ANTENNA MODEL

A model of a box truss mesh antenna is shown in Figure 3. Mesh support posts (standoffs) separate the radiating surface from the support structural. This separation provides the volume necessary to stow the mesh and mesh tie system and assures that neither the mesh nor the tie cords impinge on the deployment of the box truss. Generally, the standoffs are tubes of similar cross section to the box truss vertical members and are inserted into the corner fittings. The mesh is attached to the top of the standoffs. The vertical members on the box truss structure are vertical rather than perpendicular to the surface to assure step-by-step deployment and stowability.

To achieve the parabolic curve shape, each box truss face consisting of two vertical members and two surface tubes is sheared by using different length interior diagonal members.

Figure 3

721
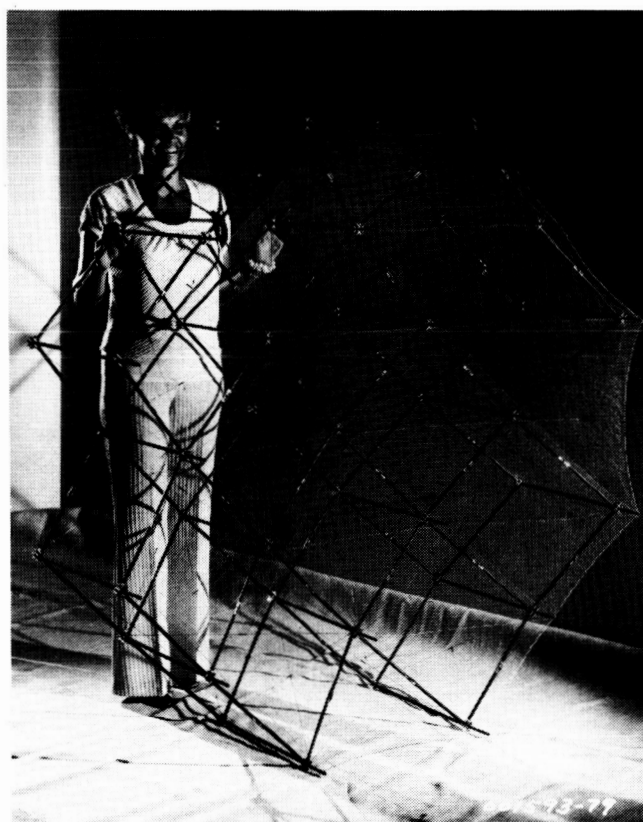
FULL-SCALE PROTOTYPE CUBE

During 1980, the design of each of the box truss components was reviewed and redesigned to achieve optimize weight, cost and thermal stability while meeting the stowed, deploying and deployed structure requirements. A prototype was made for each component and tested to verify manufacturing methods (feasibility and tolerance manageability) stiffness, strength, and weight. By the end of 1980, all components for a full-scale prototype 4.5-meter, deployable box truss cube were completed and assembly had started. Final assembly was completed in 1981. Summarized below are the design features of the full-scale prototype cube. Figure 4 shows the resulting prototype cube in a deployed configuration

> 4.5m Deployable Cube
> Stows in 0.3m square by 4.5m long (0.15m per module)
> 36 modules (28m x 28m deployed) stows in 1m by 1m by 4.6m
> All GFRP except for hinge pins and springs
> High performance (high stiffness, low CTE)
> Low Weight - 27 kg
> High Accuracy - better than 0.1mm on all axes
> All components and members fully constrained when stowed
> Corner fitting stabilized by bonded interface to vertical

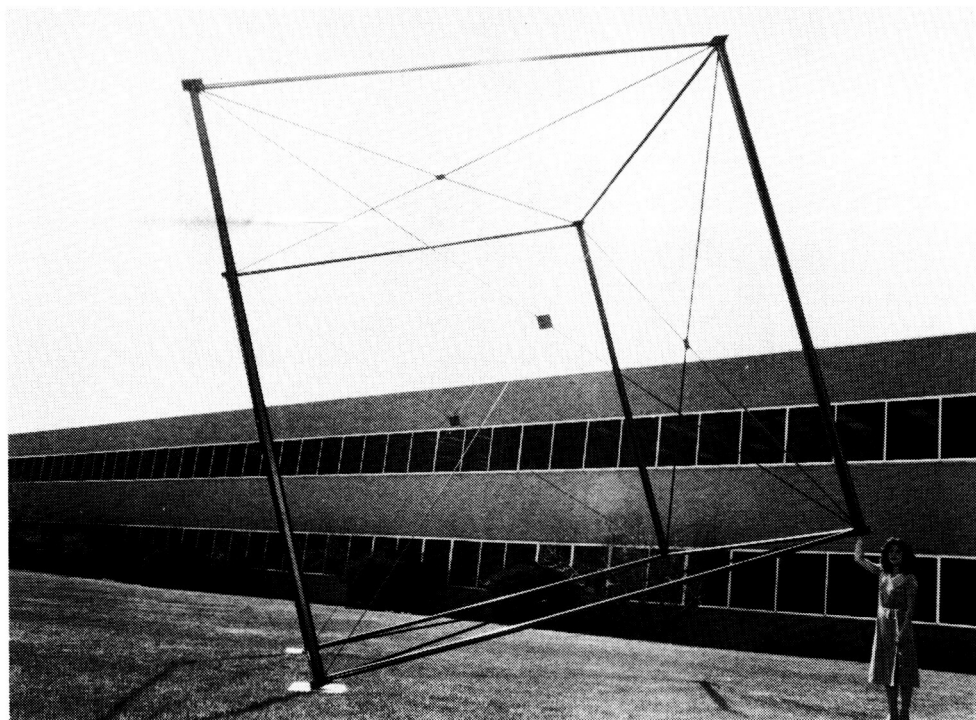A 4.5-meter diameter mesh reflector has now been integrated to the box truss cube.

Figure 4

ANALYSIS OF BOX TRUSS MESH ANTENNAS

An integrated system has been developed to model, analyze, and predict rf performance of box truss antennas with reflective mesh surfaces. This analysis system is unique in that it integrates custom-written programs for cord-tied mesh surfaces, thereby drastically reducing both the man-hours and computer-dollars required to design and analyze mesh antennas. The program can be used to analyze the effects of (1) on-orbit thermal environments, (2) solar pressure, (3) on-orbit calibration or continuous adjustment of the mesh tie system to improve surface accuracy, and (4) gravity distortions during setting.

The analysis system uses nonlinear finite-element, surface topography and interpolation, and rf aperture integration techniques. The system provides a quick and cost-effective final link in the design process for box truss antennas. (Fig. 5.)

O   PROGRAM CAN BE USED TO ANALYZE EFFECTS OF:

- ON-ORBIT THERMAL ENVIRONMENTS
- SOLAR PRESSURE
- ON-ORBIT CALIBRATION OR CONTINUOUS ADJUSTMENT OF MESH TIE
  SYSTEM TO IMPROVE SURFACE ACCURACY
- GRAVITY DISTORTIONS DURING SETTING
- MANUFACTURING ERRORS

O   PROGRAM USES:

- NON-LINEAR FINITE ELEMENT
- SURFACE TOPOGRAPHY AND INTERPOLATION
- RF APERTURE INTEGRATION

O   PROGRAM CONSISTS OF SIX CUSTOM WRITTEN INTEGRATED PROGRAMS

Figure 5

TYPICAL BOX TRUSS ANTENNA AND MESH TIE SYSTEM

Figure 6 shows that the direct tieback tie system consists of three types of cords: the surface cross cords that bisect the mesh reflective surface, the surface radial cords that extend radially from the top of the standoffs to the surface cross cords, and the tieback cords that extend from the surface cords to the bottom of the standoffs. The bottom of the standoffs correspond to the location of the corner fittings and the box truss. The tieback cords pull the surface into shape and are tied along each surface cord at a distance defined as the radial tie spacing.
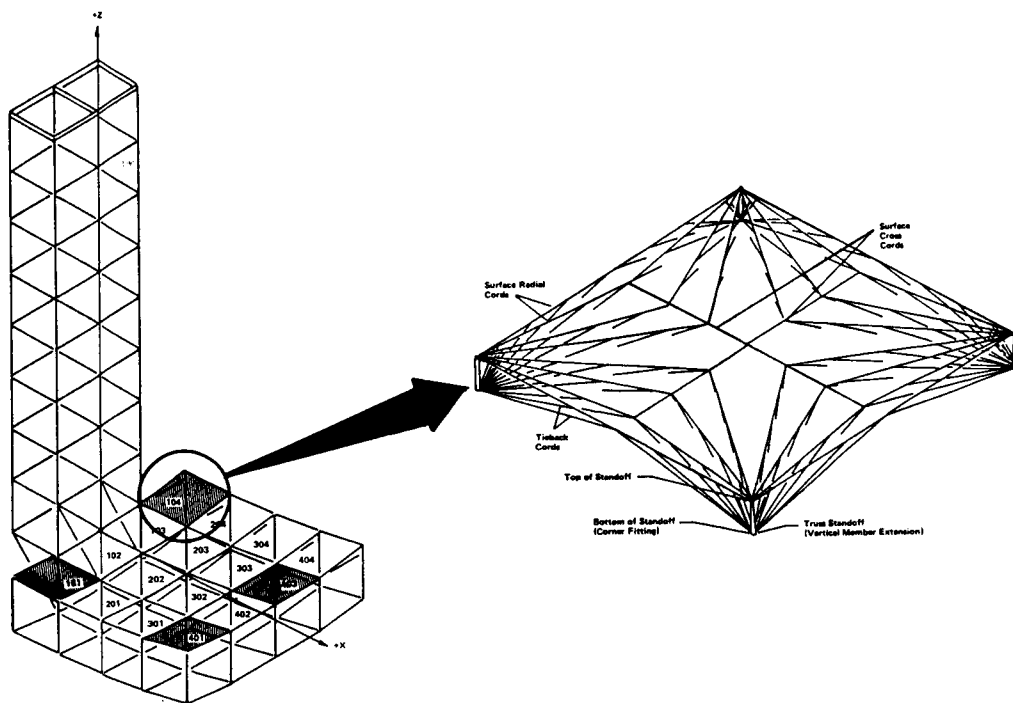
Figure 6

INTEGRATED MESH ANALYSIS SYSTEM

The complete analysis system consists of six integrated computer programs (Figure 7).
1) Mesh Tie System Generator: creates the tie system design and finite-element model of the tie system.
2) Loadcase Generator: creates the loadcases to be placed on the tie system finite-element model. These loadcases can represent any operational or manufacturing environment.
3) Model Optimizer: generates the optimized finite-element input file for the model solver.
4) Model Solver: determines the tie system distortions by solving the tie system finite-element model for the above specified loadcases.
5) Antenna Surface Topography Solver: determines the best-fit paraboloidal surface, effective feed scan, axial defocus, and minimum rms surface error to match surface distortions.
6) RF Performance Solver: determines the far-field pattern, antenna gain, and beam efficiency of the antenna.

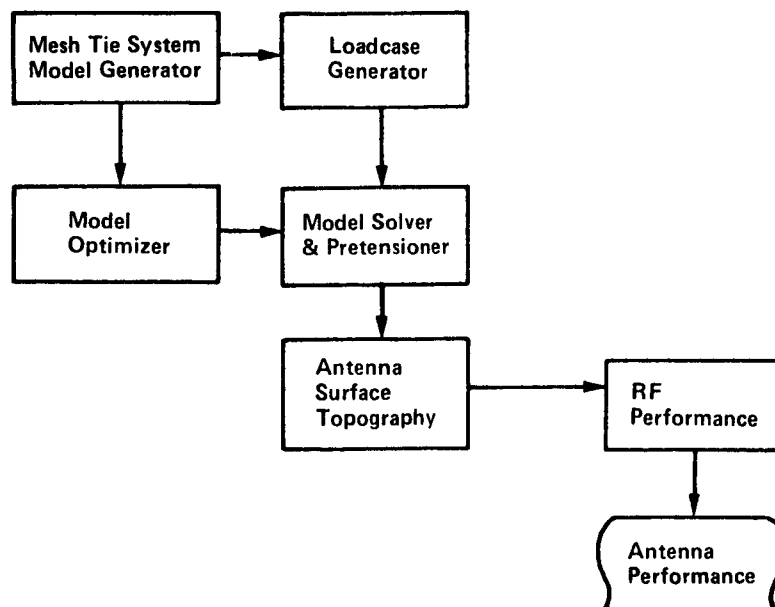Figure 7

725

PROGRAM INPUTS AND OUTPUTS

Figure 8 describes the user inputs and program outputs for each program. Illustrated is the fact that the Mesh Tie System Model Generator and the Loadcase Generator programs are used to define all inputs necessary for analyzing a mesh reflector. This allows the larger, more time consuming programs, e.g., the Model Solver, to be run in a batch mode thereby reducing run costs. In the example shown in Figure 8, effects due to tie cord temperatures and g-loading are being analyzed via the Loadcase Generator. Other options allow point loads and pressures to be analyzed.
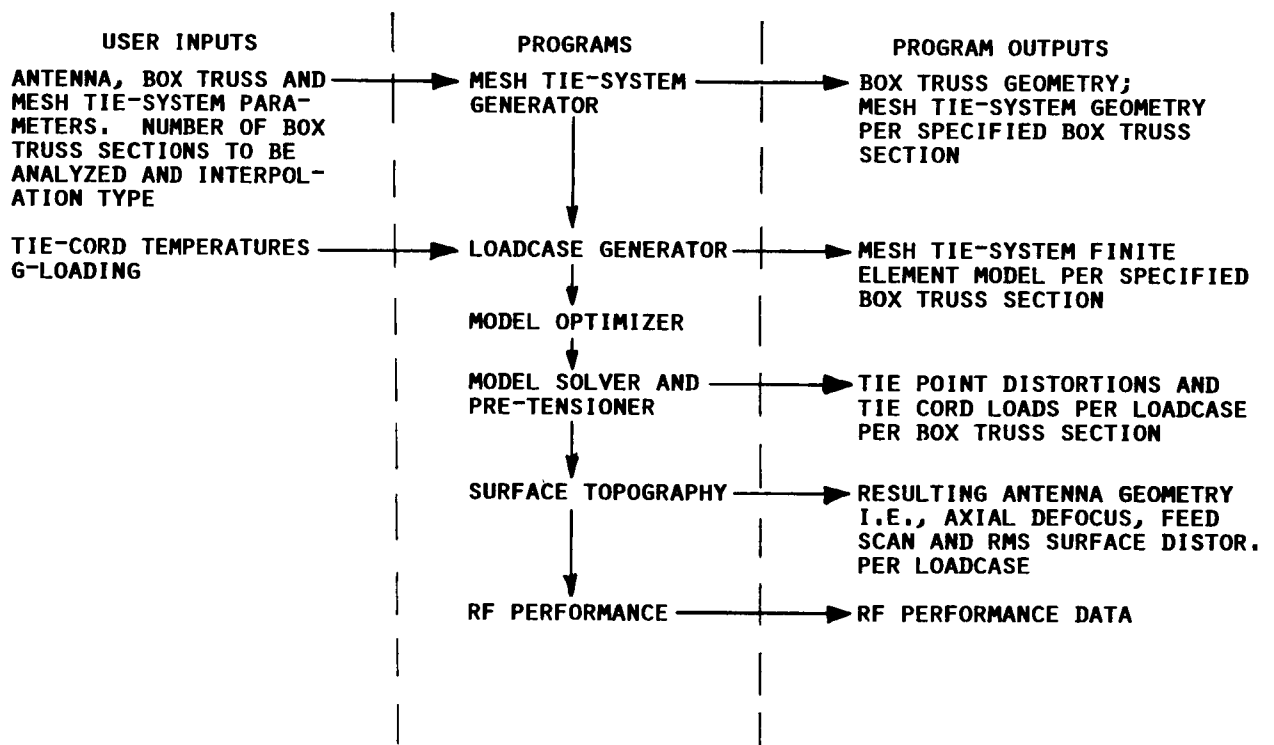
USER INPUTS	PROGRAMS	PROGRAM OUTPUTS
ANTENNA, BOX TRUSS AND MESH TIE-SYSTEM PARAMETERS. NUMBER OF BOX TRUSS SECTIONS TO BE ANALYZED AND INTERPOLATION TYPE	MESH TIE-SYSTEM GENERATOR	BOX TRUSS GEOMETRY; MESH TIE-SYSTEM GEOMETRY PER SPECIFIED BOX TRUSS SECTION
TIE-CORD TEMPERATURES G-LOADING	LOADCASE GENERATOR	MESH TIE-SYSTEM FINITE ELEMENT MODEL PER SPECIFIED BOX TRUSS SECTION
	MODEL OPTIMIZER	
	MODEL SOLVER AND PRE-TENSIONER	TIE POINT DISTORTIONS AND TIE CORD LOADS PER LOADCASE PER BOX TRUSS SECTION
	SURFACE TOPOGRAPHY	RESULTING ANTENNA GEOMETRY I.E., AXIAL DEFOCUS, FEED SCAN AND RMS SURFACE DISTOR. PER LOADCASE
	RF PERFORMANCE	RF PERFORMANCE DATA

Figure 8

726

DYNAMIC TESTING OF BOX TRUSS STRUCTURE

Testing was performed to quantify the effects of joint freeplay on a multi-bay statically determinate truss, and then assess the effects when the structure was modified to incorporate pretensioned diagonals producing a statically indeterminate truss. Also evaluated were the effects of levels of dynamic load on the dynamic performance of the truss. Testing of four truss configurations was performed:

1) Truss with tight joints.
2) Truss with joints having normal freeplay.
3) Truss with joints having excessive freeplay (3 times or more than normal freeplay).
4) Truss with normal freeplay and cross-tensioned diagonals.

The effect of magnitude of dynamic load was assessed for each test.

0   OBJECTIVE:

-    UNDERSTAND EFFECTS OF JOINT FREEPLAY ON DYNAMIC TRUSS BEHAVIOR

0   APPROACH:

-    BUILD AND TEST 2M x 20M 10-BAY TRUSS WITH NO FREEPLAY. 1 MIL FREEPLAY AND 3 MIL FREEPLAY. ALSO TEST CROSS-TENSION DIAGONALS.

Figure 9

DYNAMIC TEST ARTICLE

A test article for this purpose was designed and built. The test article consisted of ten bays of planar truss, each measuring 2-meters per side, suspended by long wires at each joint. Each side was made of square aluminum tubing, and all corner fittings were made of cast aluminum. Pins of varying size were used to assemble the truss thereby simulating various joint freeplay conditions. All joints could be shimmed and bolted tight to assure a no freeplay condition. Single, unloaded tube diagonals were interchangeable with dual, pretensioned steel rod diagonals. Modal analyses of the suspended tube diagonal configuration were conducted and used to calculate frequency response functions simulating proposed test conditions for the purpose of evaluating the suspension system. Figure 10 shows the test article with the pretensioned steel rod diagonals installed.
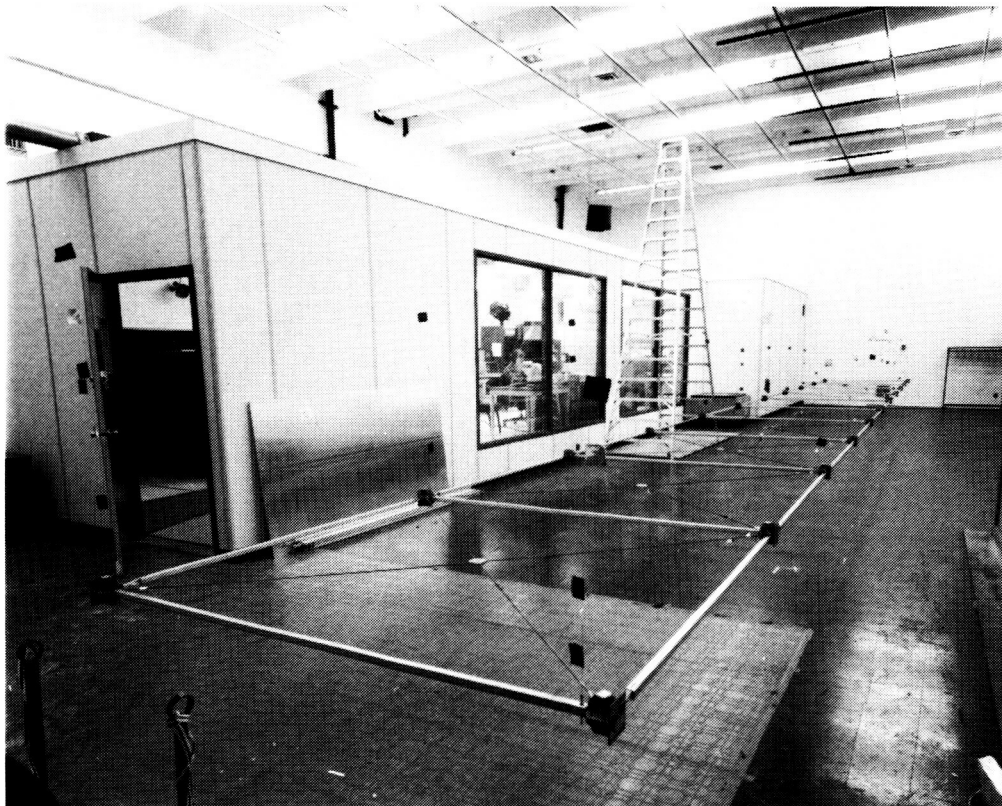
Figure 10

GENERAL TRENDS

General trends were observed for the various test models relative to the zero freeplay test model. At 1-mil freeplay both a small decrease in frequency and an increase in damping were observed. At low-level force input the structure did exhibit some nonlinear behavior. At high-level force input the structure behaved as a linear structure.

However, at 3-mil freeplay the structure was extremely nonlinear regardless of the force level. It also exhibited high damping which would be expected in a very sloppy structure. (Fig. 11.)

O   1 MIL FREEPLAY

- DECREASES FREQUENCY
- INCREASES DAMPING
- LINEAR STRUCTURE AT HIGHER INPUT
- NON-LINEAR RESPONSE AT LOWER INPUTS

O   3 MIL FREEPLAY

- EXTREME NON-LINEAR RESPONSE
- HIGH DAMPING

Figure 11

The existence of local pinned-pinned bending frequencies of the 2-meter truss member in the range of global truss bending frequencies caused the introduction of a multitude of local/global bending modes. Because the shape and frequency of such modes depend on unknown and nonlinear effects, such as joint fixity and local bending frequency variations due to oscillating loads in global modes, exact analytical predictions were difficult.

Quantification of the effect of joint freeplay was met. The tube diagonal configuration test data provided the information for this objective. The 1-mil freeplay resulted in a drop in frequency. (First global truss bending mode was identified at 20 Hz without freeplay and at 17.72 Hz with freeplay.) This frequency shift was consistent with that predicted by the Martin Marietta Denver Aerospace developed "Modal Freeplay" method, indicating that this method could be applied in future large space structures.

Damping is the least accurate parameter identified by curve fitting test transfer functions. Therefore, the uncertainties of the identified mode shapes and frequencies were of such magnitude as to preclude any exact definition of the effect of freeplay or preload on modal damping. (Fig. 12.)

O   THE TEST ARTICLE EXHIBITED A MULTITUDE OF LOCAL/GLOBAL COUPLING MODES.

O   INSTRUMENTATION WAS INSUFFICIENT TO IDENTIFY ALL MODES.

O   LOCAL/GLOBAL COUPLING PREVENTED THEORETICAL/EXPERIMENTAL CORRELATION IMPROVEMENT OF MODES THAT WERE IDENTIFIED.

O   SUFFICIENT DATA WERE OBTAINED TO EVALUATE THE MODAL FREEPLAY METHODOLOGY.

O   ASSESSMENT OF THE EFFECTS OF PRETENSIONED DIAGONALS WAS IMPEDED BY LOCAL/GLOBAL COUPLING EFFECTS.

O   QUALITY OF TEST DATA DID NOT ALLOW IDENTIFICATION OF RELIABLE MODAL DAMPING VALUE.

Figure 12

FABRICATION OF 4.5-METER BOX TRUSS ANTENNA

A 4.5-meter diameter offset mesh reflector was fabricated and integrated to an all graphite epoxy box truss cube. The reflector surface was designed to operate at X-Band (10 GHz) with a surface accuracy of 1/20 of a wavelength. Three objectives were achieved during the fabrication, setting and measurement of the antenna. These objectives were to: 1) demonstrate the fabrication methods for both mesh and tie system, 2) demonstrate performance of modular tie system to precisely position and hold mesh surface, and 3) verify empirical relationships for predicting rms surface errors due to mesh pillowing and manufacturing tolerances. (Fig. 13.)

O   OBJECTIVES:

-     DEMONSTRATE FABRICATION METHODS FOR MESH AND TIE SYSTEM
-     DEMONSTRATE MODULAR TIE SYSTEM
-     CHARACTERIZE PILLOW SHAPES

O   APPROACH:

-     BUILD 4.5 METER DIAMETER OFFSET MESH REFLECTOR INTEGRATED TO THE
      ALL GRAPHITE EPOXY BOX TRUSS DESIGNED TO OPERATE AT X-BAND

Figure 13

DIRECT TIEBACK TIE SYSTEM FEATURES

The depth of the mesh tie system can be optimized to produce either minimum packaging or maximum stability (thermal and structural). Also, the tie system cords do not span the entire width of the box section. This feature enables the tie system of each box section to be manufactured separately. This also helps to eliminate interaction between the tie systems of adjacent box sections, allowing each tie system of each box to operate independently. Consequently this produces a more stable reflector surface because local environmental effects such as shadowing of a single box section will not affect the precision of other box sections. Because each tie system operates independently, analysis and testing of the complete reflective surface can be performed on a per box section basis. (Fig. 14.)

o   THE MESH IS ATTACHED TO STANDOFFS WHICH CAN BE DESIGNED FOR MINIMUM THERMOELASTIC DISTORTION OF REFLECTOR (LONGER STANDOFFS) OR MINIMUM PACKAGING VOLUME (SHORTER STANDOFFS)

o   CONTINUOUS MESH SURFACE IS MADE BY SEWING THE INDIVIDUAL BOX SECTION MESH PANELS TOGETHER

o   EACH INDIVIDUAL BOX SECTION MESH TIE SYSTEM IS MODULAR (INDEPENDENT OF ADJACENT BOX MESH TIE SYSTEMS)

o   TIE SYSTEM MODULARITY FEATURE SIMPLIFIES MANUFACTURING AND SETTING OF ANTENNA. NO MATTER HOW LARGE THE ANTENNA, INDIVIDUAL BOX SECTIONS (MUCH SMALLER $\approx$ 3-10 M) CAN BE SET INDEPENDENTLY

o   TIE SYSTEM MODULARITY IMPROVES OPERATIONAL STABILITY BY ISOLATING LOCAL EFFECTS (EG. SHADOWING)

Figure 14

MESH AND TIE SYSTEM PRIOR TO SETTING

Integration of the reflector onto the box truss was completed in two main steps. First the mesh and tie system were installed onto the standoffs and the surface coarsely set to shape while the standoffs were installed in ground level wooden stands. Then, the standoffs and reflector were installed onto the box truss and the fine surface adjustment was completed. This two step process was used so no major scaffolding was needed to either mate the tie cord system to the mesh or set the surface to the paraboloidal shape. Figure 15 shows the reflector surface immediately after the tie system had been mated to the mesh and installed on the standoffs.

Figure 15

MESH TIE SYSTEM DURING SETTING

Figure 16 shows the next assembly step of the mesh reflector. Each tieback cord was inserted into the adjustment fittings and the surface was coarsely adjusted to shape. The adjustment fittings are an integral part of the standoff. Also shown in Figure 16 is the fact that each radial surface cord has been tensioned by attaching a weight to the end of the cord and hanging the weight over the top of the standoff. The weight is free to move thereby applying a constant tension of the surface cords. The amount of weight (1/4 lb per cord) was based on the relationship between surface cord tension, bi-axially tensioned mesh and the maximum allowed rms surface error due to mesh pillowing.
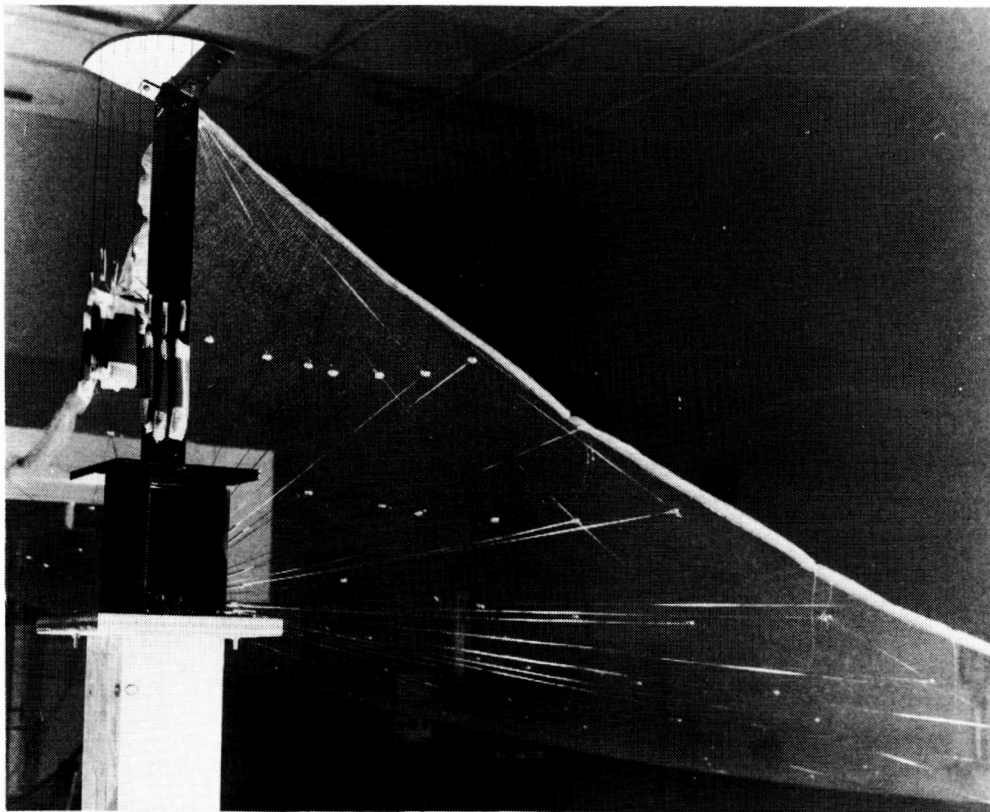
Figure 16

COMPLETED 4.5 METER ANTENNA

Figure 17 shows the completed 4.5-meter mesh reflector installed on the box truss just prior to having the surface verified by metric camera measurements. Although the box truss is rigid enough to be set upright, the metric camera measurements required the reflective surface to be parallel to the floor.
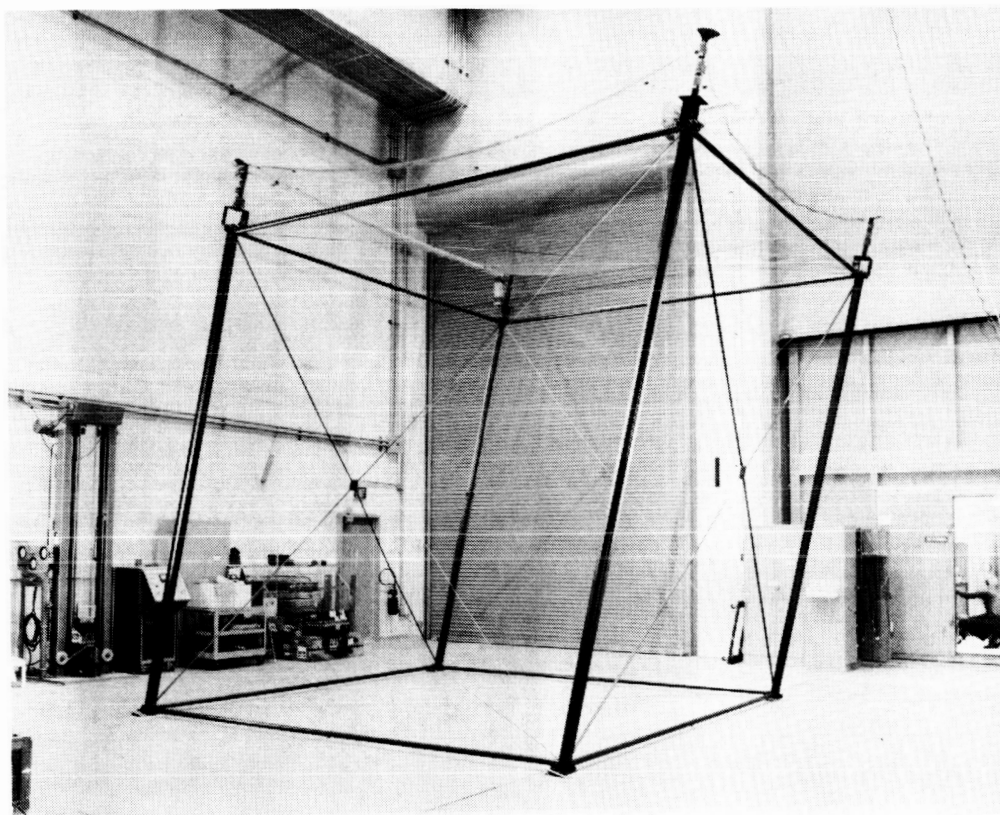
Figure 17

MEASUREMENT RESULTS FOR THE 4.5 METER ANTENNA

Figure 18 summarizes the surface verification results for the reflector. The results were obtained by using the metric camera measurements of the 176 tie points and 40 special mesh targets. The coordinates of 176 tie points were then used in a 'best-fit' analysis to determine the rms manufacturing error. The coordinates of the 40 mesh targets were used to determine the rms surface error due to mesh pillowing.

To determine the repeatability of the reflector two sets of surface measurements were performed. Set 1 was completed immediately following the theodolite surface setting. Set 2 was completed after the reflector had been partially stowed and redeployed.

In addition, during the 'best-fit' analysis, we found that one particular area of the reflector had been set lower than the rest of the surface due to improper initialization of the theodolite system. Therefore, the 'best-fit' analysis was completed for both the whole surface and the part of the surface that was unaffected by the improper initialization procedure.

	WHOLE SURFACE/ SET 1	PARTIAL SURFACE/ SET 1	WHOLE SURFACE/ SET 2	PARTIAL SURFACE/ SET 2
RMS MANUFACTURING ERROR, IN	0.050	0.040	0.049	0.041
RMS PILLOWING ERROR (AVE), IN	0.026	0.026	0.026	0.026
WORST - CASE SUM, IN	0.076	0.066	0.075	0.067
RSS OF RMS ERRORS,	0.056	0.048	0.055	0.049
AVERAGE OF WORST - CASE/RSS, IN	0.066*	0.057**	0.065△	0.058△△

* - REPRESENTS SURFACE ACCURACY OF 1/18 OF A WAVELENGTH

** - REPRESENTS SURFACE ACCURACY OF 1/21 OF A WAVELENGTH

△ - REPRESENTS SURFACE ACCURACY OF 1/18 OF A WAVELENGTH

△△ - REPRESENTS SURFACE ACCURACY OF 1/20 OF A WAVELENGTH

Figure 18

HOOP/COLUMN AND TETRAHEDRAL TRUSS
ELECTROMAGNETIC TESTS

M. C. Bailey
NASA Langley Research Center
Hampton, Virginia

# SURFACE DISTORTION FOR HOOP/COLUMN REFLECTOR ANTENNA

The distortion of the hoop/column antenna was measured with a metric camera system at discrete target locations on the surface. This figure shows a plot of the deviation from a perfect paraboloidal surface for one quadrant of the hoop/column reflector. The height of the distortion is amplified on the plot in order to show the surface features.

(QUADRANT-4)
(RMS = 0.167 CM)

MAXIMUM = +0.50 centimeter
MINIMUM = -0.80 centimeter
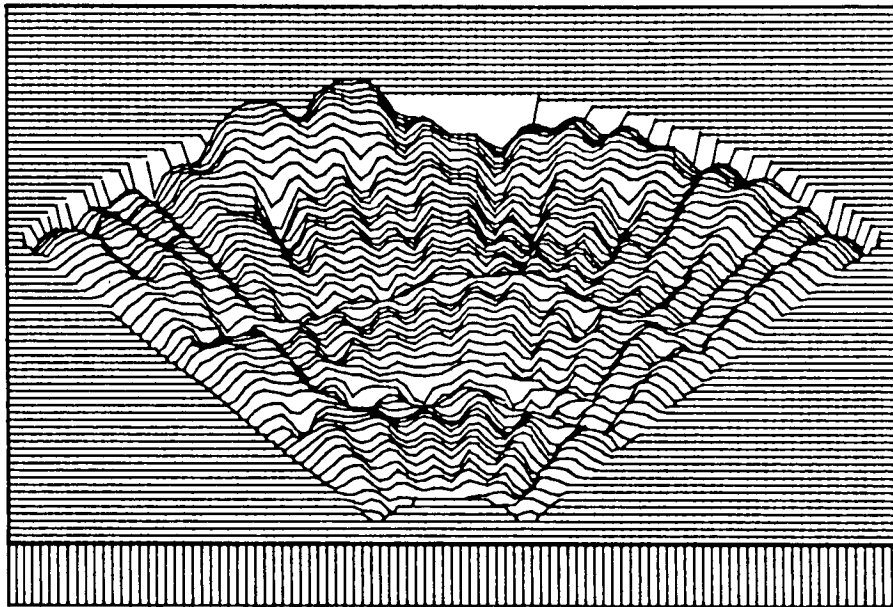
2.27-GHZ RADIATION PATTERNS FOR THE HOOP/COLUMN ANTENNA

The E-plane and H-plane radiation patterns are presented in this figure at 2.27 GHz. At this low frequency, the performance of the antenna is almost the same as a smooth surface.
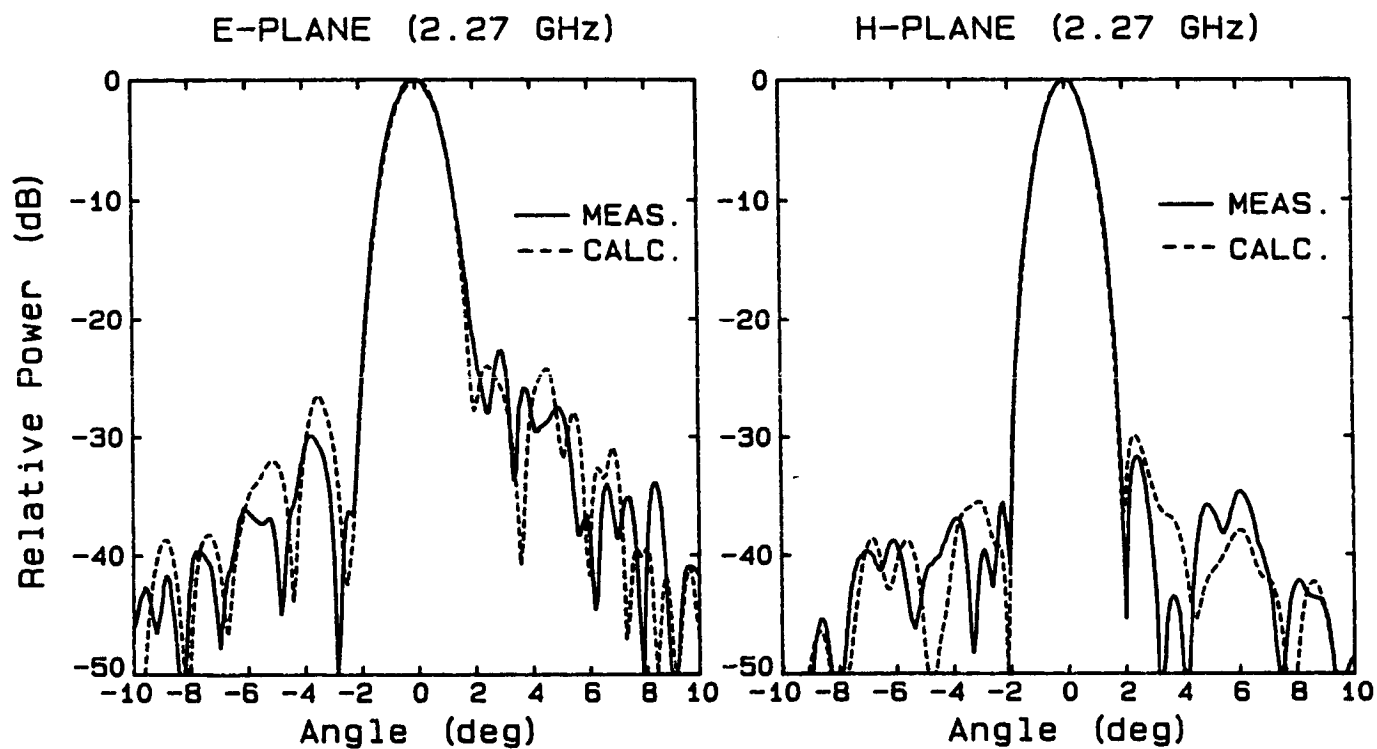
4.26-GHZ RADIATION PATTERNS FOR THE HOOP/COLUMN ANTENNA

At 4.26 GHz, the H-plane radiation pattern shows the formation of two sidelobes symmetrically located about the main beam. These lobes are characteristic of periodic errors in an antenna, or referred to as "grating" lobes.
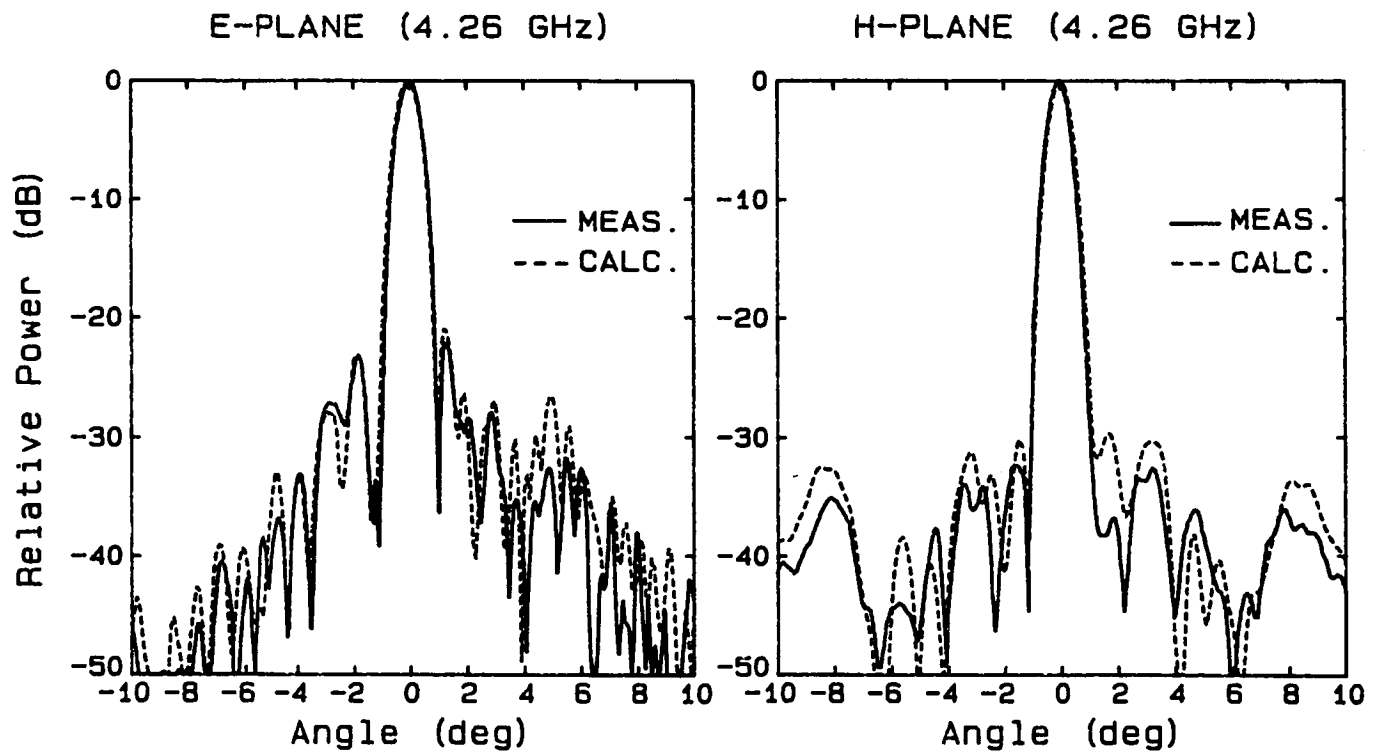
7.73-GHZ RADIATION PATTERNS FOR THE HOOP/COLUMN ANTENNA

At higher frequencies, these "grating" lobes increase in height and move closer to the main beam. In addition, the E-plane also shows sidelobes symmetrically located about the main beam and at a much lower level. One of these lobes (+6 degrees) in the E-plane shows some interference due to feed spillover onto the opposite quadrant of the reflector.

E-PLANE (7.73 GHz)   H-PLANE (7.73 GHz)
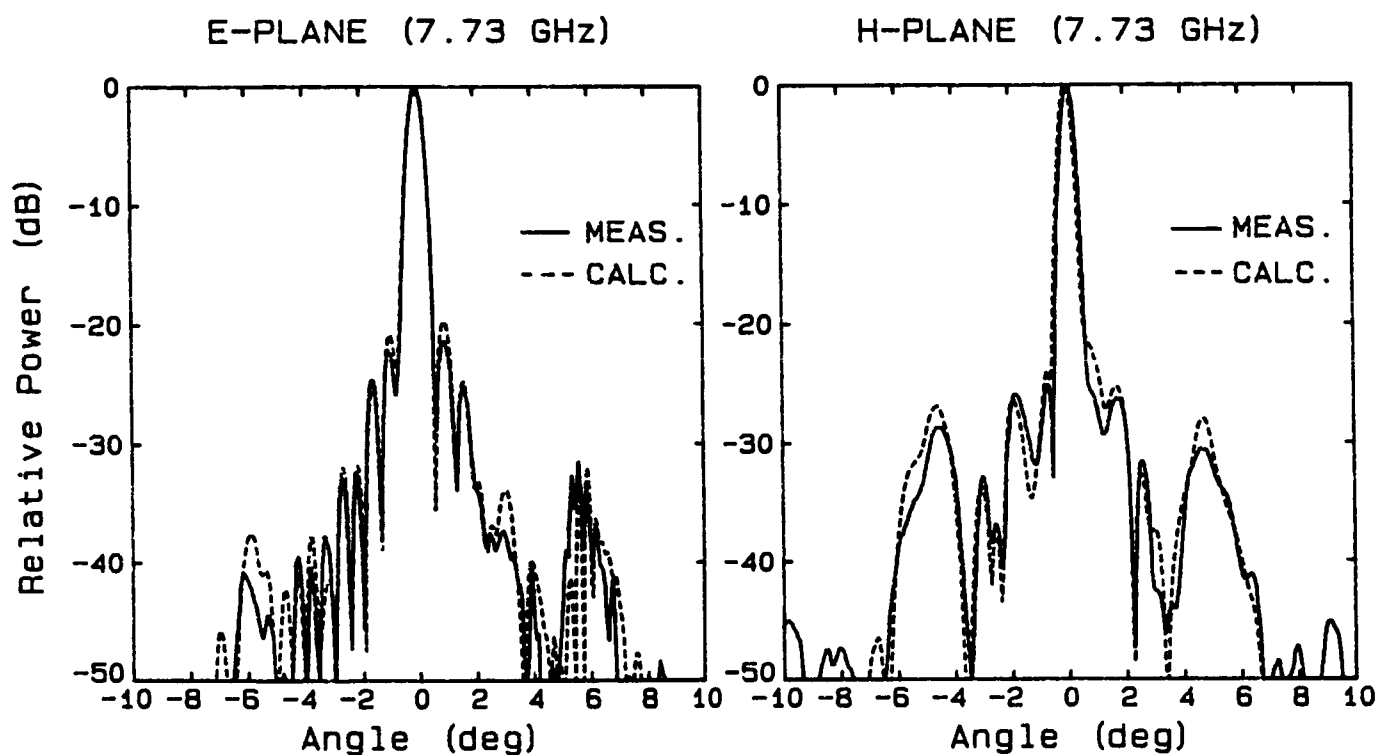
The contour plots of the radiation patterns show the "grating" lobes are actually several lobes located in a circular arc about the main beam. This arrangement of the "grating" lobes is due to the ripple in the surface being periodic in the circumferential direction rather than in a linear direction as is characteristic of truly periodic grating lobes.
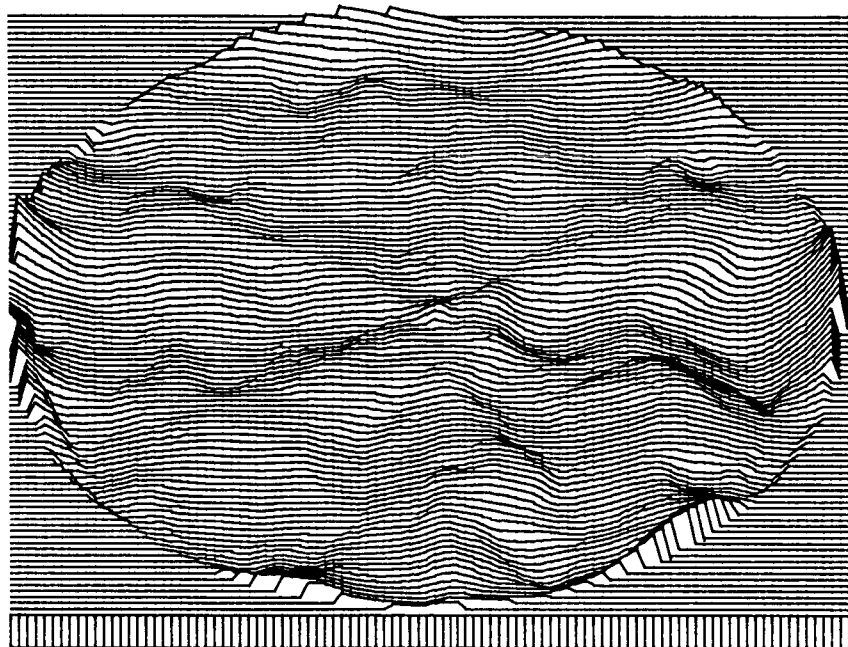
(11.6 GHz) (10dB increments) (0 to -30dB)

CALCULATED

MEASURED
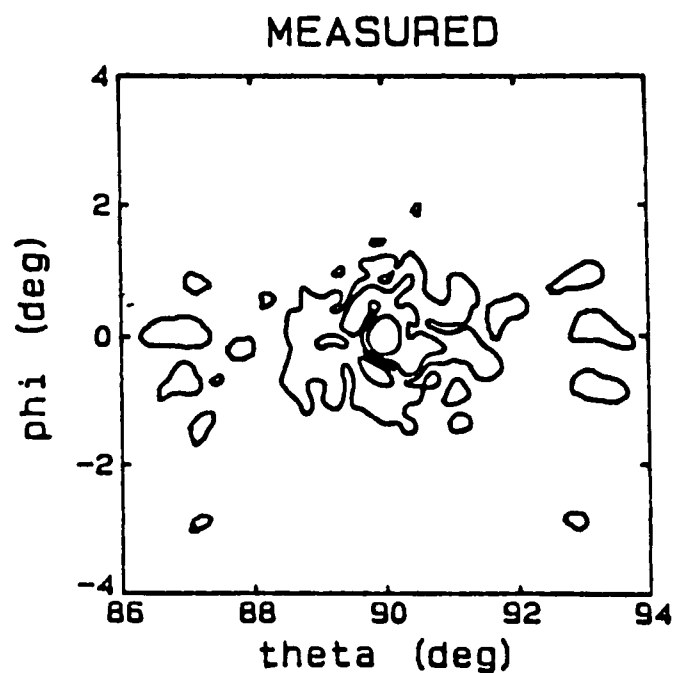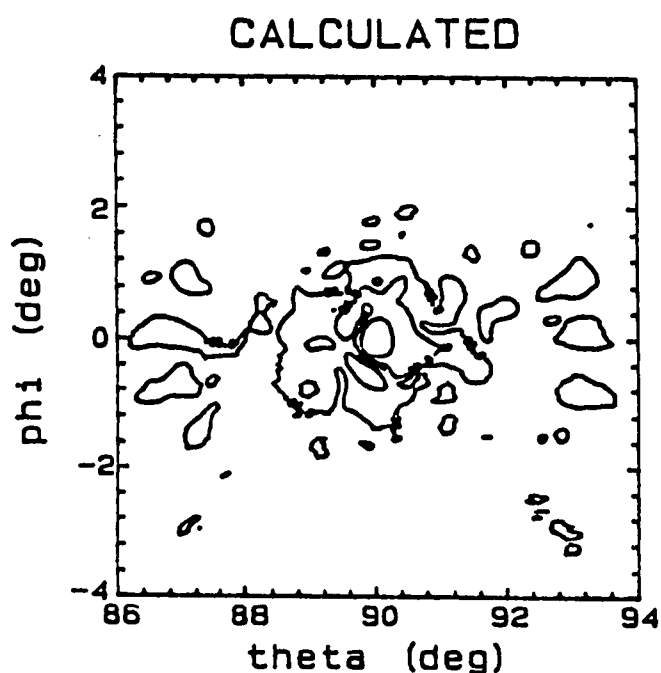
SURFACE DISTORTION FOR THE TETRAHEDRAL TRUSS REFLECTOR ANTENNA

The surface tie-points for the tetrahedral truss reflector were placed more randomly in order to avoid the periodic "pillowing" of the surface. This plot shows the deviation from a perfect paraboloidal surface with the height of the distortion also amplified on the plot.
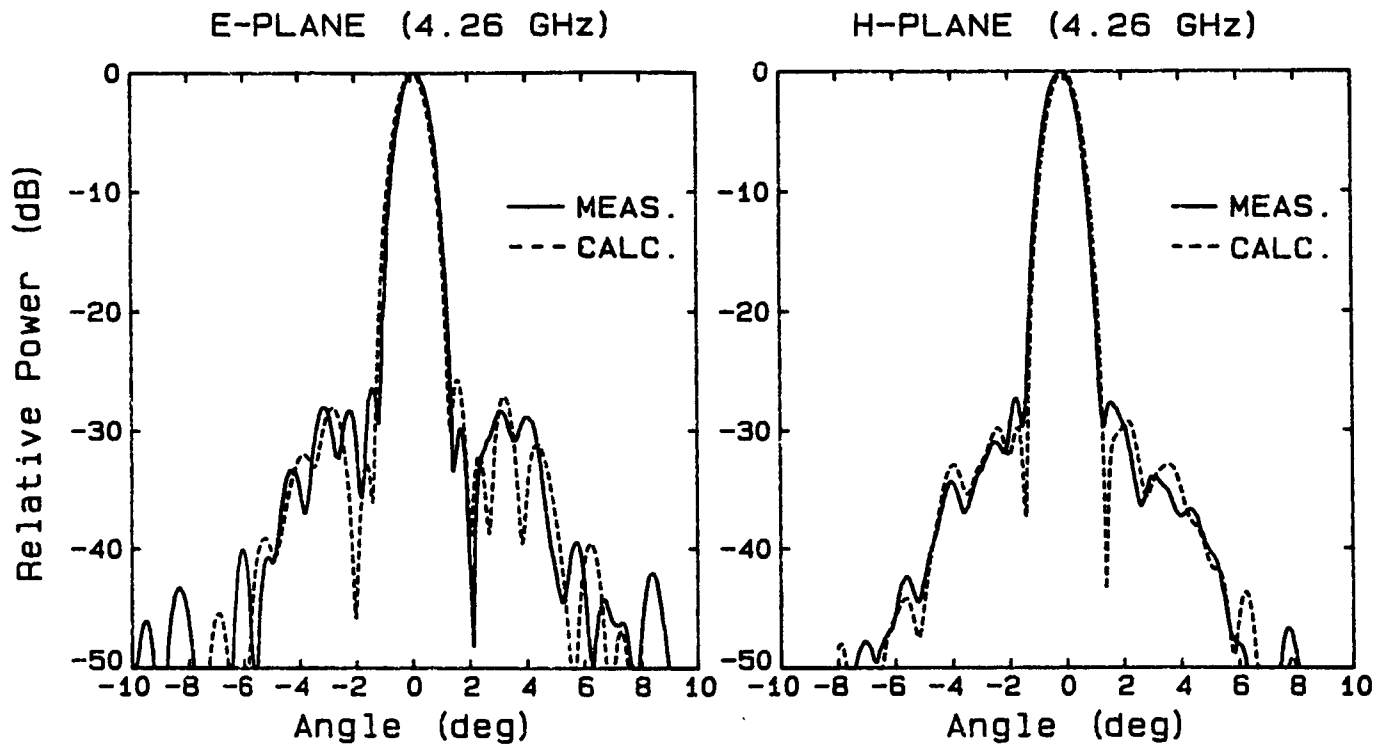
(RMS = 0.091 CM)

MAXIMUM = +0.60 centimeter
MINIMUM = -0.37 centimeter

4.26-GHZ RADIATION PATTERNS FOR THE TETRAHEDRAL TRUSS ANTENNA

Due to the randomizing of the surface tie-points, the radiation patterns for the tetrahedral truss do not have the "grating" lobes that were characteristic of the hoop/column antenna.
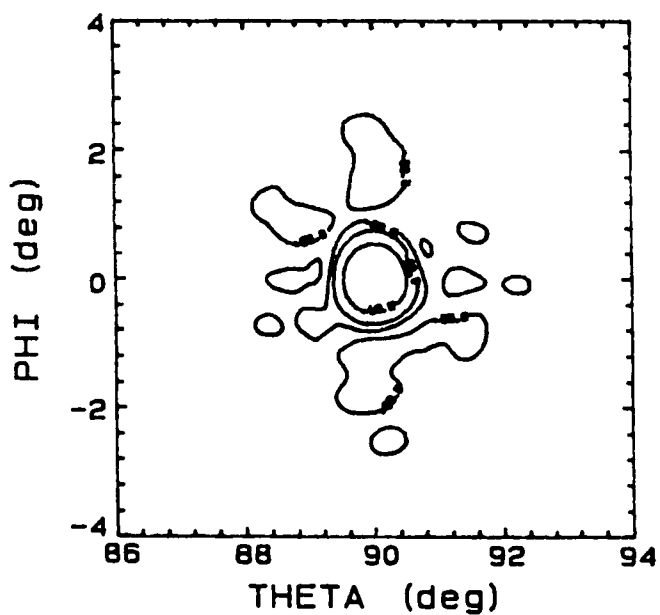

744

7.73-GHZ RADIATION PATTERNS FOR THE TETRAHEDRAL TRUSS ANTENNA
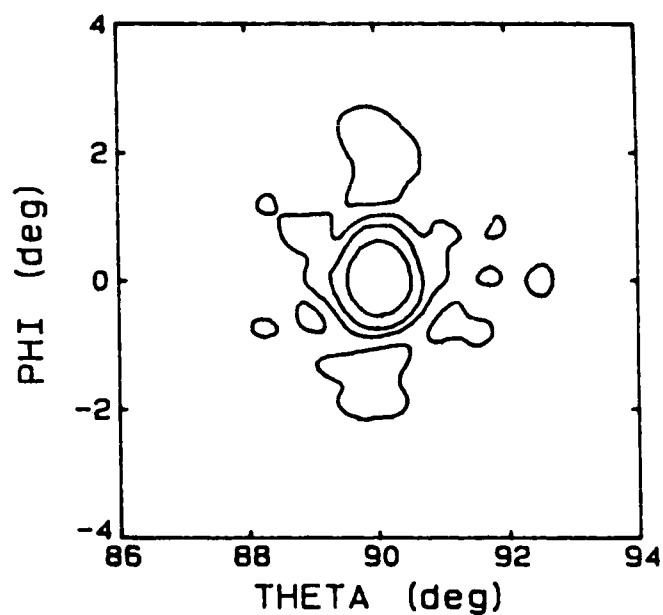
The contour radiation patterns at 7.73 GHz for the tetrahedral truss antenna do show symmetric lobes which appear to be trying to form in a six-fold symmetry about the main beam.

## (7.73 GHz) (10dB increments) (0 to -30dB)

CALCULATED

MEASURED

SURFACE DISTORTION CONTOURS FOR THE TETRAHEDRAL TRUSS REFLECTOR

Close examination of the surface distortion contours for the tetrahedral truss antenna indicates that a six-fold symmetry does appear to exist in the surface, thus creating the sidelobe structure observed in the previous radiation patterns.

CONTOUR INTERVALS OF 0.020 INCHES
dashed lines indicate negative contour levels
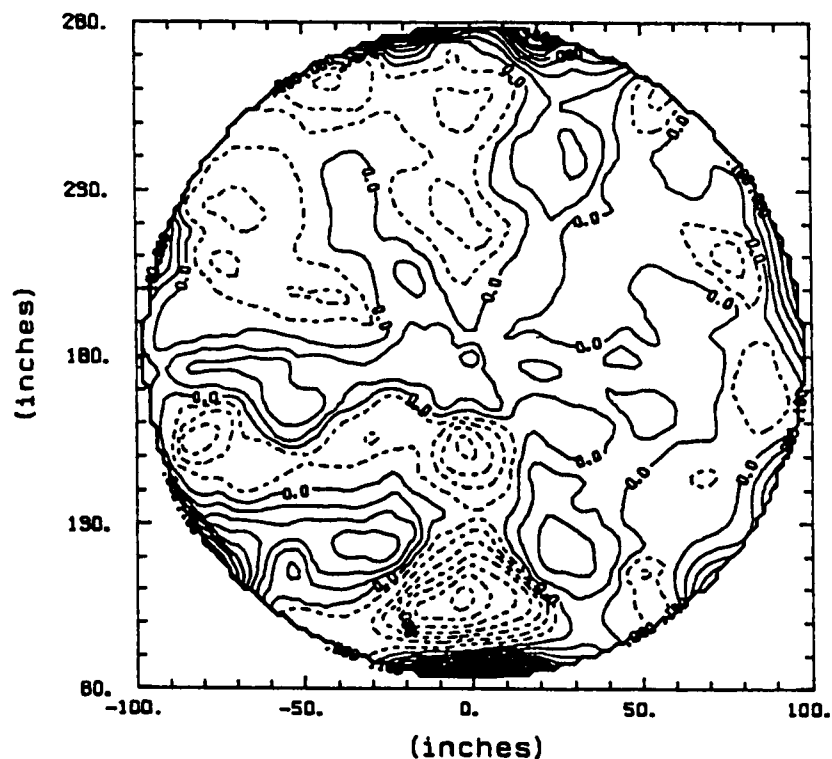
APPLICATION OF PHYSICAL PARAMETER IDENTIFICATION TO
FINITE-ELEMENT MODELS*

Allen J. Bronowicki,
Michael S. Lukich, and Steven P. Kuritz
TRW Space and Technology Group
Redondo Beach, CA

C - 3

Abstract

The time domain parameter identification method described in Volume I is applied to TRW's Large Space Structure Truss Experiment. Only control sensors and actuators are employed in the test procedure. The fit of the linear structural model to the test data is improved by more than an order of magnitude using a physically reasonable parameter set. The electro-magnetic control actuators are found to contribute significant damping due to a combination of eddy current and back EMF* effects. Uncertainties in both estimated physical parameters and modal behavior variables are given.

1 Summary

The availability of transient test data from TRW's Large Space Structure Truss Experiment (LSSTE) allowed the parameter identification procedure to be verified against actual hardware. Various member stiffness and mass properties, structural damping, magnetic damping in the control actuators, and actuator gains were the parameters which were adjusted to better match the model to reality. Using the approximation concepts approach, an orders of magnitude improvement in computational efficiency was obtained over previous efforts.

The use of Prony's method to fit exponentially damped sinusoids to the test data allowed visual verification of the linear damping assumption. This revealed that the primary source of damping in the control actuators for moderately large motions was due to magnetic hysteresis, and not friction. The large amount of damping available from electro-magnetic control actuators suggests their use for suppression of high frequency vibrations outside an active control system's bandwidth.

2 Test Sequence

The LSSTE is shown in Figure 1. The structure is basically a frame, with a fairly rigid top plate made of honeycomb supported by four thin columns. The primary modes are two lateral modes and a torsional mode of the top plate which involve primarily bending flexibility of the columns. The diagonal members carry no axial loads other than friction and damping forces, and control forces when the active vibration suppression system is turned on. The control system is designed to actively damp out vibrations induced by a pair of random disturbance generators located on the top plate. In order to employ a strong control algorithm, an accurate knowledge of plant behavior is necessary, hence, the need for parameter identification. It was the objective of this test–analysis correlation effort to employ only control sensors and actuators in order to simulate an on–orbit procedure.

A series of five **tests** were performed using various combinations of the four control actuators to apply initial forces and then suddenly release the load. Two lateral

---

* EMF (electro–motive force)

EXCITATION
ACTUATORS

ALIGNMENT
SENSOR
TARGET (2)

4 IN. THICK
ALUMINUM
HONEYCOMB
PLATE (2)

1 IN.
DIAMETER
ALUMINUM
TUBES
(0.049 IN.
WALL
THICKNESS)

CONTROL
ACTUATORS
(4)

ALIGNMENT
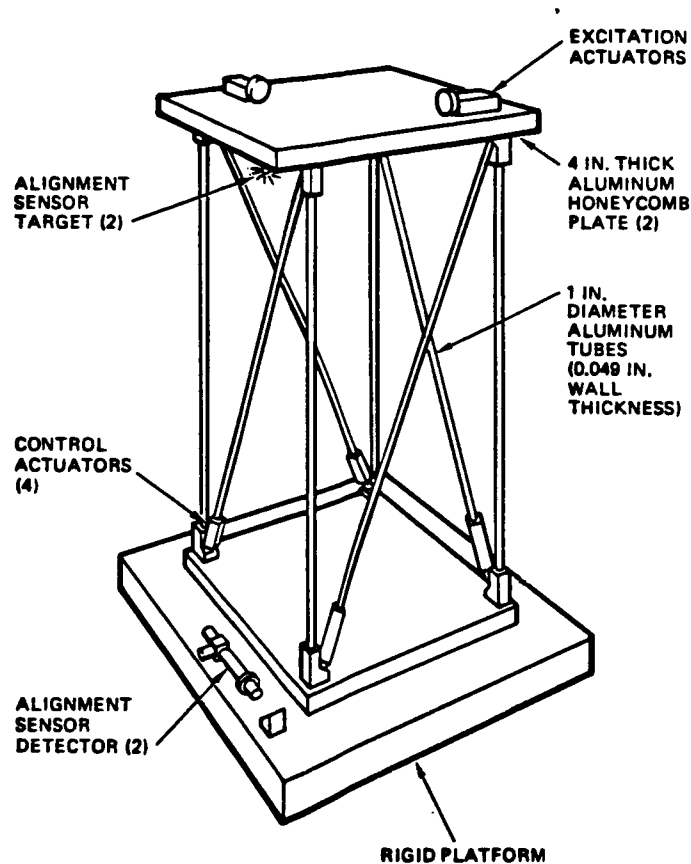SENSOR
DETECTOR (2)

RIGID PLATFORM

Figure 1:   Large Space Structure Truss Experiment Configuration

displacements at each of two Surface Accuracy Measurement Sensors (SAMS) were recorded from each of these events for a total of twenty observations. The original sampling rate was 200 samples per second,* which implies a Nyquist frequency of 100 Hz. To improve the ability of the Prony algorithm to resolve low frequency modes, which are around 1 Hz, the sampling rate was reduced to 40 sps. The data were pre–filtered to prevent aliasing using a five point Hanning smoothing algorithm developed at TRW. This algorithm preserves low frequency content and initial conditions while preventing phase shifts.

The Prony fits were employed only on the strong motion portion of the response time histories, up to 5.2 seconds. The goodness of fit was calibrated using a root mean square error norm between the Prony estimate and the actual data for each measurement. This error norm was used to assign uncertainty estimates to each of the measurements used in the Bayesian estimation procedure. Uncertainty estimates on physical parameters were chosen heuristically. The general rule was to assign large uncertainties (low weights) to prior parameter estimates in order to allow the model to match the test data as closely as possible.

* (sps)

3 Damping Models

The test data for all four sensors in one of the events designed to excite a lateral mode are shown in Figure 2. Also shown are the results of the Prony fit to the test data. It is readily apparent that exponentially damped sinusoids provide a good fit to the measured responses for moderately large motions. Hence a linear viscous damping model is valid in this regime. For small motions the response is seen to decay rapidly, indeed, it terminates entirely after 8 seconds of response. This suggests that Coulomb friction predominates in the small motion regime. (Recall that a Coulomb friction model results in a linear decay envelope.) The "grabbing" of the actuators suggests a transition from a dynamic coefficient of friction to a larger static coefficient as relative velocity in the actuators becomes small. A Dahl fiction model [1] was considered but rejected. The Dahl model provides a hyperbolic decay envelope which implies diminishing damping forces as response becomes small, contrary to our observations.

Modal damping ratios were assumed to be given by a superposition of intrinsic structural damping and viscous damping in the actuators, as expressed below for a given mode n:

$$\varsigma_n = \varsigma_{struct} + \Phi_n^T C \Phi_n / (2\omega_n)$$

The voice coil actuators used for active control employ powerful cobalt-samarium magnets surrounding copper coils. Using energy principles one can derive the actuators' damping constant from their electro-magnetic properties. The result is

$$c = c_{EMF} + c_{eddy} = K_B^2 / R \quad + \quad k_o B^2 V / \rho$$

The damping term due to back electro–motive force (EMF) is .269 lb/in/sec. The back EMF constant K_B and resistance R were supplied by the manufacturer and are 1.7 volts/foot/second and .66 ohms, respectively. The resistance of the control circuit power amplifiers was assumed to be negligible. The damping term due to eddy current or magnetic hysteresis was not known a priori since the magnetic field strength, B, and the volume of conductive material within the field, V, were unknown. The other variables are material resistivity ρ and a constant k_o. Note that both forms of magnetic damping are proportional to the square of the magnetic field and inversely proportional to resistance. Their effect can be profound when the magnetic field is large and resistance is small. Since the eddy-current portion of damping was not known it was assumed to equal the back EMF portion in the prior model used for estimation.

An excellent fit to the test data was obtained with a reasonable set of physical parameters. The sequence of events for a typical sensor is shown in Figure 3. One can see that the Prony fit to the test data is quite good, and that the model's response predictions were greatly

---

[1] Philip R. Dahl, "Solid Friction Damping of Mechanical Vibrations", *AIAA Journal*, Vol. 14, No. 12, December 1976.

improved by the estimation procedure. Only three finite element analyses were required for the identification procedure to converge. Each design iteration took about five minutes of CPU time on an IBM 3084. Following is a list of the design variables employed.

Column Stiffness The effects of the end fittings on column stiffness were unknown. The thickness of a short thin-walled tube element at the top and bottom of the column was chosen to model this effect.

Plate Mass The honeycomb top plate contains a large, unknown amount of adhesive and the mass of the corner fittings is also unknown. The center plate thickness and a corner plate thickness were chosen to model total mass and torsional inertia. The model of the plate was stiffened by a set of rigid elements to allow only mass properties to be estimated.

Structural Damping The overall level of material damping was estimated. A lower bound of $\varsigma_{struct} = .1$ % was enforced. (An advantage of the structural optimization approach to parameter ID is that reasonable bounds can be placed on parameters.)

Actuator Damping A linear viscous damping constant representing the sum of all damping effects in the actuators was chosen.

Actuator Gain The amount of force delivered by each actuator in each event was estimated. Due to the effects of stiction, this varied from event to event.

Initial and final values of the physical model parameters along with their standard deviations are given in Table 1. The large increase in corner plate thickness makes it clear that a large proportion of the mass is in the column fittings. The column stiffness was increased somewhat to reflect the rigidity of these end fittings.

Table 1: Initial and Final Physical Parameters

Parameter Description	Units	Value Initial	Value Final	Standard Deviation Initial	Standard Deviation Final	% Improvement
Tube t	inches	.049	.105	.2	.066	67
Corner Plate t	inches	4.	16.7	15.	4.78	68
Center Plate t	inches	4.	.594	8.	.35	96
Material Damping	%	.5	.1	5.	4.53	9.4
Actuator Damping	lb/in/sec	.54	1.14	5.	.805	84

Initial and final modal parameters along with their uncertainties are given in Table 2. (Uncertainty in modal damping was not computed). A large amount of modal damping was provided by the actuators. Modal damping coefficients on the order of six percent in the lateral modes and eight percent in the torsional modes were obtained.

An advantage of the Bayesian statistical approach to parameter identification is the availability of variance or uncertainty estimates on dependent variables such as weight and frequency. The algorithm directly identifies physical parameters such as element stiffness, mass and damping. The behavior variables are found indirectly as a result of the model predictions. As a result, uncertainty in model parameters can be cascaded through the analysis to provide uncertainty in model predictions. For example, the lateral mode frequency was estimated to be .704 Hz ±.0045 Hz, and the torsional mode was not estimated quite as well, being .992 Hz ±.016 Hz. It is reassuring that the modal parameters predicted by the estimated model are less uncertain than the physical model parameters themselves. One can see from the test data that the natural frequencies are well known. A large uncertainty in an estimated physical parameter will not be manifested in large behavior uncertainties if the sensitivities to that parameter are small.

Table 2: Initial and Final Behavior Variables

Parameter Description	Units	Value Initial	Final	Final Standard Deviation
Total Weight	lb	389.	328.	60.1
Lateral Mode f	Hertz	.614	.704	.0045
Torsional Mode f	Hertz	1.044	.992	.016
Lateral Mode ς	%	3.77	6.21	
Torsional Mode ς	%	5.42	7.70	

4   Conclusions

This relatively simple structure has demonstrated the validity of the parameter identification procedure for small to moderately sized structures. The procedure was found to be computationally efficient with the exception of mode shape sensitivity to model parameters, which consumed ninety percent of the entire computing budget. Scaling up to large models will require a much more efficient eigenvector derivative algorithm or the selective elimination of these computations for all but the most significant modes.

The use of physical parameter identification requires a great deal of thought in the selection of parameters which are both uncertain and have a large effect on response. This was found to be an iterative process between the analyst and the identification software. Initially a large set of parameters was chosen. This set was pruned down greatly as it was found that most parameters were not important or unidentifiable. The percent improvement in parameter uncertainty was very beneficial in this process. It was found that as parameters were removed from the estimation set, confidence in the remaining parameters increased. The choice of a minimum number off parameters is thus important. This process can take considerable analyst and computer time even for simple models.

The simplicity of the structure led to the lack of significant modes to identify. This procedure was exacerbated by the use of displacement sensors only. Accelerometers would measure response of high frequency modes with much greater resolution. It would be instructive to try this procedure on a more complex structure with accelerometers in addition to, or in lieu of displacement sensors.

The large amount of damping due to magnetic effects in the control actuators was a surprise. The use of this damping to augment an active vibration suppression system outside its computational bandwidth is a promising concept.
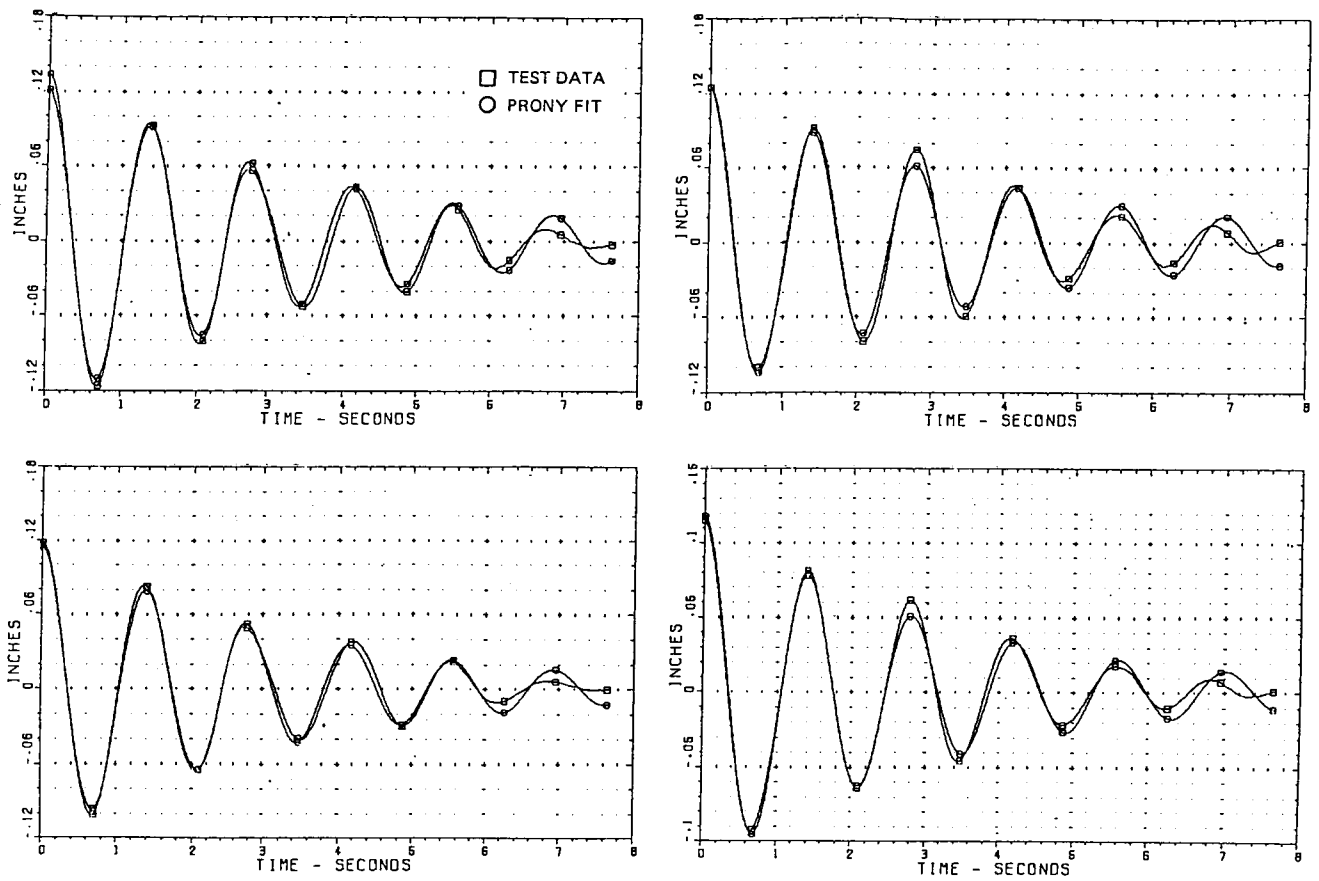
Figure 2: Prony Fit vs. Test Data for All Four Actuators in a Typical Load Event

Test Data Versus Prony Fit
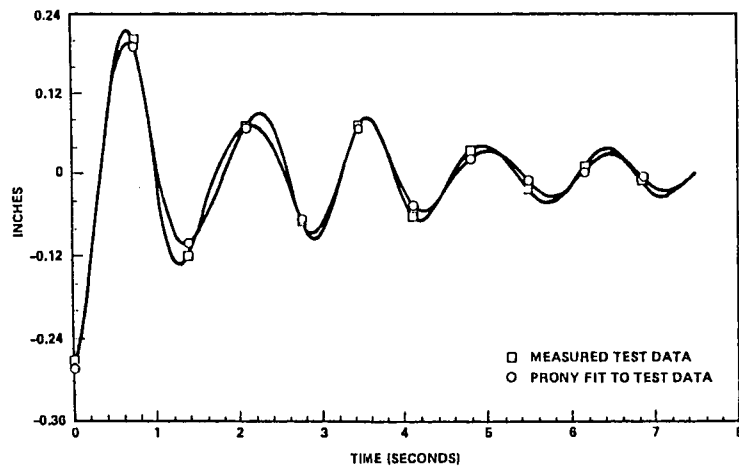
Initial NASTRAN Model Versus Prony Fit
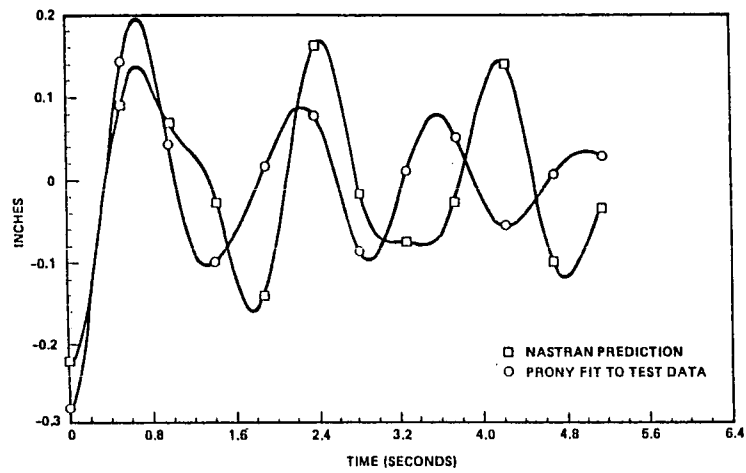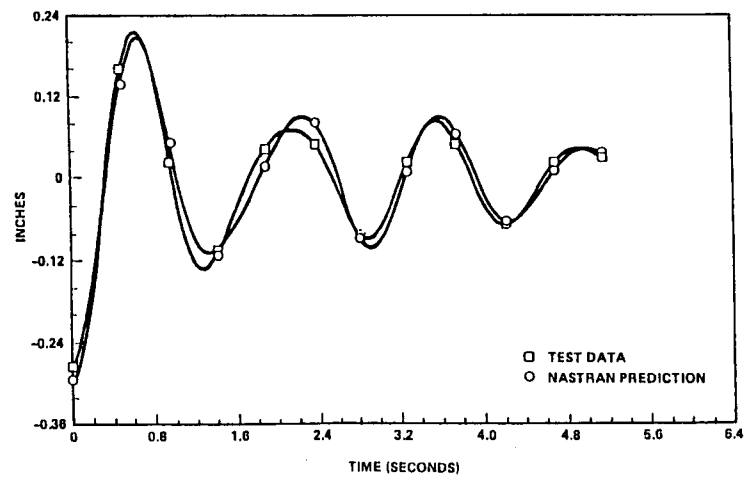

Final NASTRAN Model Versus Test Data

Figure 3: Identification Sequence for a Typical Sensor

COFS III
MULTIBODY DYNAMICS AND CONTROL TECHNOLOGY*

Robert Letchworth and Paul E. McGowan
NASA Langley Research Center
Hampton, Virginia

Marc J. Gronet
Lockheed Missiles and Space Company, Inc.
Sunnyvale, California

One of the results from the model definition study showed that the maximum scale factor for a replica model is .25. This is dictated by the fixed dimensions of the Large Spacecraft Laboratory or LSL (150 ft. height and 310 ft. diameter). Suspension analyses indicated the necessity to test the model in three planar orientations. The orientation depicted in the lower right-hand side of the figure requires the most test height, thus it limits the allowable scale factor.

SIZE OF LaRC LSL DICTATES A MAXIMUM SCALE FACTOR OF .25
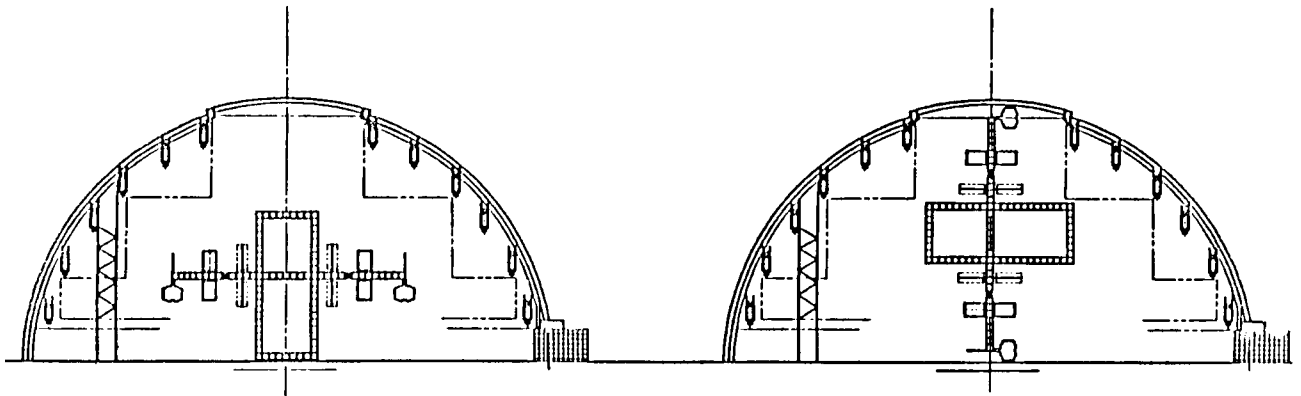
MODEL DEFINITION STUDY: SCALING ANALYSIS

Replica scaling laws were applied to simplified theoretical models of joints and the joint/tube/joint system. The practical interpretation of the results for the specific Space Station configuration under study yielded a number of conclusions. One is that if proper replica scaling is employed, the nonlinear behavior of the joints can be scaled. Another is that the stiffness of the joint/tube/joint system is not strongly dependent on the stiffness of the highly preloaded, erectable joint because almost all of the strain energy is in the tube. For the configuration studied, the stiffness (and hence the mode shapes and frequencies) of the model depends on the material used and the model suspension to first order, while the joint dynamics, gravity preloads, and airloads are at worst second-order effects.

Theoretically, the damping in the joints due to friction and impact can probably be matched as well if perfect replica scaling is employed. However, the scaling laws require that the joints be machined to precisely scaled tolerances. In addition, the damping due to other dissipation mechanisms such as the suspension system may contribute to first order. Thus, it will be a challenge to obtain reliable damping data from the scale model.

- **MODE AND FREQUENCY DATA CAN BE OBTAINED**

- **OVERALL STIFFNESS NOT STRONGLY DEPENDENT ON JOINTS**

- **RELIABLE DAMPING DATA DIFFICULT TO OBTAIN**
    - **COMPLEX JOINT BEHAVIOR MAKES REPLICA SCALING DIFFICULT BELOW 1/4 SCALE**
   - **SUSPENSION MAY ACT AS TUNED MASS ABSORBER**

MODEL DEFINITION STUDY: SUSPENSION ANALYSIS

Detailed suspension analyses were conducted to evaluate the ability of the suspended scale model to emulate the dynamic behavior of the free-free Space Station. The results indicated only a slight preference for smaller scales. Significant suspension system interaction occurred for all of the scale factors studied, requiring that the model be suspended in 3 planar orientations in order to test for most of the modes. The study also identified a number of potential problems with the cables in the suspension system. The interaction of the suspension system complicates the interpretation of the test data and places an increased dependence on the analyst's ability to accurately model the suspension dynamics.

- **BEST TO SUSPEND MODEL AT LARGE RIGID MASSES & FLEXIBLE APPENDAGES**

- **SUSPENSION NEEDED IN 3 PLANAR ORIENTATIONS**
  - **MOST MODES PLANAR**
  - **SOME 3-D MODES MAY NOT BE OBTAINABLE**
  - **ACTIVE SUSPENSION WOULD BE HELPFUL**

- **POTENTIAL PROBLEMS WITH CABLES**
  - **MUST BE TUNED TO PRESCRIBED STRESS LEVEL (65 CABLES MIN.)**
  - **"STRING" MODE INTERACTION**
  - **CABLE WEIGHT**
  - **SPURIOUS MODES MAY COMPLICATE DATA INTERPRETATION**

- **SLIGHT PREFERENCE FOR SMALLER SCALES**

MODEL DEFINITION STUDY: FREQUENCY INTERACTIONS

This figure presents some of the results of the suspension system trade study. Detailed finite element models were used to analyze the scale model suspended by steel cables in the proposed LaRC Large Spacecraft Laboratory (LSL). The frequencies of the system modes of the ISS Space Station model are indicated by the set of monotonically decreasing lines. The line near the bottom of the plot indicates the rigid-body pendulum mode frequencies. The shaded area represents the 1st mode frequencies of the cable string modes. The range of frequencies is greater at larger scales due to the fact that the LSL has a constant height, providing larger models with a wider variation in cable lengths. The overlap of the system modes and the cable string modes illustrates the strong potential for the cables to function as tuned-mass dynamic absorbers, as mentioned previously.
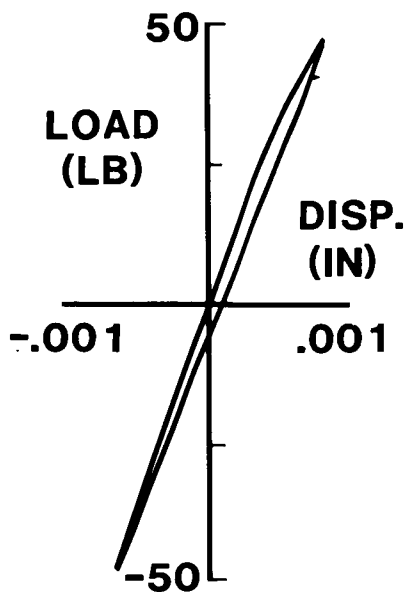
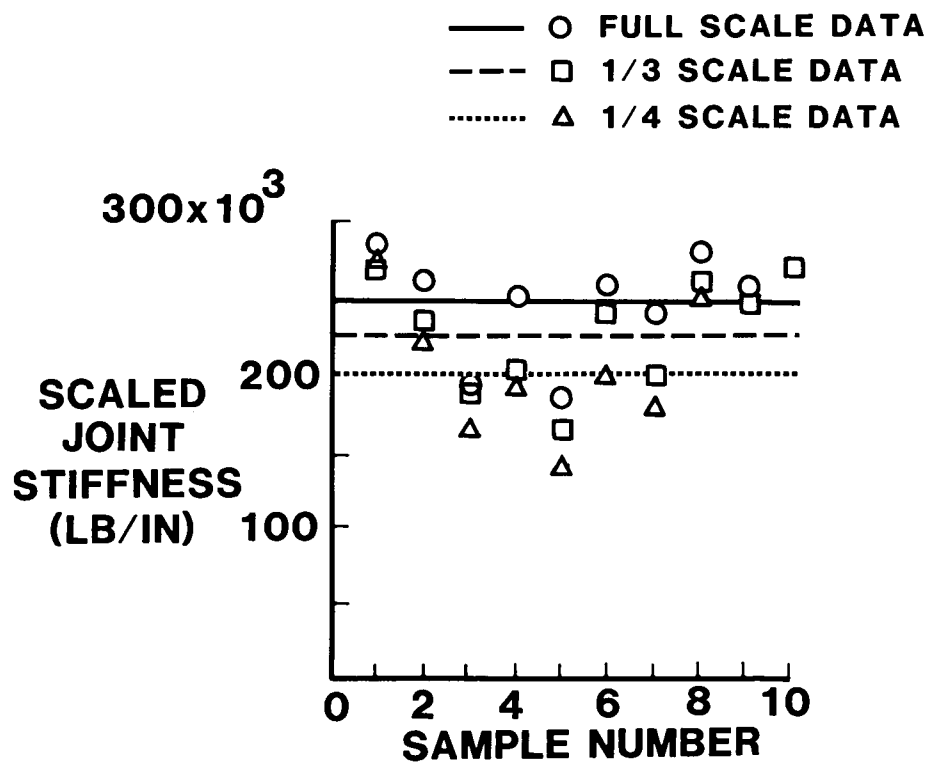

(STEEL CABLE, 10 KSI ALLOWABLE STRESS)
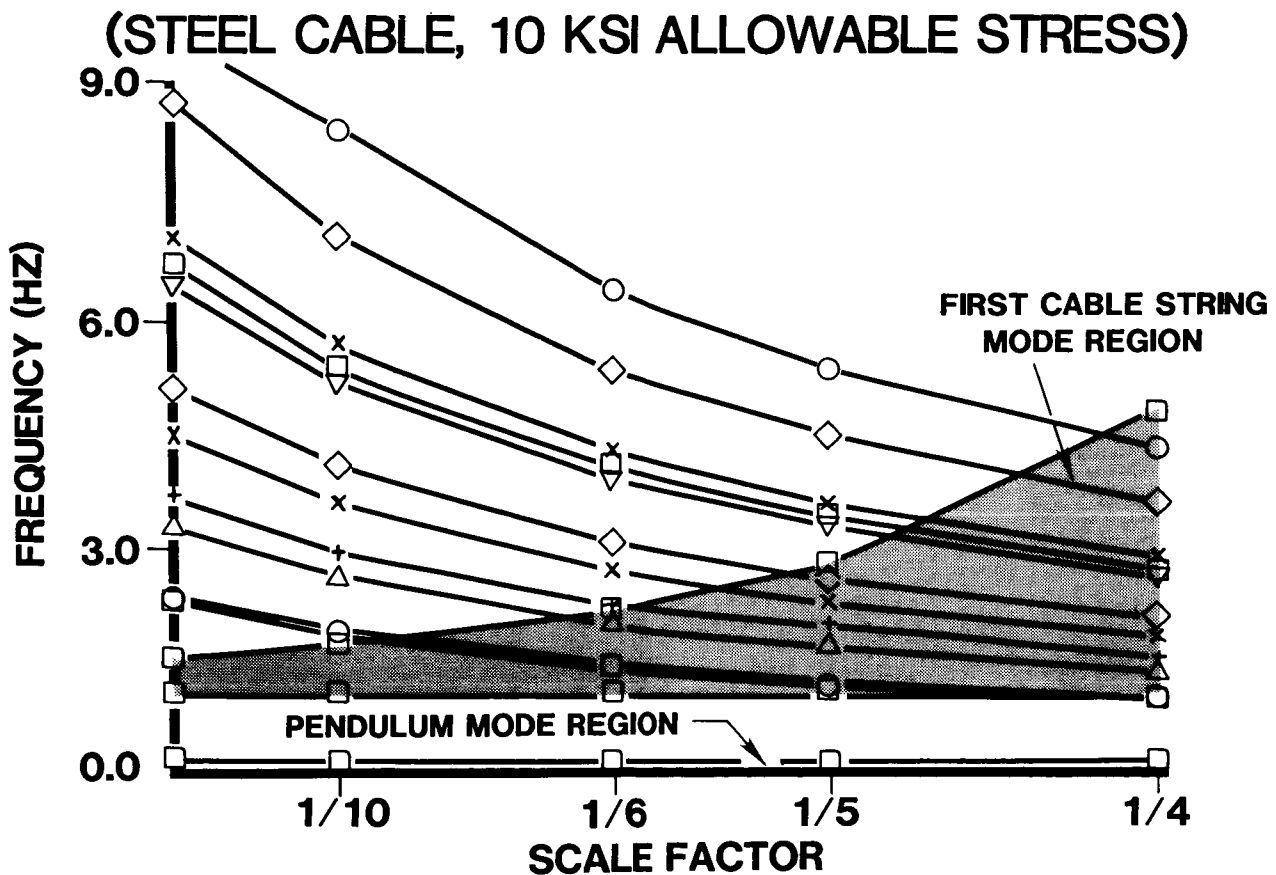
(INTERACTIONS BETWEEN SYS., PENDULUM, & CABLE MODE FREQ.)

A candidate erectable Space Station joint was fabricated at full scale and at 1/4 and 1/3 scales in order to assess the comparability of the scaled joints to the full-scale behavior. The scaled joints were intended to be close replicas of the full scale; however, certain features such as screw threads and machining tolerances were not scaled. Static tests were performed on the various joints and the joint axial stiffness was computed from the measured test data. For replica scaling, the joint axial stiffness should scale linearly with the scale factor. Thus, a 1/4-scale joint should have one-fourth the stiffness of a full-scale joint. The test results showed appreciable scatter due to variability from joint to joint; however, on average the 1/3 and 1/4 scale joints were only 8% and 13% below the theoretical values, respectively. These results are encouraging and it is believed that with better control over fabrication procedures joint stiffness can be properly scaled.

Typical Joint Static Test Data

Variation in Joint Stiffness

─── O FULL SCALE DATA

--- □ 1/3 SCALE DATA

········· △ 1/4 SCALE DATA

LOAD (LB)

DISP. (IN)

50

-.001   .001

-50

300×10^3

SCALED JOINT STIFFNESS (LB/IN)

200

100

0   2   4   6   8   10

SAMPLE NUMBER

JOINT DAMPING CORRELATIONS ENHANCED WITH INCREASED MODEL FIDELITY

Another important question is how well the inherent damping characteristics of the scaled joints compare to those of the full scale joint. Preliminary scaling analyses have shown that theoretically if replica conditions, then the damping energy loss factor should remain constant and independent of scale. This implies that all geometry, surface finish and tolerances be scaled, which is difficult in practice. A damping loss factor was computed for each size joint using the static test load deflection curves as depicted in the figure. On average the 1/3 and 1/4 scale joints were in error by 13% and 33% respectively. The larger error in the smaller joints is attributed to the tolerances which were not scaled. These results are encouraging; yet, it is noted that a series of dynamic tests need to be conducted in order to draw conclusions on the scaling of joint damping.

## Typical Static Load-Deflection Test Data
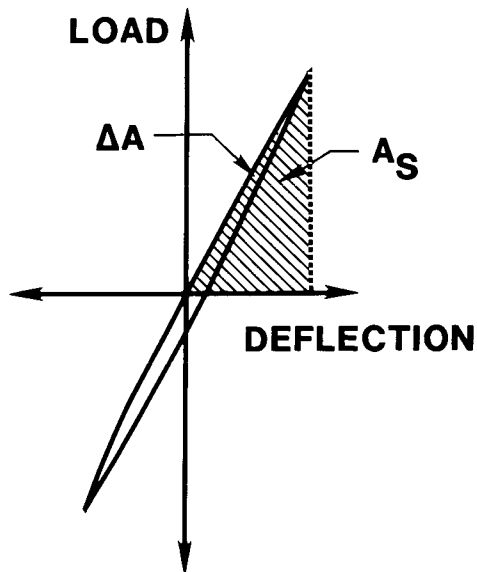
Damping Loss Factor (LF)

$$LF = \frac{\Delta A}{2\pi A_S}$$

JOINT	AVG. LF	% DIFF.
FULL SCALE	.030	-
1/3 SCALE	.026	13
1/4 SCALE	.040	33

GR/EP TUBES SCALED BY REDUCING NUMBER OF LAYERS

Graphite/epoxy tubes were fabricated at various scales to assess the feasibility of scaling Space Station truss members. A simple uni-directional lay-up was chosen for the full scale tubes. The scaled tubes were fabricated by reducing the number of layers proportionate to the scale factor. A measure of the performance of the scaled tubes is the tube weight to stiffness parameter. For replica scaling this parameter should vary with the square of the scale factor. Plotted in the adjoining figure is the ratio of the weight to stiffness for the scaled tubes to that of the full scale tubes raised to the 1/2 power, a quantity which should be linear for replica scaling. The preliminary test data show excellent correlation with the theoretical values.
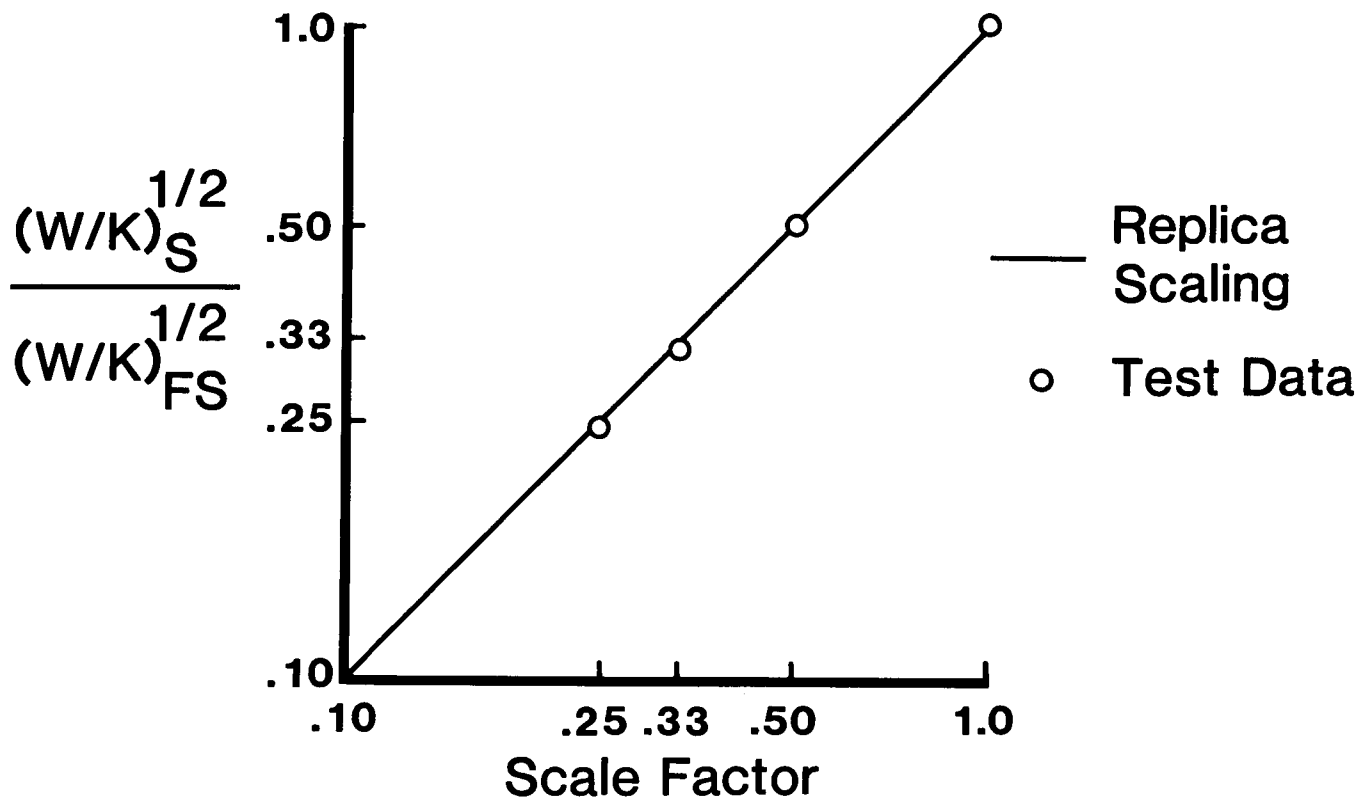
MODEL DEFINITION STUDY: SCALE FACTOR RECOMMENDATIONS

The preliminary definition study yielded three separate scale factor recommendations for the scale model. Systems analyses favored a scale factor between 1/4 and 1/5 for a replica model, a scale factor of 1/5 for a model with simulated joints, and did not overwhelmingly favor a particular scale factor for a fully simulated model. Constructing a replica scale model maximizes the utility of the model for anticipated and as yet unanticipated tests. Given that the Space Station joints are still under development, it may be prudent to initiate the test program with simulated joints and then replace them with replica joints at a later date, if necessary.

- **REPLICA MODEL**
    - **COST CONSIDERATIONS FAVOR 1/4 SCALE**
    - **DYNAMIC CONSIDERATIONS FAVOR 1/5 SCALE**

- **SIMULATED MODEL WITH AN OPTION FOR LATER REPLICATION**
    - **RECOMMEND 1/5 SCALE**

- **FULLY SIMULATED MODEL (LINEAR JOINTS)**
    - **COMPARATIVELY LOW SENSITIVITY TO SCALE FACTOR**

CONTROL TECHNOLOGY OVERVIEW IN CSI

J. B. Dahlgren and A. F. Tolivar
Jet Propulsion Laboratory
Pasadena, California

The chart illustrates the evolution of some representative on-board control systems designs. While the chart is not intended to be all-inclusive it does represent major trends in spacecraft control systems. Typical of the first generation controllers flown was that of the Viking orbiter that estimates spacecraft angular velocities from celestial reference measurements. The estimator was a simple second-order analog system based on a linearized single-axis model for the vehicle dynamics. In Voyager a digital implementation became possible because of the introduction of a digital processor for reprogrammable implementation. In the second-generation systems, a more advanced class of estimator designs provides the capability for on-board attitude determination. The Shuttle and Galileo dual-spin spacecraft designs are typical of this generation. Future space systems requiring high dimensional advanced control/estimation designs including: large antenna systems with the need for static and dynamic shape determination; Space Station with the capability for relative position/attitude determination for intervehicle control, configuration tracking, and system identification to establish knowledge of poorly known vehicle dynamics; and advanced astrophysic missions such as the Large Deployable Reflector where the requirements for active vibration control and the precise maintenance of the overall figure of a multi-segmented aperture will involve sensing and control of perhaps 1000 degrees of freedom.
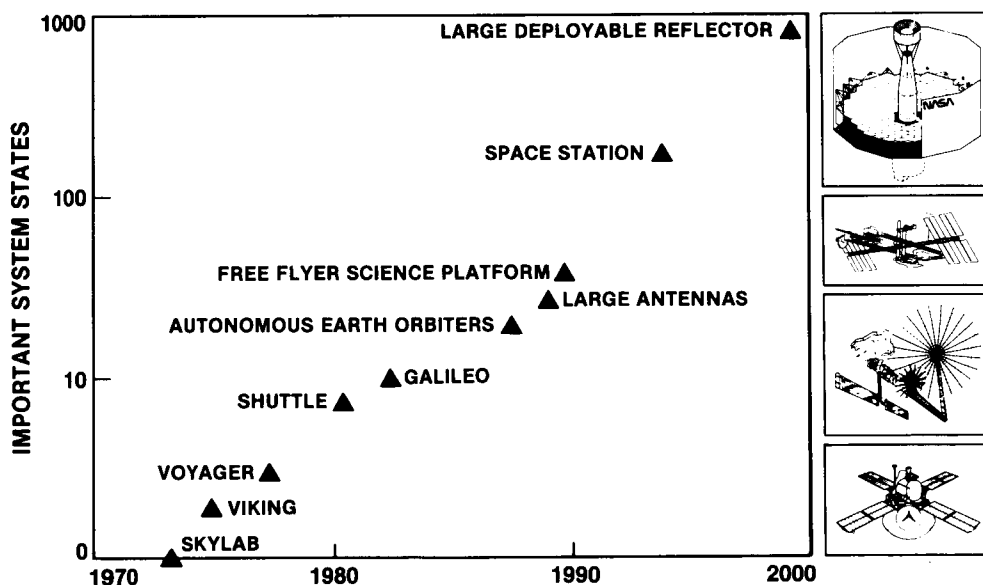
KEY CSI TECHNOLOGY NEEDS

There are a number of key technology needs requiring attention in the CSI development. These are shown in the table. Development of appropriate truncation criteria and techniques of finite element models for space structures is still immature, and therefore a crucial area in CSI technology continues to be the area of analytical modeling and model reduction. New structural concepts for space system application need to be pursued recognizing the goal of an optimal control system design, in addition to conventional goals such as lightweight, efficient packaging, and reliable and predictable deployment. System identification, where the structural and dynamic characteristics are inferred from observed response to known disturbances, provides for in-flight tuning of the controlled "plant" to achieve high control performance. Another important CSI area is in control law design methodology where control authority, parameter uncertainty, and robustness must be appropriately traded- off to provide a unified conceptual and theoretical architecture. For the case of simplified structures the control systems robustness may be measured by the typical "gain" and "phase" margins. These concepts are largely unusable for CSI designs and therefore new robustness criteria are required. The increased number of new types of sensors and actuators required for CSI control systems together with the need for in-flight characterization and relatively complex near real-time matrix calculations create a substantial computational requirement for new digital implementation approaches. Since CSI technology differs from conventional control-structure approaches new synthesis and design software tools are needed. Technology validation programs through ground and on-orbit testing are essential as part of the qualification/acceptance sequences for new CSI control strategies. The cost of large space systems will be significant and the implementation of CSI control technologies, as described, to these flight articles will require special attention to reliability and fault-tolerance.

1) ANALYTIC MODELING AND MODEL REDUCTION

2) STRUCTURAL CONCEPTS

3) SYSTEM IDENTIFICATION

4) CONTROL LAW DESIGN METHODOLOGY

5) ROBUSTNESS CRITERIA

6) SENSOR AND ACTUATOR DEVELOPMENT

7) DIGITAL IMPLEMENTATION TECHNOLOGY

8) SYNTHESIS AND DESIGN SOFTWARE TOOLS

9) GROUND TESTING

10) ON-ORBIT TESTING

11) RELIABILITY ISSUES (FAULT-TOLERANCE)

The JPL technology development program related to CSI is directed at a range of space applications including space platforms, large antennas, and large segmented optics systems. Many of these advanced spacecraft may be characterized by tens of modes below 1 Hz with poor a priori knowledge of system dynamics, 20-100m apertures whose figure/alignment needs to be controlled with sub-millimeter accuracy, and spacecraft/payload pointing to stringent requirements. New and advanced control theories and methodologies are under development to cope with these challenges including system identification, adaptive control and unified modeling and design. These areas are covered in the following charts.

In the advanced hardware components area a sensor in under development which applies to a number of CSI areas. The objective for the sensor, given the name of SHAPES for Spatial High-Accuracy Position Encoding Sensor, is to provide high date rate, multipoint, 3-D position sensing to submillimeter accuracy which lends itself to performing dynamic measurements of large space structures.

Another important element in the program is the validation of these technologies through appropriate ground and flight experiment testing. Plans are in place to carry out an extensive ground test program of evolving control methodologies such as figure sensing/control, open and closed loop identification, active vibration control, and others. Appropriate flight experiment planning for many of these same technologies is also under way in support to the Control of Flexible Structures Programs (COFS) and the Antenna Technology Shuttle Experiment (ATSE).

- THEORY/METHODOLOGY
  - SYSTEM IDENTIFICATION
  - ADAPTIVE CONTROL
  - UNIFIED MODELING AND DESIGN

- ADVANCED HARDWARE COMPONENTS
  - SHAPES 3-D FIGURE SENSOR

- GROUND VALIDATION/TESTING
  - FIGURE SENSING/CONTROL
  - OPEN/CLOSED LOOP IDENTIFICATION
  - ACTIVE VIBRATION CONTROL

- FLIGHT EXPERIMENT PLANNING
  - CONTROL OF FLEXIBLE STRUCTURES PROGRAM
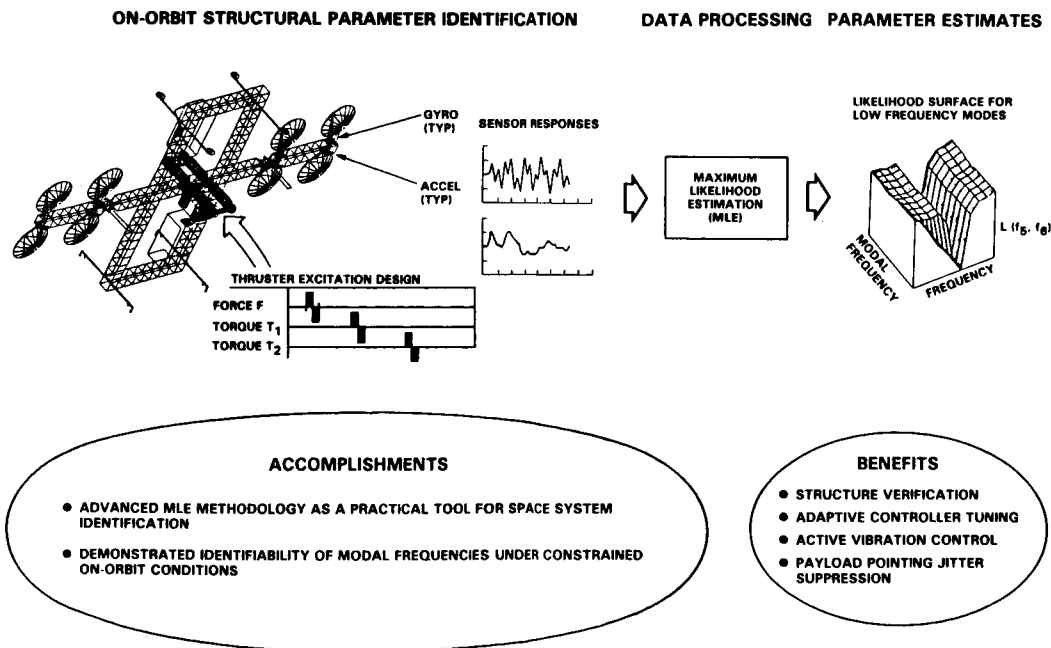 - ANTENNA TECHNOLOGY SHUTTLE EXPERIMENT

ON-ORBIT SYSTEM IDENTIFICATION

The identification of modal parameters provides information required for structure verification, controller tuning, active vibration control, payload pointing jitter suppression, and vehicle stabilization.

The objective of the On-orbit System Identification task is to develop methodology, techniques and algorithms required to perform in-flight control dynamics identification and characterization of key structural and environmental parameters. The technical approach is to develop and combine state-of-the-art linear and non-linear estimation techniques with realistic on-orbit experimentation and application procedures.

Accomplishments during FY'86 included the integration and evaluation of optimal excitation design techniques and Maximum Likelihood Estimation (MLE) methodology as a practical tool for system identification of Large Space Structures (LSS), and also demonstrated system identifiability of modal frequencies under constrained excitations and sensing. These results advance the methodology for on-orbit testing of LSS under operational constraints.

Future research plans include: Development of actuation and sensing strategies which extract parameter information efficiently (i.e., optimal design of experiment) given a constrained on-orbit configuration and testing environment; focus on the identification of parameters which directly support on-board controllers; and development of end-to-end methodology for synergistic use of frequency and time domain identification techniques.

ON-ORBIT STRUCTURAL PARAMETER IDENTIFICATION   DATA PROCESSING   PARAMETER ESTIMATES

ACCOMPLISHMENTS

- ADVANCED MLE METHODOLOGY AS A PRACTICAL TOOL FOR SPACE SYSTEM IDENTIFICATION
- DEMONSTRATED IDENTIFIABILITY OF MODAL FREQUENCIES UNDER CONSTRAINED ON-ORBIT CONDITIONS

BENEFITS

- STRUCTURE VERIFICATION
- ADAPTIVE CONTROLLER TUNING
- ACTIVE VIBRATION CONTROL
- PAYLOAD POINTING JITTER SUPPRESSION

AUTONOMOUS ADAPTIVE CONTROL SUBSYSTEM DEVELOPMENT

The research objective of this task is to develop an autonomous adaptive control subsystem for application to emerging space systems, including future large flexible structures and aeromaneuvering vehicles. The overall approach is to develop and integrate high level intelligent control technology with state-of-the-art adaptive control techniques, resulting in a controller design which is robust to both gross system changes, such as large parameter changes, hardware failures, model-order variations, anomalies, operational disturbances and changes in mission objectives, as well as to local phenomena including drifting parameters, model uncertainties, and environmental disturbances. This concept will provide robust stabilization and control with enhanced performance for future space systems.

Accomplishments in FY 86 included development of the direct output gain weighting concept for providing increased control effectiveness in large multivariable adaptive control systems, sufficient conditions for global stability of the extended algorithm, and application of these techniques to high precision adaptive payload articulation/tracking control.

Future plans include the testing and experimental validation of these techniques in the JPL/RPL 3-D control technology experiment through a sequence of increasingly demanding demonstrations. The theoretical work during FY 87 will address several new and important areas: 1) the development of systematic algorithms for choosing design parameters for improved adaptive performance/robust controller, and 2) the introduction of intelligent control techniques to incorporate in-flight dynamics and performance knowledge with the appropriate design rules towards realization of a completely autonomous adaptive control subsystem.
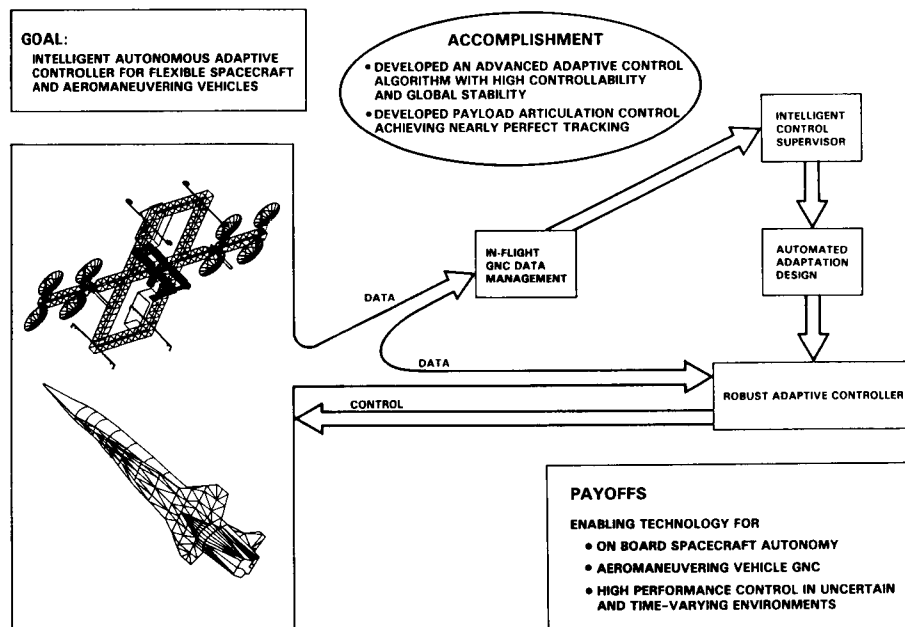
UNIFIED CONTROL/STRUCTURE MODELING FOR CONTROL SYSTEM DESIGN

This task addresses the fundamental theoretical issues arising in the modeling of CSI systems where performance objectives require control systems which interact with the structure. The ultimate program goal is to develop a computer-aided design package for modeling and control design that incorporates elements from distributed parameter system theory, control-driven modeling, model reduction methodologies, and robust control design methods. This package will enable the designer to develop control systems that satisfy the multi-objective criteria that are imposed in an operational setting, e.g., accommodation of model truncation, parameter errors, actuator/sensor bandwidth limitations, finite computer memory size and computational overhead constraints.

Work to date has been very successful in designing reduced order compensators that are tuned to both the system model and performance objectives. Current work focuses on making these designs more robust while maintaining their excellent performance characteristics. The conventional approach to making a control system more robust with respect to parameter uncertainties follows a conservative path that ultimately sacrifices performance for robustness. Recent advances in robustness research have led to the development of design methods that simultaneously address the dual objectives of performance (control system bandwidth, settling time, etc.) and robustness, and that exploit the context in which uncertainties arise in physical systems. The derived control designs have been validated in simultations with a large-order flexible antenna model. The figure shows that the new methods lead to significantly greater regions of stability and reduced sensitivity to parameter errors, while simultaneously retaining control system performance. Future work will address the extension of the current results to discrete-time (digital) system design and their application to fine-resolution piecewise models for complicated simulated and physical structures.
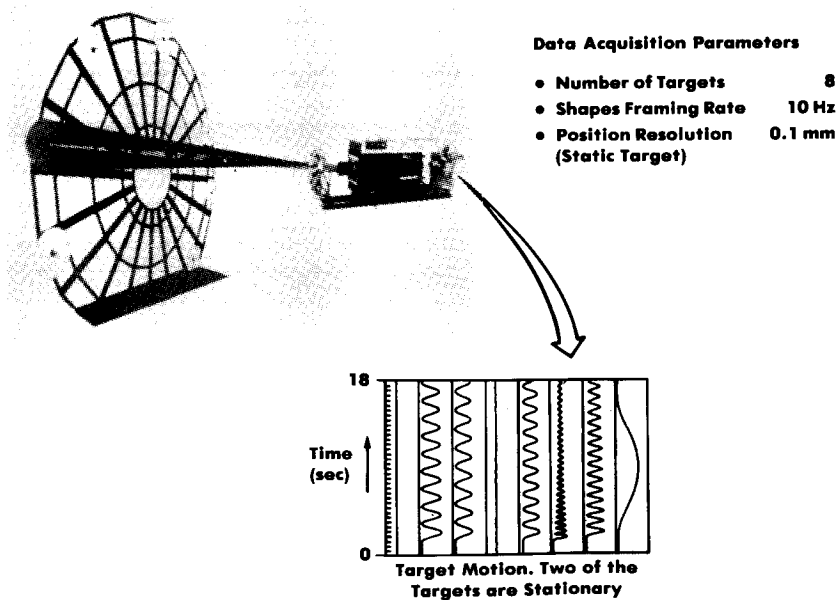

773
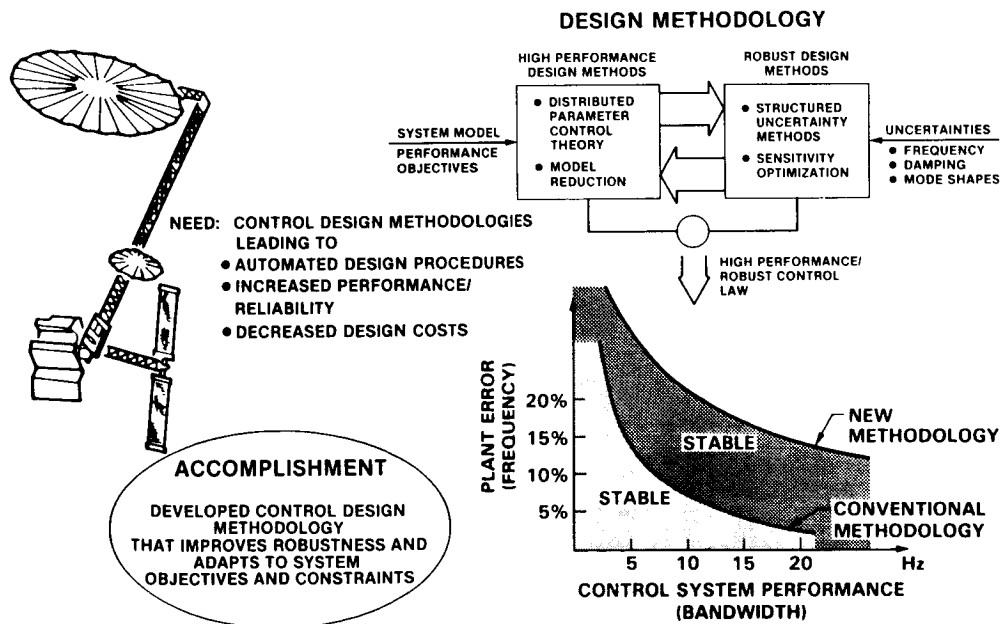
SHAPES: SPATIAL, HIGH-ACCURACY POSITION ENCODING SENSOR

The objective of the SHAPES task is to develop a control sensor for making 3-D simultaneous position measurements of multiple (50-100) targets with sub-millimeter accuracy and with sufficient data bandwidth for system identification, and shape and vibration control of large space structures. The technical approach is to develop and integrate angular and range measurement techniques based on multi-pulse time-of-flight ranging, fast semiconductor laser diodes, charge coupled device (CCD) imaging detectors, and picosecond resolution electro-optic signal-processing detectors.

A major accomplishment has been achieved the past year: the successful first-time demonstration of simultaneous optical ranging of 8 independent targets at an update rate of 10 measurements per second, with a measurement resolution of 10 microns (0.4/1000 in). These results have clearly demonstrated the viability of the multi-pulse, multi-target optical ranging concept. The next phase of the development will address the incorporation of angular measurement to obtain the full 3-D measurement capability.
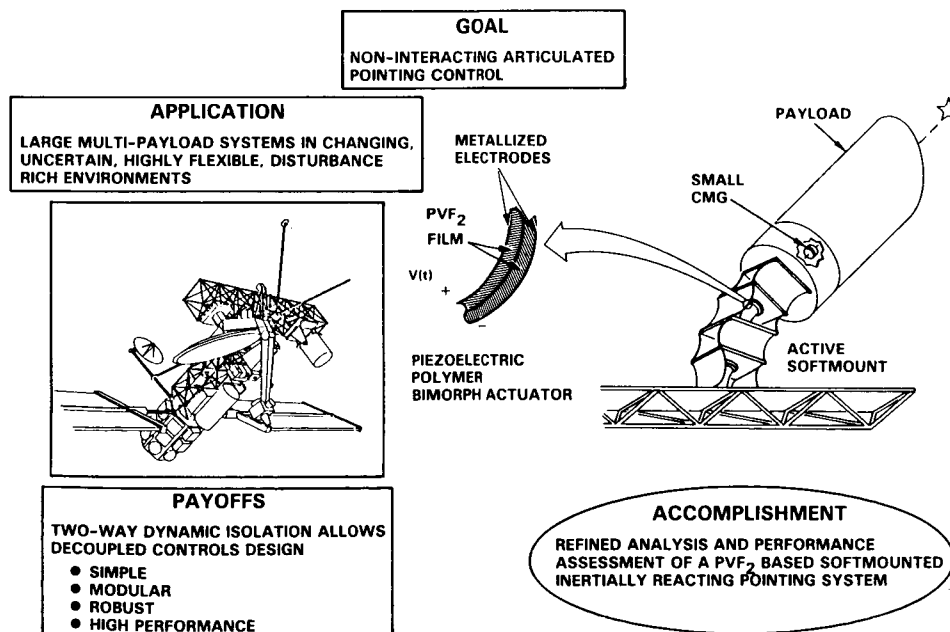
Currently, SHAPES is the only sensor to have demonstrated this simultaneous multi-target tracking capability, which is required for determining both static figure/alignment control, as well as dynamic in-flight characteristics of Large Antennas, Platforms and the Space Station (both during assembly and operational phases). In a typical application to space station and platforms, SHAPES can provide the sensing and instrumentation capability that will be needed during initial on-orbit tests and checkout. Such instrumentation will also be needed to support periodic diagnosis and verification during the station's operational lifetime. Specific applications include assembly, alignment, geometry certification, and measurement of in-orbit dynamics for structural verification and for updating control system gain. SHAPES can also be configured as a rendezvous and docking sensor with an acquisition range of 40 Km.

Data Acquisition Parameters

- **Number of Targets**   8
- **Shapes Framing Rate**   10 Hz
- **Position Resolution**   0.1 mm
  (Static Target)

Target Motion. Two of the Targets are Stationary

ADVANCED PRECISION POINTING TECHNOLOGY

The trend in payload pointing is toward combining multiple instruments on a common large basebody. Such large flexible base vehicles will present articulated payload pointing system designers with three significant challenges: an unprecedented level of dynamic disturbances, a set of extremely low frequency base vehicle strucutral modes (e.g. 0.1 Hz for Space Station/Space Platforms), and a system that is guaranteed to continually evolve as new instruments and other modules are added to the basebody and old instruments are removed or replaced. The first challenge represents a quantitative change over current systems; the latter represents a quantitative and qualitative change since for such systems it will be impossible to maintain the traditional separation between structural frequencies and pointing control bandwidth, and the control design cannot rely on fixed system dynamics.

These considerations motivate the development of a pointing concept that incorporates a mechanically soft (but actively controlled) interface between payload and base vehicle with primary pointing control authority resident on the payload in the form of a reaction wheel or control moment gyro. Such an approach provides two way isolation between payload and basebody and mitigates the problem of control bandwidth - structural frequency interaction. The concept under development is that of an active "softmount" incorporating the use of a piezoelectric polymer material (PVF$_2$) to implement the soft active interface. The principal accomplishment of FY '86 was a refined analysis of the conceptual design of such an active "softmounted" pointing system. Performance analysis of a planar model was performed, and a six DOF analytical model for a proof of concept analysis was developed. The next step is to complete the analytical proof of concept, with breadboard development and test to follow.

GOAL
NON-INTERACTING ARTICULATED POINTING CONTROL

APPLICATION
LARGE MULTI-PAYLOAD SYSTEMS IN CHANGING, UNCERTAIN, HIGHLY FLEXIBLE, DISTURBANCE RICH ENVIRONMENTS

METALLIZED ELECTRODES

PVF$_2$ FILM

V(t)

PIEZOELECTRIC POLYMER BIMORPH ACTUATOR

PAYLOAD

SMALL CMG

ACTIVE SOFTMOUNT

PAYOFFS
TWO-WAY DYNAMIC ISOLATION ALLOWS DECOUPLED CONTROLS DESIGN
- SIMPLE
- MODULAR
- ROBUST
- HIGH PERFORMANCE

ACCOMPLISHMENT
REFINED ANALYSIS AND PERFORMANCE ASSESSMENT OF A PVF$_2$ BASED SOFTMOUNTED INERTIALLY REACTING POINTING SYSTEM

# CONTROL TECHNOLOGY VALIDATION

The objective of this program is to develop and conduct technology experiments to validate and demonstrate large space system static and dynamic control technologies in sensing, modeling, identification, and adaptive control, which are required for the control of future spacecraft, such as large antennas and space platforms. JPL is actively engaged in the development of these large space system control technologies including: figure sensing/control, dynamic identification, adaptive control, and unified control/modeling/ design. Ground validation of these technologies is crucial for establishing confidence and reducing risks in their future large space system applications. Evaluation of these fast developing control technologies through actual implementation on ground test is also essential to validate and compare the performance of different methodologies and algorithms, providing a valuable research tool to enable the further development of effective theories and solutions.

The Control Technology Validation program is a joint activity with the Air Force Rocket Propulsion Laboratory. The approach is to define, develop, and conduct technology experiments in a 3-dimensional flexible test article. The test article resembles an antenna, with a horizontal dish of 7.2 meter diameter (consisting of 12 ribs attached to a rigid central hub) and a 3.6 meter long flexible boom hanging vertically downward from its center. The ribs are coupled together by two concentric rings of stretched wires under tension. To achieve the desired low frequencies (0.2 Hz), the ribs are very flexible and each is supported at two location by levitators. The sensing instrumentation includes a two- axis hub angle sensor, 28 rib displacement sensors, and an electro-optical sensor, SHAPES, which will provide 16 position measurements. Actuation is provided by a two-axis hub torquer and twelve rib root actuators, with one actuator acting on each rib. The experimental apparatus has been designed and fabricated and is being assembled. The first set of four experiments will be conducted during April-September, 1987.

FLIGHT EXPERIMENTS

Work in FY '86 included control experiment definition and planning activities with the COFS and ATSE programs. The chart illustrates an experiment configuration and approach to an ATSE in-orbit control experiment, whose objectives are:

(1) Demonstrate active pointing and jitter and vibration control and antenna boresight pointing performance of 0.01 deg.

(2) Demonstrate the capability to characterize the over-all system dynamics and disturbance environment based on in-orbit measurements.

(3) Validate the methodology used to design the initial control system and the process of upgrading it in-flight based on in-orbit measurements.

(4) Demonstrate in-orbit shape determination and control technology to measure the antenna shape (ribs, mesh and feed misalignments) to an accuracy of 0.3 mm rms (knowledge), and to control it with actuators (rib-root and feed) to an accuracy of 1.0 mm rms.

(5) Update/refine analytical tools and prediction models with test data base.

(6) Advanced control technology readiness to support operational systems such as MSAT second- and third-generation and orbiting VLBI/QUASAT missions.

777
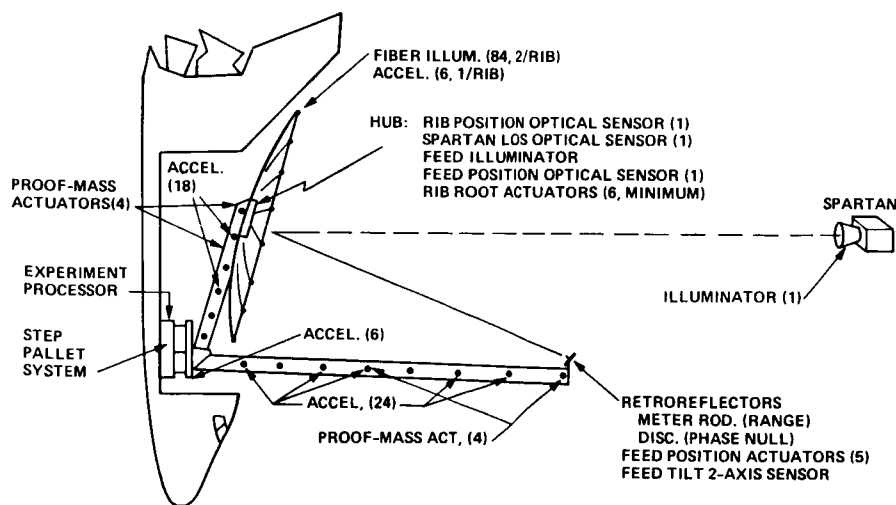
SUMMARY

The paper has attempted to give a brief control technology overview in CSI by illustrating that many future NASA missions present significant challenges as represented by missions having a significantly increased number of important system states which may require control and identifying key CSI technology needs. Many of these technologies require extensive development and tests before commitment to space initiatives which may face serious design constraints if CSI-based design options are not available. The JPL CSI-related technology developments were discussed to illustrate that some of the identified control needs are being pursued.

Since experimental confirmation of the assumptions inherent in the CSI technology is critically important to establishing its readiness for space program applications, the area of ground and flight validation requires high priority. Valid real-time closed-loop hardware/software test beds as well as extensive simulation tools should be developed as part of any strong ground test validation program. In many cases the uncertainties in extrapolating ground test results to on-orbit environments will make on-orbit testing through flight experiments a prerequisite to technology readiness.

NASA has made some in-roads in developing some of the required near-term CSI technologies to a state-of-flight readiness by the focused R&D ongoing programs. However, much more remains to be done to recognize DOD needs and closely coordinate the overall activities. An expanded joint program between NASA, DOD, Industry, and universities must be encouraged and supported. This CSI focused conference has been useful in giving this effort a start. The NASA Civil Space Technology Initiative (CSTI) proposed for a FY 88 start and related programs could serve as a catalyst to accelerate further joint activities.

- FUTURE NASA MISSIONS PRESENT SIGNIFICANT CSI CHALLENGES

- MANY CRITICAL CSI TECHNOLOGIES STILL IN INFANCY - CONSIDERABLE DEVELOPMENT IS REQUIRED

- NEED A STRONG GROUND VALIDATION PROGRAM

- CSI BASED FLIGHT EXPERIMENTS MUST DEMONSTRATE TECHNOLOGY READINESS

- AN EXPANDED JOINT PROGRAM BETWEEN NASA/DOD/INDUSTRY/UNIVERSITIES MUST BE ENCOURAGED AND SUPPORTED

ANTENNA TECHNOLOGY
SHUTTLE EXPERIMENT
(ATSE)

R. E. Freeland, E. Mettler, L. J. Miller,
Y. Rahmat-Samii, and W. J. Weber III
Jet Propulsion Laboratory
California Institute of Technology
Pasadena, California

Numerous space applications of the future will require mesh deployable antennas of 15 meters in diameter or greater for frequencies up to 20 GHz. These applications include mobile communications satellites, orbiting very long baseline interferometry (VLBI) astrophysics missions, and Earth remote sensing missions. Ground testing of these antenna systems is extremely difficult and expensive, and the results can be of questionable value. A flight test of the entire antenna system would greatly reduce the risk and uncertainty of launching such an antenna and would at the same time validate ground test procedures for future antenna systems. The NASA STS is ideally suited for performing the majority of 0 g, dynamic, and thermal tests required to space qualify this type of antenna system.

- GENERAL

  - REDUCE RISK IN UTILIZING LARGE DEPLOYABLE ANTENNAS, THEREBY ENABLING APPLICATIONS SUCH AS
    - 2nd GENERATION MSAT
    - ORBITING VLBI
    - REMOTE SENSING

- SPECIFIC

  - DEMONSTRATE CRITICAL TECHNOLOGIES AND VERIFY IN-FLIGHT PERFORMANCE OF AN ANTENNA SYSTEM REPRESENTATIVE OF ABOVE APPLICATIONS

  - DEMONSTRATE IN-FLIGHT MEASUREMENT OF LARGE SPACE ANTENNAS

ANTENNA CHARACTERISTICS FOR CANDIDATE APPLICATIONS

Listed below are some of the characteristics for candidate applications: second and third generation mobile communications satellites (MSAT), orbiting VLBI (such as the proposed QUASAT mission), and a general range of Earth remote sensing missions.

	FREQ (GHZ)	DIAM (M)	CONFIG	FEATURES	SURFACE ACCURACY
MSAT – 2ND GEN	1.6	15-20	OFFSET	MULTI-BEAM LOW SIDELOBES	3 mm (1.6 GHz)
MSAT – 3RD GEN	1.6	25-35	OFFSET	MULTI-BEAM LOW SIDELOBES	(AS ABOVE)
ORBITING VLBI	1.4-22	15-20	AXI-SYM	MULTI-FREQ HIGH GAIN	0.8 mm (22 GHz)
REMOTE SENSING	1-20	10-100	AXI-SYM & OFFSET	HIGH GAIN LOW SIDELOBES	$\lambda/30$

SPECIFICATIONS FOR LOCKHEED TEST ANTENNA

For the purposes of this study, a Lockheed wrap-rib antenna was used as the test article. Based on the requirements for the various applications in the 20 meter antenna class, a candidate test antenna was specified as outlined in the list below.

The offset configuration was chosen for the MSAT applications and is considered to be more demanding than the axisymmetric feed configuration. The 3mm surface accuracy will satisfy the MSAT L-band requirements while the 0.8 mm accuracy of the inner 10 meters will satisfy the 22 GHz requirements of the orbiting VLBI missions, such as QUASAT.

REFLECTOR TYPE	WRAP-RIB AUTOMATIC DEPLOYMENT/ REFURLMENT
REFLECTOR DIAMETER	20 METERS
CONFIGURATION	OFFSET FED
MAST TYPES	TETRAHEDRAL TRUSS MANUAL DEPLOYMENT/ REFURLMENT
FOCAL LENGTH/ DIAMETER	1.5
RMS SURFACE ERROR	3 mm (ENTIRE SURFACE) 0.8 mm (INNER 10 METERS)
FEED ALIGNMENT ERROR	5 mm

EXPERIMENT OBJECTIVES

Based on the project objectives the following list of experiment objectives was defined. These experiment objectives cover a broad range of structural, control, and RF discipline objectives which, if fulfilled in total, would greatly reduce the risk of employing these antenna systems in future space applications.

1. DEMONSTRATE THE RELIABLE DEPLOYMENT OF THE ANTENNA STRUCTURE (REFLECTOR, MASTS, AND FEEDS)

2. VERIFY PREDICTED REFLECTOR SURFACE PRECISION AND THE FEED/REFLECTOR ALIGNMENT IN ZERO G

3. MEASURE THE THERMAL STRUCTURAL CHARACTERISTICS OF THE REFLECTOR AND MASTS

4. MEASURE THE DYNAMIC STRUCTURAL CHARACTERISTICS OF THE REFLECTOR AND MASTS

5. VERIFY RF PERFORMANCE WITH:

    - SIMPLE RF FOCAL POINT FEED

    - FEED SCANNED OFF AXIS (SIMULATED MULTIPLE BEAM)

    - MULTIPLE BEAM FEED AT 0.9 OR 1.6 GHZ

6. DEMONSTRATE THE FEASIBILITY OF IN-FLIGHT SHAPE SENSING AND CONTROL

7. DEMONSTRATE ANTENNA POINTING STABILITY/JITTER CONTROL

8. VERIFY DEPLOYMENT REPEATABILITY OF SURFACE CONTOUR

9. DEMONSTRATE ASTRONAUT IN-FLIGHT ASSEMBLY

10. SCIENTIFIC AND ENGINEERING DEMONSTRATIONS OF THE ANTENNA SYSTEM (E. G., ORBITING VLBI, RADIOMETRY, ETC)

ANTENNA INTEGRATION AND DEPLOYMENT

The figures show the stowed experiment package and the sequence of the
deployment of the antenna system. The entire experiment package is mounted on
the NASA Langley developed STEP pallet which contains the mechanical and
electrical interfaces to the Shuttle. When fully deployed, the antenna feed is
in the offset configuration and is located at the top of the feed mast tower.
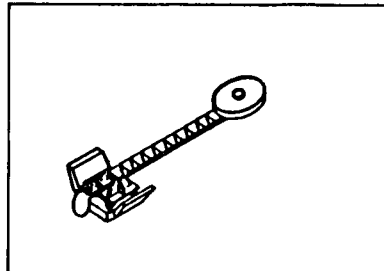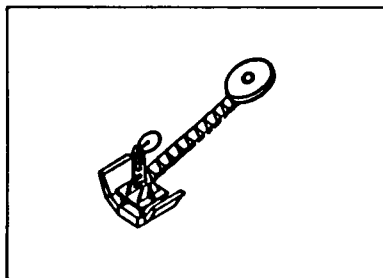The boresight of the RF pattern is perpendicular to the roll axis of the
shuttle.

STOWED CONFIGURATION
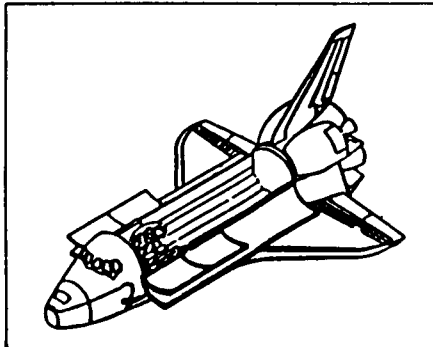
STOWED CONFIGURATION
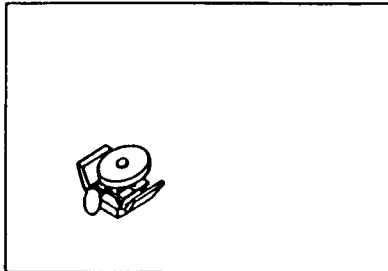
ANTENNA MAST DEPLOYMENT

FEED MAST DEPLOYMENT

FEED MAST DEPLOYMENT
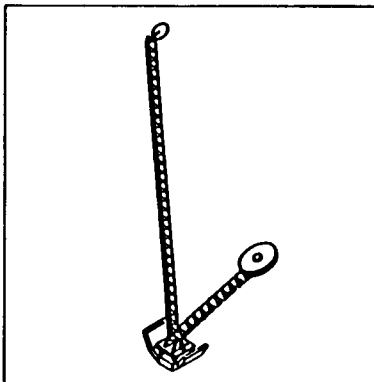
FULLY DEPLOYED CONFIGURATION
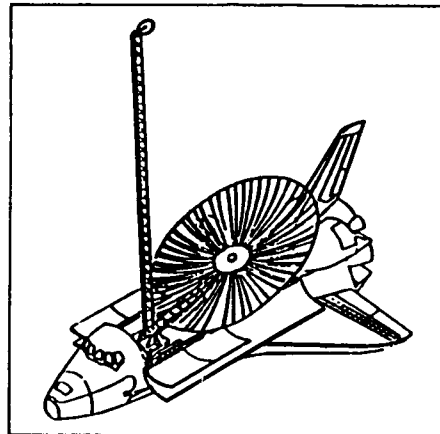
The RF pattern of the antenna is measured in the far field by employing an RF beacon on a derivative of the Spartan retrievable spacecraft. The Spartan is deployed and checked out prior to the deployment of the wrap-rib antenna and is subsequently retrieved after the wrap-rib antenna has been refurled.

The operational configuration will be with the Shuttle in a gravity gradient orientation (nose toward Earth) and its minus Z-axis aligned with the velocity vector. This orientation will allow the antenna to be in the Shuttle wake region and will minimize the interaction of free-stream oxygen with the reflector and mast structures.

The SPARTAN, equipped with an omni-directional antenna and beacon transmitter, will trail the Shuttle at a distance that places it in the far field of the test antenna. The upper limit is chosen to keep the power requirements on the SPARTAN to a reasonable level.

OMNI-
DIRECTIONAL
ANTENNAS

SHUTTLE
VELOCITY
VECTOR

FREE-FLYER
WITH
BEACONS

9 TO 21 Km
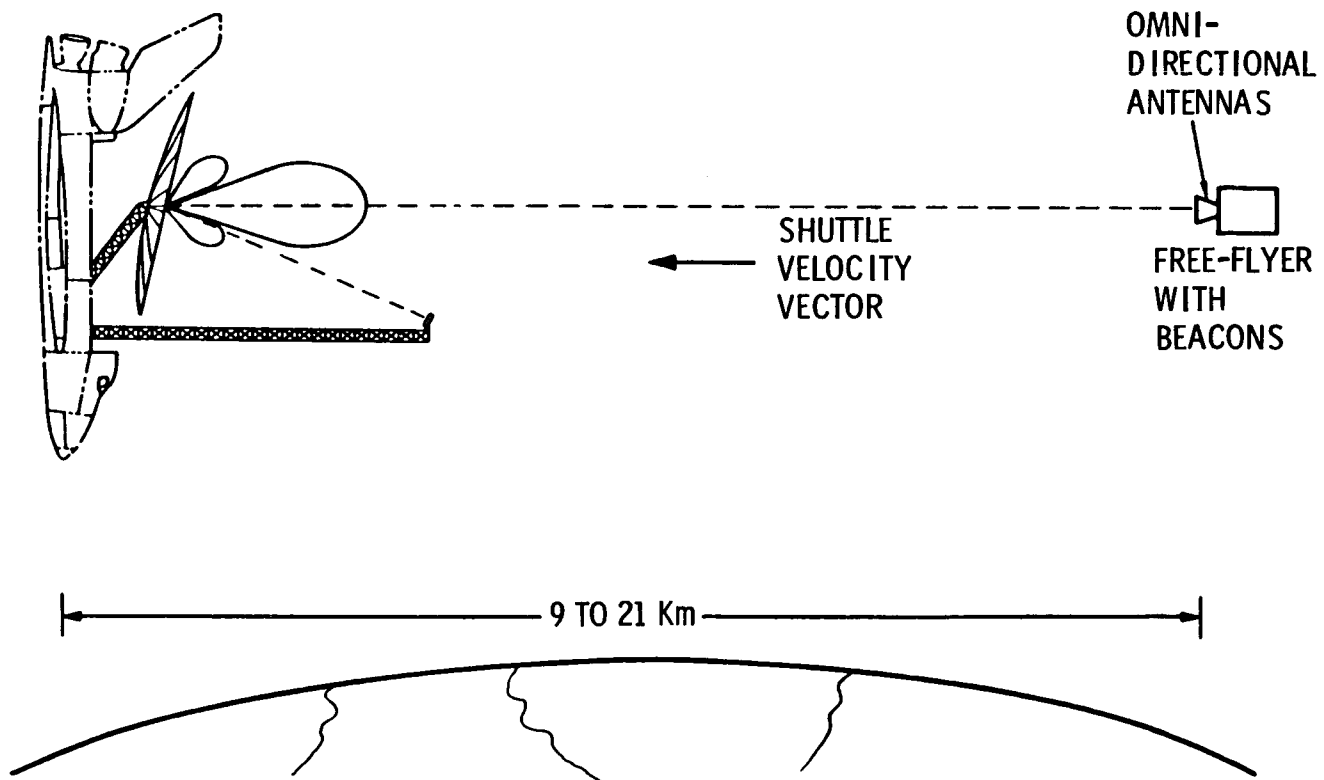
MISSION DESCRIPTION

In the baseline scenario, the experiment will be conducted in a 28.5°, 250 N.M. orbit. Such an orbit affords the opportunity to conduct the antenna experiment during a flight in which other payloads are carried. Other (e.g., high inclination, high-altitude) orbits have also been studied. Some high inclination orbits afford opportunities for full illumination (constant thermal input) slowly precessing into orbits with varying shadowing. Higher altitudes minimize the deleterious effects of atomic oxygen on the antenna. Unfortunately, both of these orbit types imply less payload mass in orbit thus reducing the possibility of a multi-payload flight.

After launch and deployment of the other payloads, the SPARTAN will be checked out and deployed. The operational configuration will be attained. Then the various antenna structures will be deployed and aligned with EVA astronauts assisting.

- LAUNCH INTO 28.5°, 250 N.M. ORBIT

- DEPLOY OTHER PAYLOADS

- CHECKOUT AND DEPLOY SPARTAN

- SEPARATE FROM SPARTAN 9-21 km

- ROTATE TO G-G ATTITUDE

- DO EVA DEPLOYMENT OF ANTENNA BOOM, FEED BOOM, ANTENNA REFLECTOR

- DO COARSE AND FINE ALIGNMENTS OF ANTENNA STRUCTURES

After calibrations are performed, the antenna undergoes passive characterization. The RF patterns will be traced by performing attitude maneuvers using the Shuttle VRCs. This is done manually by an astronaut who is observing the SPARTAN optical beacon via a sensor mounted on the hub of the antenna. Several scenarios for the attitude maneuvers have been proposed. These include a roster scan pattern that requires frequent motion reversals with antenna settling time required after the corresponding accelerations. One alternative scheme is a continuous roll (barbecue mode) with a slow pitch maneuver superimposed on it.

Throughout the experiment, it will probably be necessary to perform periodic Shuttle propulsive maneuvers to remove the effects of differential atmospheric drag on the Shuttle and SPARTAN thus maintaining the desired relative range between the two objects. The Shuttle in g-g mode and the SPARTAN have similar ballistic coefficients, thus station keeping maneuvers may need to be performed relatively infrequently, perhaps no more than once per day.

Significant parts of the controls experiment can be performed independently of the RF characterization and may even be performed during astronaut sleep periods. The final part of the experiment will be a test of antenna surface repeatability performed by unlatching and relatching the antenna mesh and measuring the antenna surface.

Finally, the antenna is stowed by the astronauts and the SPARTAN is recaptured.

- PERFORM CALIBRATIONS AND PASSIVE CHARACTERIZATION OF ANTENNA

- PERFORM RF PATTERN TRACING VIA MANUAL STS VRCS TURNS

- PERIODICALLY CORRECT SPARTAN RELATIVE RANGE VIA VRCS OR PRCS

- PERFORM SOME OBSERVATIONS (CONTROLS AND STRUCTURES) DURING SLEEP PERIODS

- PERFORM ANTENNA SURFACE REPEATABILITY TESTS

- DO EVA STOW OF ANTENNA STRUCTURES

- RECAPTURE SPARTAN

ATSE STRUCTURAL SYSTEM EXPERIMENT
OBJECTIVES

The structural experiment objectives are to demonstrate reflector kinematic deployment reliability and the capability for man to assist the deployment of a high precision feed support structure. Repeated partial restowing and then complete deployment is expected to help characterize the reflector initial position variations. Direct measurement of aperture precision and fee structure alignment is required to validate the mechanical design. Measurements of structural thermal distortions are required for design verification, but distortions and actual temperature distributions are needed for comparison with analytical models. Measurements of a few fundamental mode shapes, natural frequencies and associated damping are needed for characterizing the structural design and correlating analytical models.

- DEMONSTRATE LARGE ANTENNA DEPLOYMENT IN ZERO-G
  - 20 METER ANTENNA
  - PARTIALLY MAN ASSISTED

- CHARACTERIZE DEPLOYMENT INITIAL POSITION VARIATION

- MEASURE APERTURE PRECISION AND FEED STRUCTURE ALIGNMENT

- MEASURE THERMAL DISTORTIONS AND TEMPERATURE DISTRIBUTIONS
  - REFLECTOR
  - FEED STRUCTURE

- MEASURE FREQUENCIES, MODE SHAPES, AND DAMPING

- VALIDATE AND REFINE THERMAL AND STRUCTURAL ANALYTICAL MODELS

ATSE ANTENNA STRUCTURE CONFIGURATION DESIGN

The antenna structure configuration design is based on an advanced version of the Lockheed wrap-rib system developed by the NASA sponsored Large Space System Technology Program. The offset reflector is a segment of the parent paraboloid with an F/D of 1.5. There are 42 graphite-epoxy lenticular ribs. The RF reflective mesh is made from 1.2 mil diameter, gold-plated molybdenum wire. It is a tricot knit with 4 cells per inch. Rib deployment is accomplished by controlling the strain energy with a mechanism on each rib. The baseline deployable booms are based on a 3 longeron Astro Industries configuration design. The longerons, battons, and diagonals are based on graphite-epoxy tubes that interface with titanium fittings. Graphite-aluminum metal matrix composite tubes are also under consideration as an alternate to graphite-epoxy. The boom configuration designs lend themselves to astronaut assisted deployment.

FEED BOOM
BAYS = 27
MASS = 147 Kg
FEED MASS = 13 Kg

BOOM STRUCTURES

MEMBERS = GRAPHITE EPOXY
FITTINGS = TITANIUM
LONGERONS
    DIA. = 20 mm
    WALL = 2 mm
BATTONS AND DIAGONALS
    DIA. = 15 mm
    WALL = 1.5 mm

REFLECTOR
F/D = 1.45
RIBS = 42
GRAPHITE EPOXY
MASS = 260 Kg

32.28 m
31.15 m
28.5 m
2.15°
18.92°
21.65°
39.99°
10.90 m
19.67 m
1.07 m
20 m
STEP SURFACE
0.70 m
10.5°
11.09 m
12.3 m
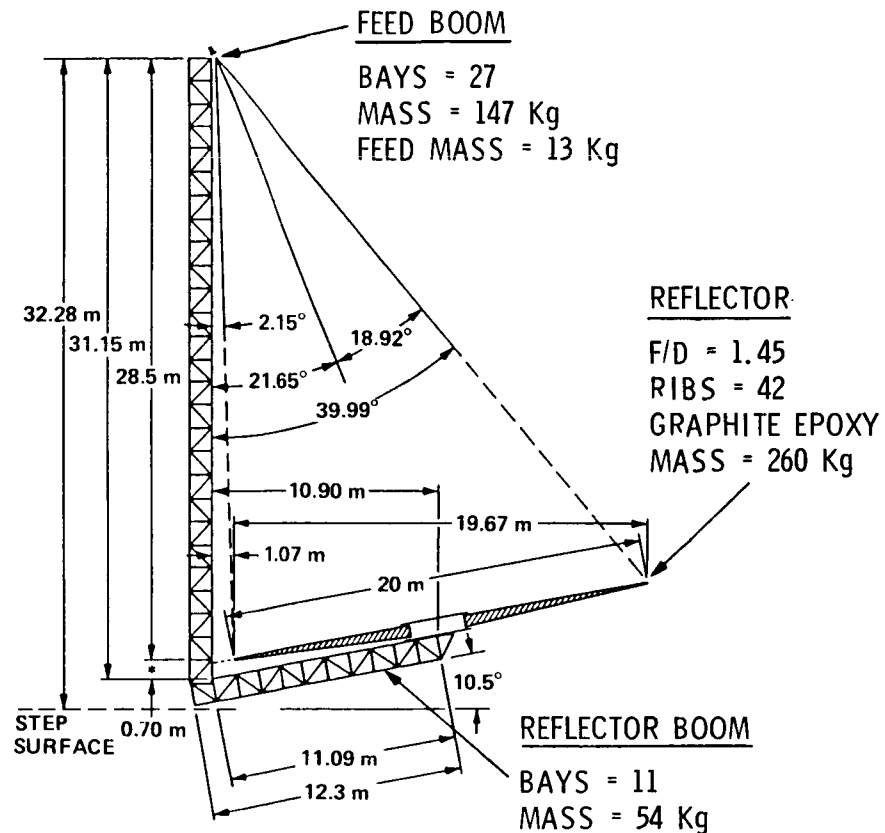
REFLECTOR BOOM
BAYS = 11
MASS = 54 Kg

There are a number of sources of error that must be considered when designing a reflector to a specified level of precision. The concept approximation error for the wrap rib antenna is the mesh flats between the ribs. Because of the difference between the radial and circumferential tensions in the mesh, there is a low amplitude pillowing of the mesh between the ribs. Component and assembly tolerances usually result in a randomly distributed surface error. Deployment dimensional repeatability results from the variations of surface initial position each time a complex structure is deployed. Thermal distortion is a function of the antenna configuration, material properties, internal heat sources and orbit. Since a large part of the antenna structure is made from graphite-epoxy, the long-term dimensional stability of this material must be considered.

- CONCEPT APPROXIMATION ERROR

- MESH PILLOWING

- COMPONENT TOLERANCES

- ASSEMBLY TOLERANCES

- DEPLOYMENT DIMENSIONAL REPEATABILITY

- THERMAL DISTORTION

- LONG-TERM MATERIAL DIMENSIONAL STABILITY

ATSE FEED BOOM STRUCTURAL ANALYTICAL MODEL

The 28 bay feed support structure has 9 truss members and 3 nodes per bay. This results in 81 nodes with 3 degrees of freedom for a model with a total of 243 degrees of freedom. Since the base of the feed support structure is supported directly by the STEP, the resulting modes are similar to those of a cantilever beam.
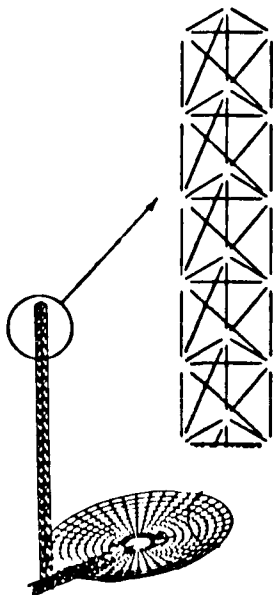
BOOM MODEL

BAYS 28
NODES/BAY 3
TRUSS ELEMENTS/BAY 9
NODES WITH 3 DOF 81
TOTAL DOF 243

FEED BOOM
MODE 1 = 1.01 Hz

MODE 2 = 1.01 Hz

MODE 4 = 6.41 Hz

MODE 5 = 6.41 Hz

MODE 7 = 17.44 Hz

MODE 8 = 17.45 Hz

STRUCTURAL DYNAMICS IDENTIFICATION EXPERIMENT

The structural dynamics identification experiment is based on measuring the response of the antenna structure resulting from excitations produced by Shuttle thruster firings and proof mass dampers located on both boom structures. Dynamic response will be measured with accelerometers. Near real-time and post-flight data analysis will be utilized.

OBJECTIVE: CHARACTERIZE STRUCTURAL DYNAMICS OF REFLECTOR BOOM, FEED BOOM, AND REFLECTOR.

REQUIREMENTS: CHARACTERIZE SELECTED MODAL FREQUENCIES, DAMPING, AND MODE SHAPES FOR CORRELATION WITH ANALYTICAL MODELS.

APPROACH: MEASURE STRUCTURAL DYNAMIC RESPONSE TO DESIGNED EXCITATION SEQUENCES.

- IDENTIFY SIGNIFICANT PARAMETERS THROUGH GROUND BASED DATA PROCESSING.
- EXCITATIONS INCLUDE STS THRUSTER FIRING AND INPUT FROM PROOF MASS ACTUATORS.
- RESPONSES MEASURED BY ACCELEROMETERS
- QUICK SURVEY, NEAR REAL TIME, AND POST-FLIGHT PROCESSING.

METHOD: INPUT EXCITATION

- SHUTTLE THRUSTER FIRING SEQUENCES (IMPULSIVE INPUT)

ATSE ORBITAL THERMAL REGIONS

The ATSE orbit consists of regions of solar illumination and Earth shadow. The maximum thermal transient occurs when the structure first enters Earth shadow or solar illumination. The extreme temperature cases for the test structure, both hot and cold, occur at the terminator portions of each thermal region.
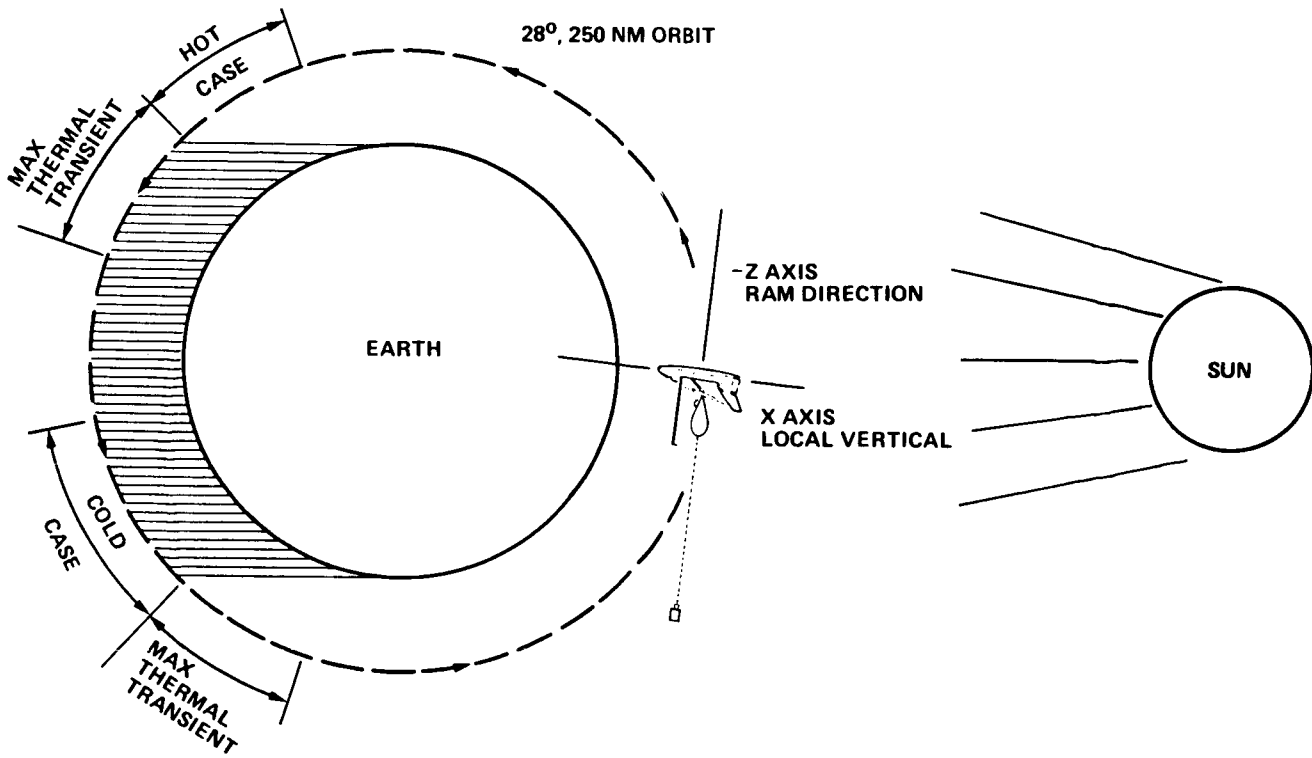
ATSE ANTENNA FEED BOOM THERMAL CHARACTERISTICS

The temperature of the base of the boom is relatively higher than at the tip because it is closer to the Shuttle. During solar illumination, there is a lot of reflected energy from the Shuttle. In Earth shadow, there is heat radiating from the Shuttle and a smaller view to space than at the tip of the boom. Even though there are significant temperature variations at each point along the boom as a function of orbit position, the temperature differences between the longerons, at equal distances along the boom, is very small.
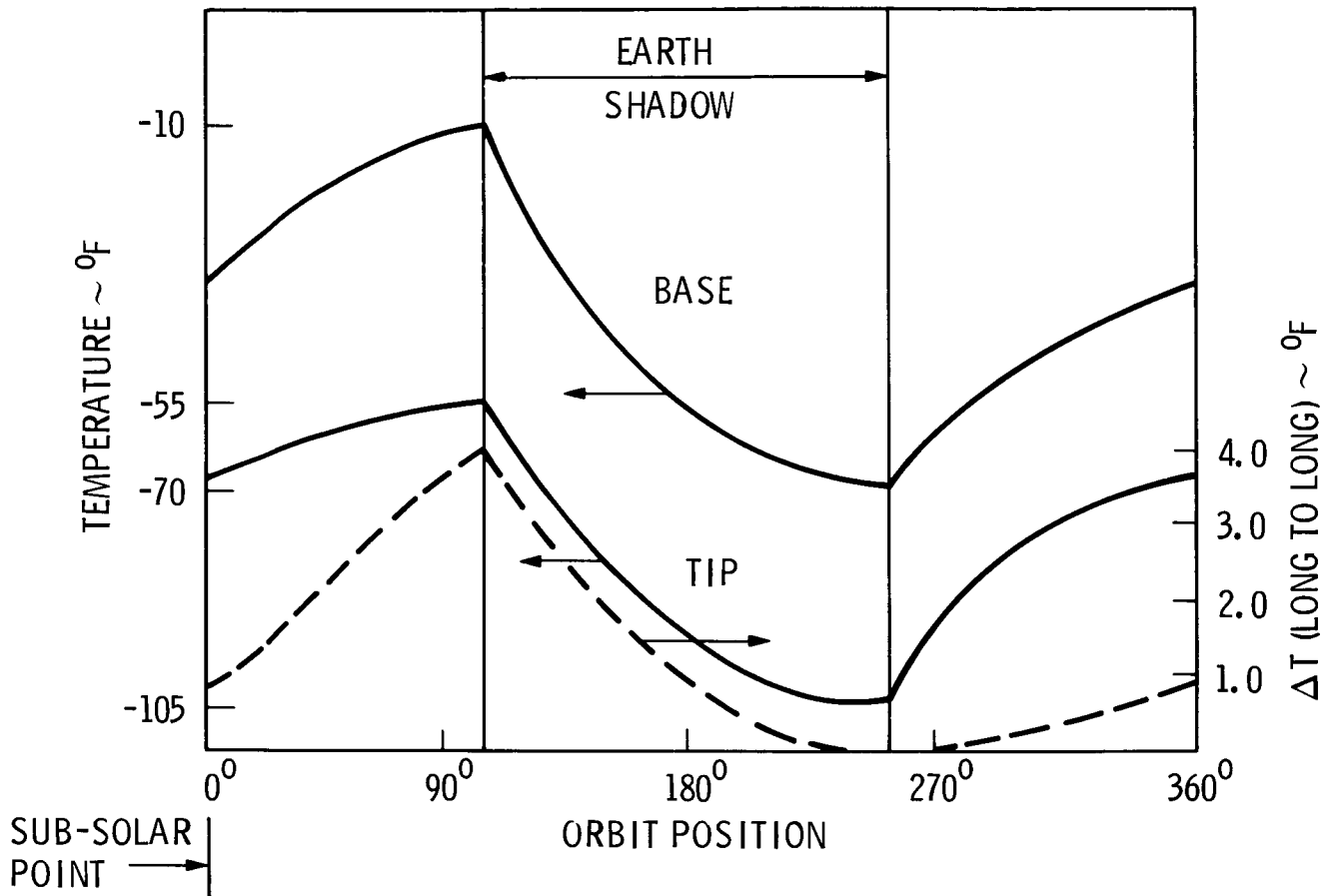
ATSE ANTENNA FEED BOOM THERMAL DISTORTION

The "hot case" portion of the thermal orbit produces the maximum temperature changes and differentials for the structure. The large temperature change from ambient to orbital results in an axial deformation of 2.0 millimeters. Since the graphite-epoxy boom has a negative coefficient of thermal expansion, there is a decrease in the length of the boom. This change in length is fairly constant with respect to orbital position because the differences in temperature between the tip and base of the structure are also fairly constant. The lateral thermal distortion results from differences in temperature of the longerons. This difference in temperature varies from 0 to a maximum of $4^{\circ}F$, as a function of orbital position, and produces a lateral deformation of 1.25 millimeters.

SOLUTION RESULTS FOR
  SUBCASE..........1

  MAX DEFORMATION.   0.08
  SCALE X, Y, Z...... 1500.93

. . . READY

$\Delta T = 4^{\circ}F$

1.25 MM

2.0 MM
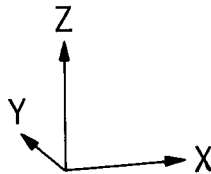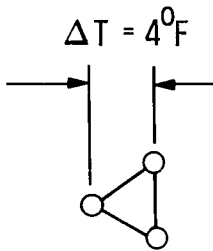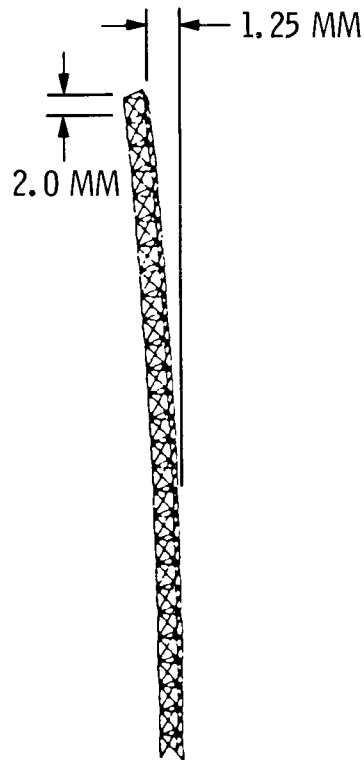
MSC/GRASP (VAX)   2   14-APR-86 14:12:15

THERMAL SYSTEM IDENTIFICATION REQUIREMENTS

Results of the thermal modeling of the ATSE provide temperature distributions as a function of orbital position. These results when used in conjunction with the structural analytical model provide estimates of actual thermal deformation. Consequently, measurement of temperature and deflection are required for model validation. The number and location of sensors for characterizing temperature distributions represent the minimal accompaniment for obtaining temperature magnitudes and differentials. Similarly, the quasi-static instrument requirements reflect characterization of the most significant structural deformations.

| STRUCTURE | QUASI-STATIC DEFL. | | TEMP. DISTRIBUTIONS | |
	LOCATION	DIRECTION	LOCATION	POSITION
FEED BOOM	3 ALONG BOOM	2 LATERAL 1 AXIAL	3 ALONG BOOM	1/LONGERON
REFLECTOR BOOM	2 ALONG BOOM	2 LATERAL 1 AXIAL	2 ALONG BOOM	1/LONGERON
REFLECTOR RIB	1 TIP 1 INTERMEDIATE EACH RIB	OUT OF PLANE	20 ON TBD RIBS	TOP & BOTTOM
MESH GORES	TBD/GORE ALL GORES	OUT OF PLANE	--	--

STRUCTURE/ENVIRONMENT INTERACTION EXPERIMENT IMPACT

Detailed contamination analysis has shown that a number of combinations of aft PRCS engines in operation simultaneously could result in permanent damage to significant portions of the antenna mesh. However, preferentially selected and operated PRCS in a pulse mode will preclude a problem.

Analysis results indicate that deposition of mass from the forward PRCS firings will change the thermal radiative properties of the forward portion of the thermal surfaces of the feed tower. This could significantly increase the thermal distortion of this structure. This problem could be somewhat minimized by preferential use of the forward engines.

Portions of the ATSE structures will be exposed to direct impact from atomic oxygen for the duration of the experiment. Exposure of the unprotected graphite-epoxy, as proposed for the test structure, would result in unacceptable damage. However, this type of material, when covered with the appropriate thermal control paint or multilayer insulation, will have no problem with the environment.

- MESH WILL BE DAMAGED UNLESS PRCS ENGINES ARE PREFERENTIALLY SELECTED AND OPERATED IN A PULSE MODE.

- POTENTIAL TOWER/FEED THERMAL DISTORTIONS DUE TO EXCESSIVE CONTAMINATION FROM FORWARD ENGINES.

- ATOMIC OXYGEN EROSION A NON-ISSUE AS LONG AS GRAPHITE/EPOXY STRUCTURES ARE OVERCOATED (PAINT OR MLI).

Since RF pattern measurements will provide the ultimate characterization of the antenna performance, a series of RF measurements are planned with the following objectives: (a) to demonstrate and develop the technological capabilities to measure large space antennas in space; (b) to measure the on-axis and off-axis beam patterns under various thermal conditions and after on-orbit surface and feed adjustment; (c) to correlate the measured RF performance with the measured surface and feed alignment; (d) to verify and update the mathematical and computer models of RF performance analysis and prediction; and (e) to project the RF performance of an operational system. These kind of data should establish an acceptable level of confidence considering large antennas for commercial and scientific applications.

- **DEMONSTRATE THE ABILITY TO MEASURE (RF) LARGE SPACE ANTENNAS**

- **MEASURE ANTENNA BEAM PATTERNS**
  - **VARYING THERMAL CONDITIONS**
  - **VARYING SURFACE AND FEED**

- **CORRELATE ANTENNA BEAM PATTERNS WITH**
  - **MEASURED SURFACE**
  - **MEASURED FEED ALIGNMENT**

- **VERIFY AND REFINE RF MODELS**

- **PROJECT THE RF PERFORMANCE OF AN OPERATIONAL SYSTEM**

CANDIDATE SCAN OPTIONS

To characterize an antenna far-field pattern, one typically displays the far-field amplitude distribution as a function of polar angle theta versus the azimuthal angle phi. This representation is shown for several values of phi which are called far-field pattern cuts. Clearly, the simplest way to achieve these representations is to move the antenna in a fixed phi cut and then measure the far-field variation as a function of theta. This data taking approach is called radial sampling. It is clear that such a sampling can be achieved only when the antenna motion with respect to the illuminating source is controlled with a precision gimbal mechanism aboard the Shuttle. This, however, could lead to a very costly system. An alternative approach would be to measure antenna far-field amplitude and phase at uniform sample points and then determine the standard far-field cuts from them. This scheme would also necessitate application of a gimbal mechanism which again could be very costly. Ultimately, it would be desirable to utilize a nonuniform sampling algorithm which would allow application of measured amplitude and phase data points on nonuniform sample points which could result from relative motions of the shuttle and the free-flyer (SPARTAN). Such an algorithm has recently been developed and tested, and it believed that it can enhance the capability of in-space measurement without the utilization of a gimbal mechanism.
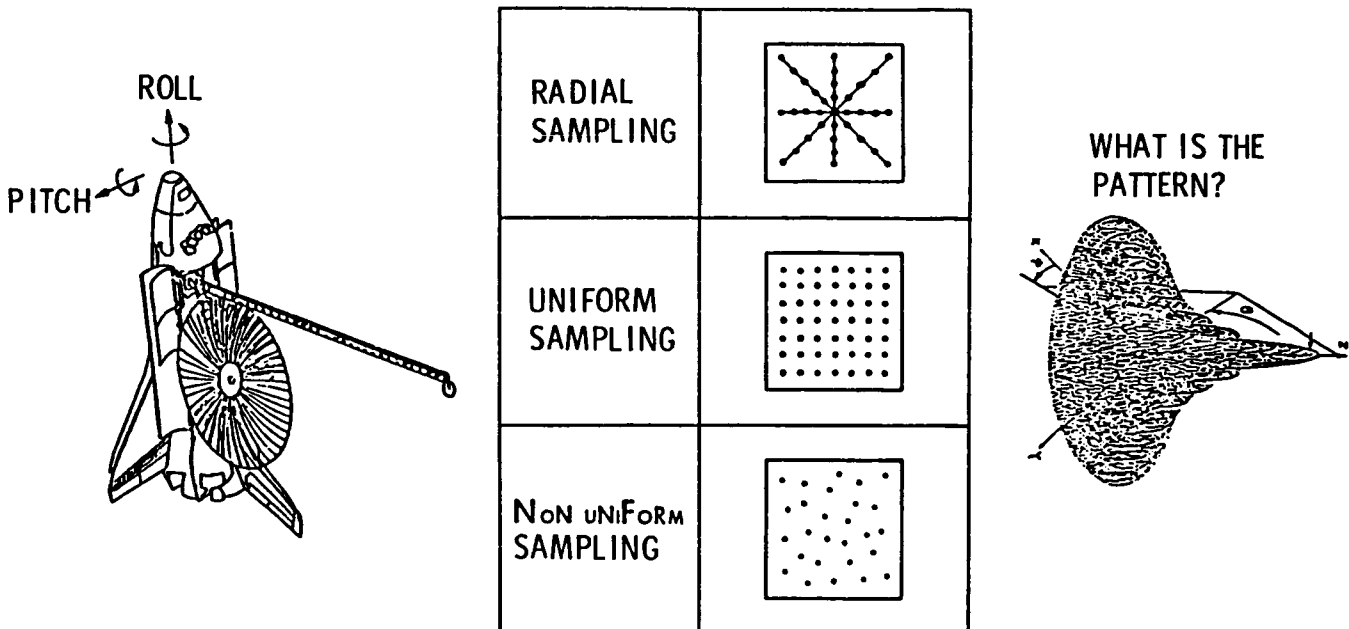
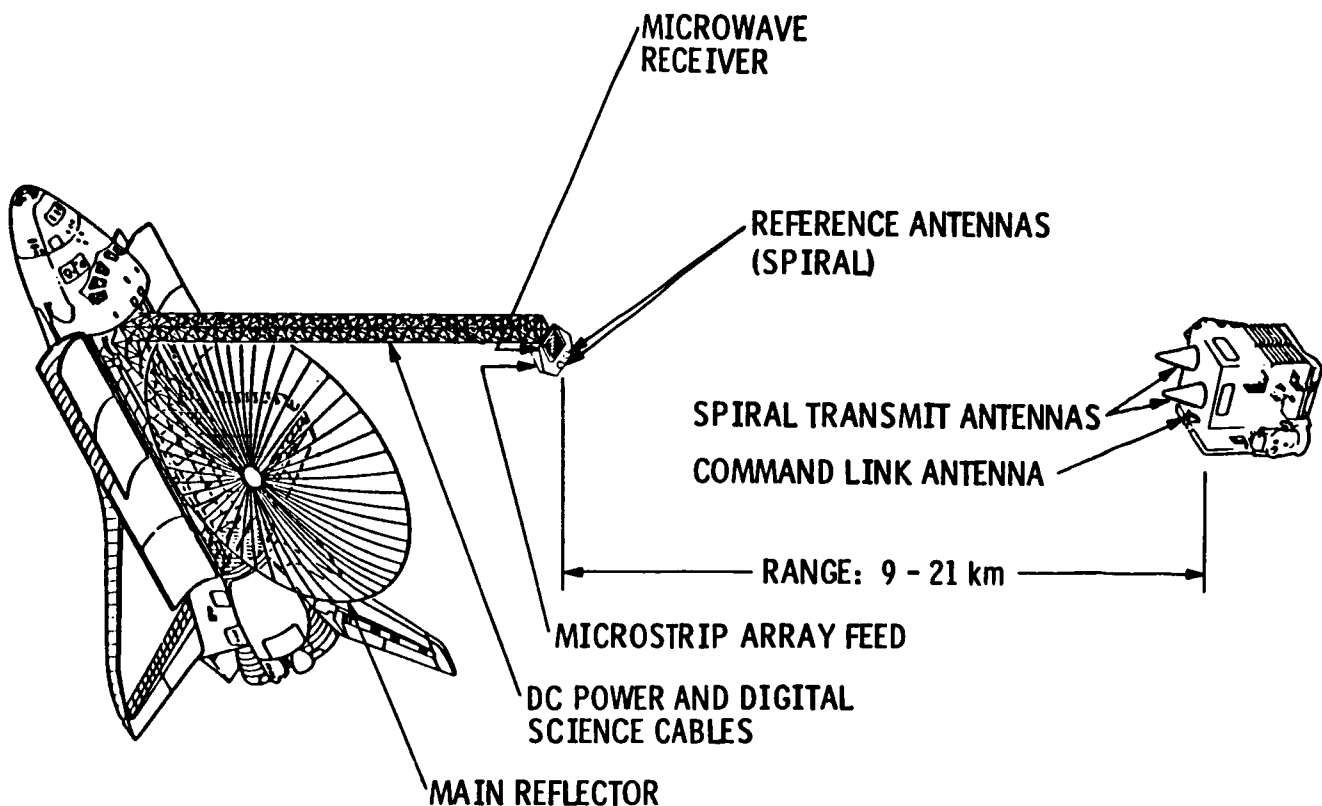- WE MUST BE PREPARED TO USE ANY OF THE ABOVE OPTIONS BASED ON THE ACHIEVABLE SHUTTLE AND FREE-FLIER MANEUVERS

Since the test antenna operates in the receive mode and the RF illumination is performed by the radiating antennas aboard the free-flyer (SPARTAN), one has to determine the relative location of the SPARTAN with respect to the test antenna as the Shuttle maneuvers on its roll and pitch axes. This relative location determination is achieved by utilizing an optical sensor which allows a precise evaluation of the location of the SPARTAN at the instant when the RF signal is measured. Based on the achievable maneuvering dynamics of the Shuttle and the SPARTAN, an image window, as depicted in the figure, could be traced which provides the nonuniform sampling data distribution.

800
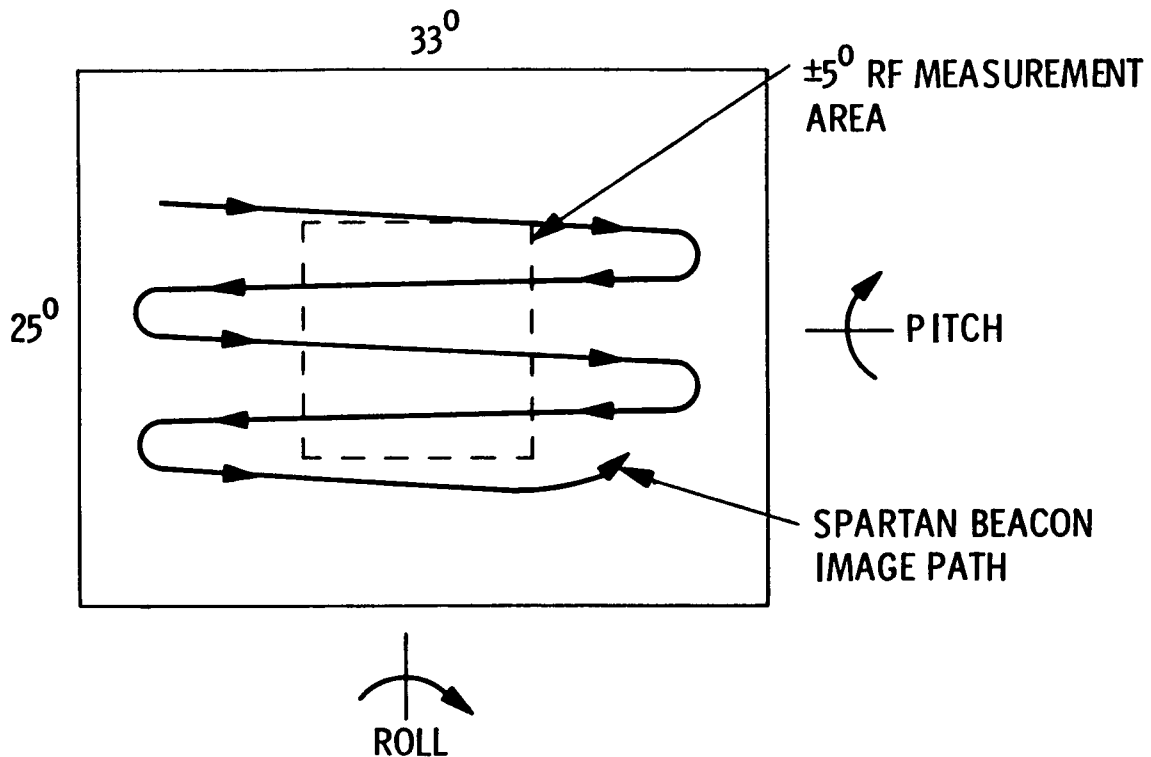
RF MEASUREMENT SYSTEM

In order to satisfy the required far-field distance criterion, a minimum separation of 9 km between the test antenna aboard the Shuttle and the SPARTAN will be needed at the operating frequency (L-band). However, in order to meet the link budget requirements based on the available radiating power from the radiating antennas aboard the SPARTAN, the maximum separation must be kept under 21 km. Since the utilization of the nonuniform sampling algorithm demands the measurements of both the amplitude and phase of the received signal, the RF measurement system will consist of the following subsystems: (a) test antenna and its feed array; (b) reference antenna for the amplitude and phase measurements; (c) calibrated microwave receiver; (d) dc power and digital science cables for data recording; (e) transmitter unit and antennas aboard the SPARTAN and (f) command link antennas and units.

MICROWAVE RECEIVER

REFERENCE ANTENNAS (SPIRAL)

SPIRAL TRANSMIT ANTENNAS

COMMAND LINK ANTENNA

RANGE: 9 - 21 km

MICROSTRIP ARRAY FEED

DC POWER AND DIGITAL SCIENCE CABLES

MAIN REFLECTOR

REFLECTOR SHAPE, POINTING AND VIBRATION CONTROL EXPERIMENTS

The control system experiments take place after the completion of the RF pattern measurements. The control system tests consist of evaluating the performance of different types of dynamics identification and control algorithms. For each set of software, the response of the antenna to commanded structural excitation via the RCS, VRCS and proof mass actuators will be measured and evaluated.

The objectives of the reflector shape, pointing and vibration control experiments are to:

1. Demonstrate on-orbit shape and alignment sensing and control technology in order to measure the overall antenna shape (ribs, mesh and feed misalignments) to an accuracy of 0.3 mm root-mean-squared (rms) knowledge, and to control it with actuators (rib-root and feed) to an accuracy of 1.0 mm rms.

2. Validate the control design methodology used to design the initial control system and the process of in-flight updates of the control parameters based upon on-orbit dynamic identification.

3. Demonstrate active line-of-sight pointing and vibration control design to show stability improvement over a passive system and demonstrate antenna boresight pointing stability performance of 0.01 degrees.

4. Update and refine analytical tools and prediction models with the test data base.

- DEMONSTRATE ON ORBIT SHAPE AND ALIGNMENT SENSING AND CONTROL

- VALIDATE CONTROL DESIGN METHODOLOGY
    - INITIAL CONTROL SYSTEM
    - ON-ORBIT DYNAMIC IDENTIFICATION
    - IN-FLIGHT UPDATES OF CONTROL PARAMETERS

- DEMONSTRATE ACTIVE CONTROL
    - LINE-OF-SIGHT POINTING
    - VIBRATION

- UPDATE AND REFINE ANALYTICAL TOOLS AND MODELS

CONTROL EXPERIMENT HARDWARE ARCHITECTURE

The antenna control system functions consist of RF feed and antenna position sensing, rib root and feed plane actuation, and feed and dish boom active dynamic control. The angular position of the RF feed will be determined in real time by viewing the tracking beacon(s) on the SPARTAN via a CCD sensor. This sensor and associated electronics will be located on the hub of the reflector and be aligned along the antenna boresight. The position sensing function will determine in real time the angular location of the reflector ribs, the location and orientation of the feed, and the position of the feed mast with respect to the reflector hub. This information is necessary for static control of the reflector and the feed. In general both range and orientation information will be determined via a CCD sensor in combination with point light sources and retroreflectors.

Attached at the root of a subset of the reflector ribs will be a micromotor driven, screw-type actuator. These actuators will be used collectively to adjust the rib positions and thus the reflector shape. They will be capable of single DOF rotation of the rib-root so as to cause translation of the rib tip in the direction perpendicular to the plane of the reflector surface. Attached to the feed plane will be translational and rotational actuators to control the feed position in three DOF and the orientation in two DOF. These actuators will be used for static control of the position and orientation of the feed relative to the reflector hub after the fee mast is deployed. Attached to the feed and dish booms at the appropriate locations will be accelerometers and proof mass actuators. The accelerometers, along with the control algorithms, will provide the commands to drive the proof mass actuators for dynamic control of the feed-hub line-of-sight jitter.

803
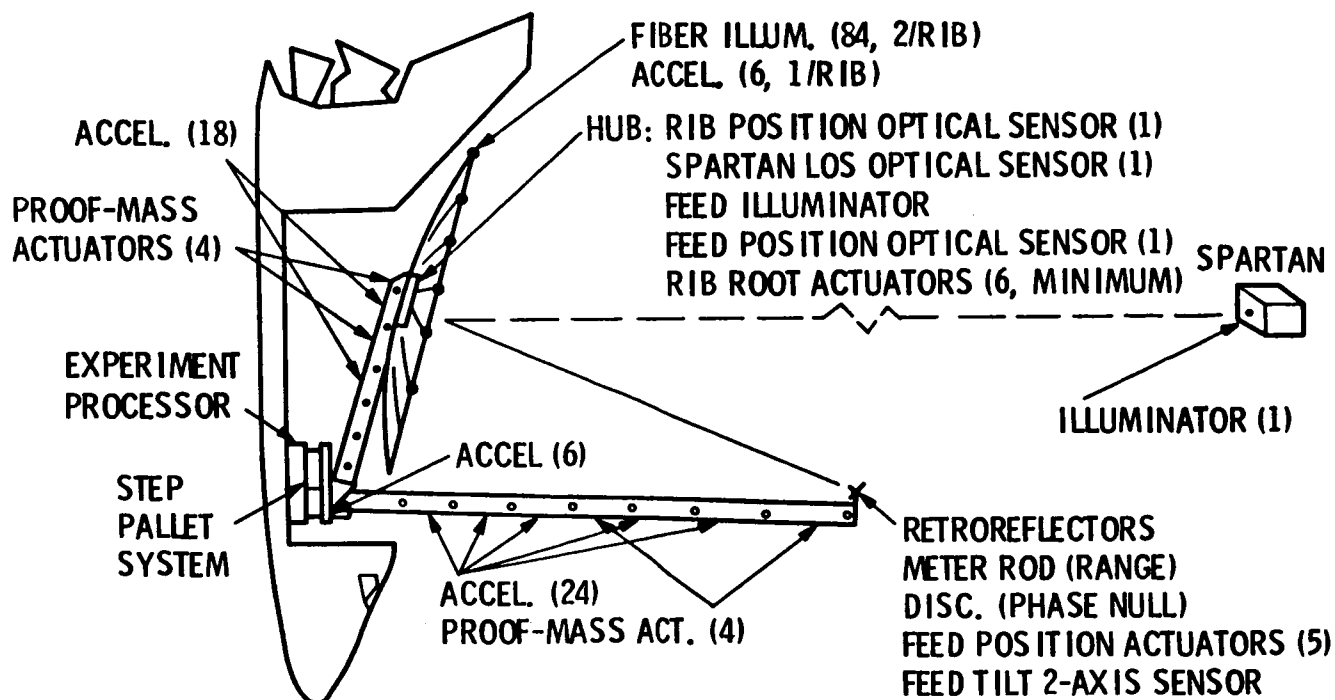
PHOTOGRAMMETRY

The purpose of the photogrammetry subsystem is to characterize the reflector static shape. The subsystem will locate a large number of points on the mesh and ribs defined by a retroreflective target attached to that point. The number of points that can be measured is limited by the range of change in position resulting from shape distortion. The envelope of possible locations of one point must not enter the envelope of adjacent points. An additional limit to the number of measurement points may be the available mesh packing volume to handle the retroflector array.

Three film cameras located in the Shuttle bay will be mounted in position to measure the underside of the reflector (mesh, ribs, and hub) to cover the central 10 meters. An additional camera is required to measure the full 20 meters to the desired accuracy. Approximately 130 frames of film are available per camera. The film is processed post-flight to yield approximately 1500 points on the antenna mesh to a location accuracy of 0.2 mm rms.
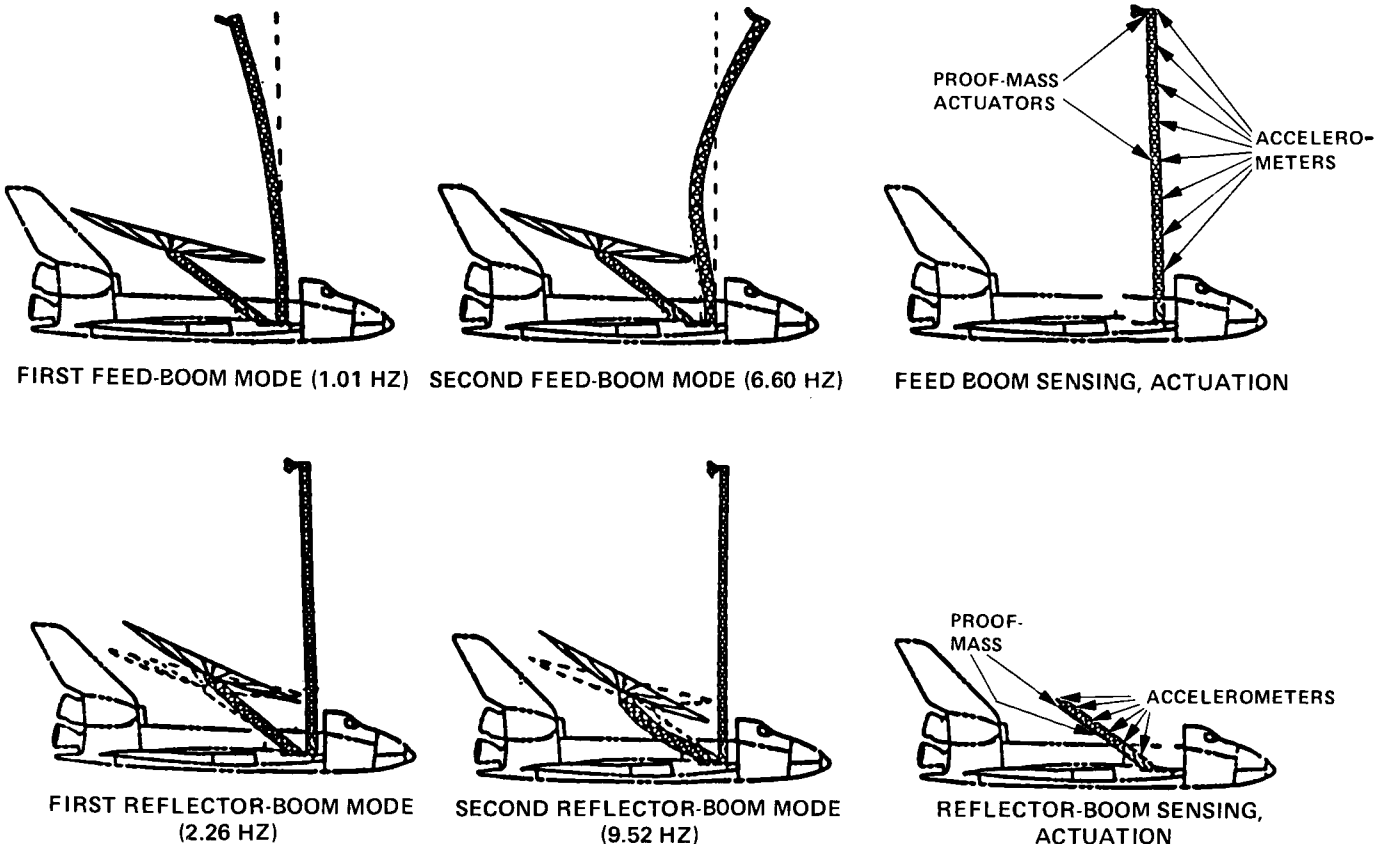

4 FILM CAMERAS LOCATED IN SHUTTLE BAY
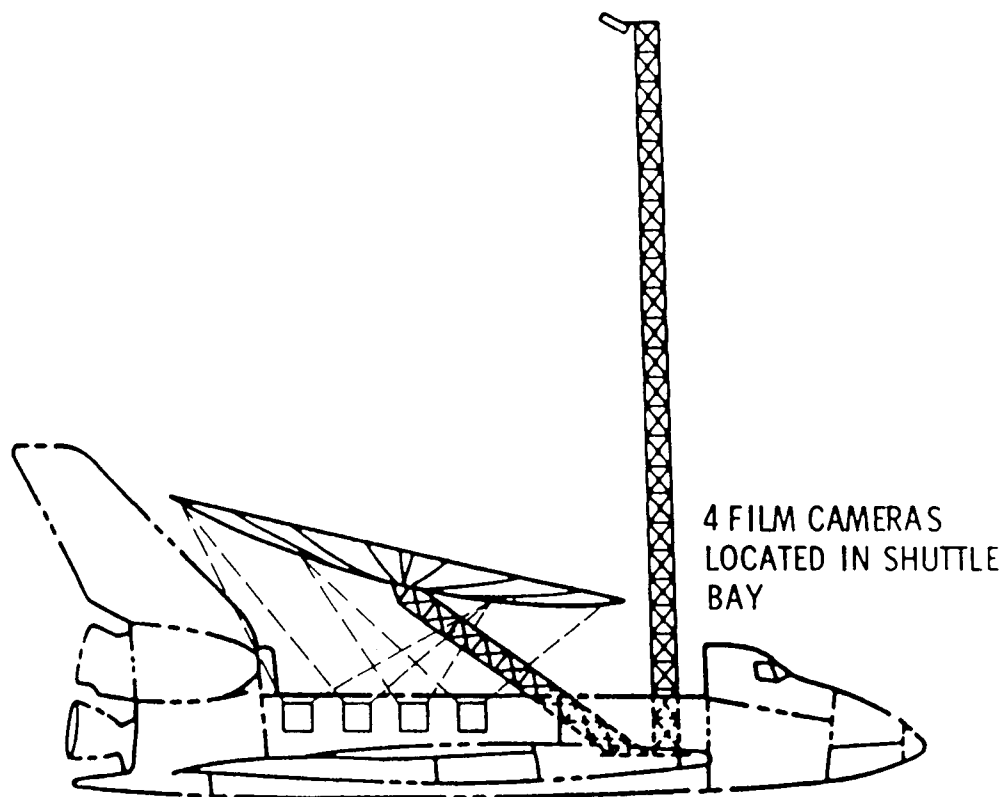
PHOTOGRAMMETRY SUBSYSTEM
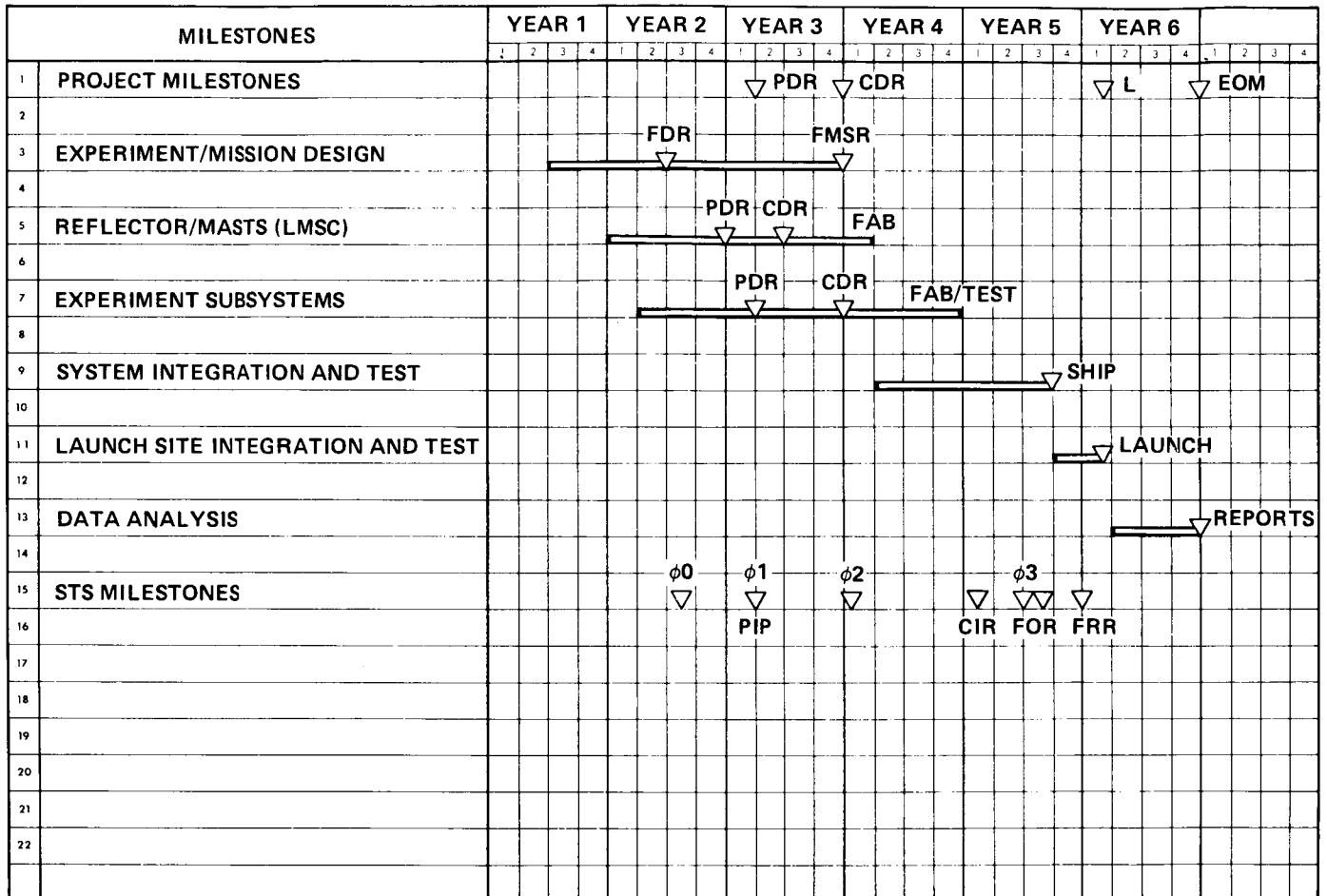
STRUCTURE CONTROL DYNAMICS IDENTIFICATION

Dynamics Identification: An initial wideband characterization of the antenna system dynamic response to induced disturbances will be performed after the passive behavior of the antenna has been measured and analyzed (to first order). Induced impulsive disturbances, encompassing the range expected during the period of the experiment, will be made utilizing controlled VRCS and/or RCS thruster firings. Measurement of the antenna dynamic response will be made via accelerometers placed at the appropriate locations on the feed and reflector booms to determine the nominal, modal frequencies and damping. The wideband data will be used to initialize more precise narrowband excitation using proof-mass actuators located on the antenna and feed booms. Results of the narrowband-frequency-domain modal estimates and transfer functions will be used to optimize the subsequent inputs for recursive-time-domain algorithms, and for data-block-MIMO identification methods such as Maximum Likelihood Estimation. Data processing will be done by the ground payload operations control, with parameter updates transmitted to on-board controllers.

Pointing and Vibration Damping Control: The purpose of this experiment is to demonstrate that the feed-reflector alignment can be actively controlled to reduce inherent perturbations. This will be accomplished using proof mass actuators on the feed and dish booms to control the structure's oscillations and the feed plane actuators to control the feed-hub line-of-sight position. Data obtained from the characterization experiment may be evaluated in mission time and used to adjust and tune the onboard control models. A series of active pointing and jitter suppression experiments will be performed that include both regulation and tracking control laws.

FIRST FEED-BOOM MODE (1.01 HZ)   SECOND FEED-BOOM MODE (6.60 HZ)   FEED BOOM SENSING, ACTUATION

PROOF-MASS ACTUATORS   ACCELEROMETERS

FIRST REFLECTOR-BOOM MODE (2.26 HZ)   SECOND REFLECTOR-BOOM MODE (9.52 HZ)   REFLECTOR-BOOM SENSING, ACTUATION

PROOF-MASS   ACCELEROMETERS

PROJECT MASTER SCHEDULE

The master schedule for this flight experiment shows that Year 1 would consist of preproject studies and analyses followed by a project start in Year 2. The project would take roughly four years to the launch and flight experiment in Year 6. A significant amount of data analysis and modeling would follow the experiment itself.

MILESTONES	YEAR 1	YEAR 2	YEAR 3	YEAR 4	YEAR 5	YEAR 6	
1 PROJECT MILESTONES			▽ PDR ▽ CDR			▽ L ▽ EOM	
2							
3 EXPERIMENT/MISSION DESIGN		FDR ▽	FMSR ▽				
4							
5 REFLECTOR/MASTS (LMSC)		PDR ▽	CDR ▽ FAB				
6							
7 EXPERIMENT SUBSYSTEMS			PDR ▽ CDR ▽ FAB/TEST				
8							
9 SYSTEM INTEGRATION AND TEST					▽ SHIP		
10							
11 LAUNCH SITE INTEGRATION AND TEST						▽ LAUNCH	
12							
13 DATA ANALYSIS						▽ REPORTS	
14							
15 STS MILESTONES		φ0 ▽	φ1 ▽ φ2 ▽		φ3 ▽ ▽▽ ▽		
16			PIP		CIR FOR FRR		
17							
18							
19							
20							
21							
22							

CONCLUSIONS FROM THE FY '86 ATSE STUDIES

The studies conducted at JPL and Lockheed over the past year have concluded that a flight experiment of a relatively large mesh deployable reflector is achievable with no major technological or cost drivers. The test article and the instrumentation are all within the state of the art and in most cases rely on proven flight hardware. Every effort was made during the course of the studies to design the experiments for low cost, either through hardware inheritance or design simplicity. The net result is an experiment design which is relatively low in cost yet achieves the global objectives of the project, which were to enable new applications of large deployable space antennas and to advance the state of the art in the structural, control, and RF aspects of these antenna systems.

- ANTENNA EXPERIMENT IS TECHNICALLY FEASIBLE

- NO TECHNICAL "SHOW-STOPPERS"

- EXPERIMENT WOULD ENABLE NEW APPLICATIONS

- EXPERIMENT WOULD ADVANCE TECHNOLOGY STATE OF THE ART

STRUCTURAL CONTROL BY THE USE OF PIEZOELECTRIC ACTIVE MEMBERS

J. L. Fanson and
J.-C. Chen
Jet Propulsion Laboratory
Applied Technologies Section
California Institute of Technology
Pasadena, California

LARGE SPACE STRUCTURE CONTROL PROBLEM

Large Space Structures (LSS) exhibit characteristics which make the LSS control problem different from other control problems. LSS will most likely exhibit low-frequency, densely spaced and lightly damped modes. In theory the number of these modes is infinite. Because these structures are flexible, Vibration Suppression is an important aspect of LSS operation. There are a number of implementability issues which must be dealt with by any "space realizable" actuation and sensing scheme. In terms of Vibration Suppression, we would like the control actuators to be as low mass as possible, have infinite bandwidth, and be electrically powered. In addition, we argue that actuators which produce "internal forces" in the structure have distinct advantages for the Vibration Suppression application. Since velocity sensing may be very difficult at low vibration levels and low frequencies, we prefer to use strain as the only measurement. Finally, we propose that actuators be built into the structure as dual-purpose structural elements in the interest of efficiency of design.

- **LOW FREQUENCY, DENSELY SPACED AND LIGHTLY DAMPED MODES ARE COMMON. ACCURATE SYSTEM CHARACTERISTICS ARE DIFFICULT TO OBTAIN**

- **VIBRATION SUPPRESSION IS AN IMPORTANT ASPECT OF LSS OPERATION**

- **ACTUATOR REQUIREMENTS ARE LIGHT WEIGHT, INTERNAL FORCE PRODUCING, ELECTRICAL POWERED, INFINITE BANDWIDTH, etc.**

- **ACCURATE VELOCITY SENSING MAY BE UNREALISTIC**

- **STRAIN SENSORS SHOULD BE CONSIDERED**

- **INTEGRATED DUAL PURPOSE LOAD CARRYING/ACTUATION MEMBERS SHOULD BE CONSIDERED**

Initial work investigating vibration suppression in LSS using internal forces centered on the one-dimensional vibrating string. The string has low inherent out-of-plane stiffness, like some Large Space Structures. It was found that by varying the tension in the string as a function of state variables and time, damping could be introduced. The lower figure shows a plot of the motion of the string in the phase plane. The distance of the curve from the origin is an indication of the energy in the motion at a particular point in time. The damping is evident by the spiraling of the locus into the origin.

VIBRATING STRING

$$\rho \frac{\partial^2 y}{\partial t^2} = \frac{\partial}{\partial x}\left(T \frac{\partial y}{\partial x}\right)$$

$$T = T\left(y, \frac{\partial y}{\partial t}, t\right)$$
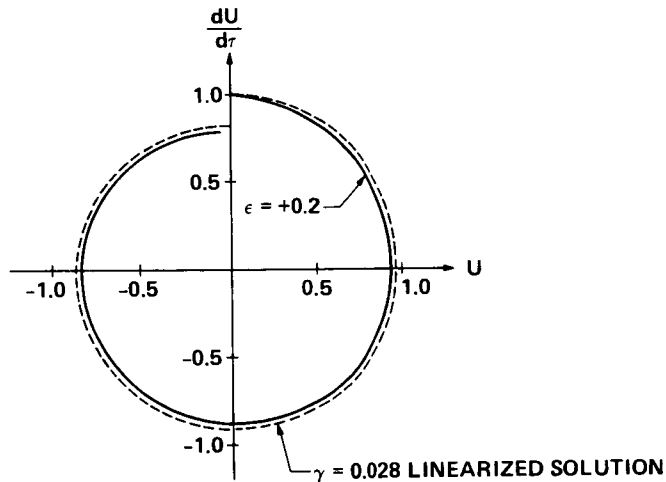
EXAMPLES OF ACTIVE MEMBERS

The concept of an active member is to replace a passive structural ele-
ment, such as a diagonal of a space-truss beam, with a structure which is also
a control actuator and sensor. We propose a piezoelectric active member for
the control of LSS. Such devices would consist of a piezoelectric actuator
and sensor for measuring strain, and screwjack actuator in series for use in
quasi-static shape control. Several concepts for active-members are shown.
One variation is to beam a laser through a hollow strut to measure movement
between the two ends of the member. We envision these devices as being self-
contained, possibly containing their own electronics for effecting Vibration
Suppression.

SINGLE BAY
DETAIL

TEST
SPECIMEN

ACTIVE MEMBER
(TYPICAL)

← EXCITATION

PIEZOELECTRIC
SENSOR/ACTUATOR

SCREW JACK

SPACE TRUSS

A = ACTUATOR
S = SENSOR

END FITTING

LASER TARGET

PIEZOELECTRIC
ACTUATOR

LASER

TRUSS MODEL

ACTIVE MEMBER WITH LASER
DISPLACEMENT SENSOR
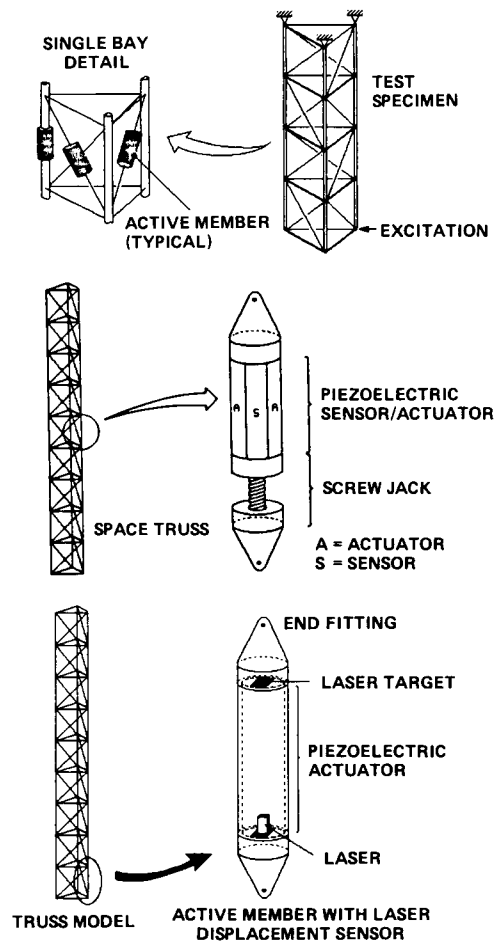
FEASIBILITY STUDY --- PIEZOBEAM EXPERIMENT

In order to investigate the feasibility of using piezoelectric active members to perform Vibration Suppression in LSS, a simple experiment was designed. The objective of the experiments is to simulate an active member using piezoelectric ceramic thin sheet material on a thin, uniform cantilever beam. The structure was designed to have low stiffness, low mass density, and to have a first mode at 5 Hz. We use collocated piezoelectric ceramics as both actuators and strain sensors. The layup of the ceramics and the dimensions of the composite piezobeam are shown.

- OBJECTIVE - SIMPLE DEMONSTRATION OF VIBRATION SUPPRESSION
- INTEGRATED STRUCTURAL MEMBER/ACTUATOR
- LSS CHARACTERISTICS
    - LOW STIFFNESS
    - LOW MASS
    - HIGH MODAL DENSITY AT HIGHER FREQUENCY
- COLLOCATED ACTUATORS/SENSORS
- SPACE REALIZABLE APPROACH
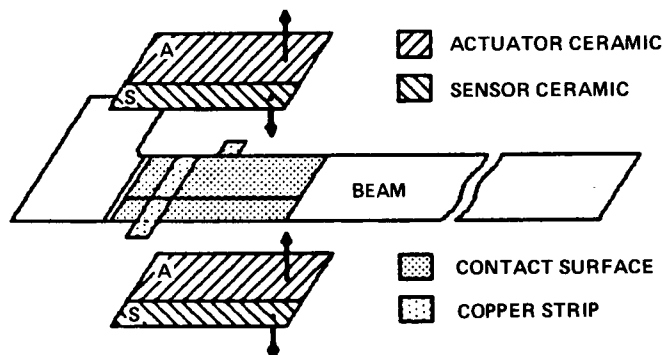
| | PIEZOELECTRIC CERAMICS | |
	BEAM	ACTUATOR	SENSORS
LENGTH:	12.50 in	1.25 in	1.25 in
WIDTH:	0.648 in	0.50 in	0.25 in
THICKNESS:	0.020 in	0.0095 in	0.0095 in
MATERIAL:	ALUMINUM	LEAD-ZIRCONATE-TITANATE (PZT)	

The cantilever beam was supported in a vibration test fixture shown in the figure. The beam was supported in a clamping flange which was bolted to a linear bearing table. The table was excited by means of a stinger attached to a small shaker. A wide variety of waveforms were used to test the open-loop and closed-loop performance of the piezobeam.
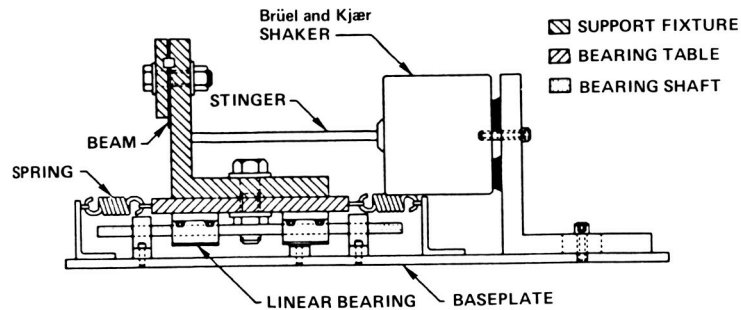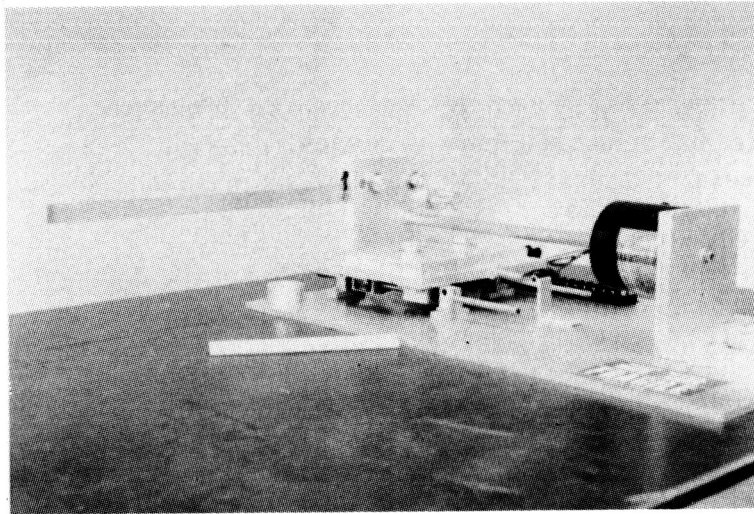
MECHANICS OF PIEZOELECTRICS

The piezoelectric ceramic material is an inherent electromechanical trans-
ducer. If an electric field is applied to the material, it tends to strain by
an amount proportional to the strength of the applied field. The proportion-
ality constant is the d_{31} coefficient. If, on the other hand, the material is
stressed, an electric field is generated spontaneously. The proportionality
constant between stress and generated electric field is the g_{31} coefficient.
Both the d_{31} and the g_{31} coefficients are material properties of the piezoelec-
tric.

The piezoelectrics are arranged on the test beam in a sandwich fashion.
The actuators are arranged such that a voltage applied to the outer electrode
surfaces causes one ceramic to expand while the other contracts. Since the ce-
ramics are adhered to the beam, a bending moment is produced. Similarly, the
bending of the beam stresses the sensor ceramics which in turn produce a volt-
age which is measured.

(a.) ACTUATOR PIEZOELECTRIC

E_f POLARITY

CERAMIC ← 1.0 → ← ϵ_E

$\epsilon_E = d_{31} E_{f'}$
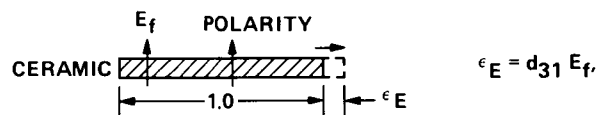
(b.) SENSOR PIEZOELECTRIC

E_f POLARITY

$\sigma \rightarrow$ ← σ

$E_f = -g_{31} \sigma'$
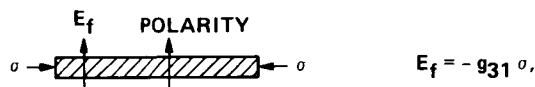
V_a = ACTUATOR VOLTAGE

d_{31} = PIEZOELECTRIC STRAIN CONSTANT

g_{31} = PIEZOELECTRIC VOLTAGE CONSTANT

t_a = THICKNESS OF THE ACTUATOR CERAMICS

PUSH-PULL BENDING ACTUATOR

POLARITY V_a

CERAMIC

ALUMINUM

CERAMIC

POLARITY V_a

The moment applied by the piezoelectrics is determined by integrating the stress produced. The magnitude of the applied moment is found to be proportional to the width of the actuator ceramic W_a, the product of the Young's Modulus and piezoelectric strain constant $d_{31}E_a$, the "lever arm" (or distance from the neutral axis), and the applied voltage V_a. The measured voltage was about 25% less than the predicted value which is consistent with the simplifying assumptions of the analysis.

ACTUATOR INDUCED BENDING MOMENT

NEUTRAL AXIS

POSITIVE CURVATURE
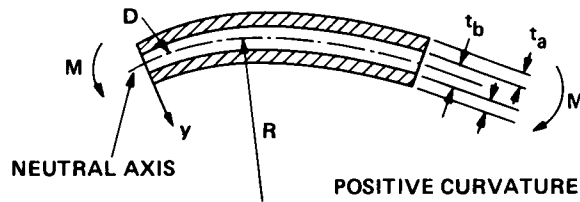
$$M = \int_A \sigma_x (y - D)\, dA = \int_A E\, \epsilon_x (y - D)\, dA.$$

$$= \int_{\substack{\text{UPPER} \\ \text{CERAMICS}}} E_1 (-\epsilon_E)(y - D)\, dA + \int_{\substack{\text{LOWER} \\ \text{CERAMICS}}} E_3 (\epsilon_E)(y - D)\, dA.$$

$$M = W_a E_a d_{31} (t_a + t_b)\, V_a.$$

$$M = 1.02 \times 10^{-3}\, V_a \, \frac{\text{in} \cdot \text{lb}_f}{\text{VOLT}}$$

ACTUAL MEASUREMENT: $M = 0.714 \times 10^{-3}\, V_a \, \dfrac{\text{in} \cdot \text{lb}_f}{\text{VOLT}}$

The sensor responds to the applied stress. Assuming that the stress at the midthickness is the sensor stress σ_s, we find that the sensor responds to the curvature of the beam $\frac{\partial^2 y}{\partial x^2}$. Again, using the modal expansion, we find that the sensor voltage is a function of the curvature of the mass-normalized mode shape. This measurement is related to the bending strain of the beam which is a generalized displacement.

SENSOR: PLANT TRANSFER FUNCTION

THE SENSOR SENSES THE MODAL "DISPLACEMENT"

$$\sigma_s = -\frac{1}{2}(t_s + t_b)\frac{M}{I}.$$

$$V_s = -\frac{1}{2}g_{31} t_s (t_s + t_b)\frac{M}{I}.$$

$$V_s \doteq \underbrace{\frac{1}{2}f_s g_{31} t_s (t_s + t_b) E_b}_{a_2}\frac{\partial^2 y}{\partial x^2},$$

f_s = SENSOR CALIBRATION FACTOR = 0.75

$$V_s = a_2 C\left(\frac{\partial^2 y}{\partial x^2}\right),$$

C = FACTOR FOR CURVATURE VARIATION

$$V_s = a_2 \xi_i(t) C\left(\frac{\partial^2 \phi_i(x)}{\partial x^2}\right) = a_2 \xi_i(t) C_i.$$

*THE SENSOR SENSES THE MODAL "DISPLACEMENT".

EQUATION OF MOTION FOR PIEZOBEAM

    The partial differential equation of motion for the piezobeam is shown. It involves the second spatial derivative of the applied moment. The actuators are modelled as applying a uniform distributed follower moment over part of the length of the beam. The applied moment is modelled mathematically using a Heaviside Step function to turn the moment on and another Heaviside Step to turn it off spatially. Using the standard modal expansion, the modal equations are derived. The coupling of the actuator to the modal equations involves the difference in slopes of the mass-normalized mode shapes at the ends of the actuator ceramics.

APPLIED MOMENT M

E(x), I(x), m(x)

x_1 x_2

L
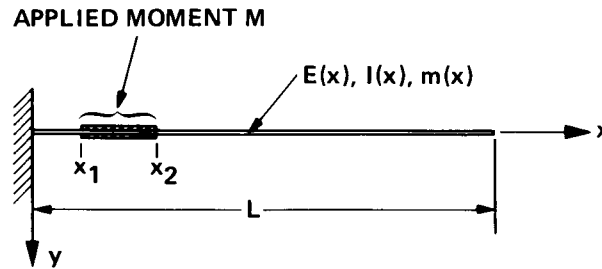
$$m(x) \frac{\partial^2 y}{\partial t^2} + \frac{\partial^2}{\partial x^2}\left(E(x)\, I(x)\, \frac{\partial^2 y}{\partial x^2}\right) = \frac{\partial^2 M(x)}{\partial x^2} \, .$$

$$M(x) = a_1 V_a \, [h(x - x_1) - h(x - x_2)],$$

$$h(\cdot) = \text{HEAVISIDE STEP FUNCTION}$$

MODAL EQUATIONS:

$$y(x, t) = \sum_{i=1}^{n} \xi_i(t)\, \phi_i(x).$$

$$\ddot{\xi}_j(t) + \xi_j(t)\, \omega_j^2 = a_1 D_j V_a.$$

WHERE $D_j \equiv [\phi_j'(x_2) - \phi_j'(x_1)],$

818

SYSTEM CONFIGURATION

The top figure is a block diagram of the control system. The actuators and sensors are modelled as non-dynamic real constant matrices. The external disturbances enter through the shaker. The control approach used in these experiments is called Positive Position Feedback. This technique uses displacement measurements to effect vibration suppression. It can be understood by considering the scalar case consisting of two equations, one representing the structure or mode ζ, and one representing a tuned control filter η. The modal displacement drives the filter, and the filter coordinate is fed back in turn to the structure. The Positive Position terminology can be understood from these equations.
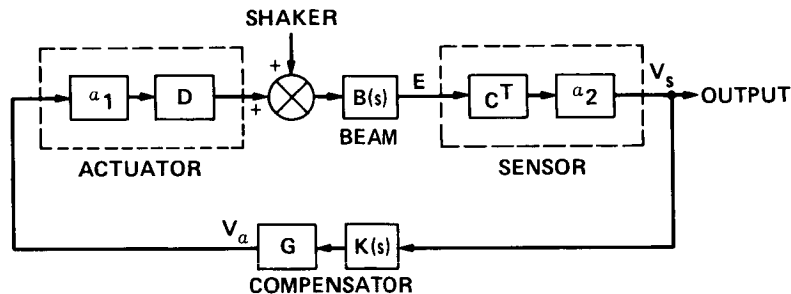
SYSTEM EQUATIONS FOR SISO:

STRUCTURE: $\ddot{\xi} + 2\zeta\omega\dot{\xi} + \omega^2\xi = g\omega^2\eta + f(t)$

COMPENSATOR: $\ddot{\eta} + 2\zeta_f\omega_f\dot{\eta} + \omega_f^2\eta = \omega_f^2\xi$

ω = MODAL FREQUENCY , ζ = MODAL DAMPING

g = GAIN FACTOR , f = EXTERNAL FORCE

ω_f = FILTER FREQUENCY , ζ_f = FILTER DAMPING

POSITIVE POSITION FEEDBACK (PPF) CONTROL

- POSITION COORDINATE OF THE STRUCTURE IS POSITIVELY FED TO THE FILTER
- POSITION COORDINATE OF THE FILTER IS POSITIVELY FED BACK TO THE STRUCTURE

PPF SYSTEM STABILITY

The system matrix equation for the scalar example shows that the coupling of the structure to the compensator occurs in the frequency or stiffness matrix. This is because displacements are used as measurement quantities. A stability analysis of the system equation indicates that stability is maintained if the gain g lies between zero and one. In particular, the point on the Nyquist plot which determines stability is the point A. If point A lies to the right of the origin, stability is maintained. Point A is the point on the locus corresponding to zero frequency. Thus the stability criterion is non-dynamic. This is characteristic of Positive Position Feedback and accounts for the improved robust stability of this method. A root locus for the scalar case shows how PPF achieves Vibration Suppression. The filter pole moves toward the imaginary axis while the structural pole moves into the left half plane. Thus, the structural pole is stabilized.

$$\left\{ \begin{array}{c} \ddot{\xi} \\ \ddot{\eta} \end{array} \right\} + \left[\begin{array}{cc} 2\zeta\omega & 0 \\ 0 & 2\zeta_f\omega_f \end{array} \right] \left\{ \begin{array}{c} \dot{\xi} \\ \dot{\eta} \end{array} \right\} + \left[\begin{array}{cc} \omega^2 & -g\omega^2 \\ -\omega_f^2 & \omega_f^2 \end{array} \right] \left\{ \begin{array}{c} \xi \\ \eta \end{array} \right\} = 0$$

THE CONTROL GAIN FACTOR IS IN THE SYSTEM STIFFNESS
MATRIX, THUS THE TERM "STIFFNESS CONTROL".

NYQUIST PLOT
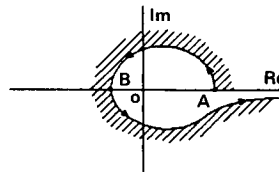
ROOT LOCUS FOR SCALAR PPF
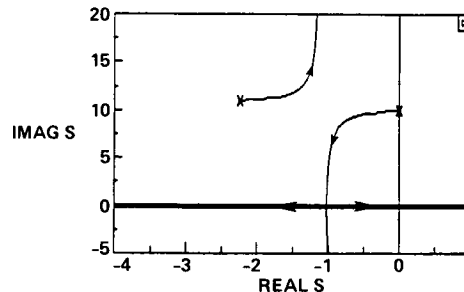
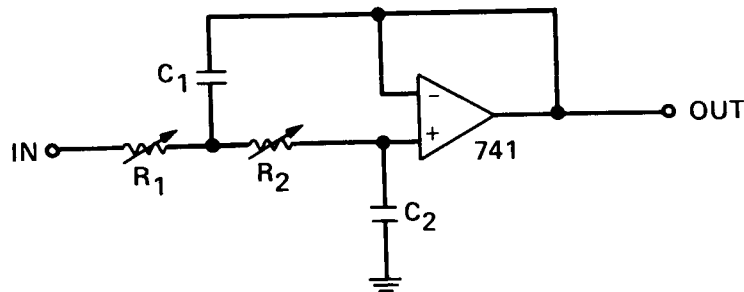The Positive Position Feedback compensator is composed of tuned filters with transfer function shown below. A simple analog filter realization with the desired transfer function is shown. The frequency and damping ratio is selected based on the results of the control synthesis.

LAPLACE TRANSFORM OF FILTER

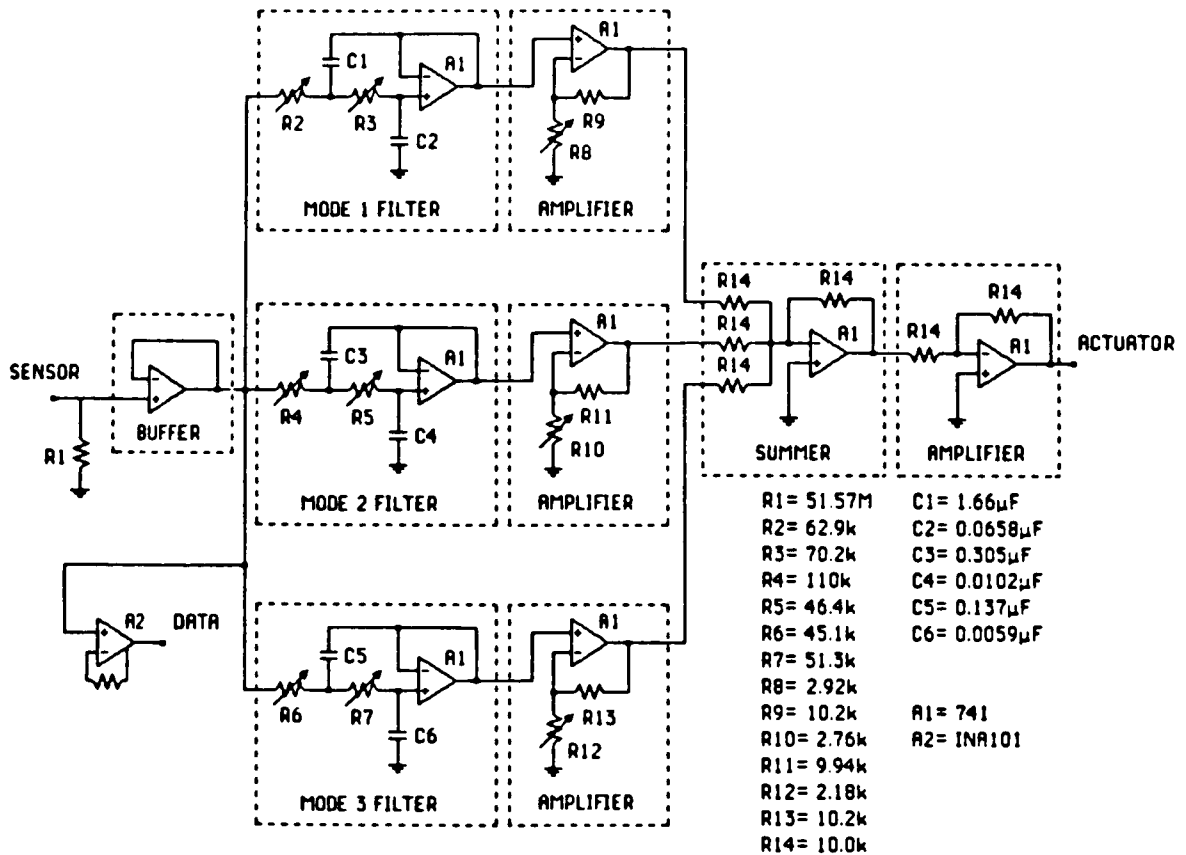$$T(s) = \frac{\omega_f^2}{s^2 + 2\zeta f\omega fs + \omega_f^2},$$

$$\omega_f = \sqrt{\frac{1}{R_1 R_2 C_1 C_2}},$$

$$\zeta_f = \frac{1}{2}\omega_f (R_1 + R_2) C_2.$$

$$R_1 = R_2 \cong 50\ K\ (OHMS)$$

Several experiments were performed. The first experiments controlled the lower modes of the beam individually with one sensor and actuator pair. Then the lower modes were controlled together. The control circuit for the control of the first three modes is shown along with the component values used. The circuit contains more amplifiers than necessary to allow more flexibility in the development of the experiment.


R1= 51.57M   C1= 1.66µF
R2= 62.9k   C2= 0.0658µF
R3= 70.2k   C3= 0.305µF
R4= 110k   C4= 0.0102µF
R5= 46.4k   C5= 0.137µF
R6= 45.1k   C6= 0.0059µF
R7= 51.3k
R8= 2.92k
R9= 10.2k   A1= 741
R10= 2.76k   A2= INA101
R11= 9.94k
R12= 2.18k
R13= 10.2k
R14= 10.0k

SISO EXPERIMENTAL RESULTS

The frequency response functions for the experiments using one actuator and sensor pair are shown. These are measured data. The dashed line represents the open-loop response, the solid line represents the closed-loop response. It can be seen that the control action on the controlled modes greatly reduces their response amplitude. In addition, the spillover into uncontrolled modes is always stabilizing. This is characteristic of Positive Position Feedback. The open-loop and closed-loop free decay for Mode 1 under Mode 1 control is also shown.
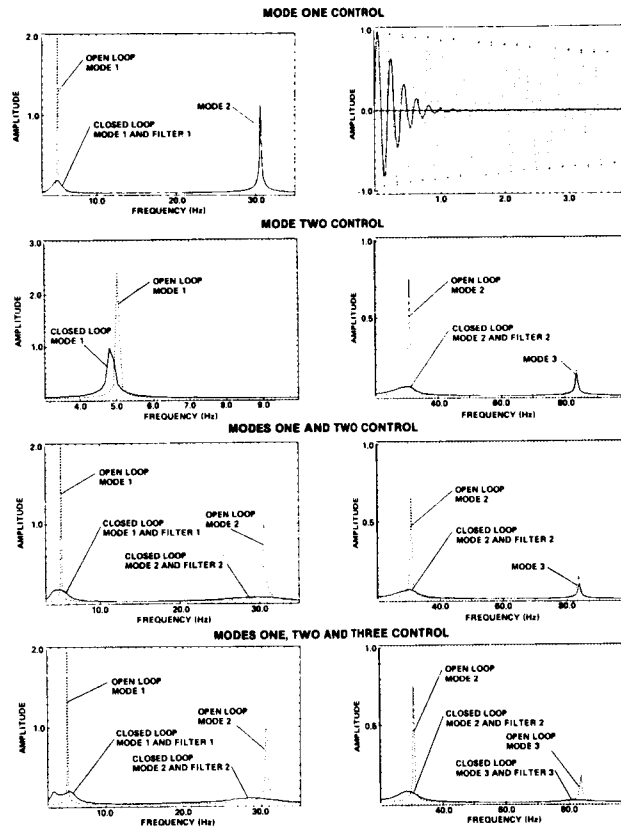
Oscilloscope photographs of the free decay of Mode 1 under three mode control are shown. Each photograph shows the open-loop decay as the outer envelope, and the closed-loop decay as the inner trace. Both photographs are of the same response only at two different time scales. The settling time of the first mode was reduce from about one minute to about one second.

OPEN AND CLOSED LOOP FREE DECAY OF MODE ONE
FOR THREE MODE CONTROL
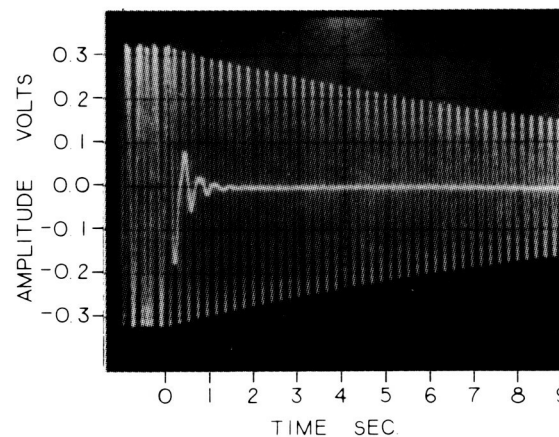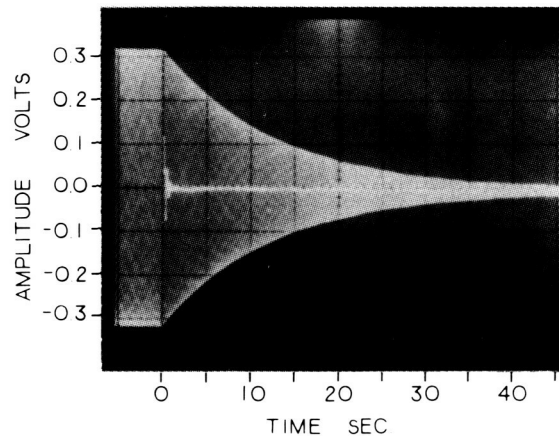
SISO EXPERIMENTAL RESULTS (CONT.)

These tables summarize the open-loop and closed-loop performance for the single-input-single-output experiments. Three quantities of interest are compared: ζ, $\zeta\omega_n$, and $\zeta\omega_n^2$. The first quantity, ζ, is the damping ratio and is a general measure of modal damping. The second quantity, $\zeta\omega_n$, is inversely related to the settling time. The third quantity, $\zeta\omega_n^2$, is inversely related to the steady-state amplitude of response to sinusoidal excitation ignoring the effects of mode shape changes. Depending on the type of dynamic response of interest one or another of these quantities is of greater interest.

EFFECT OF MODE 1 CONTROL ON MODES 1 AND 2

	MODE 1			MODE 2		
	$\zeta_1(\%)$	$\zeta_1\omega_1$	$\zeta_1\omega_1^2$	$\zeta_2(\%)$	$\zeta_2\omega_2$	$\zeta_2\omega_2^2$
OPEN LOOP	0.23	0.0721	2.27	0.15	0.289	55.5
CLOSED LOOP	16.3	4.68	135.	0.19	0.366	70.3
*PERCENT CHANGE**	*7,000*	*6,400*	*5,800*	*26.7*	*26.6*	*26.7*
PREDICTED[†]	13.3	3.96	118.	0.17	0.320	61.7

EFFECT OF MODE 2 CONTROL ON MODES 1 AND 2

	MODE 1			MODE 2		
	$\zeta_1(\%)$	$\zeta_1\omega_1$	$\zeta_1\omega_1^2$	$\zeta_2(\%)$	$\zeta_2\omega_2$	$\zeta_2\omega_2^2$
OPEN LOOP	0.23	0.0721	2.27	0.15	0.289	55.5
CLOSED LOOP	0.43	0.131	4.00	12.7	22.4	3.95×10^3
*PERCENT CHANGE**	*87*	*80*	*76*	*8,400*	*7,700*	*7,000*
PREDICTED[†]	0.37	0.112	3.40	13.3	23.5	4.18×10^3

EFFECT OF TWO MODE CONTROL ON MODES 1 AND 2

	MODE 1			MODE 2		
	$\zeta_1(\%)$	$\zeta_1\omega_1$	$\zeta_1\omega_1^2$	$\zeta_2(\%)$	$\zeta_2\omega_2$	$\zeta_2\omega_2^2$
OPEN LOOP	0.23	0.0721	2.27	0.15	0.289	55.5
CLOSED LOOP	15.3	3.81	94.7	13.8	23.7	4.05×10^3
*PERCENT CHANGE**	*6,600*	*5,200*	*4,100*	*9,100*	*8,100*	*7,200*
PREDICTED[†]	12.7	3.38	89.9	12.7	22.8	4.07×10^3

EFFECT OF THREE MODE CONTROL ON MODES 1, 2, AND 3

|	MODE 1			MODE 2			MODE 3		
	$\zeta_1(\%)$	$\zeta_1\omega_1$	$\zeta_1\omega_1^2$	$\zeta_2(\%)$	$\zeta_2\omega_2$	$\zeta_2\omega_2^2$	$\zeta_3(\%)$	$\zeta_3\omega_3$	$\zeta_3\omega_3^2$
OPEN LOOP	0.23	0.0721	2.27	0.15	0.289	55.5	0.27	1.41	738.
CLOSED LOOP	13.4	2.63	51.5	8.85	15.7	2.78×10^3	3.99	20.4	1.04×10^4
*PERCENT CHANGE**	*5,700*	*3,500*	*2,200*	*5,800*	*5,300*	*4,900*	*1,400*	*1,300*	*1,300*
PREDICTED[†]	–	–	–	–	–	–	–	–	–

* PERCENT CHANGE BETWEEN MEASURED VALUES

† PREDICTED CLOSED LOOP VALUES

825

Two sensors and actuators were used in a multi-input-multi-output experiment to control the first six modes of the beam. The location of the two sets is shown in the figure. The open-loop and closed-loop frequency response functions are shown for the first eight modes.

ACTUATOR/SENSOR LOCATIONS FOR MIMO PIEZOBEAM.
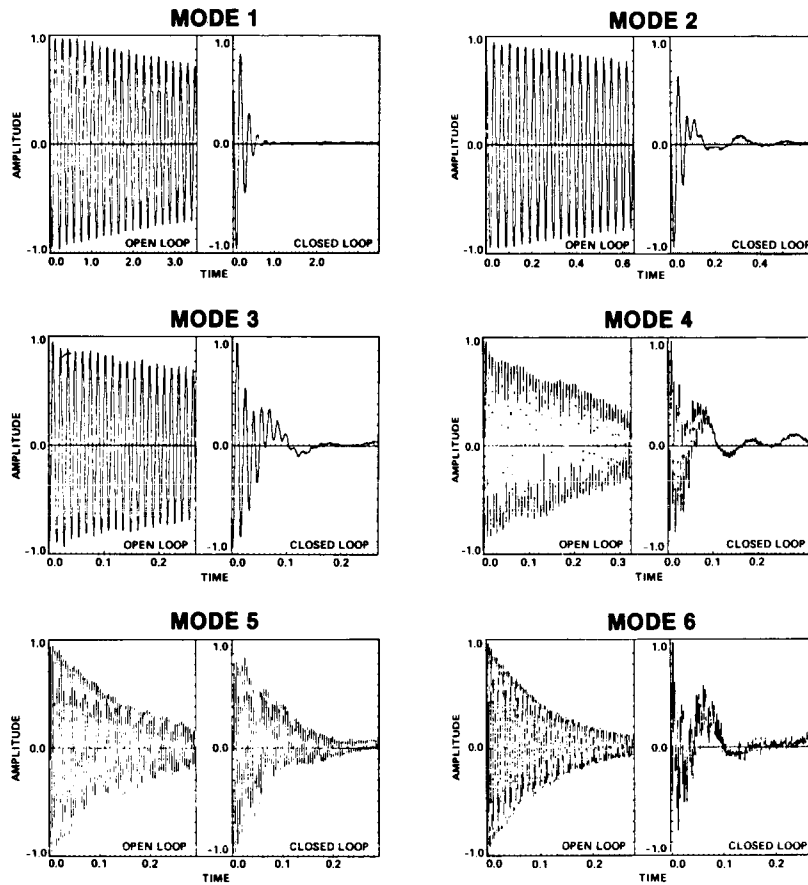## ALL DIMENSIONS IN INCHES.
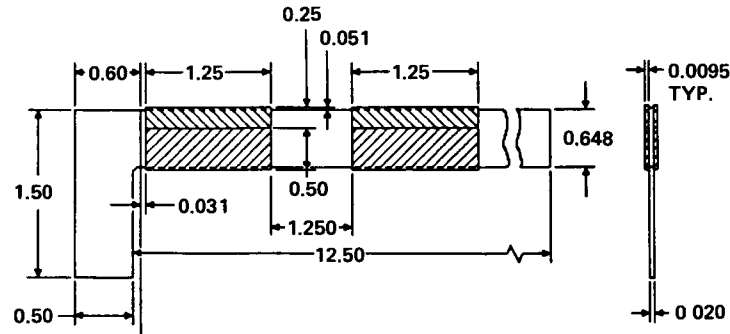
OPEN LOOP AND MIMO CLOSED LOOP FREQUENCY
RESPONSE FUNCTIONS FOR SENSOR 1.
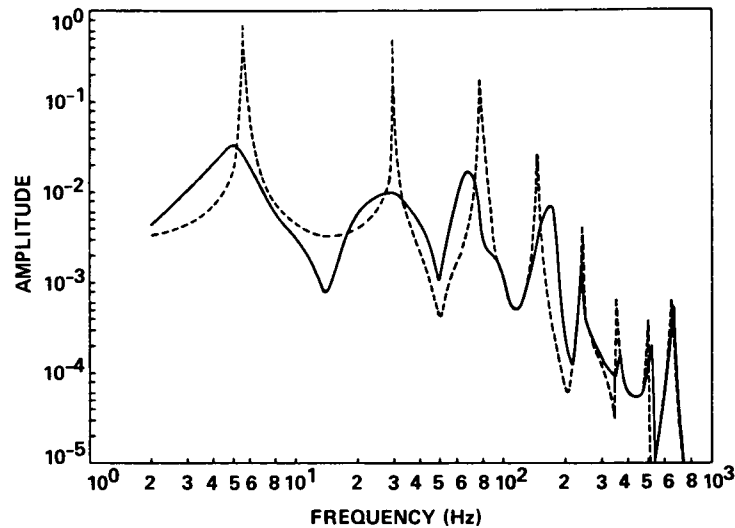
The open-loop and closed-loop free decay responses for the first six modes of the beam are shown.

OPEN LOOP AND CLOSED LOOP FREE DECAY

MIMO EXPERIMENTAL RESULTS (CONT.)

The two tables summarize the open-loop and closed-loop performance for the six mode control case.

EFFECT OF MIMO CONTROL ON MODES 1 THROUGH 8

	MODE 1			MODE 2			MODE 3			MODE 4		
	$\zeta_1 (\%)$	$\zeta_1\omega_1$	$\zeta_1\omega_1^2$	$\zeta_2 (\%)$	$\zeta_2\omega_2$	$\zeta_2\omega_2^2$	$\zeta_3 (\%)$	$\zeta_3\omega_3$	$\zeta_3\omega_3^2$	$\zeta_4 (\%)$	$\zeta_4\omega_4$	$\zeta_4\omega_4^2$
OPEN LOOP	0.33	0.116	4.11	0.19	0.352	64.1	0.23	1.05	489.	0.38	3.54	3.30×10^3
CLOSED LOOP	20.0	5.93	176.	24.8	34.0	4.65×10^3	8.00	33.2	1.38×10^4	4.05	29.8	2.19×10^4
PERCENT CHANGE*	6,000	5,000	4,200	13,000	9,600	7,200	3,400	3,100	2,700	970	740	560
PREDICTED[†]	31.5	8.47	200.	18.6	28.8	4.44×10^3	13.4	52.5	2.06×10^4	5.44	41.0	3.08×10^4

	MODE 5			MODE 6			MODE 7			MODE 8		
	$\zeta_5 (\%)$	$\zeta_5\omega_5$	$\zeta_5\omega_5^2$	$\zeta_6 (\%)$	$\zeta_6\omega_6$	$\zeta_6\omega_6^2$	$\zeta_7 (\%)$	$\zeta_7\omega_7$	$\zeta_7\omega_7^2$	$\zeta_8 (\%)$	$\zeta_8\omega_8$	$\zeta_8\omega_8^2$
OPEN LOOP	0.39	5.73	8.42×10^3	0.37	7.98	1.73×10^4	0.34	10.6	3.32×10^4	0.36	11.3	3.55×10^4
CLOSED LOOP	0.78	11.4	1.68×10^4	0.62	14.1	3.14×10^4	0.45	15.9	5.09×10^4	0.50	16.2	5.20×10^4
PERCENT CHANGE*	100	100	100	70	80	80	46	50	53	40	43	46
PREDICTED[†]	3.24	46.9	6.81×10^4	3.03	64.7	1.38×10^5	–	–	–	–	–	–

* PERCENT CHANGE BETWEEN MEASURED VALUES   † PREDICTED CLOSED LOOP VALUES

CONCLUSIONS

The conclusions drawn from this analysis and these experiments follow.

- FEASIBILITY OF USING PIEZOELECTRIC MATERIALS AS DUAL-PURPOSE STRUCTURAL ELEMENTS/ACTUATORS FOR VIBRATION SUPPRESSION IN LARGE SPACE STRUCTURES WAS DEMONSTRATED

- POSITIVE POSITION FEEDBACK (PPF) AS A VIBRATION SUPPRESSION CONTROL STRATEGY WAS IMPLEMENTED

- USING THE STRAIN SENSOR WHICH MEASURES THE ELASTIC DEFORMATION FOR CONTROL WAS SUCCESSFULLY DEMONSTRATED

- MULTI-MODE VIBRATION SUPPRESSION WAS ACHIEVED WITH DRAMATIC REDUCTION IN DYNAMIC RESPONSE

- NO DESTABILIZING EFFECTS WERE OBSERVED DUE TO EITHER THE SPILLOVER OR THE ACTUATOR DYNAMICS

- A BETTER SYNTHESIS THEORY WHICH PROVIDES PROCEDURES FOR THE SELECTION OF GAINS FOR STRONG STRUCTURE/CONTROL COUPLING SHOULD BE DEVELOPED

- A TRUE ACTIVE MEMBER NEEDS TO BE DEVELOPED AND INCORPORATED INTO MORE COMPLICATED EXPERIMENTS

GROUND TEST OF LARGE FLEXIBLE STRUCTURES

Ben K. Wada
Jet Propulsion Laboratory
Pasadena, CA

MOTIVATION

Many future mission models require large space structures which have accurate sur-
faces and/or the capability of being accurately aligned. If ground test approaches
which will provide adequate confidence of the structural performance to the program
managers are not developed, many viable structural concepts may never be utilized.
The size and flexibility of many of the structural concepts will preclude the use of
the current state-of-the-art ground test methods because of the adverse effects of
the terrestrial environment (atmosphere, gravity, etc.). The challenge is to develop
new test approaches which will provide confidence in the capability of large space
structures to meet performance requirements prior to flight. The development of
ground test methods for large space structures is one of most significant challenges
to the structural dynamicists to meet the needs of future space structures.

The objective of this paper is to describe the activities at JPL on ground testing of
large space structures. Since some of the proposed structural systems cannot be
tested in entirety, a coordinated ground test/analytical model program is required to
predict structural performance in space. This paper addresses selected concepts
under development at JPL.
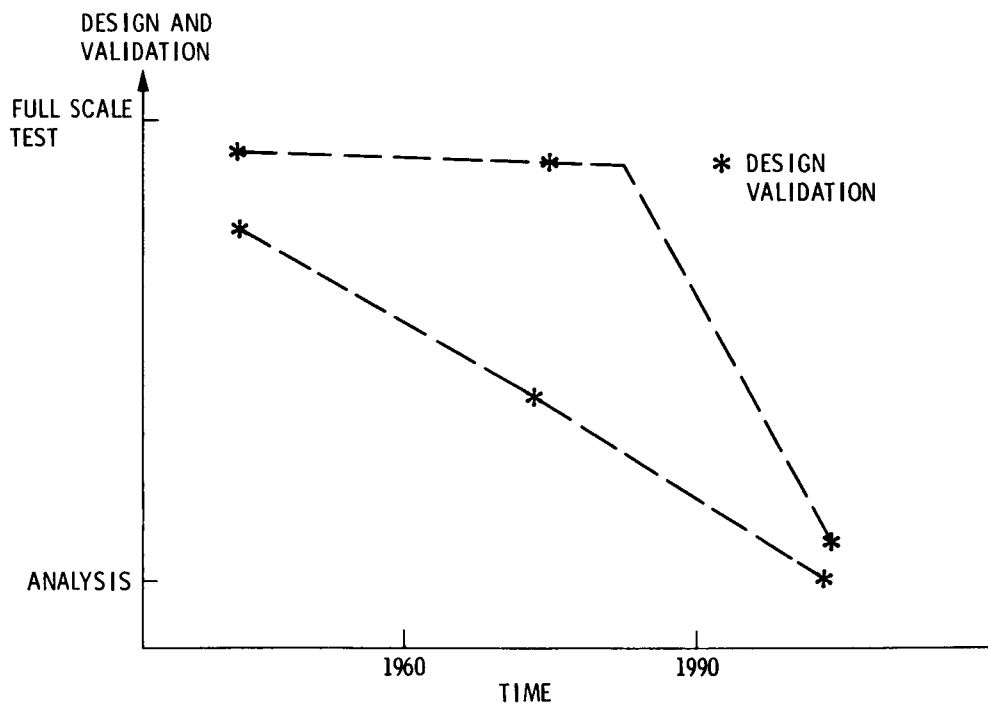
STRUCTURAL VERIFICATION

When large flexible space structures cannot be ground tested in an operational con-
figuration because of the adverse terrestrial environment (such as gravity and air),
a ground test program must be developed to validate a mathematical model which in
turn can be used to demonstrate the performance of the total structural system in
space.

The two approaches most often used are to either test the full-scale structure using
artificial restraints with the objective of simulating the operational configuration
or to ground test some or all of the subsystems comprising the total system. The
removal of the effects of the artificial restraints from the full-scale test or the
assembly of the subsystems to predict the dynamic response of the full-scale hardware
is accomplished by analysis. A third approach referred to as the Multiple Boundary
Condition Tests (MBCT) is a hybrid of the two approaches where the total structure is
tested, but the objective is to use artificial restraints to allow for good ground
test data and to obtain added test data by utilizing a large number of different sets
of artificial restraints. The analysis procedure is then to update and validate the
analytical model using a large number of experimental data and to remove the influ-
ence of the artificially imposed boundary conditions.

Finally to validate the techniques, the ground-tested hardware along with its analyt-
ical prediction should be tested in space to validate the approach. Confidence in
the technology to combine ground tests along with analytical models to accurately
predict the on-orbit dynamics will increase our ability to design and fly large space
structures to meet future space program challenges.

In this paper, the basic ideas which form the foundation of the research at JPL in
structural verification by ground tests will be presented. Since many investigators
have evaluated full-scale testing approaches, this paper concentrates on the MBCT and
some aspects of subsystem tests.

STRUCTURAL VERIFICATION

LARGE SPACE STRUCTURE

FULL SCALE

ANALYTICAL

- GRAVITY EFFECT
- SUSPENSION SYSTEM
- MULTIPLE SUPPORT
- COMBINATION
- EXTRAPOLATION

MULT. BOUN. COND TEST (MBCT)

GROUND TEST LIMITATIONS

- ORDER OF 100 m
- BUCKLING
- GRAVITY EFFECT
- ATMOSPHERE

SUBSYSTEM

VERIFICATION OF ON-ORBIT DYNAMIC CHARACTERISTICS

- COFS
- LARGE ANTENNA SYSTEM (MSAT)
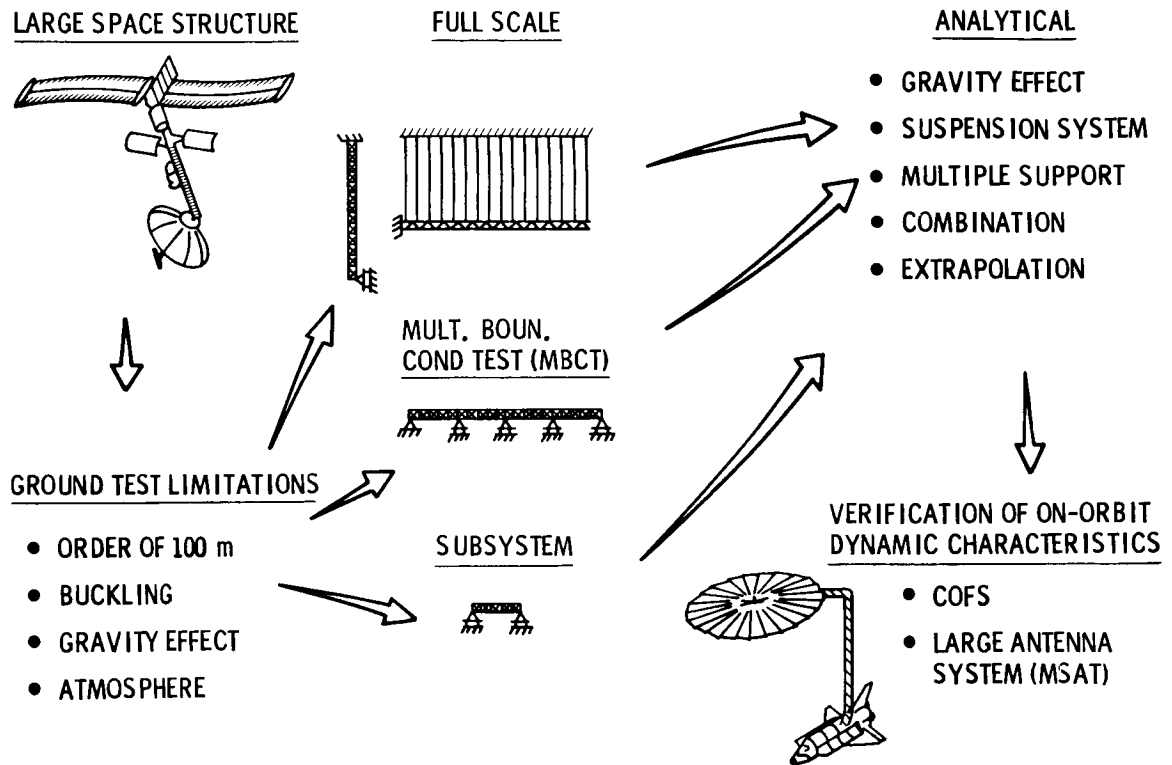
This figure represents a sector of a wrapped rib antenna built under contract to JPL by LMSC Co. The sector is part of a 55-meter-diameter antenna and thus is approximately 27 meters in length. Since the antenna could not survive the 1-g gravitational field, it was supported along each rib by about 7 suspension cables. The affect of the gravitational field on distorting the structural characteristic can be seen by the "sag" in the lightweight mesh which must be near horizontal in space to meet its desired performance.

One of the objectives of this program was to evaluate different ground test methods from which experimental data could be used to help.
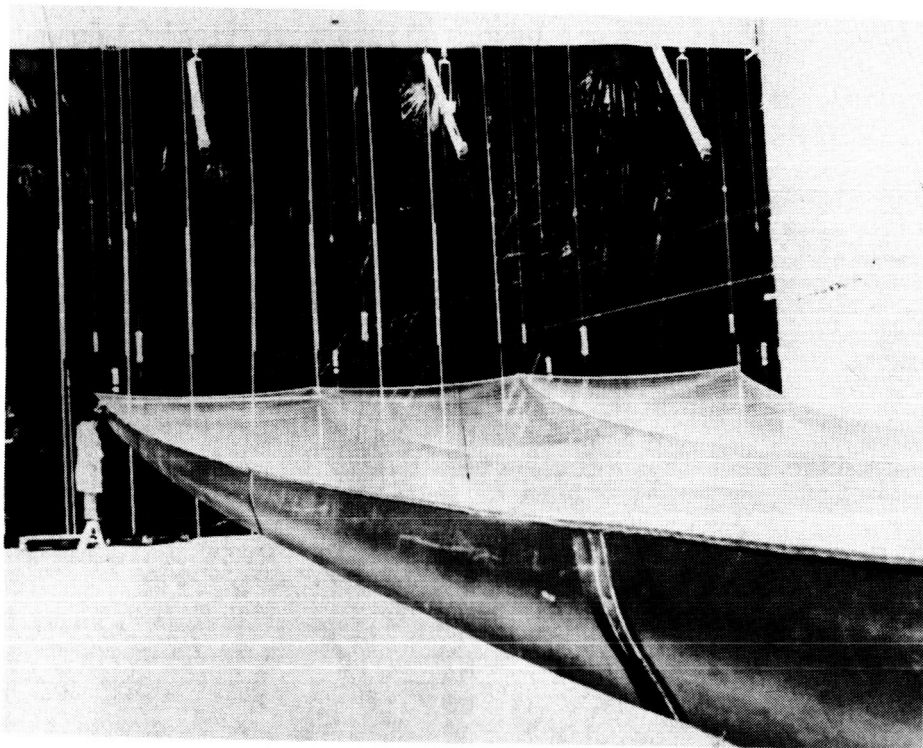
Rather than to initially explore ground tests methods to validate a sector of the rib, the goal was to ground test a single rib of the antenna. After observing the adverse affects of the terrestrial environment on the very large flexible structure, the difficulty of performing a meaningful ground test seemed to be a formidable task. The initial goal was to test a single rib in a configuration that simulated the in-orbit configuration. Subsystem test concepts for a single rib were not feasible because the structure was one continuous graphite/epoxy structure which could not be divided into subsystems without cutting the structure. Test methods considered included incorporation of active controls in the suspension system to eliminate their affects and vertically suspending the rib in a vacuum chamber. Neither appeared feasible within the available funds and schedule. The active control of the suspension system appeared to be a technical development program in itself, and the existing known vacuum chambers did not have sufficient vertical clearance.

One quickly concluded, after observing the vibration of a single rib which was supported by cables, that meaningful vibration data couldn't be obtained by testing in the configuration.
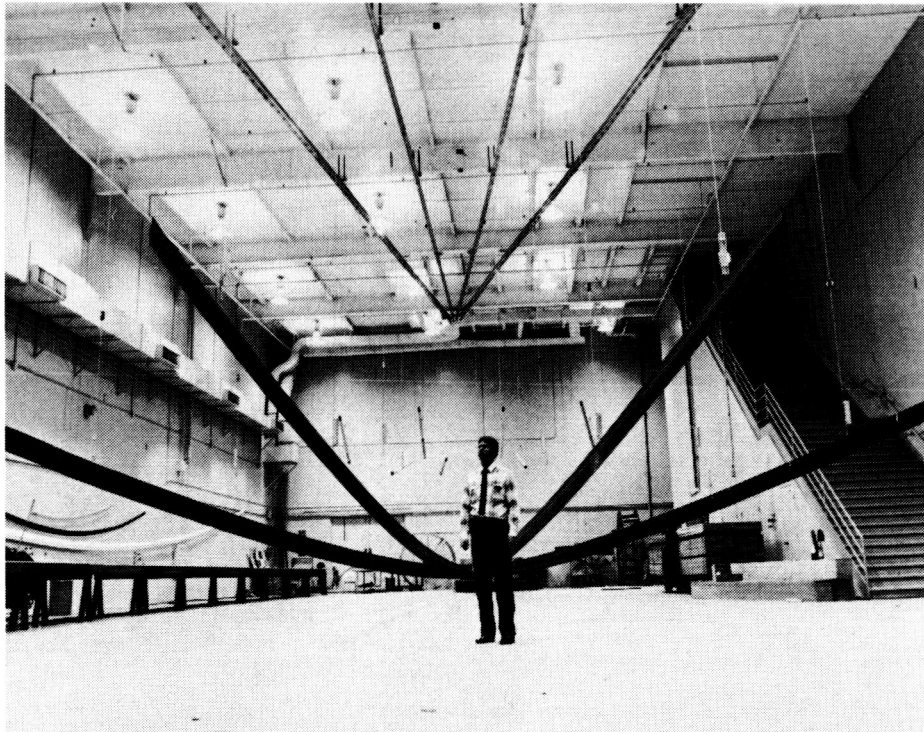
OPERATIONAL STRUCTURE SYSTEMS TEST

In many of the modal tests of the operational configuration performed to date, the objective has been to measure the largest number of mode shapes and frequencies and to attempt to identify the parameters (mass and stiffness) which should be modified to correlate the mathematical model with the test data. Difficulties exist in obtaining accurate test data as the mode number increases, and the sources of errors are difficult to isolate and identify because the number of parameters in the mathematical model may be in the tens of thousands and the number of experimental data may be in the hundreds.

B.C.* = 0

$$
\begin{bmatrix}
P_{11} & P_{12} & P_{13} & P_{14} & P_{15} & P_{16} & P_{17} \\
P_{21} & P_{22} & P_{23} & P_{24} & P_{25} & P_{26} & P_{27} \\
P_{31} & P_{32} & P_{33} & P_{34} & P_{35} & P_{36} & P_{37} \\
P_{41} & P_{42} & P_{43} & P_{44} & P_{45} & P_{46} & P_{47} \\
P_{51} & P_{52} & P_{53} & P_{54} & P_{55} & P_{56} & P_{57} \\
P_{61} & P_{62} & P_{63} & P_{64} & P_{65} & P_{66} & P_{67} \\
P_{71} & P_{72} & P_{73} & P_{74} & P_{75} & P_{76} & P_{77}
\end{bmatrix}
$$

*Boundary condition (BC)

MULTIPLE BOUNDARY CONDITION TEST (MBCT)

In an attempt to determine an alternate test approach to validate the mathematical model of a rib of the wrapped rib antenna, the concept of the MBCT approach was devised. A subsystem test approach could not be directly used because the continuous rib could not be physically "cut" for the subsystem tests.

The approach is to place artificial restraints along the structure in order to measure valid ground test data. In this example, when the artificial restraint is placed at node four, the dynamic test of the structure will only impact the parameter terms in the lower right-hand corner. Thus with this set of data, one estimate of the analytical parameters can be more easily obtained.

B.C. = 1

$$
\begin{bmatrix}
& & & & & & \\
& & & & & & \\
& & & & & & \\
& & & & & & \\
& & & & \dot{P}_{55} & \dot{P}_{56} & \dot{P}_{57} \\
& & & & \dot{P}_{65} & \dot{P}_{66} & \dot{P}_{67} \\
& & & & \dot{P}_{75} & \dot{P}_{76} & \dot{P}_{77}
\end{bmatrix}
$$
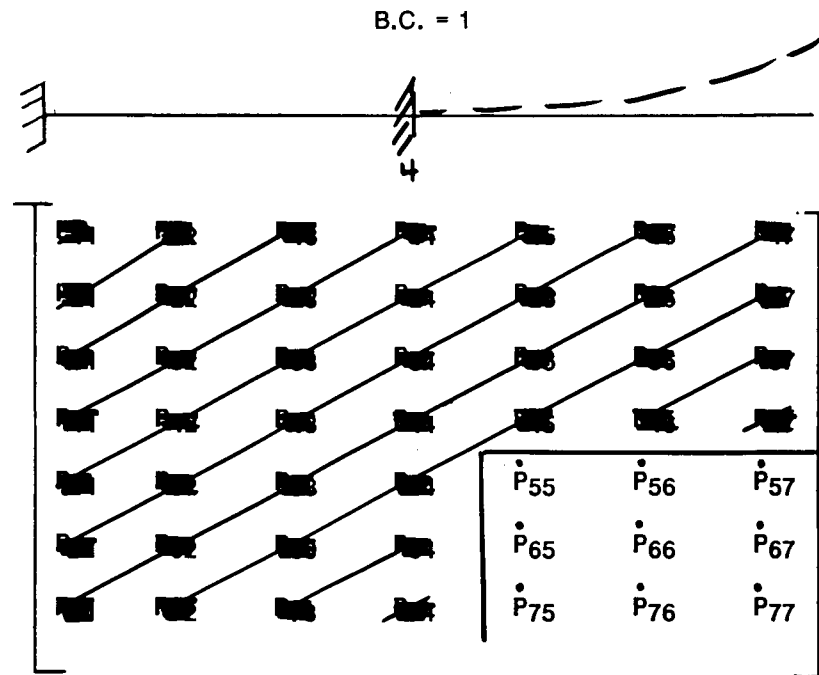
ANOTHER SET OF RESTRAINTS

If another set of restraints is selected, the resulting test data only affect another subset of the total mathematical model of interest. Note that in Boundary Condition (BC) #2, the updated terms of the mathematical model are shown. The engineer can arbitrarily select the restraints in order to isolate and concentrate on the parameters that are considered to be significant.

B.C. = 2

$$
\begin{array}{ccc}
\dot{P}_{44} & \dot{P}_{45} & \dot{P}_{46} \\
\dot{P}_{54} & \dot{P}_{55} & \dot{P}_{56} \\
\dot{P}_{64} & \dot{P}_{65} & \dot{P}_{66}
\end{array}
$$
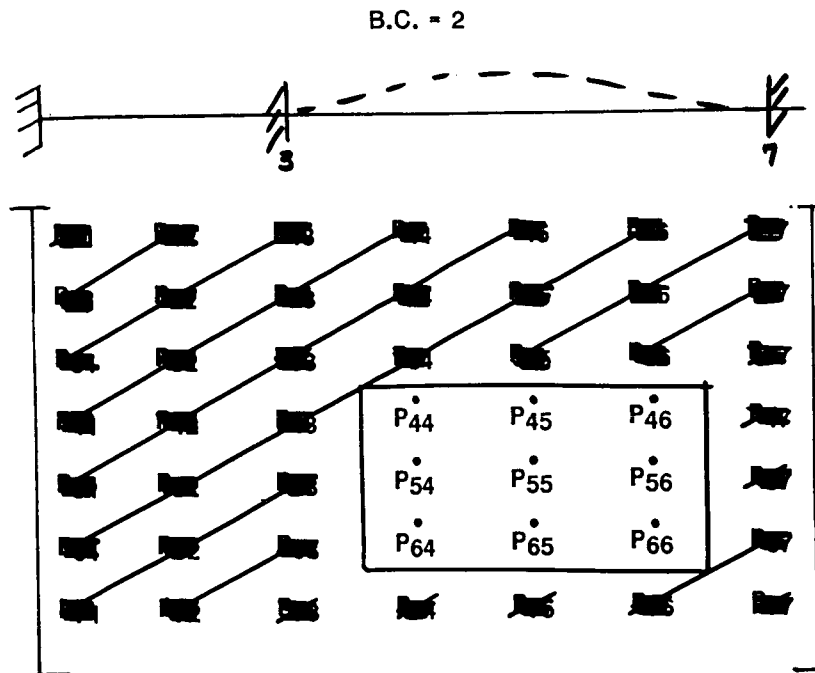
COMBINING THE RESULTS FROM TESTS PERFORMED
ON BC #1 AND BC #2

Note that by combining the results of the updates of the mathematical terms from tests of BC #1 and BC #2, two estimates of the parameters associated with nodes 5 and 6 are obtained. By extending the steps illustrated, a large number of estimates of any parameter can be obtained by the selection of the restraints. The large number of parameter estimates can be obtained by obtaining a large number of modes from a few tests or a small number of modes from a large number of tests with various restraints.

A statistical analysis has indicated that by using the MBCT approach, a better estimate of the parameters can be obtained than if good test results from a modal test of a large space structure can be obtained.

B.C. = 1,2

$$P_{55} \quad P_{56}$$
$$P_{65} \quad P_{66}$$
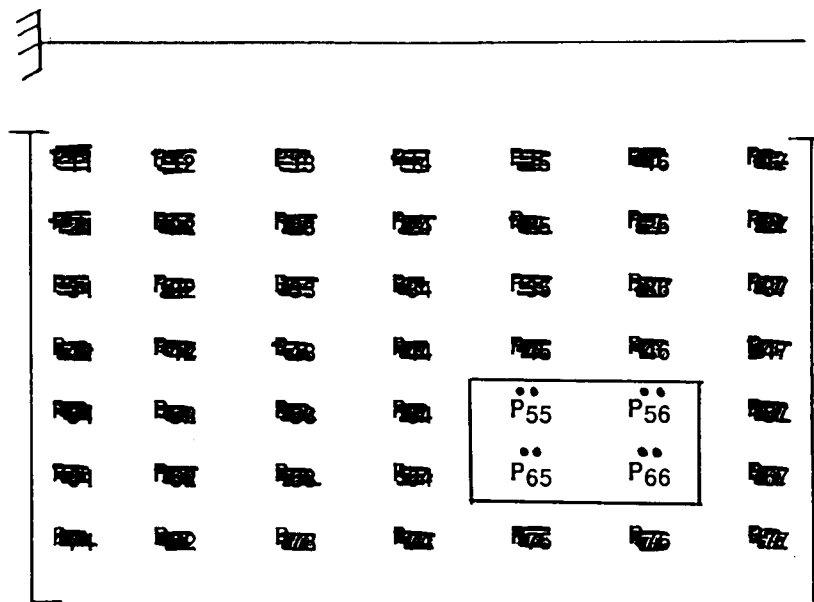
CAN TESTS REQUIRED FOR THE MBCT
BE PERFORMED?

Since the concept of the MBCT is only valuable if the tests necessary to obtain good experimental data can be performed, a modest test program was undertaken. As noted in this figure, sectors of the antenna rib were clamped at the discretion of the engineer. The objective was to constrain the hardware to alleviate the adverse terrestrial conditions and yet obtain good meaningful data. A large number of different boundary conditions were imposed, and excellent data were readily obtained; in fact, the extremely low stiffness of the overall structure helped in the constrained tests. The lowest resonant frequencies with the restraints were approximately 10 Hz., and meaningful static displacements were measured. Within a 2-day period, up to 30 different restraint conditions were tested for the first two modes. The accuracy of the experimental data appeared to be good. The test indicated the ease by which a limited number of modes could be obtained for a large number of conditions with various restraints. Our experience validated the ability to obtain good reliable test data for the MBCT approach.
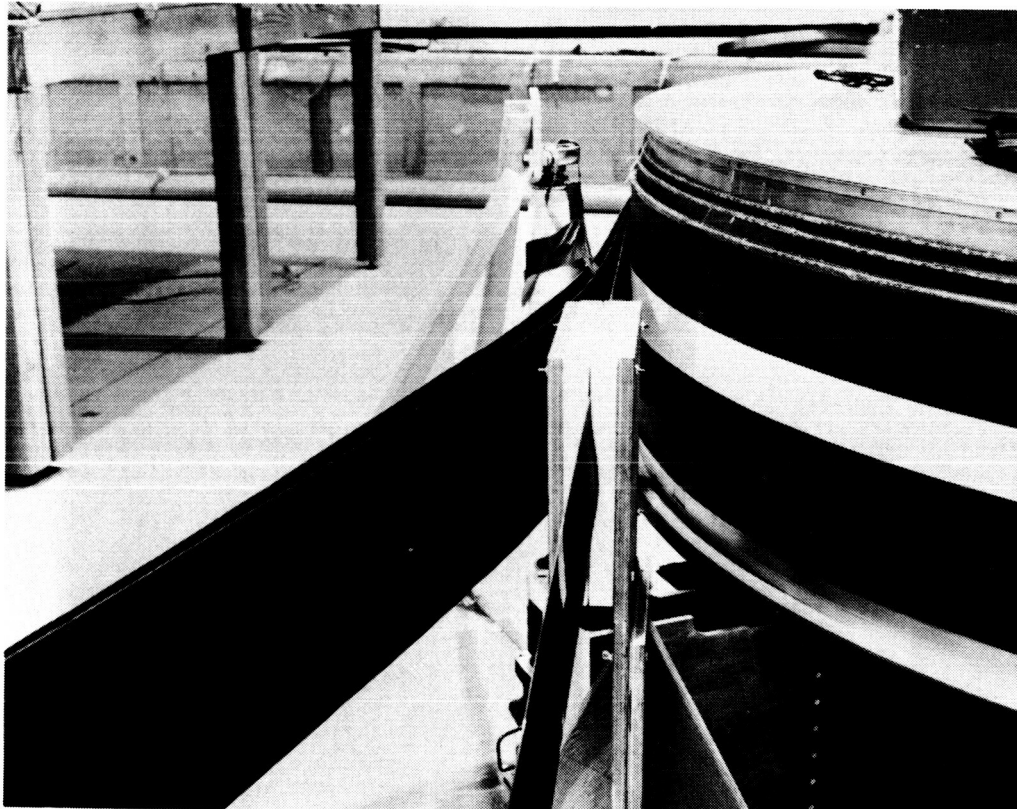
A numerical simulation of the MBCT approach was performed to validate the approach. The beam consists of 16 beam elements and is simply supported at both ends. The objective is to find the 10-percent error in element 4 and the 20-percent error in element 10 using the MBCT approach.

CURRENT APPROACH

| 1 | 2 | 3 | 4 | 5 | 6 | 7 | 8 | 9 | 10 | 11 | 12 | 13 | 14 | 15 | 16 |

10%   20%
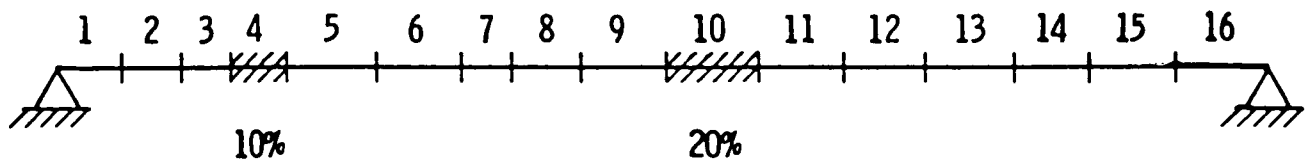
In the simulation study, the following arbitrary restraints were selected. Although six different boundary conditions are shown, only two will be used in this paper.

BC#1

BC#2

BC#3

BC#4

BC#5

BC#6

C-4
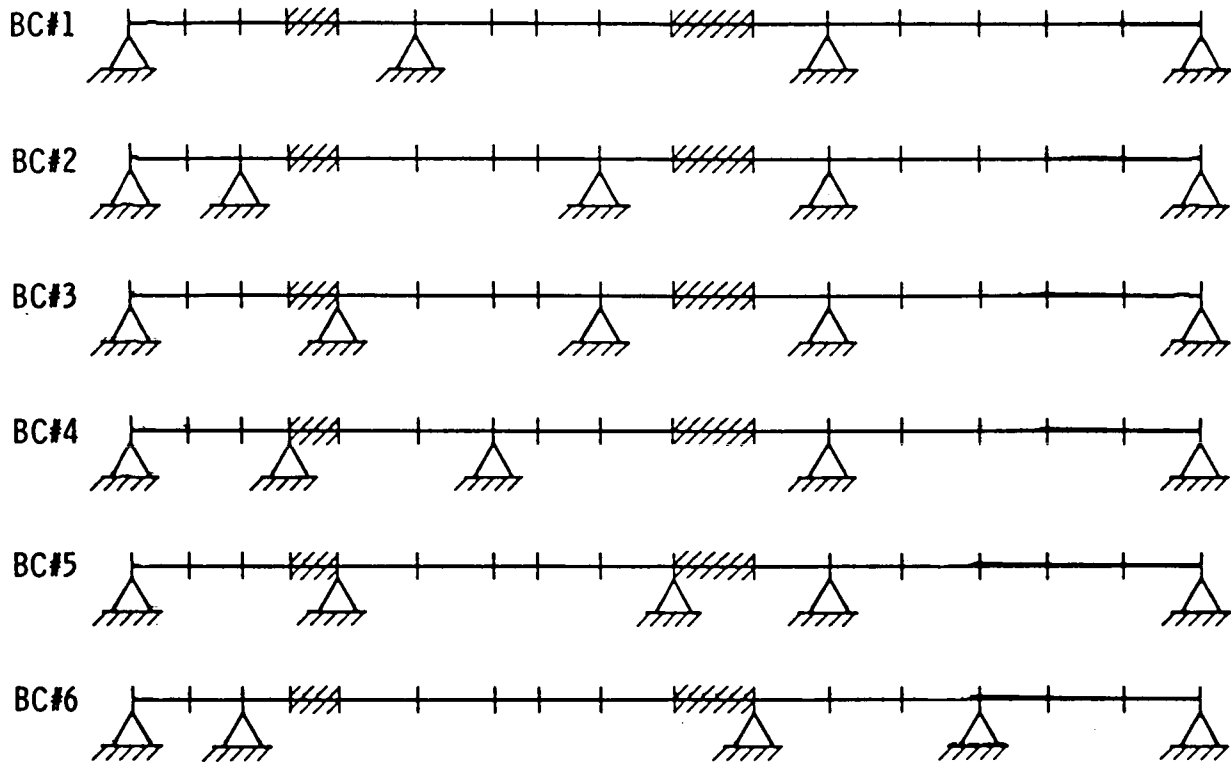
This chart shows that if a conventional modal test could be performed, then the errors in the mathematical model could be corrected to within 96 percent in two test/analysis update iterations. However using the MBCT approach of using 2 to 5 frequencies from each of the first two MBCT configurations, the mathematical model could be corrected to within 99 percent with the same amount of effort.

ESTIMATED PARAMETERS,
ITERATIONS 1 AND 2 ΔI_4 AND ΔI_{10}
(THEORETICAL VALUES ΔI_4 = 0.00834, ΔI_{10} = 0)

(CASE 2)

CASE	ITERATION 1		ITERATION 2		CONFIGURATION
a ΔI_4	0.005897	71%	0.007971	96%	CONVENTIONAL MODAL TEST
ΔI_{10}	0.000657		0.000523		10 FREQUENCIES TOTAL
b ΔI_4	0.007031	84%	0.008166	98%	MBCT CONFIGURATION 1-2
ΔI_{10}	0.000323		0.000034		10 FREQUENCIES TOTAL
c ΔI_4	0.007690	92%	0.008268	99%	MBCT CONFIGURATION 1-2
ΔI_{10}	0.000028		-0.000006		8 FREQUENCIES TOTAL
d ΔI_4	0.006322	76%	0.008273	99%	MBCT CONFIGURATION 1-2
ΔI_{10}	0.000881		-0.000030		6 FREQUENCIES TOTAL
e ΔI_4	0.005358	64%	0.008255	99%	MBCT CONFIGURATION 1-2
ΔI_{10}	0.000678		-0.000012		4 FREQUENCIES TOTAL

INFLUENCE OF TERRESTRIAL ENVIRONMENT
ON THE DYNAMICS OF STRUCTURES

Another important consideration in the ground validation of structures is to establish the ground test conditions under which the terrestrial environment can adversely affect the test results. These data are of value in establishing the artificial boundary conditions in the MBCT approach or in subsystem testing.

The efforts are to investigate the influence of the forces in the structure and structural displacement due to gravitational forces and their impact on the dynamics of structures. This figure shows the influence of the gravitational field on the frequencies of a beam for the various types of modes.

● LINEARIZED FREQUENCY EQUATION

$$\frac{\omega_{gn}}{\omega_{on}} = \left[1 + \frac{NL^2}{n^2\pi^2EI} + \frac{AW_i^2}{2I}\right]^{1/2} \quad ; n = i = 1,3,5,\ldots$$

$$\frac{\omega_{gn}}{\omega_{on}} = \left[1 + \frac{NL^2}{n^2\pi^2EI}\right]^{1/2} \quad ; \text{FOR } n = 2,4,6,\ldots$$

(a) n = 1

(b) n = 2 AND n = 3

845
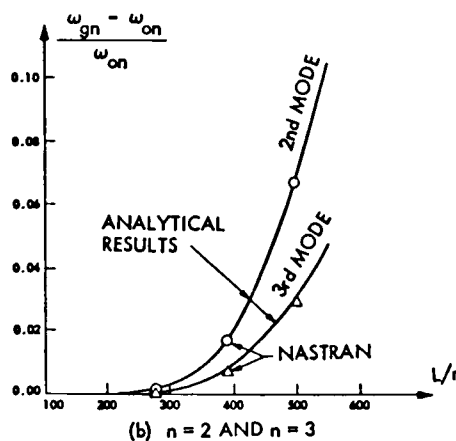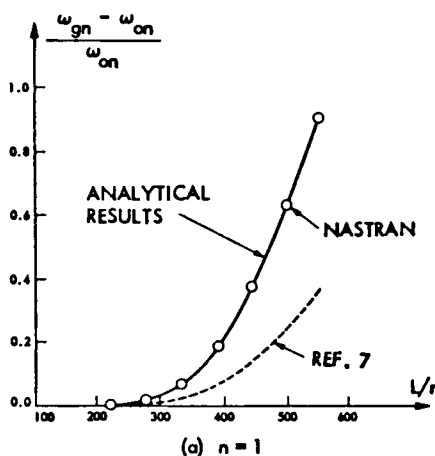
A truss-type structure was selected to illustrate the extension of the ideas developed in the previous figure.

TRUSS-COLUMN TYPE STRUCTURE

A-A CROSS SECTION
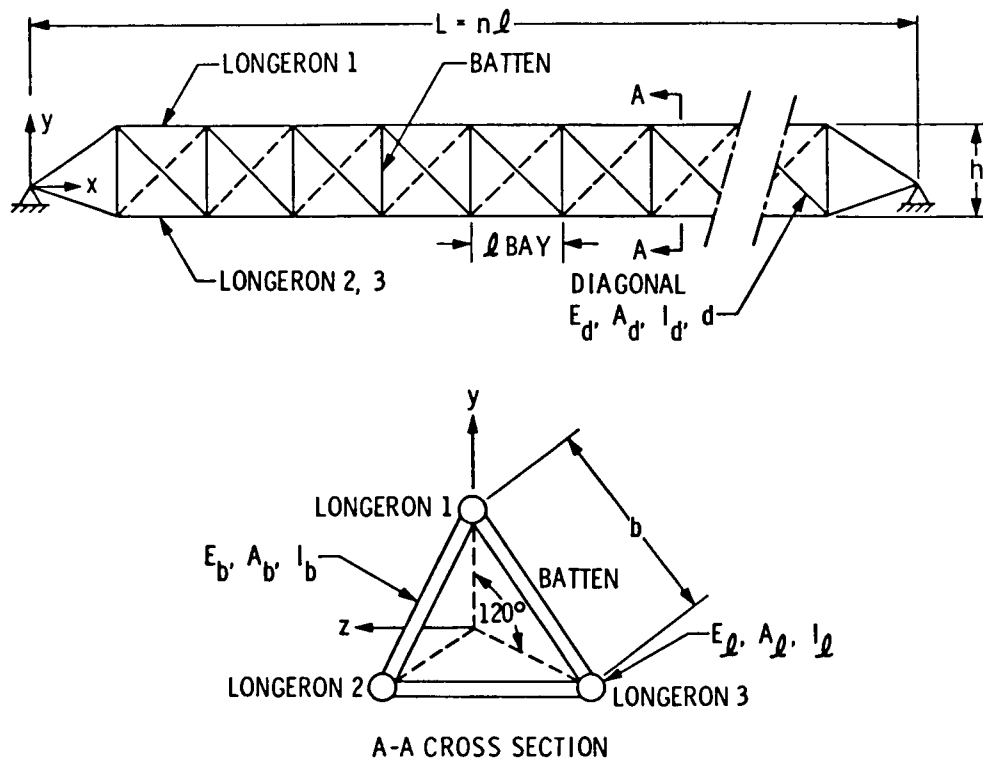
This figure depicts other aspects of the research performed to predict the dynamics of large space structures utilizing ground test data and analyses. Step number one is to perform a buckling analysis to determine the number of bays which can physically maintain its geometry and retain its basic stiffness characteristics. Step number two is to select the number of bays for the ground test. Step number three is to correct the results of the test data from step number two for a zero gravity condition. Step number four is to extrapolate the results of steps number three to the full beam in a zero gravity condition. Step number five compares the test/analysis approach to the results of the total beam if an accurate test on the beam could have been performed; the comparison is within .003 Hz.

VERIFYING THE NATURAL FREQUENCY
OF A LARGE TRUSS-COLUMN (60-BAY)
PROCESS

1. BUCKLING ANALYSIS FOR A 60-BAY TRUSS-COLUMN
   (RESULTS: BUCKLED IF $n > 53$)

2. GROUND TESTS FOR A 40-BAY STRUCTURE
   (RESULTS: N, W_0, ω_g ARE MEASURED)

3. NATURAL FREQUENCY OF A 40-BAY TRUSS-COLUMN IN 0-g FIELD CAN BE PREDICTED BY USING LINEARIZED FREQUENCY EQUATION

4. NATURAL FREQUENCY OF A 60-BAY TRUSS-COLUMN IN 0-g FIELD CAN BE EXTRAPOLATED BY USING SCALING LAW

5. NUMERICAL DEMONSTRATION:

   NASTRAN:

   ω_0(60-BAY) = 0.415 Hz

   $\begin{cases} \omega_g(40\text{-BAY}) = 0.953 \text{ Hz} \\ \omega_0(40\text{-BAY}) = 0.905 \text{ Hz} \\ \omega_0(60\text{-BAY}) = 0.418 \text{ Hz} \end{cases}$

In many structures, the entire system may not be assembled on the ground prior to assembly in space. An example may possibly be the Space Station. In these situations, testing of subsystems or groups of subsystems may have to be performed to validate and update its analytical model; then the analytical model of the subsystems may be combined to predict the dynamics of the total system.

History has shown that subsystem testing and validation have concentrated on those elements which are loaded during the subsystem test and not loaded through the interconnection of the subsystems.

$$
\begin{bmatrix}
a_{11} & a_{12} & a_{13} & a_{14} \\
a_{21} & a_{22} & a_{23} & a_{24} \\
a_{31} & a_{32} & a_{33} & a_{34} \\
a_{41} & a_{42} & a_{43} & a_{44}
\end{bmatrix}
$$
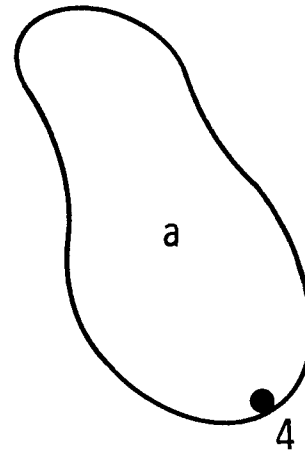
USE OF THE MBCT APPROACH TO
SYSTEMATIC SUBSYSTEM TESTING

An evaluation of a comparison between the analytical model generated by test verified subsystem models and the final system modal test indicates that most often the discrepancies occur because of the errors in the analytical model at the subsystem interconnection points.

In order to test for these important parameters at the interconnection points during the subsystem testing, concepts developed for the MBCT have been adapted. The initial step is to a priori determine the terms in the overall system which are important to the dynamic characteristics which affect the overall system performance. This can be accomplished in many ways; an approach used is to evaluate the elements with large strain energy distribution in the important system modes. The second step is to determine the elements validated by the standard subsystem modal test methods to evaluate the elements which require additional test verification. In most cases these elements can be verified by a large number of tests which load the interface at the subsystem interconnection points. The type and number of tests are selected such that all the important elements, not previously validated, are loaded a sufficient number of times to obtain a good statistical estimate.

SYSTEM

$$\begin{bmatrix} a_{11} & a_{12} & a_{13} & a_{14} \\ a_{21} & a_{22} & a_{23} & a_{24} \\ a_{31} & a_{32} & a_{33} & a_{34} \\ a_{41} & a_{42} & a_{43} & a_{44} \end{bmatrix}$$

$$\begin{bmatrix} b_{11} & b_{12} & b_{13} & b_{14} \\ b_{21} & b_{22} & b_{23} & b_{24} \\ b_{31} & b_{32} & b_{33} & b_{34} \\ b_{41} & b_{42} & b_{43} & b_{44} \end{bmatrix}$$

$$\begin{bmatrix} c_{11} & c_{12} & c_{13} & c_{14} \\ c_{21} & c_{22} & c_{23} & c_{24} \\ c_{31} & c_{32} & c_{33} & c_{34} \\ c_{41} & c_{42} & c_{43} & c_{44} \end{bmatrix}$$

SUMMARY

The basic ideas behind the research being performed at JPL in the area of ground test of large flexible structures for validation of its mathematical model are presented. The goal is to validate the techniques developed at JPL as a part of the MAST effort which is part of the COFS Program. The objective will be to ground test the MAST hardware, predict its dynamic characteristics by analysis using the ground test data, and to verify the predictions by using the flight measured data.

- **GROUND TEST OF LARGE SPACE STRUCTURES ENABLES USE OF STRUCTURES REQUIRED FOR FUTURE MISSIONS**

- **PRESENTED CONCEPTS PURSUED IN JPL R&AD**

    - **INFLUENCE OF TERRESTRIAL ENVIRONMENT ON TESTING**

    - **SUBSYSTEM TEST/ANALYSIS ----> SYSTEM**

    - **MULTIPLE BOUNDARY CONDITION TESTS**

- **PARTICIPATE IN COFS**

SLEW MANEUVERS ON THE SCOLE LABORATORY FACILITY

Jeffrey P. Williams
Spacecraft Control Branch
NASA Langley Research Center
Hampton, Va.

INTRODUCTION

The Spacecraft Control Laboratory Experiment (SCOLE) has been conceived to provide a physical test bed for the investigation of control techniques for large flexible spacecraft. The control problems to be studied are slewing maneuvers and pointing operations. The slew is defined as a minimum time maneuver to bring the antenna line-of-sight (LOS) pointing to within an error limit of the pointing target. The second control objective is to rotate about the line of sight and stabilize about the new attitude while keeping the LOS error within the 0.02 degree error limit. The SCOLE problem is defined as two design challenges. The first challenge is to design control laws for a mathematical model of a large antenna attached to the Space Shuttle by a long flexible mast. The second challenge is to design and implement a control scheme on a laboratory representation of the structure modelled in the first part [1]. Control sensors and actuators are typical of those which the control designer would have to deal with on an actual spacecraft. Computational facilities consist of micro-computer based central processing units with appropriate analog interfaces for implementation of the primary control system, and the attitude estimation algorithm.

This report gives preliminary results of some slewing control experiments which demonstrate the capabilities of the recently completed experimental facility.

* EXPERIMENT CONCEIVED TO PROVIDE A COMMON "DESIGN CHALLENGE FOR INTERESTED INVESTIGATORS

* SLEWING AND POINTING CONTROL PROBLEM

* USES ANTENNA LIKE STRUCTURAL CONFIGURATION AND INERTIAL SENSORS AND ACTUATORS

* VARIETY OF SENSOR AND ACTUATOR TYPES
  - Accelerometers, rate sensors, optical position
  - Thrusters, cmg, reaction wheel

* MULTI-MICROPROCESSOR BASED COMPUTING

* WILL DEMONSTRATE EFFECT OF APPLYING RIGID-BODY CONTROL LAW TO A FLEXIBLE STRUCTURE USING THRUSTERS ONLY

SLEW MANEUVER ON THE SCOLE

The primary purpose of this paper is to demonstrate the capability of the laboratory facility to fulfill the requirements of the second part of the Design Challenge presented by Taylor and Balakrishnan [1]. That requirement is for an accessible laboratory experiment which will allow the study of slewing maneuver of flexible spacecraft.

A 20 degree single axes minimum-time slew using the reflector mounted thrusters is presented. An ad-hoc control scheme which allows the maneuver to be completed without exciting the 1st bending mode of the mast is also demonstrated. No theoretical analysis is offered to justify the performance of the controller or to generalize the technique to other flexible structures.

* PART TWO OF SCOLE DESIGN CHALLENGE (Taylor, Balakrishnan)

* SLEW 20 DEGREES USING THRUSTERS

* WILL DEMONSTRATE AD—HOC CONTROL LAW TO SLEW WITHOUT EXCITING 1st BENDING MODE

* SCOLE LABORATORY FACILITY IS PROVIDED AS A TEST—BED FOR EVALUATION OF CONTROL LAWS FOR LARGE FLEXIBLE STRUCTURES.

* IMPLEMENTATION OF A CLASSICAL RIGID BODY BANG—BANG SLEWING CONTROL LAW DEMONSTRATESD THAT FLEXIBLITY OF THE SCOLE APPARATUS WILL PRESENT CONTROL CHALLENGES SUFFICIENT FOR IDENTIFYING CONTROL DESIGN METHODOLOGIES WHICH MAY BE APPLIED TO FUTURE LARGE FLEXIBLE SATELLITES

* IMPLEMENATION OF AN AD—HOC CONTROLLER FOR VIBRATION ACCOMMODATION DEMONSTRATED THAT FLEXIBILITY OF THE STRUCTURE CAN BE SUPPRESSED

SCOLE LABORATORY APPARATUS

The laboratory experiment shown in the figure attempts to implement the definition of the modelling and control design challenge within reasonable limits of the 1g, atmospheric environment. The experimental facility exhibits the essential SCOLE characteristics of a large mass/inertia connected to a small mass/inertia by a flexible beam. Some trades are made in terms of structure, sensors, actuators, and computational capability in order to develop the experiment in a timely and cost effective manner. To this end, the basic structure is made of homogeneous continuous elements connected by welds and mechanical fasteners. The sensors are aircraft quality rate sensors and servo accelerometers. The Shuttle attitude will be determined through a combination of inertial measurements and optical sensing techniques. The Shuttle control moments are provided by a pair of 2-axis control moment gyros (CMG's). Mast mounted control torques can be applied by a pair of two-axis reaction wheels. Reflector based forces are provided by solenoid actuated jets. Reflector mounted torque devices are a trio of high authority reaction wheels.

STRUCTURES

The SCOLE is comprised of three basic structures, the Shuttle, the mast, and the reflector panel. The assembly of these individual components and the global reference frame are shown in the figure.

The Shuttle planform is made from a 13/16 inch steel plate and has overall dimensions of 83.8 by 54.0 inches. Its total weight is 501.7 pounds. The Shuttle's center of mass is located 3.4 inches below the experiment's point of suspension, and 26.8 inches forward of the tail edge.

The mast is 120 inches long. It is made from stainless-steel tubing and weighs 4.48 pounds. One-inch thick manifolds are mounted to the mast at each end.

The reflector panel is hexagonal in shape, made from welded aluminum tubing, and weighs 4.76 pounds. It is located 126.6 inches below the SCOLE's point of suspension. The center of the reflector is located at 12.0 inches in the x direction and 20.8 inches in the y direction from the end of the mast.

BASIC SCOLE STRUCTURE

Shuttle:
13/16 in. steel plate
501 lb

Mast:
3/4 × .049 in. stainless steel tube
4.48 lb

Reflector:
3/4 × .0625 in. welded aluminum tube
4.76 lb
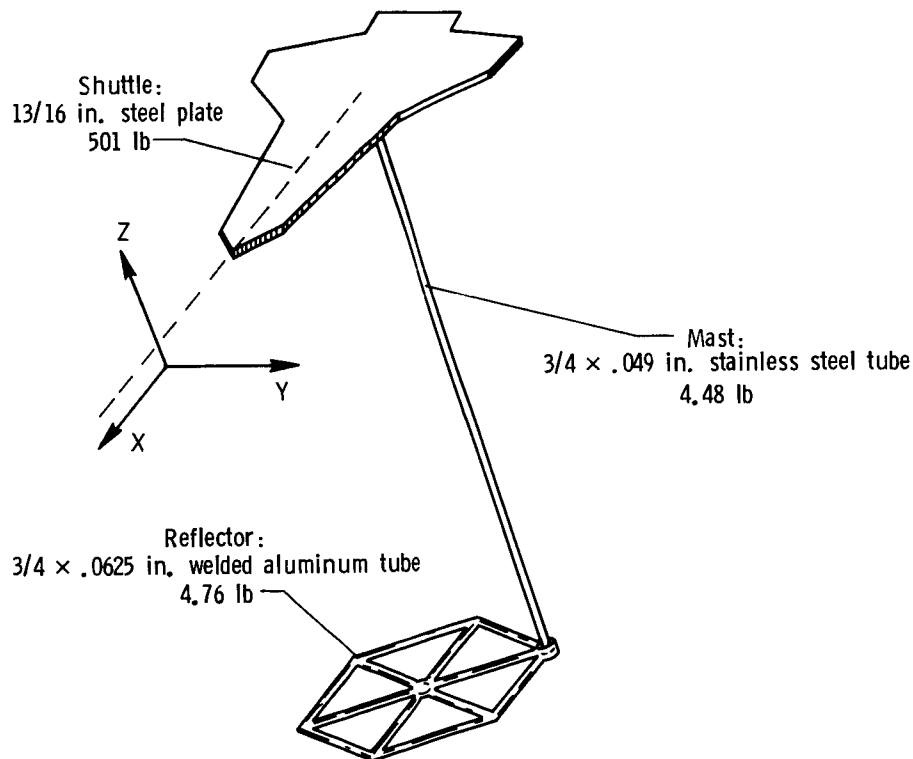
The complete system is suspended from an eleven-foot cable attached at the system center of gravity via a universal joint. The positive z-axis of the Shuttle is pointed up, thus minimizing the static bending of the antenna mast. The suspension point shown in the figure is a two-degree-of-freedom gimbal for pitch and roll rotations with yaw rotation supplied by the suspension cable. The estimated break-out torque of the gimbal is 0.1 ft-lb. The gimbal is fixed to the Shuttle plate, and the system center-of-gravity is made to coincide with the center-of-rotation by means of an adjustable counter balance system.
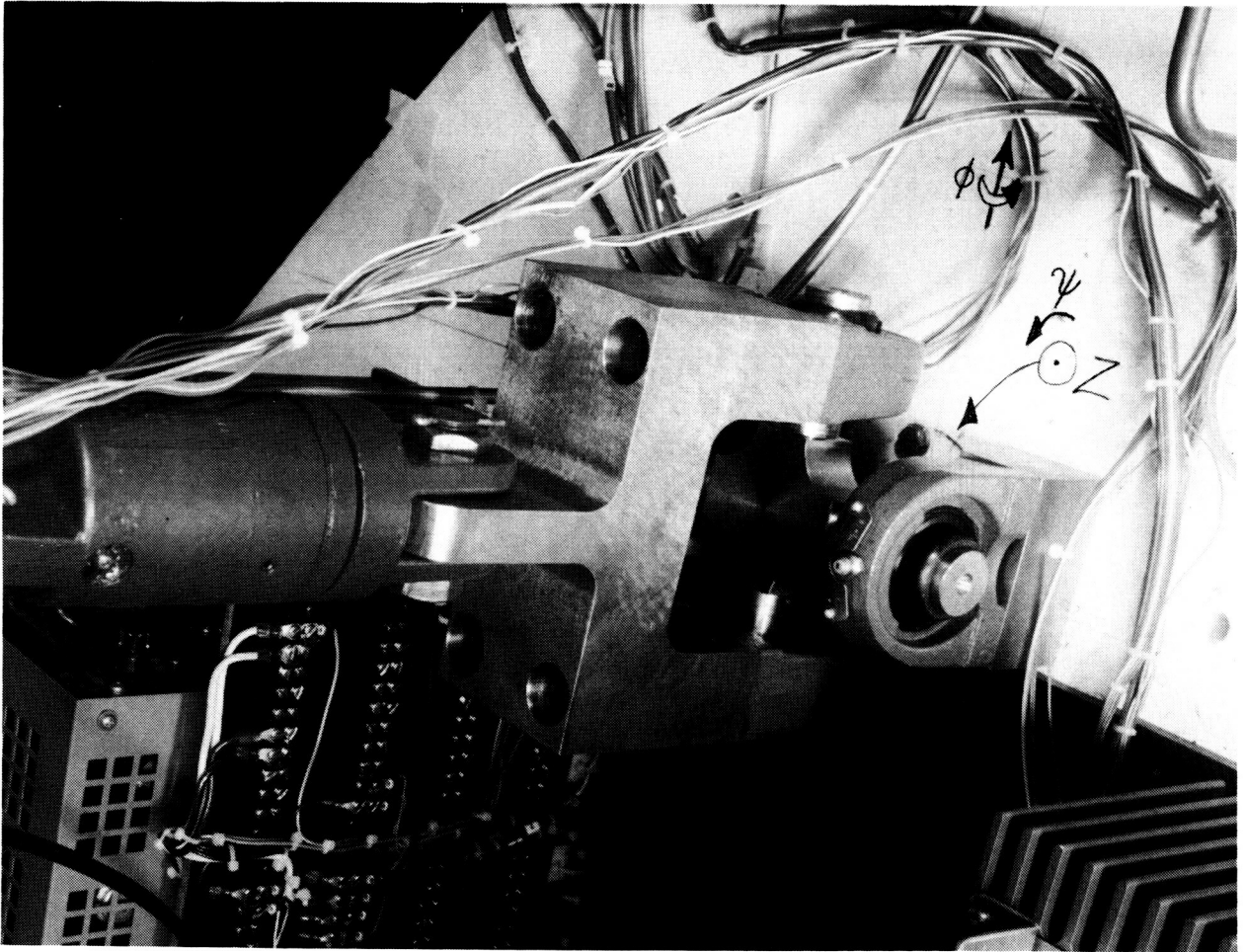
SLEW CONTROL LAW

The slewing of a rigid body spacecraft has long been accomplished with a simple on-off control algorithm which can be derived by examining the phase-plane solution of the simple forced-double-integrator dynamical system. Such a system will describe a parabolic path in the phase plane. The particular path is a function of the initial conditions and the applied torque. If one formulates the final condition problem by specifying zero attitude and zero attitude rate at the final time, backward solution of the equations of motion shows that the approach to the origin must follow the skew-symmetric parabolic curves shown in the figure. These lines will be called the control switching curves. For a given initial condition, the starting command to drive states of the body toward one of the switching curves may be determined by inspection. When the states intersect one of the curves, the control command will change sign and the states will then be driven to zero. This algorithm is shown to be minimum-time by Bryson and Ho in reference 2. If the effectiveness of the torquers is mis-estimated, the controller will still converge to zero, but more than one switch will be required. Also, to allow for practical implementation, a dead-band must be included so that the control command may be set to zero when sufficient attitude performance is achieved.

Such a control law is implemented on the SCOLE by using the reflector mounted thrusters for the control torque. The Shuttle rate sensor and accelerometers are used to estimate attitude rate and attitude by ignoring pendulumn motion of the suspension system. The cold air thrusters on SCOLE have about 0.2 lb force output and are approximately 10 ft from the center of rotation. Their rise time is about 0.032 seconds.
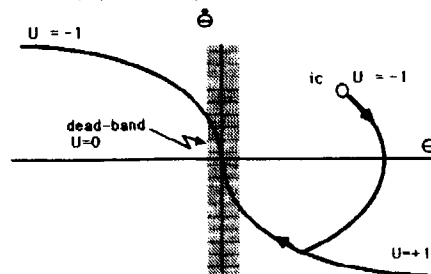
* FOR A SIMPLE RIGID BODY SLEW ABOUT ONE AXIS,

$$I\ddot{\Theta} = tu$$

* THE MINIMUM TIME MANEUVER IS GIVEN BY (Bryson & Ho):

$u = +1$ if $\dot{\Theta}^2 \text{sign}(\dot{\Theta}) < -2\ t/I\ \Theta$ or
             if $\dot{\Theta}^2 \text{sign}(\dot{\Theta}) = -2\ t/I\ \Theta$ and $\Theta > 0$

$u = -1$ if $\dot{\Theta}^2 \text{sign}(\dot{\Theta}) > -2\ t/I\ \Theta$ or
             if $\dot{\Theta}^2 \text{sign}(\dot{\Theta}) = -2\ t/I\ \Theta$ and $\Theta < 0$

* FOR IMPLEMENTATION:

$\dot{\Theta}$ derived from rate sensor
Θ derived from accelerometers by ignoring pendulumn effects

DAMPING CONTROL LAW

For a cantilevered end condition, that is to say, no rigid-body motion, a vibration suppression control law which uses the reflector mounted rate sensor and the thrusters may be derived. The control law is simply to command thrust opposite the sign of the velocity component parallel to thrust axes at the point of attachment of the thrusters. This control will cause a linear decay of the controllable vibration modes.

For implementation on the SCOLE, the velocity of the center of the reflector (attachment point of the thrusters) is estimated by calculating the cross product:

$$\underline{v} = \underline{r} \times \underline{w}$$

where $\underline{r}$ is the position vector of the thrusters with respect to the rate sensor mounted on the corner of the reflector and $\underline{w}$ is the output vector of the rate sensor.

Here again, a dead-band is required so that the thrusters will turn off when the state origin is reached.

* SUPPRESS BENDING MODE VIBRATIONS OF MAST/REFLECTOR

* FOR CANTILEVERED END CONDITIONS SIMPLE COLLOCATED FEED–BACK WILL SUFFICE:

$$U = - \text{ sign (velocity of thrusters)}$$
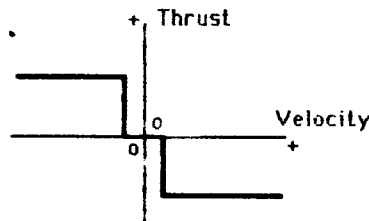
* FOR IMPLEMENTATION, VELOCITY OF THRUSTERS IS DERIVED FROM REFLECTOR MOUNTED ANGULAR RATE SENSOR BY CALCULATING:

$$\underline{V} = \underline{r} \times \underline{w}$$

where $\underline{V}$ is the thruster velocity, $\underline{r}$ is the postition vector of the thrusters w.r.t. the angular rate sensor, and $\underline{w}$ is the output angular rate sensor.

AD-HOC SLEW CONTROLLER

Observation of the structural configuration indicates that the first mode of motion for the system will be a bending mode which will have the Shuttle and the reflector bending toward each other. A command to slew would tend to excite this mode. To suppress the flexible motion would require a thruster command which is contrary to the desired attitude motion. To resolve this dilemma, use is made of the position dead-band for the bang-bang slew control law and the rate dead-band of the vibration suppression control law. By combining the thrust commands for the two controllers, a semi-consistent control command can be determined. A semi-consistent command is one which has the sign and magnitude of at least one of the individual commands. To determine the semi-consistent command, one must first recognize that the thruster can have one of three states: -1, 0, or +1. If the two commands have opposite signs, they are inconsistent and the only control choice is to command zero thrust. If the signs are the same, or if one command is zero and one is non-zero, then the command to the thrusters should be the sign of the sum of the individual commands. Admittedly, this technique does not account for more than one flexible mode, but recall that the stated purpose of the paper is to demonstrate the capability of the laboratory facility, not to develop new control theory.

* DETERMINE CONTROL COMMMANDS FOR BOTH CONTROL LAWS
  SIMULTANEOUSLY

  – IF COMMANDS CONFLICT (ARE OF OPPOSITE SIGN),
  TURN THRUSTERS OFF
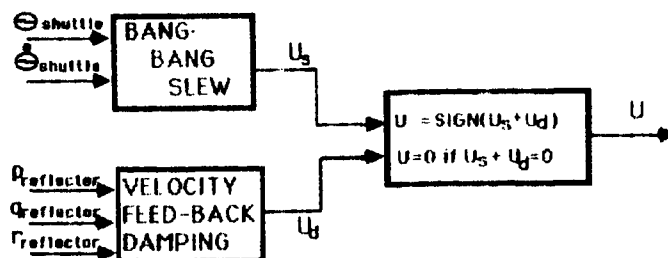
* NO MODAL DECOUPLING ATTEMPTED
 – THAT IS TO SAY, OUTPUTS OF SENSOR ARE USED DIRECTLY

* MUST RECOGNIZE THAT NO THEORY IS PRESENTED TO PREDICT
  PERFORMANCE OR GENERALIZE THIS TECHNIQUE TO OTHER
  FLEXIBLE STRUCTURES

SENSORS

The sensors for the experiment consist of three servo-accelerometers and two, three-axis rotational rate sensing units. The power supplies for these sensors are mounted on the Shuttle plate to minimize the number of large gauge wires which must cross the universal joint suspension point. Only a single 115 VAC cable and thirty-three signal wires cross the universal joint. The wires for the sensors are routed on the Shuttle and along the mast.

SHUTTLE MOUNTED ACCELEROMETERS

The Shuttle-mounted accelerometers shown in the figure sense the x,y, and z accelerations of the Shuttle and gravity. The output of the x and y accelerometers are used to determine attitude angle by neglecting pendulumn effects of the suspension system. These sensors are distributed away from the suspension point to aid inertial attitude estimation. The accelerometers have a frequency response which is nearly flat up to 350 Hz. Linearity is within .17% of the full-scale output.
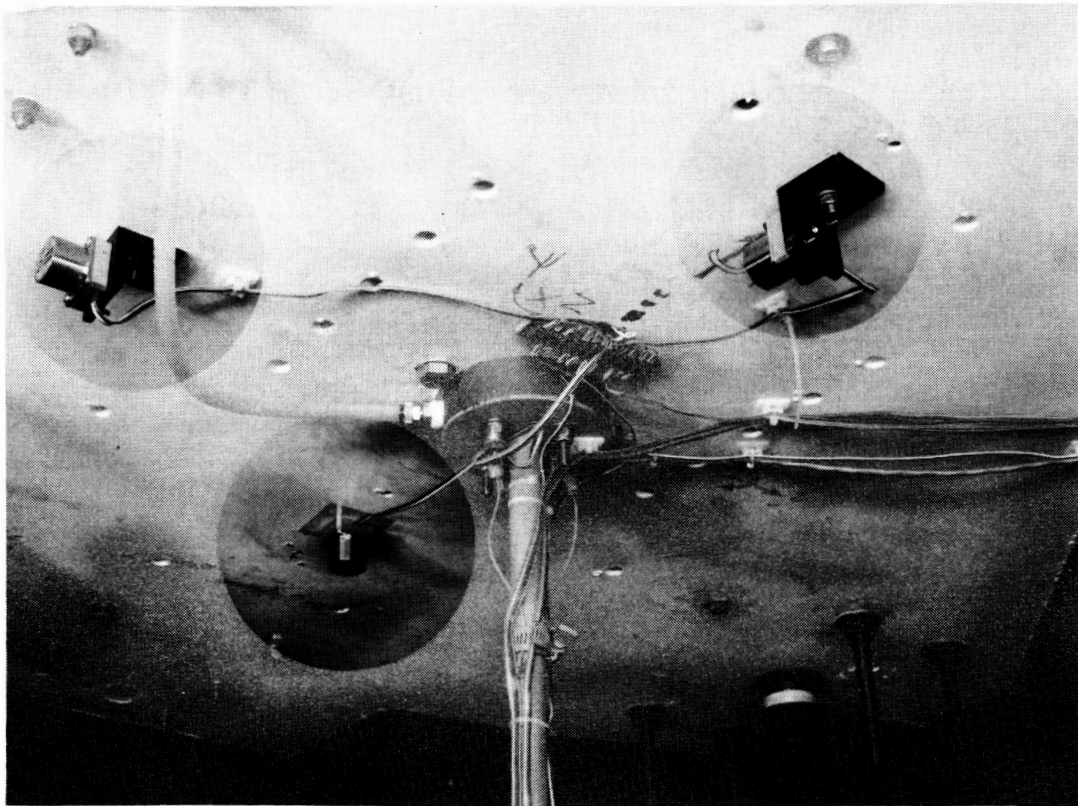
REFLECTOR-MOUNTED CONTROL DEVICES

The reflector-mounted rate sensor package, shown in the extreme left of the figure, senses three axis angular rates at the reflector end of the mast. This information is used for the vibration suppression control law.

The control forces on the reflector are provided by solenoid actuated cold gas jets. The thrusters are mounted in the center of the reflector and act in the x-y plane. The jets are supplied by a compressed air tank mounted on the Shuttle. The pressurized air travels through the mast to the solenoid manifold which gates the air flow between the regulated supply tank and the thrusters. Thrust is initiated by opening the solenoid with a discrete command.
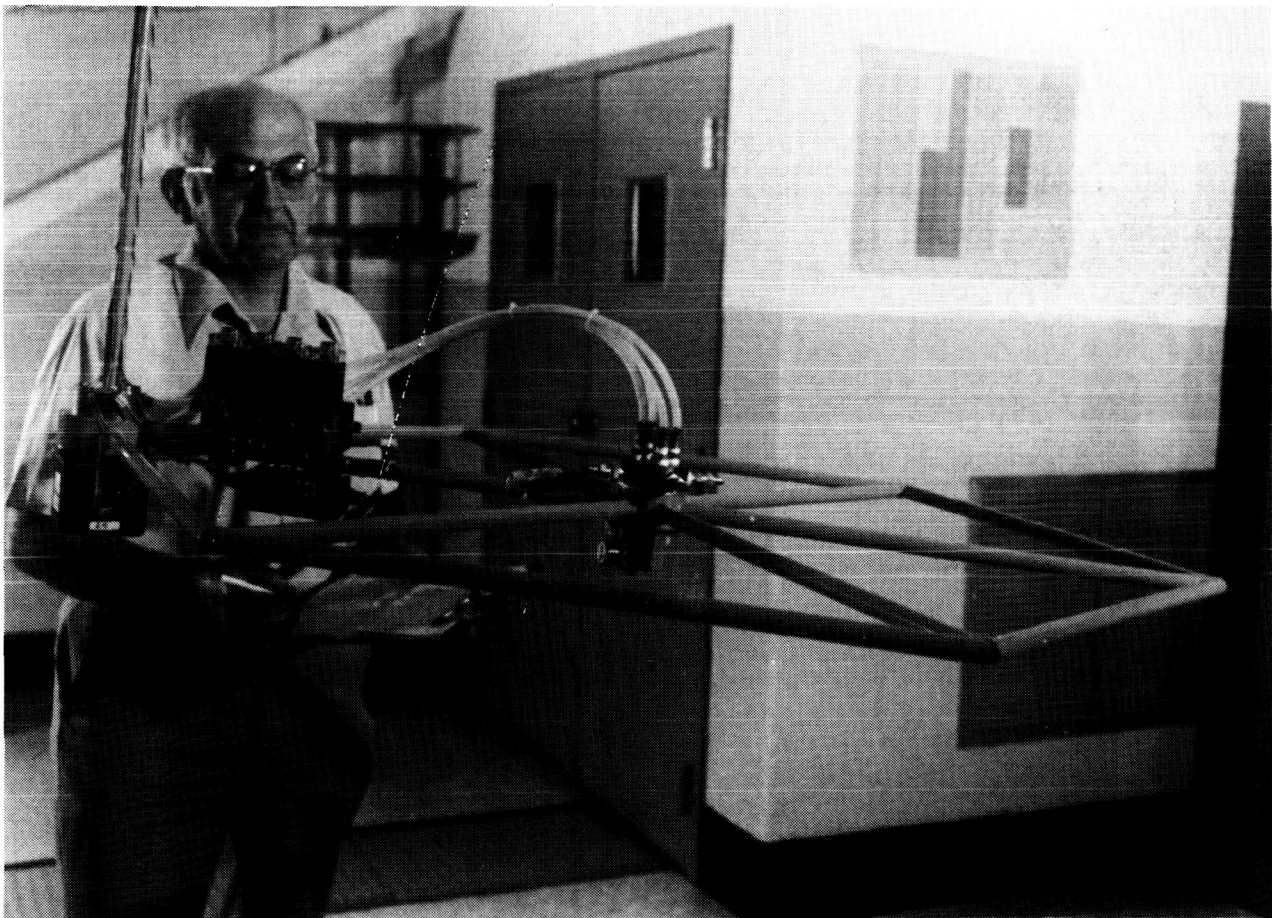
SHUTTLE RATE SENSORS

The rotational rate sensors are three axis aircraft quality instruments. The frequency response is approximately flat to 1 Hz and -6 db at 10 Hz. Linearity is about 0.6% full scale. The range is 60 deg/sec for the yaw and pitch axes and 360 deg/sec for roll. The threshold is 0.01 deg/sec.

The Shuttle-mounted rate sensor package shown in the figure, senses three axis rigid body angular rates of the Shuttle plate. These data are used for the slewing control law.

COMPUTER SYSTEM

The main computer for control law implementation will be a micro-computer based on the Motorola M68000 microprocessor. The computer has 2.0 Mbyte of random access memory and a 40 M-byte hard disk. The operating system is based on UNIX with C, Fortran and Pascal compilers available for applications programming. The computer has 12 serial ports and one parallel port. Terminals are connected on two of the ports and an answer-only modem is attached to another. One port is used for an originate only modem. A line printer is attached to another port.

Analog interfaces consist of a four-bit output-only discrete channel, eight digital-to-analog converters and sixty-four analog-to-digital converters. All converters are 12 bit devices with a range of +/-10v.
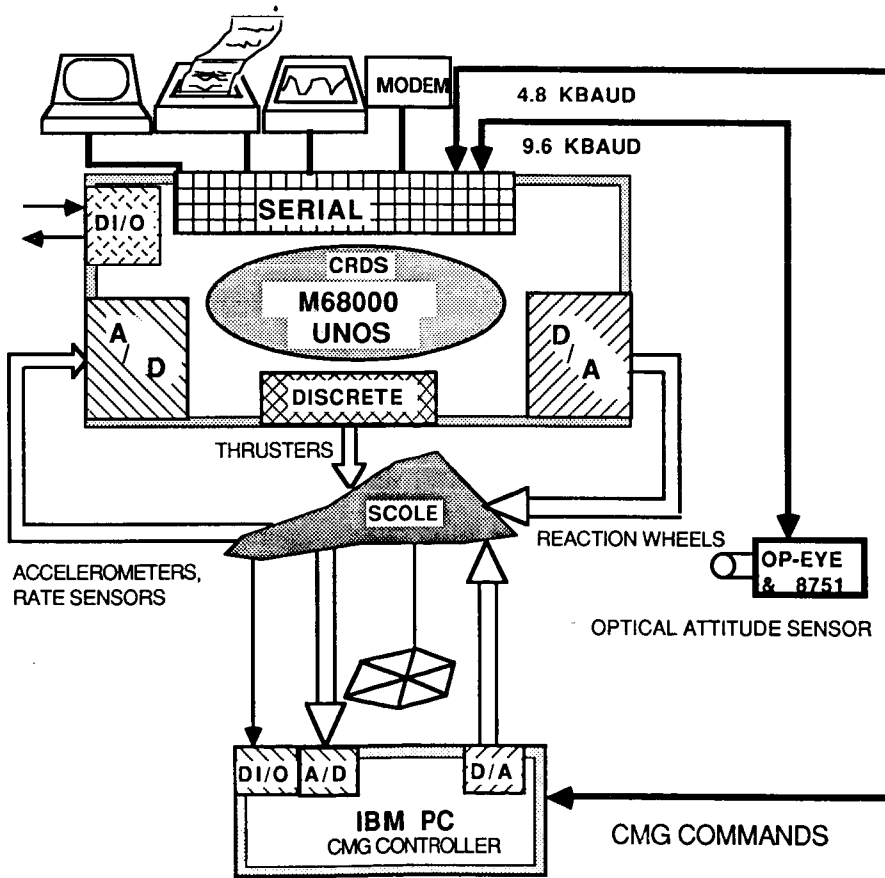
EXPERIMENTAL RESULTS

The effect of applying the rigid-body bang-bang slewing control law to a flexible structure without taking that flexibility into account is demonstrated in the top four time histories. The data presented are, from top to bottom: the Shuttle roll attitude estimate, the Shuttle roll rate estimate, the reflector roll rate measurement, and the thruster command perpendicular to the roll axis. The control law is demonstrated by applying an external torque during the first five seconds with the control disabled. After approximately 20 degrees of attitude error is built up, the control was enabled. The reduction of the attitude error and first switch of the thrust command proceeds essentially as expected for a simple double integrator plant. The oscillation of the attitude during the period from twelve to twenty-two seconds is due to an under estimate of the control effectiveness of the thrusters. Note however that the attitude error continues to decrease. The structural dynamics and control problem addressed by the SCOLE Design Challenge are evident in the oscillation of the Shuttle and reflector roll rates. After the attitude error has become very small at about nineteen seconds it is apparent that the flexible mode is completely unstable and would eventually lead to structural failure.

The effectiveness of the ad-hoc controller in accomplishing the slew without exciting the flexible motion is shown in the bottom four time histories. The same variables are plotted here as above. In this case, the consistency comparison between the slew command and the vibration suppression command allows the slew command to take effect only during short bursts which usually last only one sample period. These pulses are sufficient to drive the attitude error to zero, but the maneuver takes about six seconds longer than the slew only control law. Note however, that the flexible motion is not appreciably excited in this case. Also, because the attitude rates remain relatively small, the attitude error remains relatively low. A final special circumstance in this demonstration must be recognized – that is that the initial condition of the plant had essentially zero excitation of the flexible mode. If it had been excited prior to activation of the control, it is possible that the slew would not have been accomplished.

RIGID BODY BANG–BANG SLEW ONLY
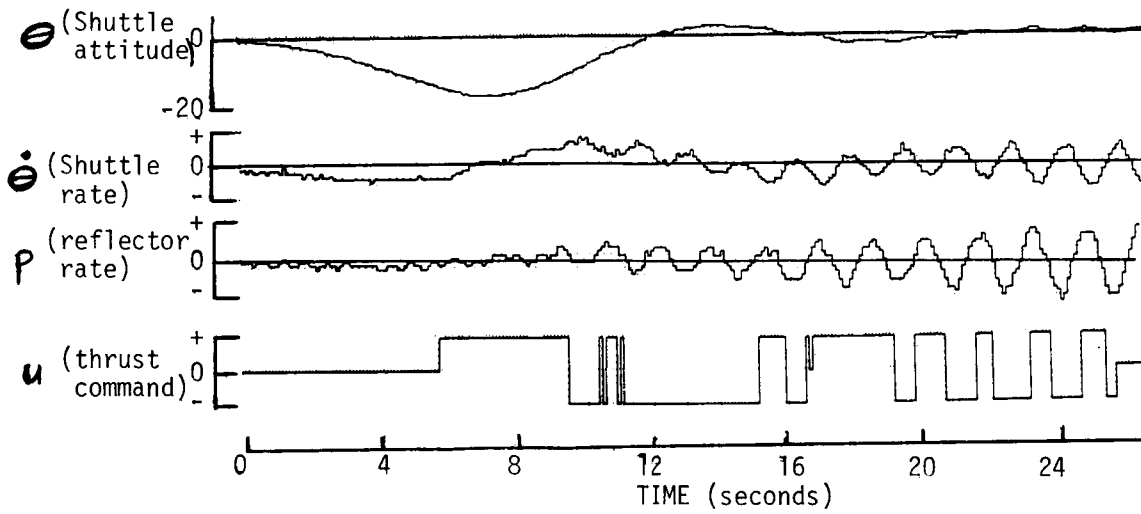
BANG–BANG SLEW & VIBRATION SUPPRESSION
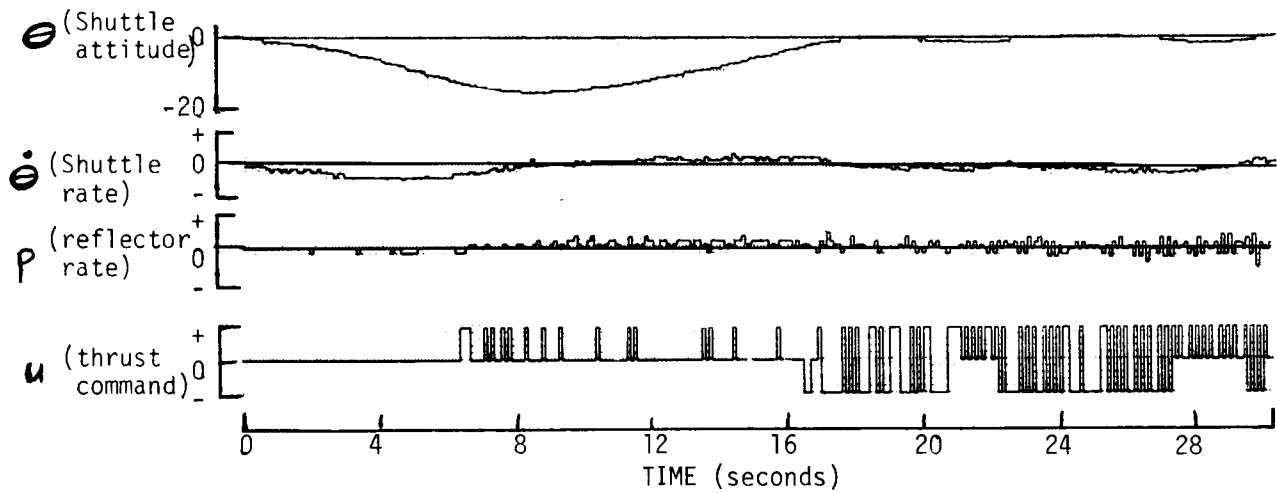
CONCLUSIONS

The SCOLE laboratory facility has been constructed to provide a test-bed for the testing and evaluation of control laws for large flexible structures. Implementation of a classical rigid body bang-bang slewing control law has demonstrated that the combination of flexiblity and control authority present on the SCOLE apparatus will present control challenges sufficient for identifying control design methodologies which may be applied to future large flexible satellites.

The implemenation of an ad-hoc controller for vibration accommodation demonstrated that flexible motion of the structure can be suppressed.

REFERENCES

1. Taylor, L.W., Jr., and Balakrishnan, A. V.: A Laboratory Experiment Used to Evaluate Control Laws for Flexible Spacecraft...NASA/IEEE Design Challenge, Proceedings of the Fourth VPI&SU/AIAA Symposium on Dynamics and Control of Large Structures, June 1983, pp. 311-318.

2. Bryson, A.E., Jr., and Ho, Y.C.: Applied Optimal Control, Optimization, Estimation, and Control, John Wiley & Sons, N.Y., 1975.

RESEARCH IN SLEWING AND TRACKING CONTROL

Jer-Nan Juang
NASA Langley Research Center
Hampton, Virginia

James D. Turner
Cambridge Research Associate
A Division of Photon Research Associates, Inc.
Cambridge, Massachusetts

INTRODUCTION

This research is intended to identify technology areas in which better analytical and/or experimental methods are needed to adequately and accurately control the dynamic responses of multibody space platforms such as the Space Station and the Radiometer Spacecraft. A generic space station model (ref. 1) is used to experimentally evaluate current control technologies and a radiometer spacecraft model is used to numerically test a new theoretical development for nonlinear three-axis maneuvers (ref. 2). Active suppression of flexible-body vibrations induced by large-angle maneuvers is studied with multiple torque inputs and multiple measurement outputs. These active suppression tests will identify the hardware requirements and adequacy of various controller designs.

OUTLINE

● **Rapid three—body maneuvering experiments**

● **Analytical development for nonlinear three—axis maneuvers**

The objective of the present experiment is to demonstrate slewing of flexible structures in multiple axes while simultaneously suppressing vibrational motion at the end of the maneuver. This experiment is designed to verify theoretical analyses concerning the application of modern control methods (refs. 3 & 4) for linear systems to the control of nonlinear systems (refs. 5).

- **Objective: To understand the suppression of vibrations in flexible structures due to large-angle multi-axis maneuvers.**

- **Approach: Perform fundamental experiments in rapid slewing of a three-body flexible system while suppressing vibrational motion at the end of maneuver.**

EXPERIMENT SETUP

Two flexible steel panels hinged to a rigid hub are used to study the slewing control for experimental validation of modern control theory. The hub is rotated in the horizontal plane by an electric gearmotor and its rotational angle is measured by a potentiometer. Instrumentation for each individual panel consists of an electric gearmotor, three full-bridge strain gages to measure bending moments and an angular potentiometer to measure the angle of rotation at the root. The electric gearmotor provides the torque at the root of the panel in the horizontal plane. The strain gages are located at the root, at twenty-two percent of the panel length, and at the mid-span. As a result, the system has three gearmotors as inputs, and six strain gages and three potentiometers as outputs. Signals from all outputs are amplified and then monitored by an analog data acquisition system. An analog computer closes the control loop, generating voltage signals for the three gearmotors based on a linear optimal control algorithm (refs. 6 & 7).
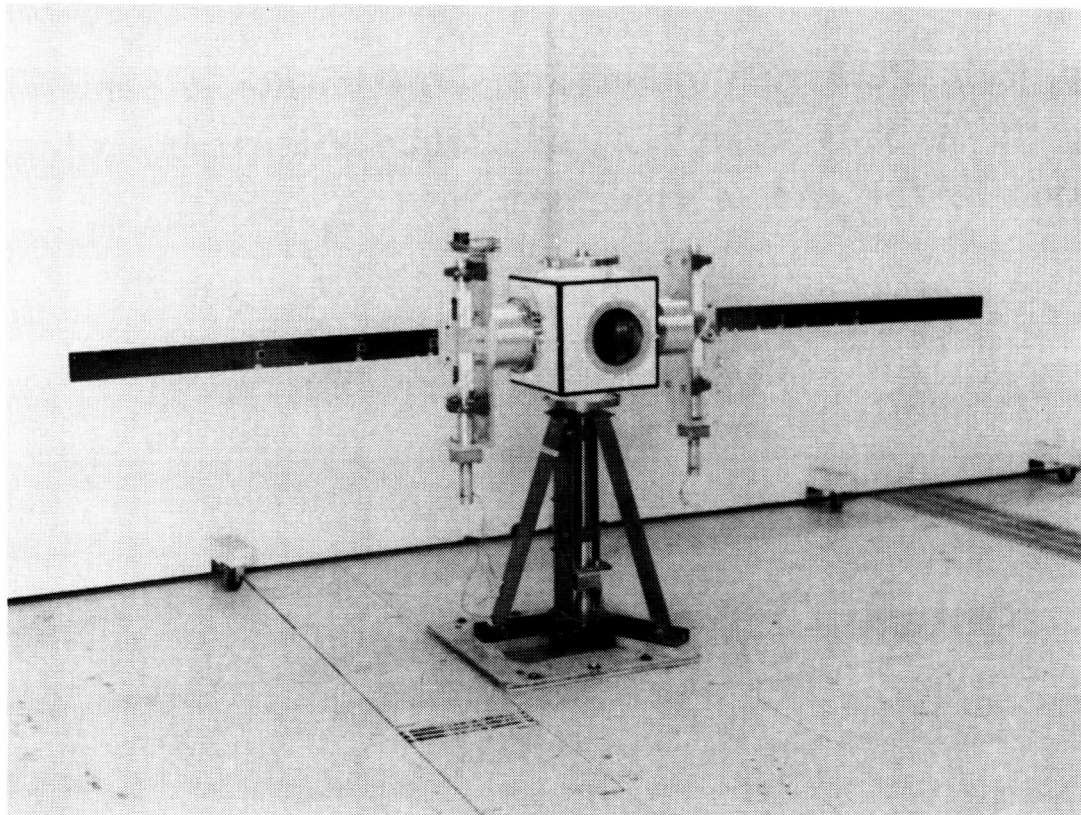
CONTROL STRATEGY FOR LARGE ANGLE MANEUVER

The control designs which use simple closed-loop feedback algorithms are considered for implementation. The basic strategy is to develop means of applying the linear control theory to the nonlinear dynamic system. The control designs are based on a linear dynamic system obtained by using the feedback linearization procedure developed in ref. 3 to isolate the kinematic nonlinearities in the state matrix and then properly treat them as the external force disturbances. The linear dynamic system includes the major portion of the couplings between the rigid hub rotation and the flexible panel motions. It has been proven that this control design is stable under certain constraints of the control gains. With this control strategy, the control procedure can be easily implemented and the three actuators work cooperately to accomplish the large-angle maneuvering and simultaneously suppress the vibrational motions.

- **Define performance requirements such as slewing rate**

- **Derive a three-body dynamic model including actuator dynamics**

- **Treat nonlinear terms as disturbances**

- **Compute direct output feedback gains**

- **Check stability of the closed-loop nonlinear system**

This figure shows the results for 45-degree maneuvers in air. No strain feedback is conducted. The root strain is shown to illustrate the experimental results. The solid line in the center figure represents the final position of the system, whereas the dashed line represents the initial position.

TRANSIENT RESPONSES FOR EXPERIMENTAL DATA

(For 45-deg maneuvers in 2.0 sec without strain feedback)
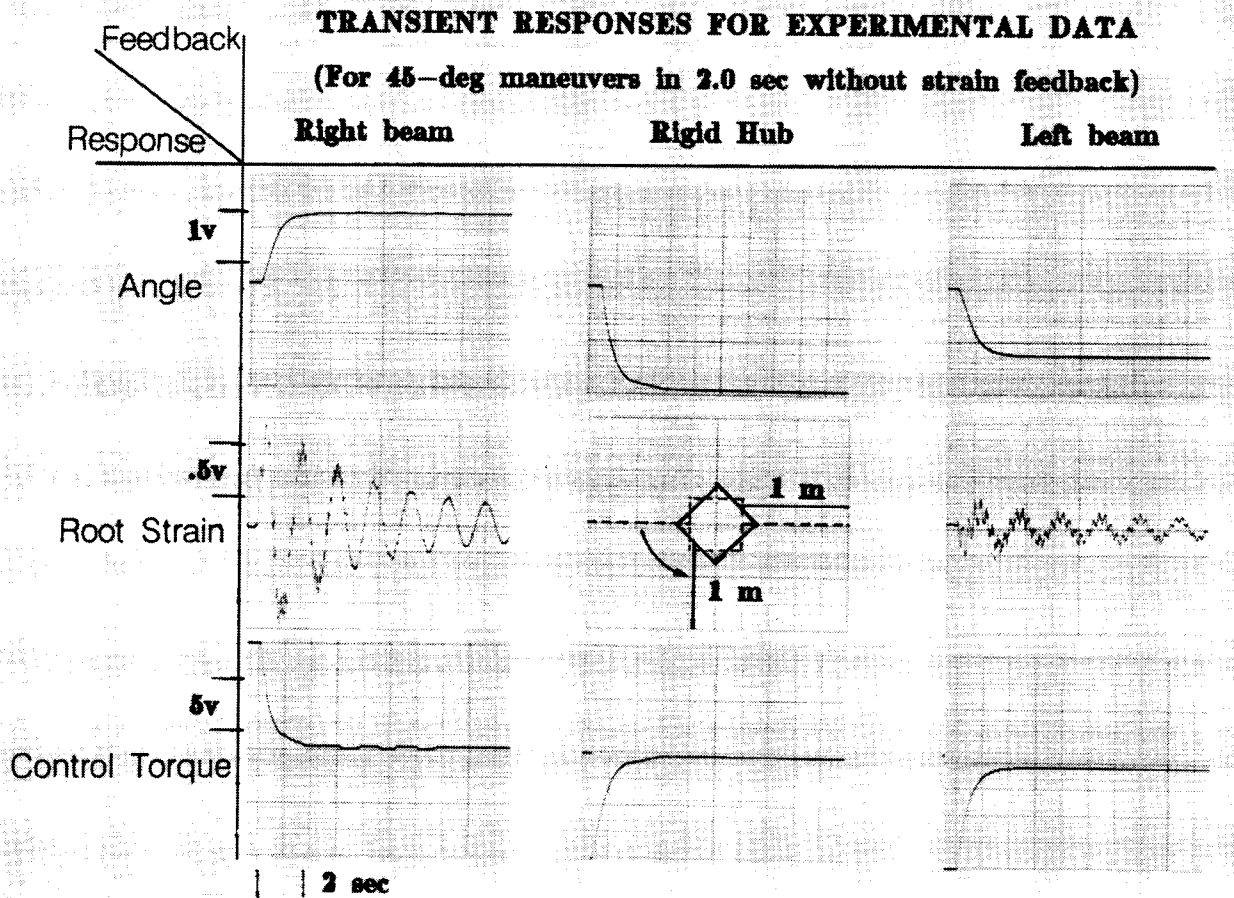
TYPICAL TEST RESULTS (CONTINUED)

This figure shows the results for 45-degree maneuvers with strain feedback. The root strain is shown to illustrate the experimental results. The solid line in the center figure represents the final position of the system, whereas the dashed line represents the initial position. Significant reduction of the root strain responses is observed because of the strain feedback. The experiment data depict a residual motion caused by air circulation in the laboratory while conducting the experiment. Nonlinear effects due to kinematic nonlinearity and large bending deflections during the maneuver did not cause significant changes in performance of the control laws, which were designed using linear control theory.

TRANSIENT RESPONSES FOR EXPERIMENTAL DATA

(For 45-deg maneuvers in 2.0 sec with strain feedback)
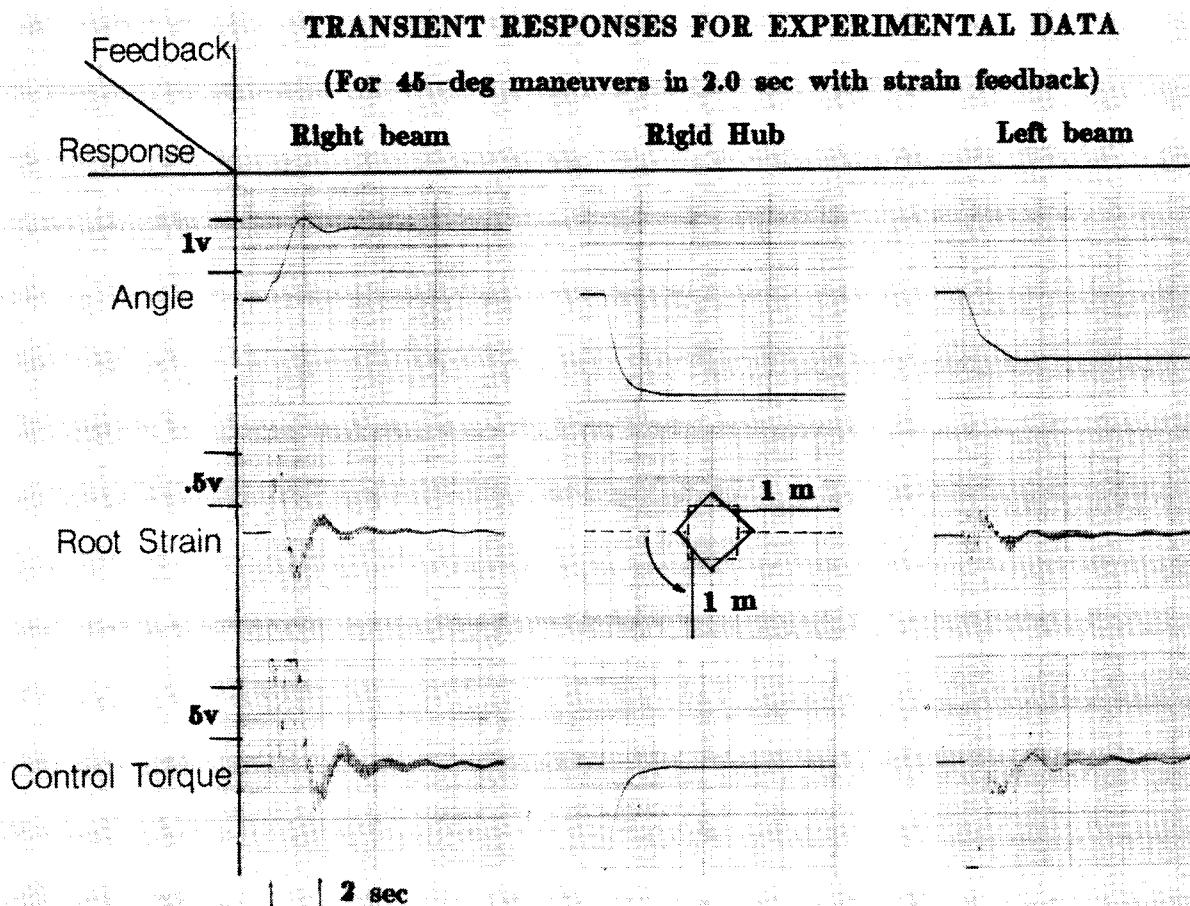
The following figures present a new approach for general nonlinear three-axis slewing maneuvers for flexible spacecraft. The approach developed here is to find the optimal solution for the rigid body model, and then to apply this open-loop rigid body optimal control to fully flexible spacecraft with a perturbation feedback controller. The perturbation feedback controller controls several flexible modes in addition to the rigid body modes, and the feedback gains are computed using the flexible plant linearized about the rigid body nominal solution at several points along the maneuver (ref. 2).

- **Use a rigid body nominal solution for the open-loop maneuver**

    - **Compute single-axis starting guess**

    - **Apply continuation method**

- **Use a closed-loop perturbation feedback for vibration suppression**

    - **Linearize flexible plant about nominal solution**

    - **Compute perturbation gains**

    - **Interpolate gains between time-points**

- **Control smoothing**

RADIOMETER SPACECRAFT MODEL

The spacecraft model used for the example maneuvers is based on a satellite model similar to the N-ROSS satellite, which consists of a more or less rigid bus and several flexible appendages including radiometer and solar array. The spacecraft bus is assumed to be rigid in this study, whereas the radiometer and the solar array are assumed to be flexible. The flexible appendages are each assumed to have five elastic degrees of freedom, and 0.1% damping.
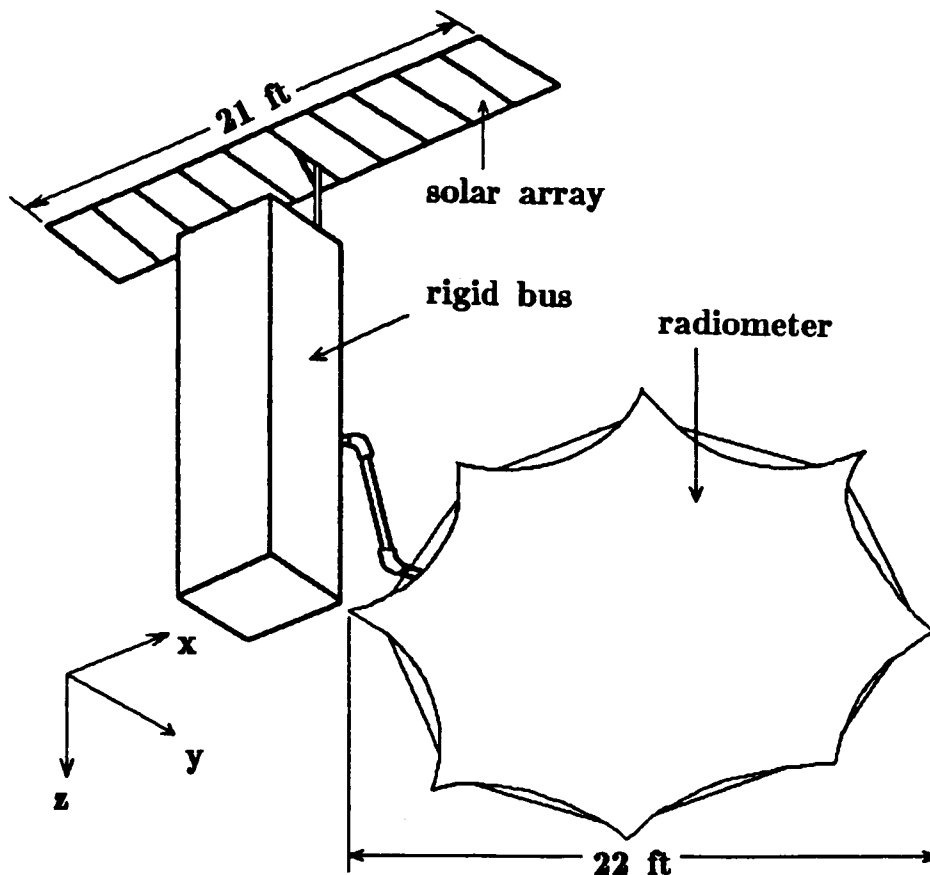
A 60 second rest-to-rest maneuver with angular displacement of 1 radian about each axis was simulated. The break frequency is chosen to be $2\pi/60$ rad/sec. For the choice of this break frequency, the resulting maneuver had controls with smooth profiles.
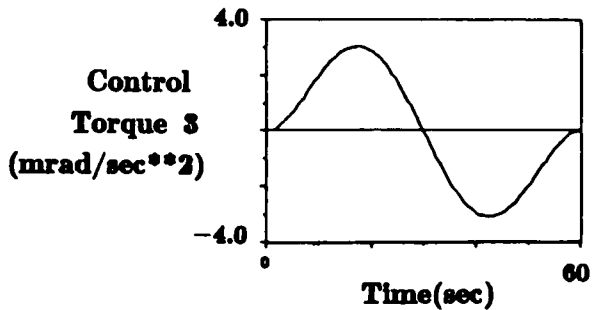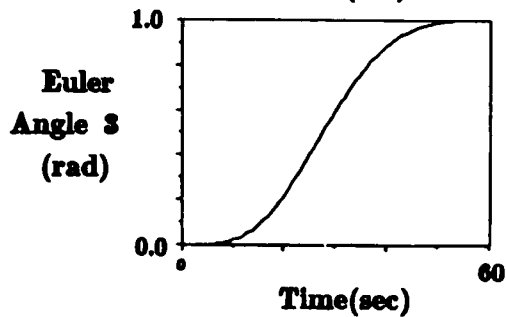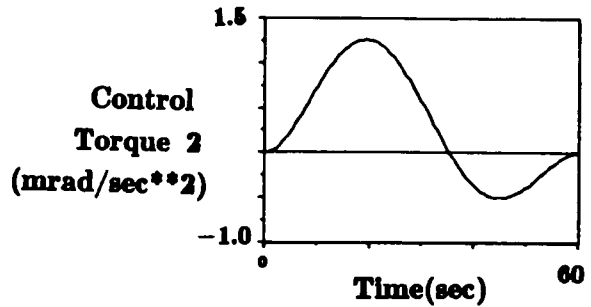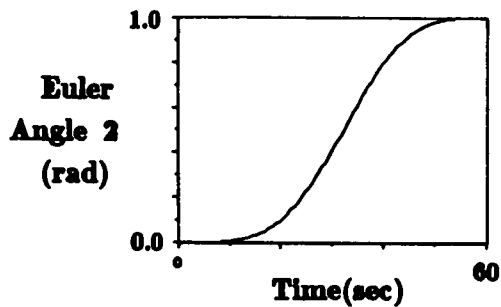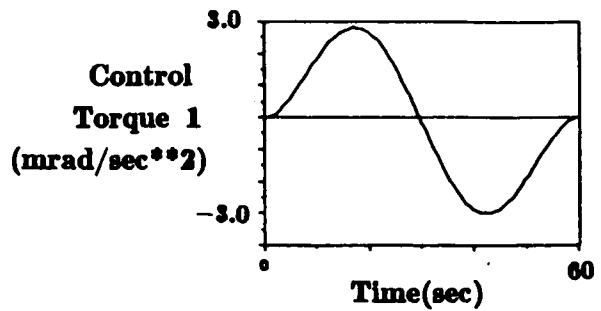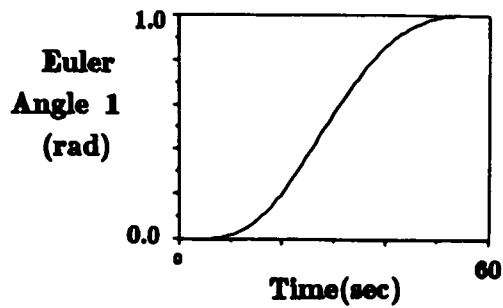
EXAMPLE MANEUVER - PERTURBATION FEEDBACK

The 60 second rest-to-rest maneuver with angular displacement of 1 radian about each axis was simulated. The flexible plant was linearized about the rigid body nominal solution at 12 second intervals. The two lowest solar array modes and the two lowest radiometer modes were chosen for inclusion in the feedback formulation. The other higher frequency modes represent residual modes. All modes are assumed to have 0.1% damping. The break frequency for the perturbation controller was chosen to be half the frequency of the highest controlled mode, so as to minimize the excitation of the residual modes. The error in the initial angle is chosen to be 5% of the total angular displacement about each Euler axis. The controlled modal amplitudes and residual amplitudes are plotted separately. All the modal amplitudes are very small by the end of the maneuver.

(Off-nominal initial angles)
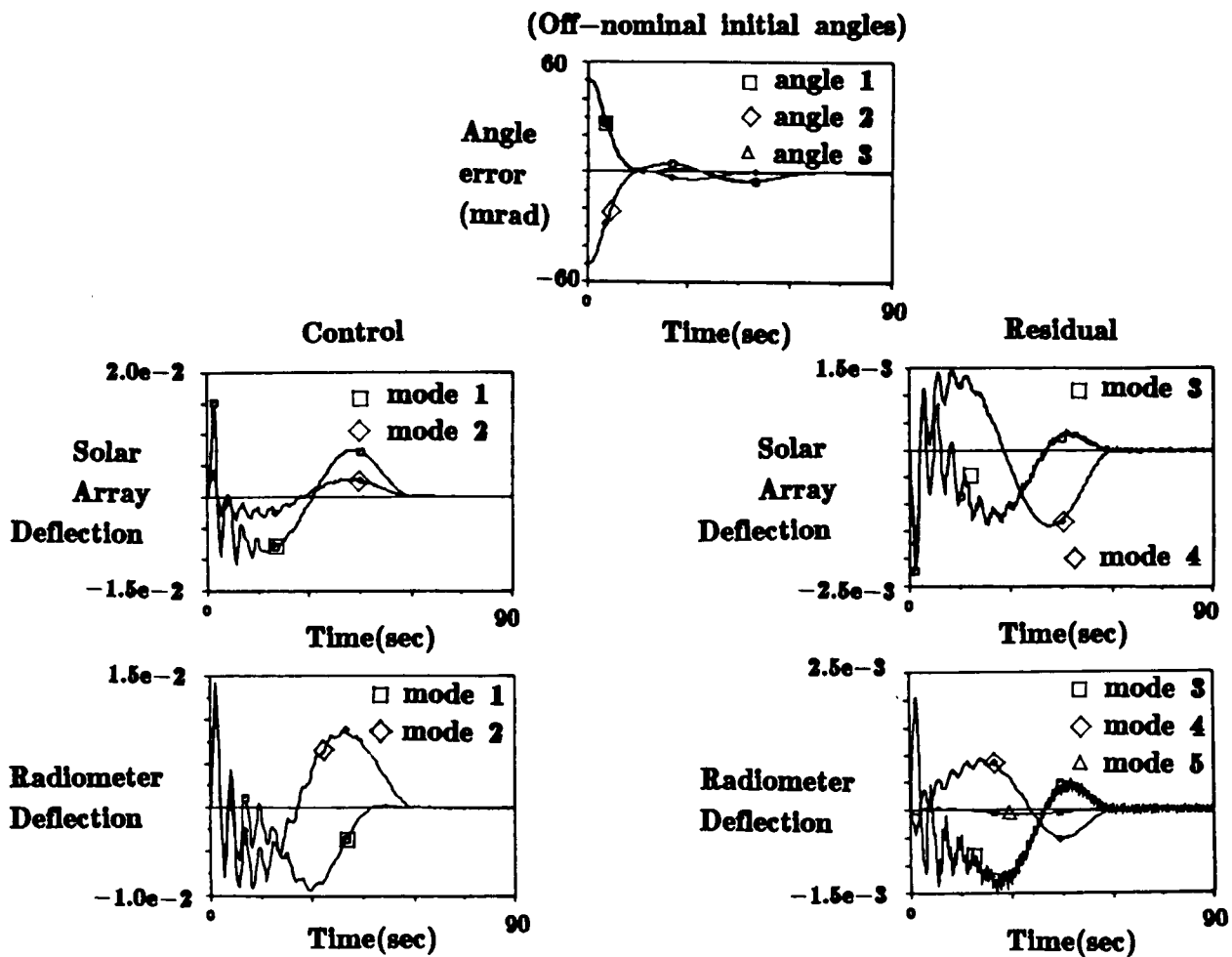
CONCLUDING REMARKS

● **Fast three–body slewing maneuvers with vibration suppression have been successfully demonstrated for flexible structures.**

● **Nonlinear three–axis maneuvers for large flexible systems are developed and numerically tested.**

REFERENCES

[1] Belvin, K. W., "Experimental and Analytical Generic Space Station Dynamic Models," NASA TM-87696, March 1986.

[2] Chun, H. M., "Large-Angle Slewing Maneuvers for Flexible Spacecraft," Ph. D. Dissertation, Massachusetts Institute of Technology, Cambridge, Massachusetts, 274 pages, Sept. 1986.

[3] Juang, J. N., Turner, J. D., and Chun, H. M., "Closed-Form Solutions of Control Gains For a Terminal Controller," Journal of Guidance, Control and Dynamics, Vol. 8, Jan.-Feb. 1985, pp. 38-43.

[4] Juang, J. N., Turner, J. D., and Chun, H. M., "Closed-Form Solutions For a Class of Optimal Quadratic Regulator Problems with Terminal Constraints," Journal of Dynamic System, Measurement and Control, Vol. 108, No. 1, March 1986, pp. 44-48.

[5] Ghammaghami, P. and Juang, J. N., "A Controller Design for Multi-body Large Angle Maneuvers, special issue in the Mechanics of Structures and Machines, 1987.

[6] Juang, J. N., Horta, L. G., and Robertshaw, H., "A Slewing Control Experiment for Flexible Structures," Journal of Guidance, Control and Dynamics, Vol. 9, No. 5, Sept.-Oct. 1986, pp. 599-607.

[7] Juang, J. N. and Horta, L. G., "Effects of Atmosphere on Slewing Control of a Flexible Structure, "AIAA Paper No. 86-1001-CP, Presented at the 27th Structures, Structural Dynamics, and Materials Conference, San Antonio, Texas, May 19-21, 1986.

1. Report No. NASA CP-2447, Part 2	2. Government Accession No.	3. Recipient's Catalog No.
4. Title and Subtitle NASA/DOD Control/Structures Interaction Technology - 1986		5. Report Date June 1987
		6. Performing Organization Code 542-06-11-01
7. Author(s) Robert L. Wright, Compiler		8. Performing Organization Report No. L-16242
9. Performing Organization Name and Address NASA Langley Research Center Hampton, VA 23665-5225		10. Work Unit No.
		11. Contract or Grant No.
12. Sponsoring Agency Name and Address National Aeronautics and Space Administration Washington, DC 20546-0001		13. Type of Report and Period Covered Conference Publication
		14. Sponsoring Agency Code

15. Supplementary Notes

16. Abstract

This publication is a compilation of the papers presented at the First NASA/DOD Control/Structures Interaction (CSI) Technology Conference held at the Omni International Hotel, Norfolk, Virginia, November 18-21, 1986. The conference, which was jointly sponsored by the NASA Office of Aeronautics and Space Technology and the Department of Defense, was organized by the NASA Langley Research Center. The conference is the beginning of a series of annual conferences whose purpose is to report to industry, academia, and government agencies the current status of control/structures interaction technology. The conference program was divided into five sessions: (1) Future Spacecraft Requirements: Technology Issues and Impact; (2) DOD Special Topics: (3) Large Space Systems Technology; (4) Control of Flexible Structures, and (5) Selected NASA Research in Control Structures Interactions.

17. Key Words (Suggested by Authors(s)) Controls Structures Control/structures interaction Large space systems Flexible structures	18. Distribution Statement Unclassified - Unlimited Subject Category 18
19. Security Classif.(of this report) Unclassified	20. Security Classif.(of this page) Unclassified	21. No. of Pages 322	22. Price A14